AD-A166 003 REGULATION & DEVELOPMENT OF MEMBRANE TRANSPORT PROCESSES(U) MEDICAL UNIV OF SOUTH CAROLINA CHARLESTON J S GRAVES 15 MAY 85 AFOSR-TR-86-0142 1/4

UNCLASSIFIED F/G 6/16 NL

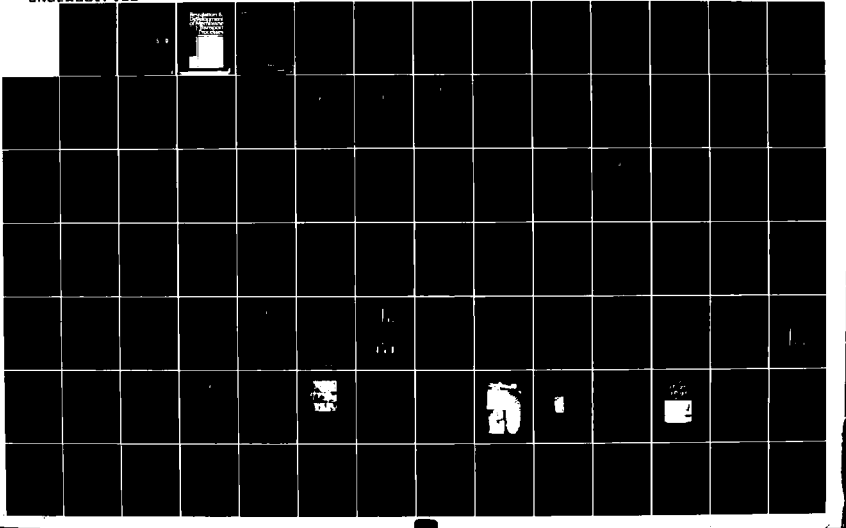

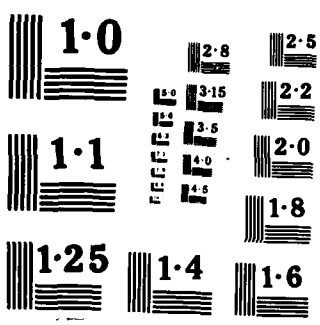
1·0
1·1
1·25
1·4
1·6
1·8
2·0
2·2
2·5
2·8
3·15
3·5
4·0
4·5
5·0

OK to take apart mc

PHOTOGRAPH THIS SHEET

(1)

AD-A166 003

DTIC ACCESSION NUMBER

LEVEL

INVENTORY

REGULATION AND DEVELOPMENT OF MEMBRANE TRANSPORT PROCESSES

AFOSR-TR-86-0142

DOCUMENT IDENTIFICATION

DISTRIBUTION STATEMENT A
Approved for public release;
Distribution Unlimited

DISTRIBUTION STATEMENT

ACCESSION FOR	
NTIS GRA&I	☑
DTIC TAB	☐
UNANNOUNCED	☐
JUSTIFICATION	
BY	
DISTRIBUTION /	
AVAILABILITY CODES	
DIST	AVAIL AND/OR SPECIAL
A-1	

DISTRIBUTION STAMP

DTIC
ELECTE
APR 0 3 1986
S D
D

DATE ACCESSIONED

QUALITY INSPECTED 6

DATE RETURNED

86 4 1 163

DATE RECEIVED IN DTIC

REGISTERED OR CERTIFIED NO.

PHOTOGRAPH THIS SHEET AND RETURN TO DTIC-DDAC

DTIC FORM 70A DEC 83

DOCUMENT PROCESSING SHEET

PREVIOUS EDITION MAY BE USED UNTIL STOCK IS EXHAUSTED.

Regulation & Development of Membrane Transport Processes

Regulation & Development

UNCLASSIFIED

SECURITY CLASSIFICATION OF THIS PAGE

REPORT DOCUMENTATION PAGE

1a REPORT SECURITY CLASSIFICATION: UNCLASSIFIED	1b RESTRICTIVE MARKINGS
2a SECURITY CLASSIFICATION AUTHORITY	3 DISTRIBUTION/AVAILABILITY OF REPORT: Approved for public release; Distribution unlimited.
2b DECLASSIFICATION/DOWNGRADING SCHEDULE	
4 PERFORMING ORGANIZATION REPORT NUMBER(S)	5 MONITORING ORGANIZATION REPORT NUMBER(S): AFOSR-TR- 86-0142
6a NAME OF PERFORMING ORGANIZATION: Society of General Physiologists, Medical Univ of South Carolina	6b OFFICE SYMBOL (If applicable)
7a NAME OF MONITORING ORGANIZATION: Air Force Office of Scientific Research/NL	
6c ADDRESS (City, State and ZIP Code): 171 Ashley Avenue, Charleston, South Carolina 29425	7b ADDRESS (City, State and ZIP Code): Building 410, Bolling AFB, DC 20332-6448
8a NAME OF FUNDING/SPONSORING ORGANIZATION: AFOSR	8b OFFICE SYMBOL (If applicable): NL
9 PROCUREMENT INSTRUMENT IDENTIFICATION NUMBER: AFOSR-83-0310	
8c ADDRESS (City, State and ZIP Code): Building 410, Bolling AFB DC 20332-6448	10 SOURCE OF FUNDING NOS.

PROGRAM ELEMENT NO.	PROJECT NO.	TASK NO.	WORK UNIT NO
61102F	2312	A5	

11 TITLE (Include Security Classification): Regulation and Development of Membrane Transport Processes

12 PERSONAL AUTHOR(S): Dr James Graves

13a TYPE OF REPORT	13b TIME COVERED	14 DATE OF REPORT (Yr., Mo., Day)	15 PAGE COUNT
Interim – Book	FROM 15 Jul 83 TO 14 Jun 84	15 May 85	One

16 SUPPLEMENTARY NOTATION

17 COSATI CODES			18 SUBJECT TERMS (Continue on reverse if necessary and identify by block number)
FIELD	GROUP	SUB GR	

19 ABSTRACT (Continue on reverse if necessary and identify by block number)

The Symposium took place on September 11-14, 1983, at the Marine Biological Laboratory, Woods Hole, MA. Approximately 150 scientists were registered, and 50 posters were contributed. Over the first three days of the meeting, seventeen invited speakers gave 40 minute oral presentations to the group assembled. On the fourth morning, two workshops were convened simultaneously with four presentations in each. The AFOSR funds were used for travel and on-site expenses of the invited particpants. The invited presentations have been published as a book by John Wiley and Sons, Inc.

20 DISTRIBUTION/AVAILABILITY OF ABSTRACT	21 ABSTRACT SECURITY CLASSIFICATION
UNCLASSIFIED/UNLIMITED ☒ SAME AS RPT. ☐ DTIC USERS ☐	UNCLASSIFIED

22a NAME OF RESPONSIBLE INDIVIDUAL	22b TELEPHONE NUMBER (Include Area Code)	22c OFFICE SYMBOL
Dr William O Berry	(202) 767-5021	NL

DD FORM 1473, 83 APR EDITION OF 1 JAN 73 IS OBSOLETE.

SECURITY CLASSIFICATION OF THIS PAGE UNCLASSIFIED

REGULATION AND DEVELOPMENT OF MEMBRANE TRANSPORT PROCESSES

VOLUME 39

IN THE SOCIETY OF GENERAL
PHYSIOLOGISTS SERIES

REGULATION AND DEVELOPMENT OF MEMBRANE TRANSPORT PROCESSES

Editor:

JAMES S. GRAVES, PH.D.

Department of Physiology
Medical University of South Carolina
Charleston, South Carolina

Society of General Physiologists and

JOHN WILEY & SONS

New York • Chichester • Brisbane • Toronto • Singapore

Library of Congress Cataloging in Publication Data:

Main entry under title:
Regulation and development of membrane transport processes.

(Society of General Physiologists series ; v. 39)
Based on the proceedings of the 37th Annual Symposium
of the Society of General Physiologists, held Sept. 1983
in Woods Hole, Mass.
Includes index.
1. Biological transport—Regulation—Congresses.
2. Cell membranes—Congresses. 3. Eukaryotic cells—
Congresses. I. Graves, James S. (James Stephen),
1945– II. Society of General Physiologists.
Symposium (37th : 1983 : Woods Hole, Mass.) III. Series.

[DNLM: 1. Biological Transport—congresses. 2. Cell
Membrane—metabolism—congresses. W1 S087G v.39 /
QH 601 R344 1983]
QH509.R44 1984 574.87'5 84-11987
ISBN 0-471-81038-X

Printed in the United States of America

10 9 8 7 6 5 4 3 2 1

CONTRIBUTORS

E. A. Adelberg Departments of Human Genetics and Physiology, Yale University School of Medicine, New Haven, Connecticut

Qais Al-Awqati Departments of Medicine and Physiology, College of Physicians and Surgeons, Columbia University, New York, New York

Robert S. Balaban Laboratory of Kidney and Electrolyte Metabolism, National Institutes of Health, Bethesda, Maryland

Dale Benos Department of Physiology and Biophysics, Harvard Medical School, Boston, Massachusetts

John D. Biggers Department of Anatomy, Dartmouth Medical School, Hanover, New Hampshire

Lewis Cantley Department of Biochemistry and Molecular Biology, Harvard University, Cambridge, Massachusetts

William A. Catterall Department of Pharmacology, University of Washington School of Medicine, Seattle, Washington

J. Chao Department of Pharmacology, Medical University of South Carolina, Charleston, South Carolina

John S. Cook Biology Division, Oak Ridge National Laboratories, Oak Ridge, Tennessee

Samuel W. Cushman Cellular Metabolism and Obesity Section, National Institute of Arthritis, Diabetes, Digestive and Kidney Disease, National Institutes of Health, Bethesda, Maryland

A. W. Cuthbert Department of Pharmacology, University of Cambridge, Cambridge, U.K.

Hector F. DeLuca Department of Biochemistry, University of Wisconsin, Madison, Wisconsin

L. Dux Institute of Biochemistry, School of Medicine, University of Szeged, Szeged, Hungary

Isidore S. Edelman Department of Biochemistry, College of Physicians and Surgeons, Columbia University, New York, New York

Douglas M. Fambrough Department of Embryology, Carnegie Institution of Washington, Baltimore, Maryland

Jordan B. Fishman University of Tennessee-Oak Ridge Graduate School of Biomedical Science, Oak Ridge, Tennessee

J. J. Gargus Department of Physiology, Emory University Medical School, Atlanta, Georgia

Haim Garty Department of Membrane Research, The Weizmann Institute of Science, Rehovot, Israel

Gerhard Giebisch Department of Physiology, Yale University School of Medicine, New Haven, Connecticut

Guido Guidotti Department of Biochemistry and Molecular Biology, Harvard University, Cambridge, Massachusetts

P. V. Halushka Department of Pharmacology, Medical University of South Carolina, Charleston, South Carolina

Thomas L. Hayden Department of Mathematics, University of Kentucky, Lexington, Kentucky

Paul J. Hissin Department of Chemistry, Mount Sinai Hospital, New York, New York

Norman J. Karin University of Tennessee-Oak Ridge Graduate School of Biomedical Science, Oak Ridge, Tennessee

Eddy Karnieli Metabolic Unit, Endocrine Institute, Rambam Medical Center, Haifa, Israel

Bruce M. Koeppen Departments of Medicine and Physiology, University of Connecticut Health Center, Farmington, Connecticut

G. Kracke Department of Biochemistry, SUNY Upstate Medical Center, Syracuse, New York

D. Louvard Department de Biologie Moleculaire, Institut Pasteur, Paris, France

Harry S. Margolius Department of Pharmacology, Medical University of South Carolina, Charleston, South Carolina

Anthony Martonosi Department of Biochemistry, SUNY Upstate Medical Center, Syracuse, New York

D. H. Miller Department of Pharmacology, Medical University of South Carolina, Charleston, South Carolina

John W. Mills Department of Anatomy, Dartmouth Medical School, Hanover, New Hampshire

Leslie L. Mix Department of Pharmacological and Physiological Sciences, University of Chicago, Chicago, Illinois

Eric W. Overström Department of Anatomy and Cellular Biology, Tufts University School of Medicine, Boston, Massachusetts

Nancy E. Owen Department of Pharmacological and Physiological Sciences, University of Chicago, Chicago, Illinois

C. Peracchia Department of Physiology, University of Rochester, Rochester, New York

Lewis R. Pollack Biology Division, Oak Ridge National Laboratory, Oak Ridge, Tennessee

David W. Pumplin Department of Anatomy, University of Maryland School of Medicine, Baltimore, Maryland

Marilyn D. Resh Department of Biochemistry and Molecular Biology, Harvard University, Cambridge, Massachusetts

Phillip M. Rosoff Department of Biochemistry and Molecular Biology, Harvard University, Cambridge, Massachusetts

Bernard Rossi National Cancer Institute, National Institutes of Health, Bethesda, Maryland

Scott J. Sherman Department of Pharmacology, University of Washington School of Medicine, Seattle, Washington

Ian A. Simpson Cellular Metabolism and Obesity Section, National Institutes of Health, Bethesda, Maryland

C. W. Slayman Departments of Human Genetics and Physiology, Yale University School of Medicine, New Haven, Connecticut

Ulf Smith Department of Medicine, University of Goteborg, Goteborg, Sweden

K. Soderberg Howard Hughes Medical Institute, University of Utah, Salt Lake City, Utah

J. A. Spayne Department of Pharmacology, University of Cambridge, Cambridge, United Kingdom

Emily H. Tate Biology Division, Oak Ridge National Laboratory, Oak Ridge, Tennessee

K. A. Taylor Department of Anatomy, Duke University Medical Center, Durham, North Carolina

Lucia M. Vicentini Department of Pharmacological and Physiological Sciences, University of Chicago, Chicago, Illinois

Mitchell L. Villereal Department of Pharmacological and Physiological Sciences, University of Chicago, Chicago, Illinois

Barry A. Wolitzky Department of Anatomy, University of Maryland School of Medicine, Baltimore, Maryland

PREFACE

The transport of ions and molecules across the eukaryote cell membrane has been the subject of intense investigation for the last several decades. Starting immediately after World War II, electrophysiologic and radioisotopic methodologies were combined to describe many ion transport processes in model epithelia and a few nonepithelial cells. The biochemical characterization of transport systems was ushered in during the late 1950s by the meticulous enzymology of Jens Skou and his collaborators in describing the (Na^+ + K^+)-activated ATPase. Confirmation of the Na^+, K^+–ATPase as the functional active transport system for Na^+ and K^+ substantiated the idea that membrane transport processes may be carried out by integral membrane proteins that are under the direct genetic control of the cell. A view of the cell membrane as a dynamic cell organelle began to emerge in the late 1960s; this resulted, in large part, from the biophysical studies of the cell surface of immunocytes. Not only could membrane proteins move laterally in the "sea of lipid," but also they could be inserted or removed as needed. Armed with this new concept of the dynamic and regulated cell membrane, cell biologists and physiologists conducted studies on the regulation of a variety of transport processes as a function of cell cycle, growth phase, malignant transformation, hormone treatment, substrate limitation, or other growth conditions. During the last decade, as these physiological studies have proceeded, molecular biologists have provided both the experimental tools for more elegant dissection of these regulatory processes and the model of membrane biogenesis from which to derive the principles of regulation. Thus today we are in the advantageous position of recognizing a variety of situations in which transport processes are regulated and of having the capability, in many cases, to study the mechanisms of the regulatory process.

The current model of membrane biogenesis provides the paradigm on which most of the studies on the regulation of membrane transport systems are based. The general scheme describes the translation of messenger RNA and insertion of the polypeptide into the membrane of the endoplasmic reticulum. After posttranslational modifications (e.g., glycosylation) in the golgi

apparatus, small vesicles that contain the transmembrane protein are liberated into the cytoplasm. The membrane protein can then be inserted into the cell membrane with the proper orientation by exocytotic fusion of the vesicle. Once emplaced in the cell membrane, the transport protein may undergo further alterations, such as oligimerization or covalent modification, to regulate its activity. In this *in situ* modification of the membrane transport systems, the cytoplasmic modulators, such as cyclic nucleotides, prostaglandins, calcium/calmodulin, and kinase/phosphatase, may play a role. Within this scheme describing the biogenesis of a membrane transport system, there are three levels that may be regulated: (1) gene expression leading to synthesis of the membrane protein, from transcription through posttranslational modification; (2) insertion and removal of membrane vesicles containing the transport system; (3) *in situ* modification of the transport system in the cell membrane. Each of these forms of regulation is addressed by several chapters in this book.

The symposium from which this book derives was organized to give a state-of-the-art assessment of the various types of regulation of transport systems. Participants from a variety of disciplines—physiology, biochemistry, genetics, and pharmacology—were invited to provide a diversity of approach and viewpoint that stimulates the cross-fertilization of ideas. The contributions dealt with regulatory processes evoked by two kinds of stimuli: (1) external stimuli, such as hormones or substrate limitation; (2) the internal stimulus of genetically programmed development. But the central theme of the meeting was to proceed from the physiological observations toward a more biochemical understanding of the mechanisms involved in regulation. Toward this goal, the question of which of the three forms of regulation described is(are) operative was the most commonly asked and answered. Therefore, many of the chapters in this volume describe the regulation of a transport system that falls within one or more of these general categories.

As is the nature of scientific inquiry, this collective contribution poses as many new questions as it answers old ones. Many of these new questions are both intriguing and addressable with current methodologies. For example, a fundamental question results from the studies on the stimulus-evoked fusion of cytoplasmic vesicles: Do these vesicles contain unique subsets of membrane proteins, and, if so, how is the appropriate subpopulation of vesicles recruited for fusion in response to the specific stimulus? Also, a question that underlies such studies with epithelial tissues concerns the mechanism(s) utilized by epithelial cells to generate the asymmetric distribution of membrane proteins. Thus we hope that the reader will find this volume to be not only a source of valuable information but also a stimulus in framing the important questions that will guide future studies.

The organization of the symposium and the preparation of this book required the assistance of many individuals, but I must acknowledge the three who played the most substantive roles. I am grateful to John Cook for his

collaboration during the early stages of selecting the topics and contributors. Isidore Edelman and Phillip Knauf were invaluable consultants throughout the organizational process. The Society gratefully acknowledges financial assistance from the National Science Foundation, the National Institutes of Health, and the Air Force Office of Scientific Research.

JAMES S. GRAVES

Charleston, South Carolina
August 1984

CONTENTS

REGULATION AND DEVELOPMENT OF MEMBRANE TRANSPORT PROCESSES

PART 1

REGULATION OF MEMBRANE TRANSPORT

PART 1

REGULATION OF MEMBRANE TRANSPORT

CHAPTER 1

REGULATION OF TURNOVER OF Na^+,K^+-ATPase IN CULTURED CELLS

JOHN S. COOK
NORMAN J. KARIN
JORDAN B. FISHMAN
EMILY H. TATE
LEWIS R. POLLACK
Biology Division, Oak Ridge National Laboratory and the University of Tennessee–Oak Ridge Graduate School of Biomedical Sciences Oak Ridge, Tennessee

THOMAS L. HAYDEN
Department of Mathematics University of Kentucky Lexington, Kentucky

A recurring theme of this book is the dynamic state of cell surface membranes. It was shown a number of years ago (30) that in certain cell types fluid-phase endocytosis occurred at a rate that internalized, in times on the order of one hour, an amount of surface membrane equivalent in area to the entire cell surface. Since this far exceeded the rate of membrane biogenesis, it followed that much of the surface must be recycled intact. Direct morphological as well as biochemical demonstrations of membrane externalization from the phagolysosomal compartment followed (e.g., refs. 23, 29). It is now apparent that the cell surface in many cell types is in continuous exchange with an internal membrane pool and that, as shown elsewhere in this symposium (see Chapter 3 by Simpson et al.; Chapter 13 by Resh and Guidotti; and Chapter 9 by Al-Awqati) certain physiological stimuli may induce the fusion of vesicles from this pool with the surface and thus rapidly elevate the cells' transport capacity by the insertion of reserve transporters into functional location.

1. MEMBRANE RECYCLING IN HeLa and HTC CELLS

In the unstimulated steady state, recycling may be observed in more than one kinetically identifiable compartment. When fluid-phase endocytosis is measured in HeLa cells by the uptake of tracer sucrose or insulin, the subsequent loss of label follows two-component kinetics (Fig. 1.1; see also

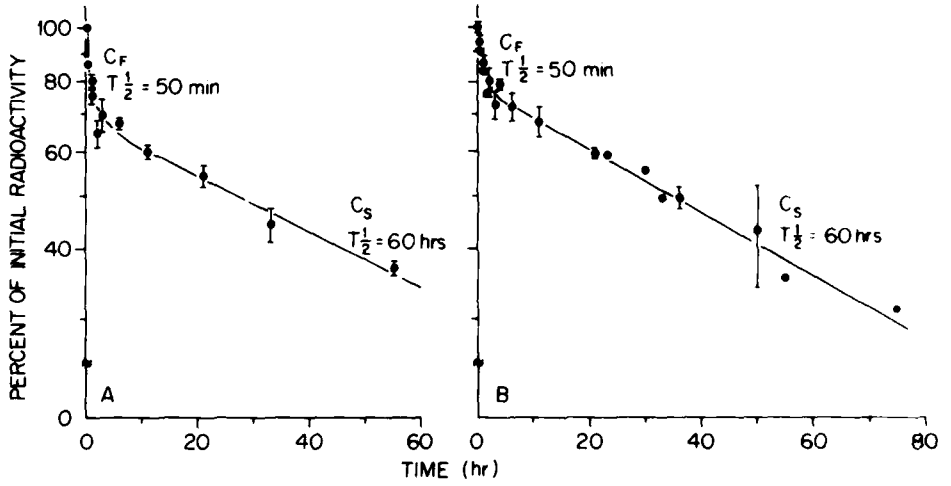

Figure 1.1. Release of [^{14}C]sucrose, a fluid-phase endocytosis marker, from HeLa cells labeled for different time periods. Error bars are ± one S.D. Cells in the left-hand panel were labeled for 2 h, those on the right-hand panel for 15 h. Control experiments showed that the fast component C_F was not due to surface binding. The half-times for both C_F and the slow component C_S were the same in all cases, but the relative compartment size for C_F became progressively smaller with time of uptake [32% after 2 h loading; 21% after 15 h; and (not shown) 10% after 48 h] From ref. 5.

ref. 2). The first component has a half-time of about 50 min, and is a progressively smaller fraction of the total intracellular label as the time allowed for uptake is increased. The second component has a half-time of 60–120 h. The kinetic properties of this component are identical with the exocytosis of internalized ouabain which, on being cleared from the cell surface, is taken up exclusively into the lysosomal compartment (8). Our preliminary interpretation of these results is that the marker is taken up in about equal amounts into two compartments. One compartment recycles to the cell surface with the 50-min half-time and releases its contents. This compartment is relatively small and becomes loaded to its steady-state level in a relatively short time period. The second compartment feeds into the lysosomes. This compartment continues loading for many hours (5). Hence the first compartment becomes a progressively smaller fraction of the total. Where the pathways for labeling these compartments diverge is not known. It may be at the cell surface in the formation of different classes of endosomes or at some later, but prelysosomal, step in endocytosis. The important factor for this discussion is the recycling. The nature of the surface membrane involved is not known.

A somewhat slower recycling can also be demonstrated by a biochemical label. In these experiments (12) we modified a labeling technique described by Van Lenten and Ashwell (31). Following periodate oxidation in intact cells, [^{3}H]borohydride reduction labels terminal sialic acids on surface glycoconjugates (Fig. 1.2). The nine-carbon sialic acid is thus converted to a seven-carbon derivative, AcNeu^7, which remains susceptible to cleavage

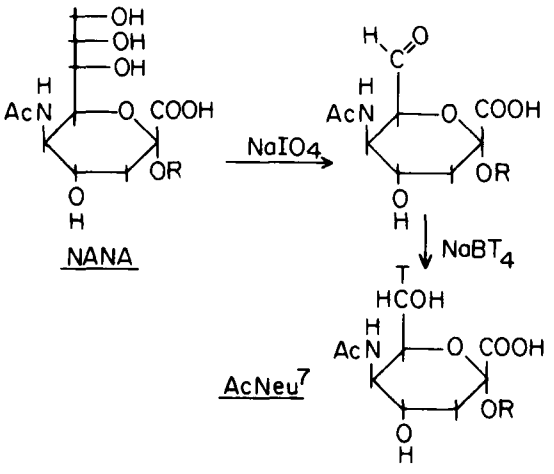

Figure 1.2. Labeling of terminal sialic acid by the Van Lenten and Ashwell (31) technique. The exocyclic triol is cleaved by $NaIO_4$, and subsequent reduction with $NaB[^3H]_4$ introduces a tritium label. The resulting [^{3}H]5-acetamido-3,5-dideoxy-L-arabino-heptulosonic acid, AcNeu^7, is the major reaction product. As a terminal sugar on sialoglycoconjugates it remains sensitive to neuraminidase, but as a monomeric sugar it is not reutilizable by the cells. Modified from ref. 31.

from the glycoconjugate by neuraminidase. Otherwise AcNeu[7] does not seem to be utilizable by the cells. We have grown cells in the presence of monomeric [^{3}H]AcNeu[7] for extended periods. The heptulosonic acid is taken up by the cells but is not metabolized, nor is it ever detectable in an acid-precipitable form, that is, it is not incorporated into glycoconjugates.

When cell-surface sialoglycoconjugates are labeled in this way, the label is subsequently lost from the cells with a complex time course (Fig. 1.3A). The pattern is very similar, although the absolute numbers are different, for both rat hepatoma cells (HTC) and the human line HeLa. The rapid phase includes some shedding from the surface as well as some fast turnover. The slow phase, with half-times of approximately 100 h, corresponds to the slow phase of membrane turnover observed in many laboratories (11, 16).

The label remaining on the cell surface is sensitive to removal by added extracellular neuraminidase. With time, the fraction of cell-associated radioactivity that can be removed this way falls from about 90% immediately after labeling to about 30% and then remains constant at this lower value (Fig.

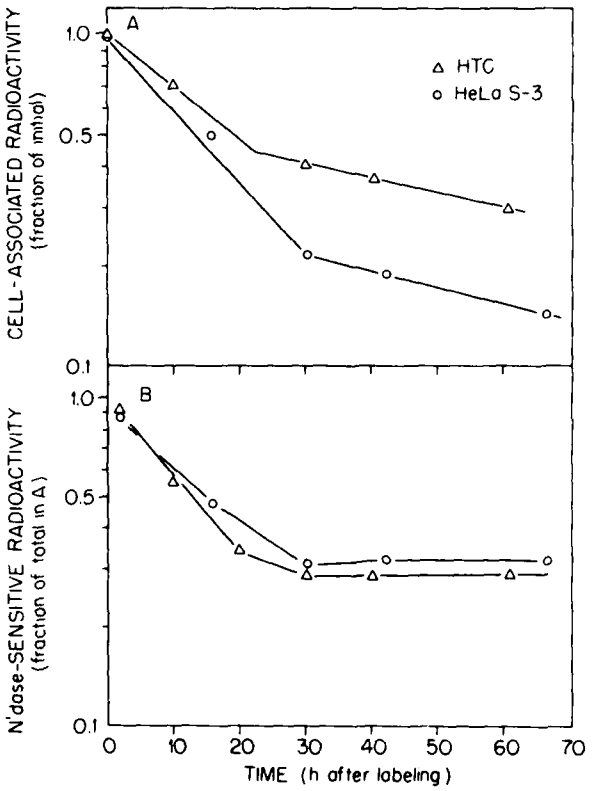

Figure 1.3. Cell-associated radioactivity in [^{3}H]AcNeu[7] and its sensitivity to removal by extracellular neuraminidase. HeLa or HTC cells were labeled at time =0 by the technique outlined in Figure 1.2 and returned to their growth medium. At intervals thereafter the cells were assayed for total radioactivity (panel A) and the fraction of that total radioactivity that could be removed by extracellular neuraminidase (panel B). From ref. 12.

1.3B). We reasoned that this decrease represented the internalization of the label, whereas the stabilization of the neuraminidase-sensitive fraction at 30% represented the recycling of internalized label back to the cell surface so that by 30 h after the initial labeling there was established a steady state of exchange between the surface and the internal pool.

To test this hypothesis we devised the experiment shown in Fig. 1.4, with the results shown in Fig. 1.5. Sialoglycoconjugates were labeled as before and their surface location demonstrated by the neuraminidase sensitivity of a small sample. The remaining cells were then allowed to internalize the label for 8 h, when the neuraminidase sensitivity had fallen to about 50% of the total. At this point the cell-surface label was removed with neuraminidase, and the cells were returned to the incubation medium. The hypothesis predicted that if the surface were in exchange with an internal pool, then the surface should become relabeled by the tritiated sialoglycoconjugates that had been internalized during the first 8 h. This is just what happens. Fifteen hours after the surface had been stripped of activity, the neuraminidase sensitivity of the total cell-associated label had returned to the 30% plateau. Since the AcNeu[7] is not reutilizable by the cells after it has been cleaved from the glycoconjugate, we concluded that the sialoglycoconjugates were recycling intact with a half-time of 5–8 h. The 30% plateau level in neuraminidase sensitivity indicated that the surface was in exchange with an internal pool twice the size of the surface itself. At some step in this recycling a small fraction, 2% per hour, of the label is siphoned off and degraded. This is the slow component of turnover.

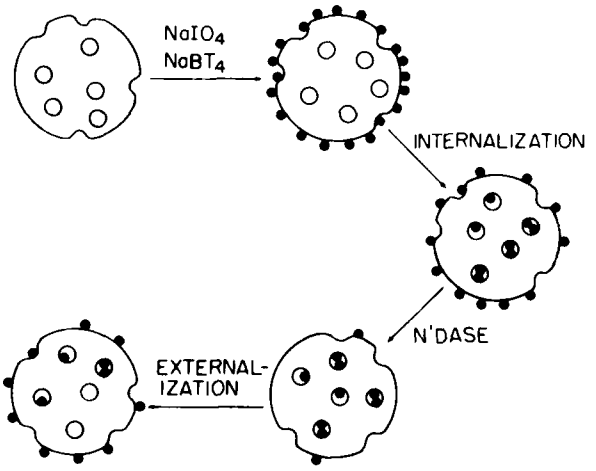

Figure 1.4. Design for the experiment demonstrating bidirectional flow of sialoglycoconjugates between the cell surface and the internal pool. Clockwise from the upper left: cells with internal vesicles and surface pits, representing forming endosomes, are labeled with $NaIO_4$/$NaB[^3H]_4$ (black dots); after incubation in growth medium a fraction of this label is internalized; virtually all of the surface label is then removed with neuraminidase, leaving the internal pool labeled, and the cells are reincubated in growth medium; the surface is relabeled from the internal pool.

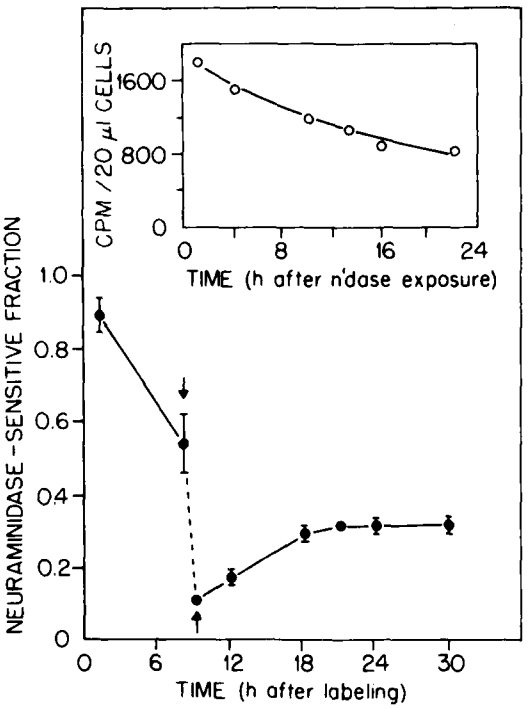

Figure 1.5. Results of the experiment diagrammed in Fig. 1.4 with HeLa cells. After the initial surface labeling with $NaIO_4/NaB[^3H]_4$, the cells were tested periodically for neuraminidase sensitivity of the cell-associated radioactivity. This fraction decreased from 90% at 0 h to about 55% at 8 h. At 8 h the surface activity was removed by neuraminidase (1 h at 0°C), and the cells were reincubated. Over the next 15 h the neuraminidase sensitivity returned to the 30% plateau level. The inset shows the decrease in total cell-associated activity, at about 2%/h, during the second incubation. From ref. 12.

Overall the results show that recycling is a real and complex phenomenon. As in many cells, receptor recycling is fast: Bleil and Bretscher (3) have shown that the transferrin receptor in HeLa cells is internalized with a half-time of 7 min and recycles in 20 min; this pathway may involve receptor-specific mechanisms. Regurgitation of endocytic markers like sucrose appears to be somewhat slower (1–2 h), and the fluid-phase markers not released in this time are captured in what appears to be the lysosomal compartment from which they are very slowly (100 h) released. It is not yet known how the steady-state recycling of sialoglycoconjugates relates to these other markers.

2. TRANSIT TIME AND TURNOVER OF Na^+,K^+-ATPase

An additional dynamic characteristic of cell membranes that has been recognized for some years is that their components are subject to turnover. At heterogeneous rates, the proteins are removed from the surface pool and

degraded. The alkali–cation transporter, identified as Na^+,K^+-ATPase or as binding sites for the specific glycoside inhibitor ouabain, is no exception.

The regulation of surface concentration of Na^+,K^+-ATPase per cell, $[E]$, may be expressed

$$\frac{d[E]}{dt} = k_i - k_{to}[E] \tag{1}$$

where k_i is a zero-order rate of insertion into the surface membrane of newly synthesized molecules in units of molecules per cell per unit time and k_{to} is the first-order rate constant for turnover in units of reciprocal time. The experiments described here for measuring turnover were done on logarithmically growing cells, and two factors related to $[E]$ must be taken into account. First, $[E]$ as measured in such populations is a mean value for cells distributed throughout the cell cycle. From [^{3}H]ouabain-binding measurements made on synchronized HeLa cells, $[E]$ appears to increase during the cell cycle in direct proportion to the growing cell-surface area (9). Second, since the cells are growing, the amount of E in the population is continually increasing, and this net increase due to growth must be allowed for with appropriate corrections. During log growth the mean value of $[E]$ per cell is constant, that is, $d[E]/dt = 0$, and equation 1 reduces to

$$[E] = \frac{k_i}{k_{to}} \tag{2}$$

and

$$k_i = k_{to}[E] \tag{2a}$$

These are steady-state relationships. For integral membrane proteins synthesis begins in the endoplasmic reticulum, and there is an extended period of transport and processing through the ER, Golgi, and post-Golgi vesicles before insertion into a functional location in the cell surface. This period is the transit time τ and is of the order of 1.5 h for insulin receptor in adipocytes (27) and for Na^+,K^+-ATPase in Sachs organ (7), 2.5 h for acetylcholine receptor in chick myoblasts (10), and 4 h for Na^+,K^+-ATPase in HeLa cells (25). During transitions from one enzyme level to another, if $[E]$ is functional surface enzyme, then

$$k_i(t) = k_{syn}(t - \tau) \tag{3}$$

where $k_i(t)$ is the insertion rate at time t and $k_{syn}(t - \tau)$ is the rate of onset of synthesis one transit time earlier. In the steady state, of course $k_i = k_{syn}$.

We have adopted two methods for the measurements of k_{to}. In the first to be described, although it was the second to be carried out, we used an antibody against the catalytic subunit of Na^+,K^+-ATPase to precipitate the enzyme from homogenates of rat hepatoma cells (HTC) that had been pulse labeled with [^{35}S]methionine. More details on the methods are given in the legend to Fig. 1.6. In pilot experiments we observed that 2 min after the onset of the pulse, labeled subunit was found in a membranous component of

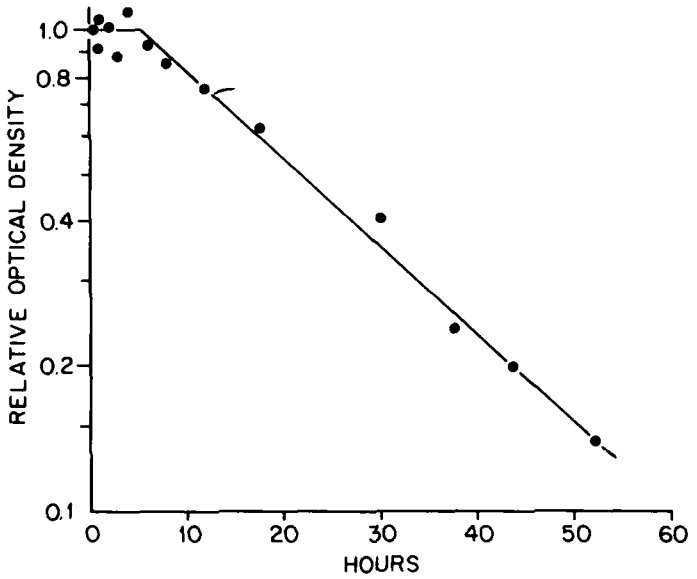

Figure 1.6. Turnover of the Na,K-ATPase in rat hepatoma cells (HTC). Cells were pulse labeled with [^{35}S]methionine for 10 min and chased with 10 mM nonradioactive methionine. At intervals thereafter an aliquot was taken, and the cells were washed and solubilized in 1% Triton X-100 and centrifuged to remove insoluble cytoskeletal elements. Saturating amounts of rabbit anti-α subunit (Na^+,K^+-ATPase) were incubated with the solubilized cells for 16 h at 4°C, and the antibody harvested on Protein-A-agarose. Na^+, K^+-ATPase was recovered by dissociation from the antibody in SDS-PAGE buffer and displayed on SDS-PAGE. The gel was fixed and dried and fluorographed on preflashed film. The density of the band at 94 K was determined with a Joyce–Loebl densitometer.

the cells, presumably the endoplasmic reticulum (not shown). In HTC cells, no labeled antigen was ever found free in the cytosol, suggesting that synthesis occurs on membrane-bound ribosomes. The specific activity of the labeled subunit increased linearly for the next 30 min (not shown). For the turnover experiment, the cells were labeled for 10 min and subsequently chased with a large excess of nonradioactive methionine. As can be seen in Fig. 1.6, following the pulse the activity in the labeled subunit remained essentially constant for about 5 h. At this time it entered a pool from which it was removed with a half-time of about 0.48 T_G, where T_G is the generation time. We take the 5-h plateau to be the transit time between the onset of synthesis and the arrival of the subunit in a turning-over pool. The latter includes the surface membrane and may include as well a population of submembrane vesicles in exchange with the surface. The first-order decay portion of the curve has a slope of $-k_{to}$. From these data we calculate that HTC cells synthesize in each generation 2.5 times the amount of enzyme needed for growth, and the excess 1.5 sets of subunits are turned over and degraded (18).

In the human HeLa cells, where we made the second set of measure-

ments, turnover is even faster. For these experiments we used a density method pioneered by Fambrough and his associates (10, 14), and the measurements were made on isolated cell membranes (25). Briefly, two populations of cells were grown in parallel, one in medium containing ^{13}C-amino acids and the other in control medium containing normal ^{12}C-amino acids. The experiment was begun by resuspending the ^{13}C-labeled cells in control medium. The measurements to be made were to follow the density shift of the ^{13}C-labeled catalytic subunit of Na^+,K^+-ATPase as it was removed from the membrane and replaced with ^{12}C-subunit. To do this we isolated membranes from both experimental and control cells and radiophosphorylated them separately, under conditions such that only the Na^+-dependent, K^+-sensitive phosphorylation of the Na^+,K^+-ATPase catalytic subunit (25, 26) was detectable as a radioactive peak on SDS-acrylamide gels or in acid-SDS-metrizamide-D_2O gradients. The experimental and control samples were distinguished by phosphorylating one with [γ-^{32}P]-ATP and the other with [γ-^{33}P]-ATP. The membranes were then mixed, solubilized in SDS, and cosedimented in acid-SDS—metrizamide-D_2O gradients. Control experiments showed that the two radioactive labels, in the absence of ^{13}C-density label, cosedimented within 0.1–0.2% of each other.

The results from two turnover experiments are shown in Fig. 1.7. After equilibration of the cells for several days in ^{13}C-medium, the density-labeled

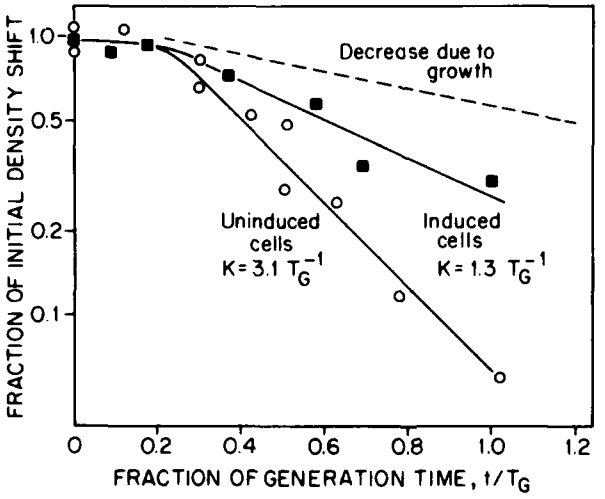

Figure 1.7. Changes in the density shift of ^{13}C-labeled catalytic subunit in HeLa cell membranes following return of the cells to control (^{12}C) medium. The density shift was assayed as described in the text. Note that the density shift remains at its initial level for 4 h (transit time) and then declines in a first-order manner. The slope of the decline is $-(k_{to} + \ln 2/T_G)$, where T_G is the generation time. The second term is an allowance for the dilution of the ^{13}C-subunit by net growth-related synthesis of ^{12}C-subunit; this component is represented by the dotted line. Open circles: control cells in normal [K^+] medium; with 1×10^6 ouabain-binding sites per cell; closed squares: K^+-stressed cells in low-K^+ (0.5 m*M*) medium with about 2.2×10^6 ouabain-binding sites per cell. Note that the transit time is the same under both conditions. From ref. 25.

subunit moves ahead of the control in the gradient by about 8%. This is the initial density shift. On return of the density-labeled cells to control medium, the same density shift at the membrane level persists for about 4 h. After this transit time, ^{12}C-subunit appears in the membrane and dilutes out the ^{13}C-enzyme. After 24 h (about one generation) the density shift is undetectable. Since the total Na^+,K^+-ATPase is constant per cell, the diminution in the shift must be due either to dilution by growth or turnover or both. The dotted line shows the decrease that can be accounted for by growth; the remainder is turnover. From this and other experiments we deduce that: HeLa cells have a mean per cell of 10^6 Na^+,K^+-ATPase molecules, measured as ouabain-binding sites; the half-time for turnover of the catalytic subunit in these cells is 5–6 h, again a mean value; the rate of synthesis (equations 2a and 3) of the subunit is about 2800 molecules per minute, of which 700 meet the growth requirement and 2100 are turned over (25).

These turnover rates should be viewed in the context of the turnover of all surface membrane proteins. It is the general finding of a number of laboratories working with cultured cells that membrane turnover kinetics are multi- (at least two) component, and that the majority of the membrane proteins turn over with half-lives of 70–200 h. The minority turn over much more rapidly with half-lives of 5–25 h. Na^+,K^+-ATPase is clearly in the minority group.

Turnover serves more than one function. In part it serves to keep the enzyme activity on the cell surface in repair, and it may turn out that the rapidly turning over proteins are the more essential to cell survival. Certainly the proper functioning of Na^+,K^+-ATPase is an essential activity. But turnover also operates in the regulation of total activity as indicated in equation 1. Na^+,K^+-ATPase is not always at a fixed concentration but can be up- and down-regulated in response to environmental factors that modulate the transporter's activity.

3. UP- AND DOWN-REGULATION OF Na^+,K^+-ATPase

Up- and down-regulation of hormone receptors are now well recognized phenomena: in general, target cells respond to reduced peptide hormone levels with an increase in the number of cell-surface receptors and vice versa. Similarly, there are now known many examples of up- and down-regulation of transport systems in which cells respond to deprivation of a transported substrate by increasing their transport capacity for that substrate (4, 6, 13, 15, 17, 21, 22, 24, 28). The available evidence suggests that this modulation is due to change in the number of transporters per cell. Such an adaptation has been observed for alkali–cation transport in cells grown in low-K^+ medium (K^+-stress; 4, 9, 15, 21, 24, 25) or in normal medium containing the transport inhibitor ouabain.

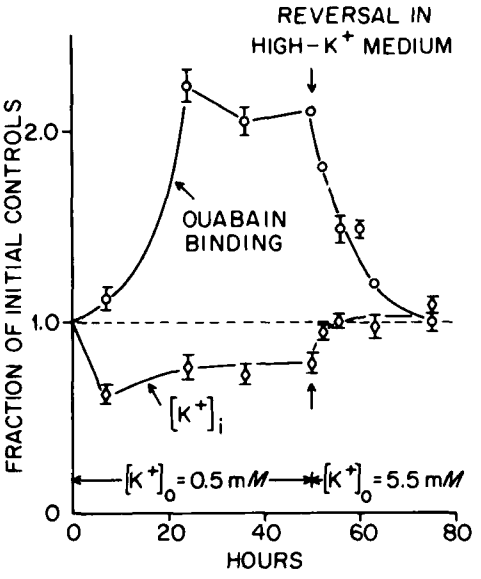

Figure 1.8. Changes with respect to controls in number of ouabain-binding sites per cell and cell $[K^+]$ in media of different K^+ concentrations. Control values at zero time are 10^6 sites per cell and 170 m*M* respectively. At zero time cells are incubated in low-K^+ (0.5 m*M* medium); at 50 h the medium $[K^+]$ is restored to control (5.5 m*M*) levels. From ref. 24.

An example of this response is shown in Fig. 1.8. HeLa cells were grown in a medium with $[K^+]$ slightly below the $K_{1/2}$ for K^+ transport, and the number of ouabain-binding sites per cell $[E]$ was measured periodically. After about 25–30 h this number had a little more than doubled and subsequently remained at the higher level. When the $[K^+]$ of the medium was restored to the normal level, $[E]$ promptly returned to the control level with a half-time for the transition of about 5–6 h. While the cells were in the up-regulated state we repeated the turnover measurements by the density-shift method (Fig. 1.7). The k_{to} had fallen to somewhat less than half the control value. From equation 2, this change in k_{to} accounts entirely for the elevated $[E]$. The up-regulation has been accomplished by modulation of the turnover rate constant with no change in the rate of synthesis. With the lower k_{to}, it is not until the number of transporters reaches twice the control value that the rate of turnover again reaches the rate of synthesis and a new steady state is established. Note that in this new steady state the transit time remains unchanged.

That turnover is responsible for these changes can again be argued from the kinetics of down-regulation (Fig. 1.8). In the K^+-stressed cells when $[E]$ is elevated, restoration of normal $[K^+]$ to the medium results in the very rapid recovery of cell electrolytes. In a few minutes cell $[K^+]$ returns to and slightly exceeds control levels. If synthesis were the mechanism regulating $[E]$, one would expect that within the cells there would be 4 h worth of Na^+,K^+-ATPase-rich membrane in transit to the surface. Even if k_{syn} changed immediately with the relief of the stress, down-regulation would not be observed at the surface until after this transit is complete. But the obser-

vation is that as soon as the stress is relieved down-regulation begins. This is the result expected if an immediate change in turnover at the membrane level were the controlling factor.

In a theoretical discussion, Berlin and Schimke (1) showed that the rate of transition in enzyme concentration from one steady state to another is dictated by the turnover rate of the enzyme in the final steady state toward which the transition is progressing. From this the generalization can be made that in regulation by turnover up-regulation will necessarily be slower than down-regulation. Fig. 1.8 is an example of this principle.

4. SIGNIFICANCE OF REGULATION BY TURNOVER

The classical concept of enzyme induction, delineated in detailed studies on *E. coli* and reinforced in studies on mammalian systems responding to various hormonal stimuli, has been that an elevated enzyme content is the consequence of an increased rate of synthesis. It has been clear in principle, as expressed in equation 2, that change in turnover can be equally effective in maintaining a new steady state, although the rate of achieving that steady state will be influenced by the mechanism the cells adopt for the transition. A number of membrane enzymes and receptors, like Na^+,K^+-ATPase, are now known to be regulated by turnover in response to a change in the concentration of their specific substrate/ligand in the environment (e.g., insulin receptor, 19; EGF receptor, 20). We asked ourselves whether there might be any particular advantage to this mode of regulation. To gain an insight into this question, we decided to model the transition from one steady state to the other in numbers of ouabain-binding sites in HeLa cells in response to step changes in concentration of extracellular K^+. As outlined here the model is simplistic; this approximation is intentional to keep the model as general as possible. The principal conclusions are not altered by a more realistic, and more complex, model (to be published).

The first version is a model of regulation by turnover. This version corresponds to our experimental observations, and real data are available to fit the required functions.

Two equations in the model have been given previously:

$$\frac{d[E]}{dt} = k_i - k_{to}[E] \tag{1}$$

and

$$k_i(t) = k_{syn}(t - \tau) \tag{3}$$

An important corollary for the model is that if under all conditions k_{syn} is invariant with time, then k_i and k_{syn} are equal. The invariance of k_{syn} is also a property of the turnover model, and, as described, the value of k_{syn} may be calculated from the known values of $[E]$ and k_{to} (equations 2 and 3). The

turnover model states that k_{to} is a function of some cellular signal Q, and the value of Q is itself regulated by the activity of the transport system:

$$k_{to} = f[Q] \tag{4}$$

$$\frac{d[Q]}{dt} = \beta(\text{transport rate}) - L[Q] \tag{5}$$

In these formulations β is the proportionality constant between the generation of Q and transport. The model is indifferent to how transport rate is modulated. Up-regulation in Na^+,K^+-ATPase is observed after either low-K^+ stress or in cells grown in sublethal concentrations of ouabain (4, 21, 24). L is a "metabolic coefficient" or rate constant for the dissipation of Q. Q is unknown. It could be cell $[K^+]$ or $[Na^+]$, or ATP flow, or ATP/ADP as influenced by the transporter, and so on. If, for example, $[Q]$ is cell $[K^+]$, L might be the leak constant for $[K^+]$ against which the pump works. Although β and L have the same sign, it can be either positive or negative.

From equation 5 it follows that in any steady state of up- or down-regulation

$$k_{to} = f\left\{\frac{\beta}{L}(\text{transport rate})\right\} \tag{6}$$

From known steady-state values of k_{to} and transport rates under various conditions, the relationships in equation 6 can be established and β/L evaluated. The function is highly nonlinear. Finally, L and thus β can be estimated by fitting the data for the transition of $[E]$ from one steady state to another at various assumed values for L. Fig. 1.9 shows one such plot for the data in Fig. 1.8. The values of $[E]$ were measured from ouabain binding in K^+-stressed cells, and the line through these points is a plot of the integral of equation 2 with k_i held constant and the initial and final values of k_{to} evaluated as described in Fig. 1.7. Note that the computed k_{to} during the transition falls from the outset of the stress, undershoots its final value, and after a slow and highly damped oscillation approaches its final new state. The initial rate at which k_{to} decreases is very sensitive to assumed values of L, which in this case was 0.1 h^{-1}. If Q were turning over rapidly, both β and L would be large, k_{to} would initially fall more precipitously, and $[E]$ would rise more rapidly than depicted. The slow onset of the increase in $[E]$ has been experimentally observed by several authors (Fig. 1.8, and refs. 15, 21, 22, 24). The oscillation observed in $[E]$ in Fig. 1.9 is again of small amplitude and heavily damped around the final value. Although slow, up-regulation is accomplished.

In this fit of the data, all of the parameters of the model, including transport parameters not detailed here, are evaluated with the exception of the transit time τ (since $k_{syn} = k_i$ throughout). Since τ for Na^+,K^+-ATPase in HeLa cells is known from other data (Fig. 1.7), we are in a position to ask a

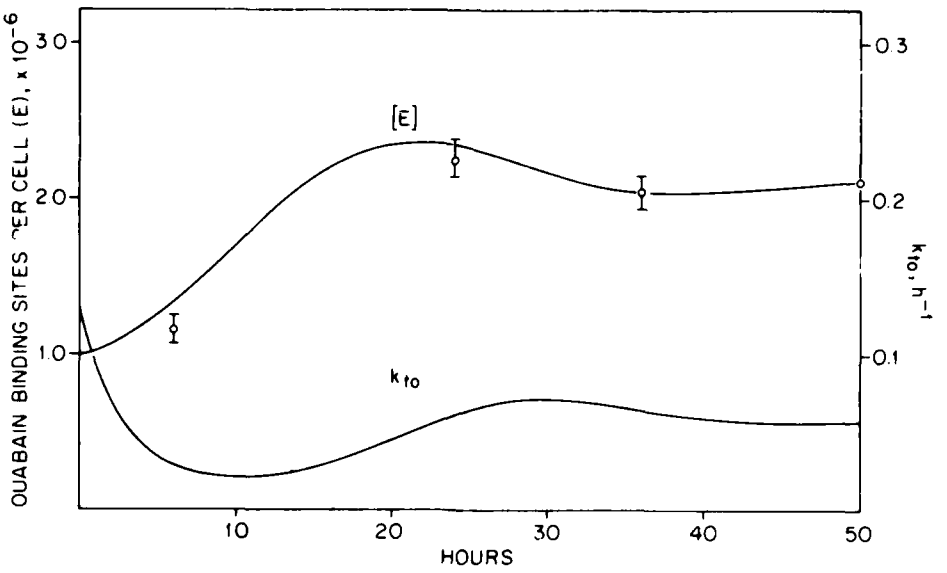

Figure 1.9. Turnover model. The computer model is for the transition in the up-regulation of Na^+,K^+-ATPase $[E]$ by change in the turnover rate constant, k_{to}. The model is fit, using equations described in the text, to data shown in Figs. 1.7 and 1.8. It describes an experiment in which, at time = 0, cells are removed from control growth medium ($[K^+]$ = 5.5 m*M*) and resuspended in growth medium with 0.5 m*M* $[K^+]$. The $K_{1/2}$ for K^+ transport is 0.8 m*M*. Left-hand ordinate: $[E]$ expressed as ouabain-binding sites per cell. Right-hand ordinate: computed k_{to}. The data points are measured ouabain-binding sites per cell, taken from Fig. 1.8. The initial measured values were $[E] = 1 \times 10^6$ and $k_{to} = 0.126\ h^{-1}$; the final values were $[E] = 2.1 \times 10^6$ and $k_{to} = 0.059\ h^{-1}$.

"straw-man" question: what would be the consequences, if any, of regulating by synthesis rather than by turnover? In this case equation 3 becomes important, k_{to} is held invariant at the known control rate, and the required k_{syn} is calculated from steady-state data (equation 2) and a variant of equation 6:

$$k_{syn} = f\frac{1}{Q} \tag{6a}$$

As before, this function can be calculated from the assumptions and the integral to equation 2 computed. Excepting the new assumption that k_{syn} regulates and k_{to} is invariant, all the remaining parameters are the same as before. Fig. 1.10 shows the computed response to the same low-K^+ stress shown in Fig. 1.9. The k_{syn} rises promptly after initiation of the stress, but, because of the 4-h transit time, there is no rise in $[E]$ at the cell surface during this period. At about 2 h, k_{syn} has doubled, and this, for a twofold up-regulated steady state, is all the response that is needed. But because $[E]$ has not yet changed, Q continues to fall, k_{syn} continues to rise and substantially

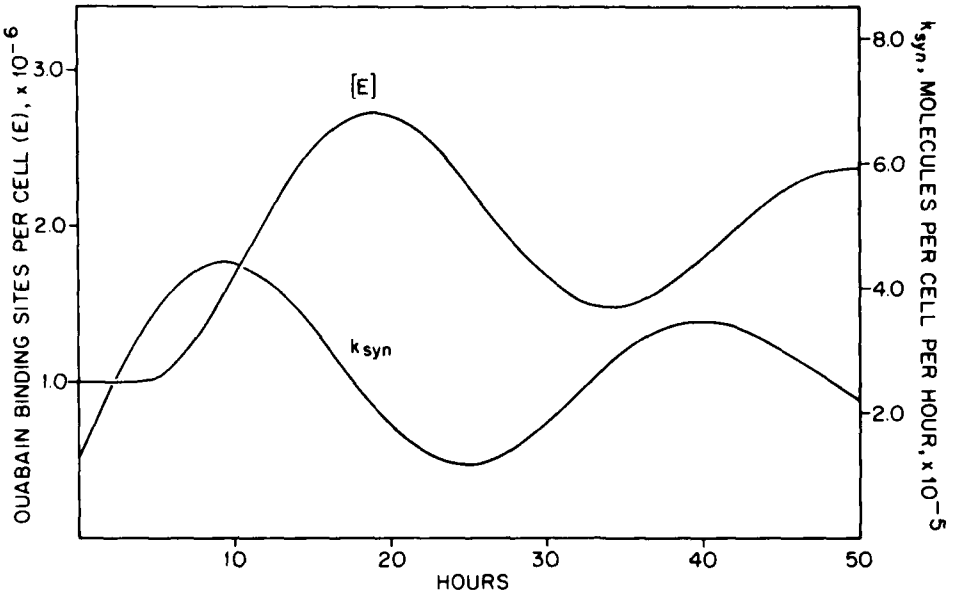

Figure 1.10. Synthesis model. This computer model for the transition in up-regulation model is based on the hypothetical supposition that regulation is mediated by change in the synthesis rate k_{syn} with no change in turnover rate constant k_{to} but with all other parameters the same as in Figure 1.9. The transit time is taken as 4 h (Figure 1.7). Left-hand ordinate: $[E]$ expressed as ouabain-binding sites per cell. Right-hand ordinate: computed k_{syn}. The initial measured values were $[E] = 1 \times 10^6$ and $k_{syn} = 1.25 \times 10^5$ molecules per cell per hour.

overshoots the required rate. After the transit time, $[E]$ begins to rise as well, the fall in Q slows, and the increase in k_{syn} therefore also slows, but the earlier overshoot in k_{syn} results in a later overshoot in $[E]$, a large increase in Q, and a consequent overrepression in k_{syn}. In brief, the interposition of the transit time between the stimulus and the functional response leads to large oscillations and poor, if any, up-regulation. In the example shown the oscillations tend to damp out at about 200 h. Assuming different values for the metabolic constant L does not improve the calculated response: lower values broaden the period of the oscillations, and higher values give more rapid oscillations that show no sign of damping, that is, no regulation, even after 200 h. Up-regulation is not accomplished.

This regulation-by-synthesis model of course does not describe what happens in the cells. What it does describe is a potential threat to a cell system that is feedback regulated but delayed in responding. It is by no means a new idea. When we showed these calculations to a colleague, he was skeptical because, as he said, of his deep faith that "cells were smarter than that." We agree. Faced with the threat of undamped oscillations in regulation by synthesis, the cells have adopted the smarter and faster-responding alternative of regulation by turnover.

ACKNOWLEDGMENTS

Research for this project was supported by the Office of Health and Environmental Research, U.S. Department of Energy, under contract W-7405-eng-26 with the Union Carbide Corporation. J. B. Fishman and N. J. Karin were supported by grant CA 09104 from the National Institutes of Health (NIH). L. R. Pollack was supported by grants T01-CA-05296 and T32-CA-09336 also from the National Institutes of Health.

REFERENCES

1. Berlin, C. M. and Schimke, R. T. (1965) *Mol. Pharmacol.*, **1,** 149–156.
2. Besterman, J. M., Airhart, J. A., Woodworth, R. C., and Low, R. B. (1981) *J. Cell Biol.*, **91,** 716–727.
3. Bleil, J. D., and Bretscher M. S. (1982) *EMBO J.*, **1,** 351–355.
4. Boardman, L., Huett, M., Lamb, J. F., Newton, J. P., and Polson, J. M. (1974) *J. Physiol.* (London), **241,** 771–794.
5. Brake, E. T. (1977) *Pinocytosis in HeLa Suspension Cells*, M. A. Thesis, University of Tennessee, Knoxville.
6. Christopher, C. W. (1977) *J. Supramol. Struct.*, **6,** 485–494.
7. Churchill, L. and Hokin, L. E. (1979) *J. Biol. Chem.*, **254,** 7388–7392.
8. Cook, J. S., Tate, E. H., and Shaffer, C. (1982) *J. Cell. Physiol.* **110,** 84–92.
9. Cook, J. S., Will, P. C., Proctor, W. R., and Brake, E. T. (1976) in Cook, J. S., Ed., *Biogenesis and Turnover of Membrane Macromolecules*, Raven Press, New York, pp. 15–36.
10. Devreotes, P. N. and Fambrough, D. M. (1975) *J. Cell Biol.*, **65,** 335–358.
11. Doyle, D. and Baumann, H. (1979) *Life Sci.*, **24,** 951–966.
12. Fishman, J. B. and Cook, J. S. (1982) *J. Biol. Chem.*, **257,** 8122–8129.
13. Frengley, P. A., Peck, W. A., and Lichtman, M. A. (1974) *Exp. Cell Res.*, **88,** 442–444.
14. Gardner, J. M. and Fambrough, D. (1979) *Cell*, **16,** 661–674.
15. Graves, J. S. and Wheeler, D. D. (1982) *Am. J. Physiol.*, **243** (Cell Physiol. 12), C124–C132.
16. Huang, C. C., Tsai, C. M., and Canellakis, E. S. (1973) *Biochim. Biophys. Acta*, **332,** 59–68.
17. Hume, S. and Lamb, J. F. (1974) *J. Physiol. (London)*, **239,** 46P–47P.
18. Karin, N. J. (1983) *Biosynthesis and Turnover of Na^+, K^+-ATPase in Cultured Rat Hepatoma Cells*, Ph.D. Thesis, University of Tennessee, Knoxville.
19. Knutson, V. P., Ronnett, G. V., and Lane, M. D. (1982) *Proc Natl. Acad. Sci. USA*, **79,** 2822–2826.
20. Krupp, M. N., Connolly, D. T., and Lane, M. D. (1982) *J. Biol. Chem.*, **257,** 11489–11496.
21. Lamb, J. F. and McCall, D. (1972) *J. Physiol.* (London), **225,** 599–617.
22. Martineau, R., Kohlbacher, M., Shaw, S. N., and Amos, H. (1972) *Proc. Natl. Acad. Sci. USA*, **69,** 3407–3411.
23. Muller, W. A., Steinman, R. M., and Cohn, Z. A. (1980) *J. Cell Biol.*, **86,** 304–314.
24. Pollack, L. R., Tate, E. H., and Cook, J. S. (1981) *J. Cell. Physiol.*, **106,** 85–97.

25. Pollack, L. R., Tate, E. H., and Cook, J. S. (1981) *Am. J. Physiol.*, **241** (*Cell Physiol.*, **10**), C173–C183.
26. Post, R. L., Sen, A. K., and Rosenthal, A. S. (1965) *J. Biol. Chem.*, **240**, 1437–1445.
27. Reed, B. C. and Lane, M. D. (1980) *Proc. Natl. Acad. Sci. USA*, **77**, 285–289.
28. Salter, D. W. and Cook, J. S. (1976) *J. Cell Physiol.*, **89**, 143–155.
29. Schneider, Y.-J., Tulkens, P., de Duve, C., and Trouet, A. (1981) *J. Cell Biol.* **82**, 466–474.
30. Steinman, R. M., Brodie, S. E., and Cohn, Z. A. (1976) *J. Cell Biol.*, **68**, 665–687.
31. Van Lenten, L. and Ashwell, G. (1971) *J. Biol. Chem.*, **246**, 1889–1894.

CHAPTER 2

REGULATION OF Na^+/H^+ EXCHANGE IN CULTURED HUMAN FIBROBLASTS

MITCHEL L. VILLEREAL
NANCY E. OWEN
LUCIA M. VICENTINI
LESLIE L. MIX
Department of Pharmacological and Physiological Sciences
University of Chicago
Chicago, Illinois

Cultured fibroblasts can be arrested in the G_0/G_1 phase of the cell cycle by deleting certain required growth factors from their culture medium. If these quiescent fibroblasts are treated with mitogens, they initiate a sequence of biochemical events that appear to begin at the level of the plasma membrane and ultimately lead to cell division. In 1978 it was demonstrated by Smith and Rozengurt (32) that a stimulation of Na^+ influx was one of the important early, membrane-associated events to occur in mitogen-treated fibroblasts. The serum-stimulated Na^+ influx is by way of an amiloride-sensitive Na^+ pathway (33, 38) that has been proposed to mediate Na^+/H^+ exchange (9, 15, 23, 25). Since it has been suggested that the rise in intracellular Na^+ or the alkalinization of the cytoplasm produced by stimulating Na^+/H^+ exchange may serve as a trigger for subsequent biochemical steps (2, 5, 11, 20, 27), it is important to determine the mechanism by which binding of mitogens to surface receptors can regulate the Na^+/H^+ exchange system. Thus, for the last several years, our laboratory has been studying the regulation of Na^+/H^+ exchange in cultured human foreskin fibroblasts (HSWP cells).

In this chapter we outline the information that we have accumulated concerning the mechanism by which binding of mitogens to receptors on HSWP cells leads to the activation of an amiloride-sensitive Na^+ transport system. We review evidence that indicates that the second messenger for the mitogen stimulus is Ca^{2+} and that the Ca^{2+} effect is mediated by calmodulin. Evidence is also presented that suggests that a stimulation of phospholipase (PLase) activity is an important step in regulating Na^+ influx in HSWP cells.

1. SERUM STIMULATION OF Na^+ INFLUX IN HSWP CELLS

When HSWP cells are removed from their normal growth medium of Eagle's minimum essential medium (EMEM) + 10% fetal bovine serum (FBS) and incubated in Hepes-buffered amino acid–free EMEM + 0.1% FBS for 4 h, their level of net Na^+ influx, following addition of a Na^+/K^+ pump inhibitor, is reduced to that seen in cells arrested in G_0/G_1 by serum deprivation. Addition of serum to the assay medium results in a dramatic stimulation of Na^+ flux over the basal, serum-deprived level (Fig. 2.1). The stimulation is very rapid, as it is evident within 30 sec, which is the shortest interval that we can accurately measure an increase in Na^+ flux. The net Na^+ influx in the absence of serum occurs through a pathway that is resistant to amiloride, a known inhibitor of Na^+/H^+ exchange in many tissues (Fig. 2.2). This is in contrast to the Na^+ influx stimulated by serum that is inhibited by amiloride, suggesting that serum activates a Na^+/H^+ exchange pathway in HSWP cells that is virtually inactive under basal conditions.

Although the doses of amiloride necessary to inhibit serum-stimulated Na^+ influx in HSWP cells are high (K_i = 0.9 mM), they are in line with doses required to inhibit Na^+/H^+ exchange in many other tissues (10, 15, 24). In addition, our recent observation that several amiloride analogs can inhibit

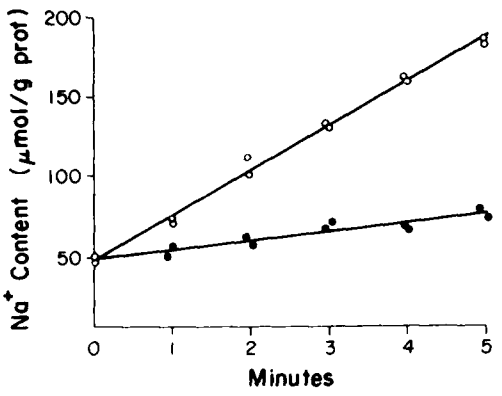

Figure 2.1. Serum stimulation of net Na^+ influx in HSWP cells. Cells were serum deprived for 4 h in amino acid–free, Tris-buffered Eagle's medium + 0.1% fetal bovine serum. Net uptake of Na^+ was initiated by the addition of medium containing 20 μM digitoxin (●) or medium containing 20 μM digitoxin + 10% fetal bovine serum (○). Cells were washed in ice cold, isotonic $MgCl_2$, extracted in 5% TCA, and the Na^+ content determined by atomic absorption.

serum-activated Na^+ flux in HSWP cells with K_i's in the 10–20 μM range (18) supports the contention that these are specific effects on the Na^+/H^+ exchange system. Data in Figure 2.3 show dose responses for inhibition of Na^+ influx by amiloride and an amiloride analog, benzamil. The higher affinity compound, benzamil, clearly shows that only the serum-activated, and not the basal, flux is sensitive to this class of inhibitors. Thus the inhibition

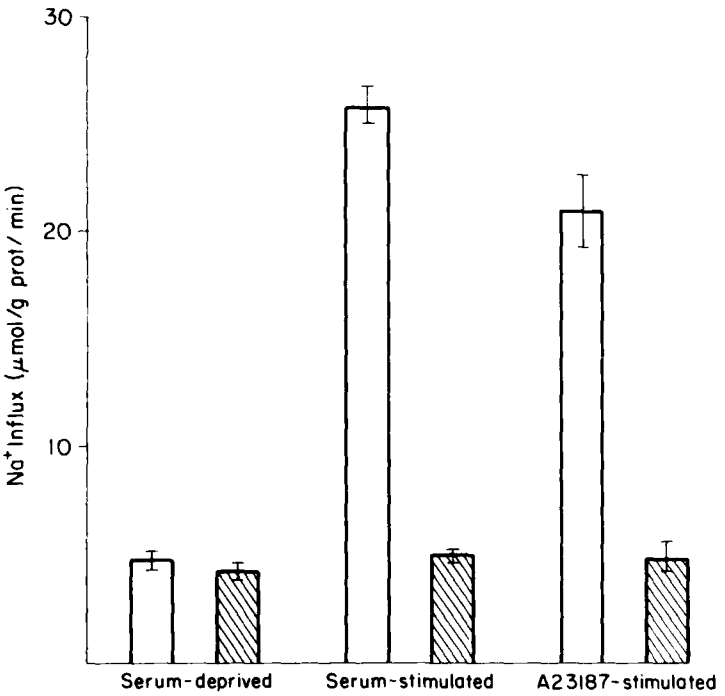

Figure 2.2. Effect of amiloride on basal and stimulated Na^+ influx. Cells were serum deprived as described in the legend to Fig. 2.1. Net Na^+ uptake was measured over a 5-min period in serum-free medium, in medium containing 10% FBS or in medium containing A23187 (5 μg/ml). Digitoxin (20 μM) was present during all flux measurements. The crosshatched bars represent flux levels in the presence of saturating concentrations of amiloride. Flux values are the means ± S.E.M. of five determinations.

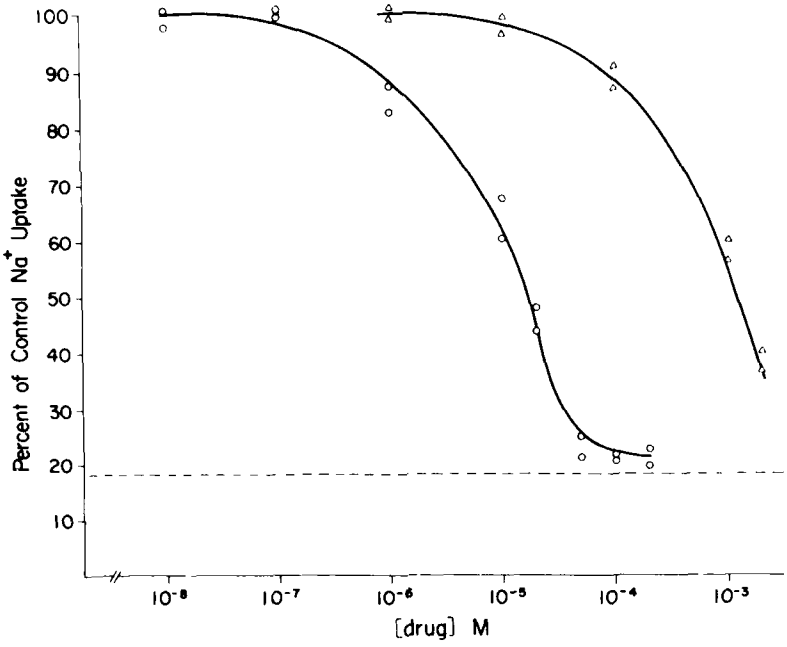

Figure 2.3. Dose-response curves for inhibition of Na^+ flux by amiloride and benzamil. Cells were serum deprived as described in the legend to Fig. 2.1. The initial rate of Na^+ uptake was measured in medium containing 10% FBS and various concentrations of amiloride (△) or benzamil (○). The dotted line represents the basal flux level measured in serum-free medium. Digitoxin (20 μM) was present during all flux measurements.

data indicate that there are two distinct Na^+ transport systems in HSWP cells: (1) a serum-independent, amiloride-insensitive pathway and (2) a serum-dependent, amiloride-sensitive pathway. The existence of two distinct Na^+ transport systems is also supported by kinetic experiments which indicate that the Na^+ concentration dependence of basal Na^+ flux can be explained in terms of a single saturating transport system, whereas the Na^+ flux in serum-stimulated cells is clearly mediated by at least two pathways (39). Although in HSWP cells and human lung fibroblasts (WI-38) the amiloride-sensitive Na^+ transport system appears to be inactive under basal conditions, this is not true in all the cells we have studied. In both Chinese hamster ovary cells (CHO) and neuroblastoma × glioma hybrids (NG108-15) there is a considerable portion of the basal Na^+ flux that can be inhibited by amiloride. It will be of interest to determine whether these are differences in species or type of cell or differences between normal and transformed cells.

2. EVIDENCE FOR SERUM STIMULATION OF Na^+/H^+ EXCHANGE

Although the amiloride inhibition data merely suggest that serum stimulates Na^+ influx by way of a Na^+/H^+ exchange system, more substantial evidence

is provided by several recent studies which have demonstrated a change in intracellular pH upon mitogen stimulation of cultured fibroblasts (14, 15, 29). In our recent studies, we have utilized the pH-sensitive fluorescent probe, 6-carboxy, 4,5-dimethylfluorescein, to monitor continuously intracellular pH of HSWP cells. The esterified form of this compound (6-carboxy, 4,5-dimethylfluorescein diacetate) readily crosses the plasma membrane and enters the cytoplasm where esterases cleave off the ester groups to produce a charged form of the molecule, which is then trapped in the cytoplasm. The trapped dye changes its fluorescence with changes in cytoplasmic pH. By monitoring fluorescence of cells continuously in a microspectrofluorometer, we have shown that the addition of mitogens to cells produces an immediate rise in intracellular pH. This rise in cellular pH is blocked by amiloride and does not occur in a Na^+-free medium (14). These observations are consistent with the hypothesis that mitogens activate a Na^+/H^+ exchange system in human fibroblasts. In addition, we have shown that Na^+ influx in the presence of serum is inhibited by extracellular protons, whereas it is stimulated by intracellular protons (22).

Finally, we have measured intracellular pH using the weak acid [^{14}C]dimethyl oxazolidine dione ([^{14}C]DMO). These studies demonstrated that the intracellular pH = 7.1 in serum-deprived cells and rises to pH = 7.35 in serum-stimulated cells. The rise in intracellular pH in response to serum is blocked by benzamil (22). Our values for intracellular pH under basal and stimulated conditions are quite consistent with values reported for 3T3 cells under similar conditions (29).

3. STIMULATION OF Na^+ INFLUX BY PEPTIDE MITOGENS

To discuss the mechanism for serum stimulation of Na^+ influx in any detail, it is necessary to ascertain which element in serum may be the active component. From previous studies of serum effects on cell proliferation, it is well known that serum contains small molecular weight peptides that are capable of acting as mitogens. Thus it seemed reasonable to test small molecular weight peptides to determine whether they would stimulate Na^+ influx in HSWP cells in a serum-free medium. In early studies it was shown that a combination of growth factors (EGF, insulin, and thrombin) would stimulate Li^+ uptake in 3T3 cells (33), and EGF would stimulate $^{22}Na^+$ influx in HSWP cells (38); however, the degree of stimulation was much less than that seen with serum. Thus it was not clear whether peptides alone could stimulate Na^+ influx as effectively as serum or whether some additional component of serum was required. In this connection, our recent observation that lys-bradykinin will stimulate Na^+ influx (and DNA synthesis) in HSWP cells (20) enabled us to find a combination of peptides that stimulates Na^+ influx (and DNA synthesis) as effectively as serum. The data in Fig. 2.4 show the effect of various combinations of EGF, lys-bradykinin, vasopressin, and insulin on

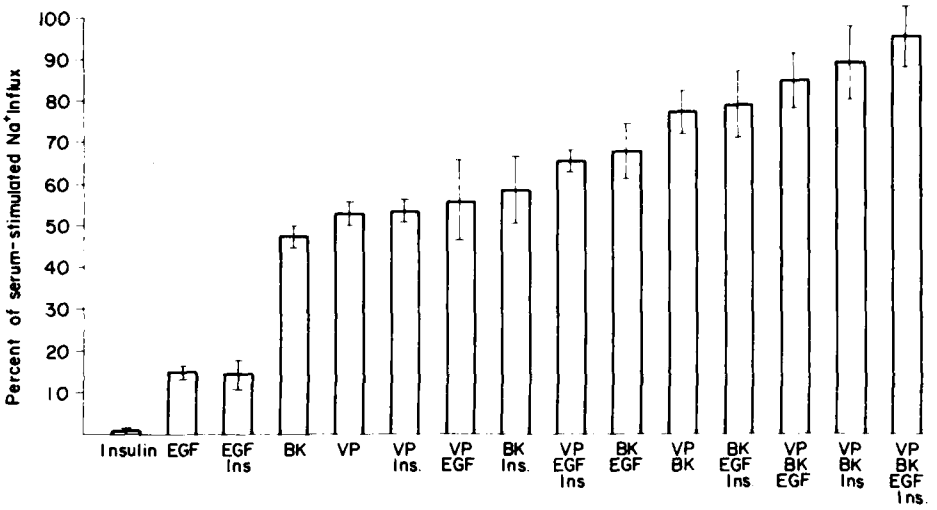

Figure 2.4. Na^+ influx in response to various combinations of four growth factors. Cells were serum deprived as described in the legend to Fig. 2.1. The initial rate of Na^+ influx was measured over a 5-min period in medium containing 20 μM digitoxin and various combinations of four growth factors [0.1 μM Lys-bradykinin (BK), 0.1 μM vasopressin (VP), 20 nM EGF, and 1 μg/ml insulin (Ins)]. Values represent mean ± S.E.M. from five determinations. For details, see ref. 20.

Na^+ influx. The net Na^+ influx in medium containing all four of these peptides is 95% of that seen in the presence of serum. Thus it is not necessary to postulate the involvement of any element of serum other than small molecular weight peptides to explain the stimulation of Na^+ influx. Since the actions of this class of peptides are known to be the result of binding at specific receptors on the cells surface, one can presume that the initial step in activation of Na^+ flux is binding of peptides to their receptors. Next we must ask how these receptors are coupled to the Na^+/H^+ transport system (e.g., by means of a second messenger).

4. STIMULATION OF Na^+ INFLUX IN SERUM-FREE MEDIUM BY A23187

In our early studies of the coupling between peptide receptors and Na^+/H^+ transporters, we examined the possibility that Ca^{2+} might serve as a second messenger for the activation process. We investigated whether elevating intracellular Ca^{2+} in HSWP cells in a serum-free medium would activate the Na^+/H^+ transport system. We found that when HSWP cells are preloaded with Ca^{2+} in the presence of the divalent cation ionophore, A23187, prior to measurement of Na^+ influx, the net Na^+ influx is stimulated dramatically (Fig. 2.2). A significant stimulation (three-fold) is observed at an A23187

concentration of 1 μg/ml with maximal stimulation (five-fold) occurring at 5 μg/ml. At a concentration of 5 μg/ml, A23187 stimulates a five-fold increase of initial $^{45}Ca^{2+}$ influx into HSWP cells, supporting the contention that this agent will increase the cytosolic Ca^{2+} concentration. The A23187 clearly stimulates Na^+ influx by the same pathway as serum, since amiloride completely blocks the increment of Na^+ influx induced by Ca^{2+} loading. These studies suggest that Ca^{2+} could act as a second messenger to activate Na^+/H^+ exchange. The next step was to demonstrate that serum or peptide mitogens do modify Ca^{2+} metabolism.

5. EVIDENCE FOR Ca^{2+} MOBILIZATION IN HSWP CELLS IN RESPONSE TO SERUM OR PEPTIDE MITOGENS

If Ca^{2+} is the second messenger in the serum activation of Na^+ influx, then cellular Ca^{2+} could rise through either an increase in Ca^{2+} influx or a mobilization of intracellular Ca^{2+}. There are examples of cellular systems where hormone-induced elevations of cellular Ca^{2+} are mediated by one or both of these processes. In the HSWP cell, the serum-stimulation of Na^+ influx can occur in a medium where Ca^{2+} is replaced by Mg^{2+}* (41) which implies that if Ca^{2+} is the second messenger in the activation process, then it must be mobilized from intracellular stores. To investigate this possibility, we measured the effects of serum and peptide mitogens on $^{45}Ca^{2+}$ efflux from HSWP cells loaded to isotopic equilibrium. The efflux of $^{45}Ca^{2+}$ from cells in the presence and absence of 10% FBS is shown in Fig. 2.5. Serum clearly stimulates $^{45}Ca^{2+}$ efflux from HSWP cells. A computer analysis of the efflux curves (see ref. 21 for details) showed that the data was best fit by a three-compartment model and suggested that HSWP cells have three physiologically distinct Ca^{2+} compartments with markedly different turnover rates. As described by Uchikawa and Borle (36) the first compartment C_1 has a very fast turnover rate and presumably represents Ca^{2+} bound to the external face of the plasma membrane; the second compartment C_2 has a fast turnover rate and presumably represents Ca^{2+} bound within the cell but readily accessible to the aqueous phase; the third compartment C_3 has a slow turnover rate and probably represents mitochondrial Ca^{2+} stores. When effluxes from the three compartments were calculated from computer-derived parameters, it was found that serum significantly ($p < 0.05$) stimulates Ca^{2+} efflux from the second and third compartments (C_2 and C_3). In the second compartment, flux is 1.84 $\pm$ 0.34 μmol/g protein/minute in serum-deprived (control) cells, and addition of serum causes the flux to increase about twofold, that is, to 3.69 $\pm$ 0.65 μmol/g protein/minute. Similarly, the third compartment flux is

* Ca^{2+} is replaced by Mg^{2+} to prevent the rise in Na^+ influx that occurs when divalent cations are removed from the assay media (40).

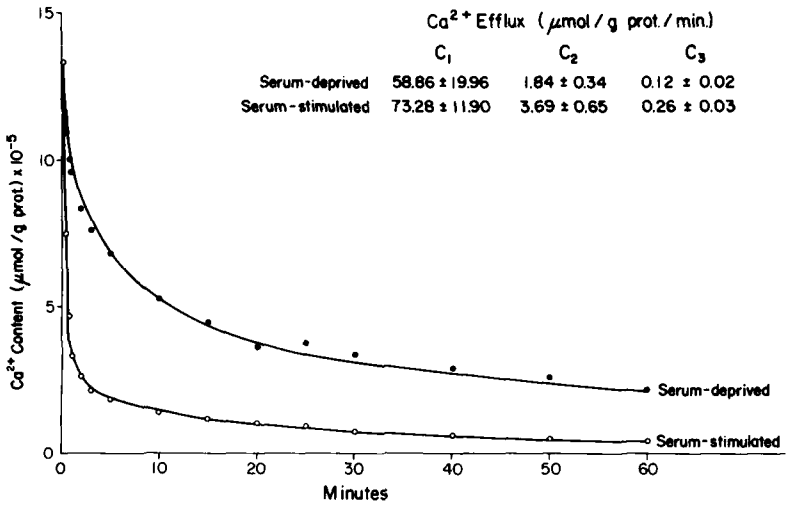

Figure 2.5. Ca^{2+} efflux from HSWP cells: the effect of serum. HSWP cells were loaded with $^{45}Ca^{2+}$ for 24 h and serum deprived for 4 h at isotopic equilibrium in amino acid–free, Hepes-buffered EMEM + 0.1% FBS. $^{45}Ca^{2+}$ efflux was initiated by addition of amino acid–free, Hepes-buffered EMEM containing 1.8 m*M* Ca^{2+} plus or minus 10% FBS. The medium was sampled from a single dish at designated times, and the $^{45}Ca^{2+}$ remaining in the cells was calculated. Points are experimentally determined, and the line is a computer fit. Values in the table are calculated from computer-derived parameters and represent mean ± S.E.M. from six determinations. For details see ref. 21.

0.12 ± 0.02 μmol/g protein/minute in control cells, and upon serum addition, the flux increases to 0.26 ± 0.03 μmol/g protein/minute.

When the combination of peptide mitogens (EGF, lys-bradykinin, vasopressin, and insulin) which fully activate Na^+ influx were tested on $^{45}Ca^{2+}$ efflux, it was found that they also significantly stimulate efflux from C_2 and C_3 (21). Specifically, in the presence of the combination of four growth factors, Ca^{2+} efflux from C_2 was 4.20 ± 0.62 μmol/g protein/minute and from C_3 was 0.38 ± 0.06 μmol/g protein/minute. Thus serum and peptide mitogens do influence Ca^{2+} metabolism in a manner consistent with their mobilizing intracellular stores of Ca^{2+}.

6. EFFECT OF TMB-8 ON SERUM-STIMULATED Ca^{2+} EFFLUX AND Na^+ INFLUX

To provide further support for the contention that mitogens stimulate Na^+ influx by mobilizing intracellular Ca^{2+}, we investigated the effect

of the intracellular Ca^{2+} antagonist 8-(*N*,*N*-diethylamino)-octyl-3,4,5-trimethoxybenzoate (TMB-8) on serum-stimulated Ca^{2+} efflux and Na^+ influx. TMB-8 has been suggested to stabilize intracellular membrane-bound Ca^{2+} (13) and has been demonstrated to block Ca^{2+}-dependent cellular functions in platelets, neutrophils, and smooth muscle (13, 26, 34). To measure the effect of TMB-8 on $^{45}Ca^{2+}$ efflux, cells were loaded with $^{45}Ca^{2+}$ and serum deprived as described previously, and then the $^{45}Ca^{2+}$ efflux was initiated by the addition of Hepes-buffered amino acid–free EMEM containing 10% FBS and 50 μM TMB-8. The data in Fig. 2.6 demonstrate that TMB-8 significantly ($p < 0.05$) inhibits the Ca^{2+} efflux from the second compartment while not affecting efflux from C_1 or C_3. Efflux from C_2 declined from 3.69 ± 0.05 μmol/g protein/minute in the presence of 10% FBS to 0.28 ± 0.01 μmol/g protein/minute in the presence of 10% FBS + 50 μM TMB-8.

Since TMB-8 blocks the serum-stimulated Ca^{2+} efflux from the second Ca^{2+} compartment, one would predict that it might block the serum-stimulated Na^+ flux, which we propose is secondary to a mobilization of intracellular Ca^{2+}. To test this possibility, HSWP cells were serum deprived for 4 h and then assayed in the presence of 10% FBS and varying concentrations of TMB-8. The data in Fig. 2.7 indicate that TMB-8 inhibits the activation of Na^+ influx by serum with a K_i = 15 μM. Maximal inhibition by TMB-8

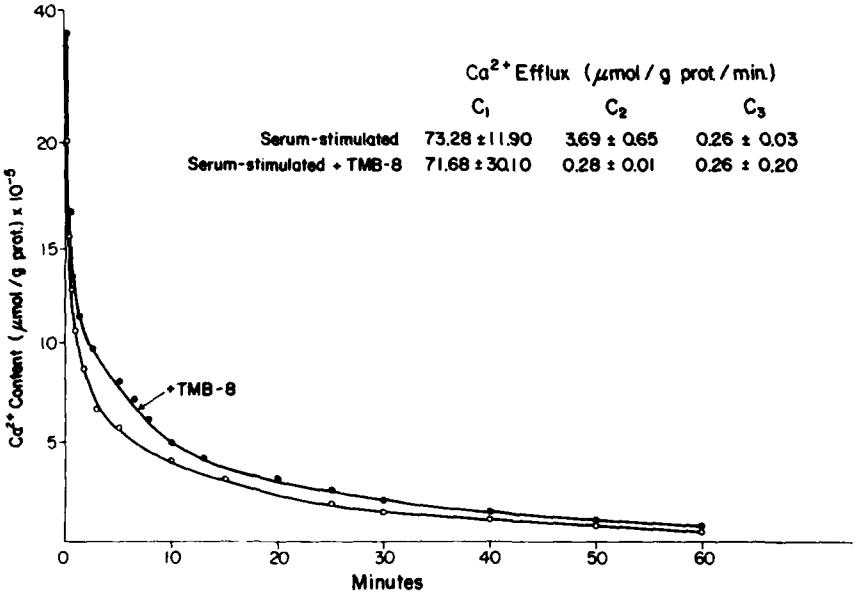

Figure 2.6. Ca^{2+} efflux from HSWP cells: the effect of serum + TMB-8. HSWP cells were loaded with $^{45}Ca^{2+}$, serum deprived, and $^{45}Ca^{2+}$ efflux was measured as described in Fig. 2.5. The concentration of TMB-8 was 50 μM. Points are experimentally determined, and the line is a computer fit. Values in the table are calculated from computer-derived parameters and represent mean ± S.E.M. from three determinations. For details see ref. 21.

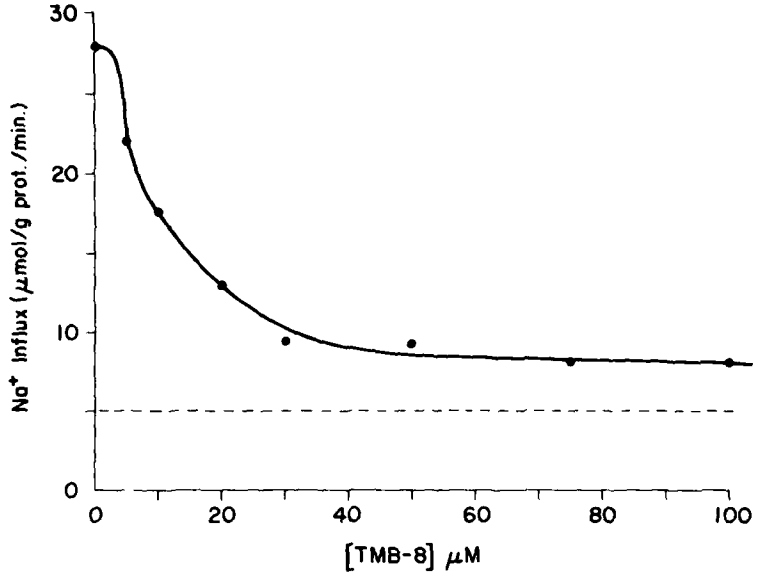

Figure 2.7. Concentration dependence of TMB-8 inhibition of serum-stimulated Na^+ influx. Cells were serum deprived as described in the legend to Fig. 2.1. The initial rate of Na^+ influx was assayed over a 5-min period in medium containing 20 μM digitoxin + 10% FBS and varying concentrations of TMB-8. The broken line represents the level of flux in serum-deprived cells.

brings the Na^+ flux in the presence of 10% FBS down near the basal level, but does not totally block the effect of serum. It is possible that a small component of the serum stimulation can be supported in the absence of a mobilization of intracellular Ca^{2+} by bringing Ca^{2+} in from outside the cell.

Although the data in Fig. 2.5 demonstrate that TMB-8 blocks the serum-induced mobilization of intracellular Ca^{2+}, it is possible that this agent's inhibition of Na^+ flux is independent of its effect on Ca^{2+} metabolism. For example, the compound could have general and nonspecific effects on the cell membrane or on the Na^+/H^+ transporter, which could directly block function of the transporter, rather than interfere with the mechanism for its activation. To support the contention that TMB-8 blocks the serum stimulation of Na^+ influx by its effects on Ca^{2+} metabolism, we tested the effect of TMB-8 on A23187-stimulated Na^+ flux. Since A23187 can elevate intracellular Ca^{2+} levels by enhancing Ca^{2+} influx, in addition to mobilizing intracellular Ca^{2+}, then A23187-stimulated Na^+ influx should not be inhibited by TMB-8 if this agent acts solely by stabilizing intracellular Ca^{2+}. The data in Table 2.1 indicate that TMB-8 had no effect on either basal or A23187-stimulated Na^+ flux, while in the same experiment it dramatically inhibited growth-factor stimulated Na^+ flux. Thus TMB-8 appears to block the activation of the transporter rather than its operation, and this block can be circumvented by providing a source of external Ca^{2+} by means of A23187.

TABLE 2.1. EFFECT OF TMB-8 ON GROWTH FACTOR– OR A23187-STIMULATED Na^+ INFLUX IN HSWP CELLS[a]

Assay Condition	Na^+ Influx (μmol/g protein per minute)
Serum-free	4.1 ± 1.3
Serum-free + TMB-8	3.3 ± 1.2
Growth factors	24.9 ± 1.5
Growth factors + TMB-8	9.7 ± 0.7
A23187	26.4 ± 2.9
A23187 + TMB-8	24.1 ± 5.2

[a] Cells were serum deprived for 4 h in amino acid–free, Hepes-buffered EMEM ± 0.1% FBS. A23187-treated samples were preincubated for 1 min in medium containing A23187 ± TMB-8. Initial rate of Na^+ influx was assayed after a 5-min incubation in amino acid–free Hepes-buffered EMEM containing 20 μM digitoxin with the indicated additions. Concentrations used were TMB-8, 50 μM; growth factors, 0.1 μM lys-bradykinin + 0.1 μM vasopressin + 20 nM epidermal growth factor + 1.0 μg/ml insulin; A23187, 10 μM. Values represent the mean ± S.E.M. from three determinations (serum-free and growth factors) or five determinations (A23187).

7. EVIDENCE FOR INVOLVEMENT OF CALMODULIN IN THE ACTIVATION OF Na^+/H^+ EXCHANGE

Since we have considerable evidence for Ca^{2+} as a second messenger in the activation of Na^+ influx in HSWP cells, it is quite reasonable to question whether the Ca^{2+}-dependent regulatory protein, calmodulin, mediates the effects of Ca^{2+}. A number of previous studies have identified calmodulin in cultured fibroblasts and have assigned a function to it in the regulation of cell growth. To test the possible involvement of calmodulin in the serum activation of Na^+ influx, we studied the effects of a variety of calmodulin antagonists on the serum stimulation of Na^+ influx. The initial studies were done with a series of psychoactive agents that previously had been shown to be calmodulin antagonists (12). For these studies, cells were serum deprived for 4 h, preincubated for 30 min in serum-free medium containing the appropriate concentration of calmodulin antagonist, and assayed in 10% FBS containing the appropriate concentration of drug. All six psychoactive calmodulin antagonists completely inhibit serum-stimulated and A23187-stimulated Na^+ influx in a dose-dependent manner (19). None of the agents inhibits the basal Na^+ flux in serum-deprived cells. Since these calmodulin antagonists exhibit a wide range of ID_{50} for their inhibition of Na^+ flux, we attempted to correlate the ability of a drug to inhibit Na^+ flux with its previously reported

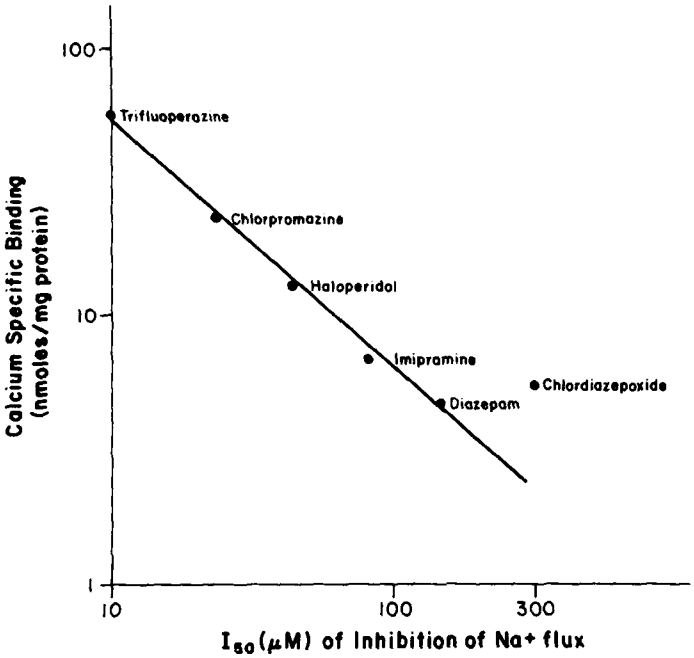

Figure 2.8. Relationship between binding of psychoactive drugs to calmodulin and inhibition of serum-stimulated Na^+ influx in HSWP cells. Cells were serum deprived as described in the legend to Fig. 2.1 and then preincubated for 30 min with medium containing calmodulin antagonists. The initial rate of Na^+ influx was measured in medium containing 20 μM digitoxin, 10% FBS, and various concentrations of antagonists. I_{50} values were determined from fractional inhibition plots (see ref. 19 for details). Calmodulin-binding data are from Levin and Weiss[12]. Correlation coefficient $r = 0.982$ (excluding chordiazepoxide).

ability to bind to calmodulin (12). As the data in Fig. 2.8 illustrate, there is an excellent correlation between a drug's ability to interact with calmodulin and its ability to block the serum activation of Na^+ influx. This strong correlation argues that the inhibition of Na^+ influx by these agents is due to their interaction with calmodulin and not to some nonspecific effects of these drugs.

Although the close correlation between inhibition of Na^+ flux and binding to calmodulin argues for a calmodulin-specific effect, it is always difficult to rule out totally involvement of the nonspecific, membrane-related effects ascribed to these agents (30). For that reason we investigated another class of calmodulin antagonists, naphthalene sulfonamide derivatives, to determine their effect on serum-stimulated Na^+ flux. As shown in Fig. 2.9, W12 is the dechlorinated homolog of W13. The absence of the chlorine in W12 greatly reduces its affinity for calmodulin in comparison to that of W13 (1). Although W12 and W13 exhibit different anticalmodulin activities, both drugs possess similar hydrophobicity indices. Thus W12 serves as an excellent control for any non-calmodulin-mediated effects of these drugs. The effects of W12 and W13 on the serum-stimulated Na^+ influx are shown in

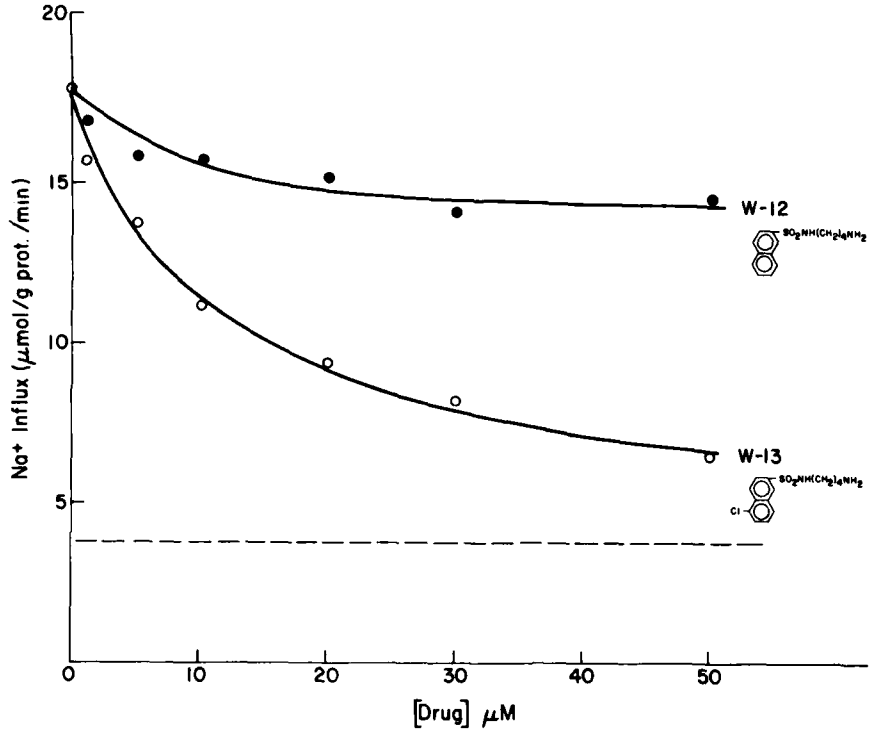

Figure 2.9. *Concentration dependence for calmodulin-antagonist inhibition of serum-stimulated* Na^+ *influx in HSWP cells. Cells were serum deprived as described in the legend to Fig. 2.1 and then preincubated for 15 min with medium containing varying concentrations of W12 or W13. The initial rate of* Na^+ *influx was measured over a 5-min period in medium containing 20* μM *digitoxin, 10% FBS, and varying concentrations of W12 and W13. The broken line represents the level of flux in serum-deprived cells. Values represent mean of five determinations.*

Fig. 2.9. It can be seen that W12 has little effect on serum-stimulated Na^+ influx in the range of concentrations tested, whereas W13 markedly inhibits serum-stimulated Na^+ influx (K_i = 9 μM). Thus the observation that six psychoactive agents and two naphthalene sulfonamide derivatives inhibit serum-stimulated Na^+ influx with the same effectiveness as these drugs interact with calmodulin provides compelling evidence that calmodulin is involved in the serum activation of Na^+/H^+ exchange.

8. EVIDENCE FOR INVOLVEMENT OF PHOSPHOLIPASE ACTIVITY IN THE ACTIVATION OF Na^+/H^+ EXCHANGE

Although there is persuasive evidence that Ca^{2+} acts as a second messenger in the mitogen activation of Na^+ flux, we do not know the mechanism by which binding of Ca^{2+} to calmodulin leads to an activation of Na^+/H^+ ex-

change. Thus it is important to determine whether certain known Ca^{2+}-regulated biochemical events might be involved in the activation process. Phospholipase (PLase) activity is a prime candidate for consideration as a component of the activation sequence for the following reasons: (1) PLase A_2 and PLase C are both Ca^{2+}-dependent enzymes that may be regulated by the level of cytoplasmic Ca^{2+} activity; (2) PLase A_2 activity in cultured fibroblasts is stimulated by bradykinin (8), a compound we have shown to stimulate Na^+ flux and DNA synthesis in HSWP cells (20); (3) PLase activity is stimulated in cultured fibroblasts by melittin, a compound that stimulates Na^+ influx in cultured mouse fibroblasts (28). Thus we tested the possibility that activation of PLase is a key step in the sequence of events leading from binding of mitogens at their receptor sites to stimulation of Na^+/H^+ exchange.

9. EFFECT OF PHOSPHOLIPASE INHIBITORS ON SERUM-STIMULATED Na^+ INFLUX

Our initial experiments to test for the involvement of PLase activity in the activation of Na^+ influx utilized two known inhibitors of PLase activity, mepacrine and the Upjohn drug U-1002 (43). Clearly if PLase activation is a key step in the stimulation of Na^+/H^+ exchange, then PLase inhibitors should block this stimulation. Cells were serum deprived for 4 h and then assayed in the presence and absence of serum and the presence or absence of PLase inhibitors. Neither mepacrinen or U-1002 has any significant effect on the basal Na^+ influx in serum-free medium (37). However, addition of 100 μM mepacrine or 200 μM U-1002 to the assay medium results in a complete block of the serum stimulation of Na^+ influx (Fig. 2.10).

Although these data are consistent with a role of PLase activity in the regulation of Na^+/H^+ exchange, it is important to demonstrate (1) that serum stimulates PLase activity in HSWP cells and (2) that a comparable dose response exists for inhibition of serum-stimulated Na^+ flux and inhibition of serum-stimulated PLase activity. Regarding the first criterion, the data in Table 2.2 show that serum does stimulate PLase activity, as measured by release of [^{3}H]arachidonic acid from preloaded cells. In five experiments serum stimulated Na^+ influx by 3–5 fold and stimulated [^{3}H]arachidonic acid release by 3–4 fold over basal levels. Regarding the second criterion, we demonstrated that both U-1002 and mepacrine were able to inhibit Na^+ influx fully with K_i's of 10 and 18 μM, respectively.* The dose-response curves for inhibition of [^{3}H]arachidonic acid release show that PLase inhibition occurs in the same concentration range of U-1002 and mepacrine as does inhibition of Na^+ flux (K_i's of 5 μM and 15 μM, respectively (37). The

* When comparing the potency of these two agents, it should be kept in mind that cells were preincubated with U-1002 for 10 min, whereas the effects of mepacrine were immediate.

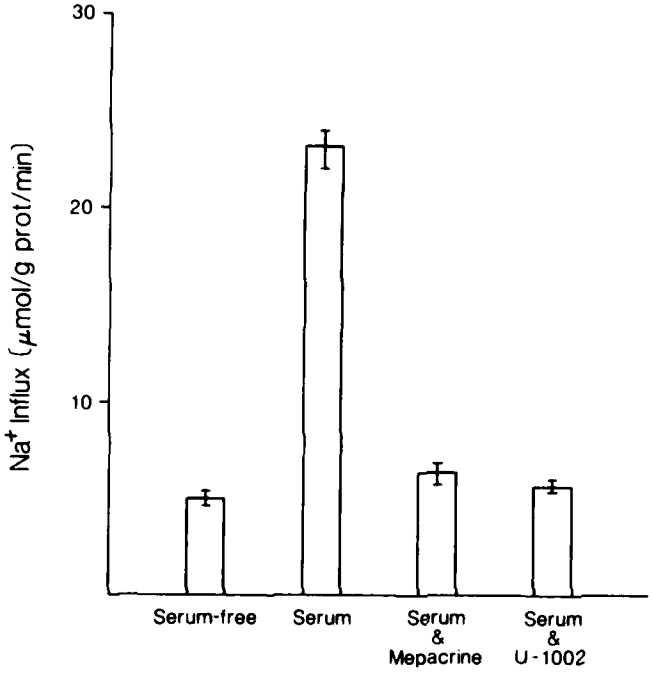

Figure 2.10. Effect of phospholipase inhibitors on serum-stimulated Na^+ influx in HSWP cells. Cells were serum deprived as described in the legend to Fig. 2.1. Initial Na^+ influx was measured over a 5-min period in either serum-free medium, 10% FBS medium, 10% FBS medium + 100 μM mepacrine or 10% FBS medium + 200 μM U-1002. Digitoxin (20 μM) was present during all assays. Values represent means ± S.E.M. for five determinations.

only discrepancy between the two inhibition curves is that the PLase inhibitors totally block the serum-activated Na^+ flux while only partially blocking the serum-stimulated [^{3}H]arachidonic acid release. This result can be easily explained by the data in Table 2.2. We found that the addition of bovine

TABLE 2.2. SERUM STIMULATION OF [^{3}H]ARACHIDONIC ACID RELEASE FROM HSWP CELLS

Assay Condition	[^{3}H]Arachidonic Acid Release (cpm/dish)
Serum-free	1500 ± 80
Serum-free + mepacrine	1542 ± 71
Serum	3500 ± 180
Serum + mepacrine	2200 ± 120
BSA	1900 ± 110
BSA + mepacrine	1940 ± 100

serum albumin (BSA) to the PLase assay medium stimulated the release of [^{3}H]arachidonic acid. This BSA stimulation is not blocked by mepacrine and is therefore presumed to be an effect on the rate of reacylation of [^{3}H]arachidonic acid into phospholipids rather than an effect at the level of the PLase. Thus it is reasonable to assume that the inhibitor-insensitive portion of the serum-stimulated [^{3}H]arachidonate release is the result of serum proteins trapping [^{3}H]arachidonic acid and thereby preventing its reacylation.

With this apparent discrepancy explained, there is a very good correlation between the dose-response curves for inhibition of Na^+ influx and PLase activity for both of these compounds. This correlation argues that the effects of mepacrine and U-1002 on Na^+ influx are by means of their effects on PLase activity and not the result of other nonspecific effects of these drugs. In addition, inhibition of Na^+ influx by mepacrine occurs with a K_i of 18 μM, whereas the nonspecific effects normally attributed to this drug occur at substantially higher concentrations (4).

10. STIMULATION OF Na^+ INFLUX BY MELITTIN

In a recent publication it was demonstrated that melittin, a known activator of phospholipase activity, would stimulate Na^+ influx in 3T3 cells (28). However, the authors of this paper argued that the Na^+ influx occurred through a nonspecific leak pathway created by the interaction of melittin with the plasma membrane. We sought to test the alternative possibility that the melittin-activated Na^+ flux occurs through the Na^+/H^+ exchange pathway. The initial studies demonstrated that melittin activated Na^+ influx in human fibroblasts when present at concentrations as low as 100 ng/ml. As shown in Fig. 2.11, a concentration of 800 ng/ml stimulates Na^+ influx to a level that exceeds that normally seen in response to 10% serum. The addition of amiloride to the assay medium completely blocks the melittin-activated Na^+ influx. These findings suggest that the stimulated Na^+ flux is mediated by the amiloride-sensitive Na^+/H^+ exchange system, rather than by a nonspecific leak pathway. The effect of melittin on Na^+ influx appears to be mediated through its effects on phospholipase activity, since mepacrine is able to block a substantial amount of the melittin stimulation of Na^+ flux. In addition, we found that melittin stimulates Na^+ influx over the same concentration range that it stimulates phospholipase activity.

In addition to the demonstration that the melittin-stimulated Na^+ flux is amiloride sensitive, there are two other observations that strongly suggest that melittin is activating Na^+/H^+ exchange rather than creating leak pathways in the plasma membrane. First, measurements of intracellular pH with a pH-sensitive fluorescent dye show that the addition of melittin to serum-deprived human fibroblasts induces a dramatic alkalinization of the cytoplasm. This alkalinization is prevented by incubation in Na^+-free medium and is blocked by addition of either amiloride or mepacrine (14). These data

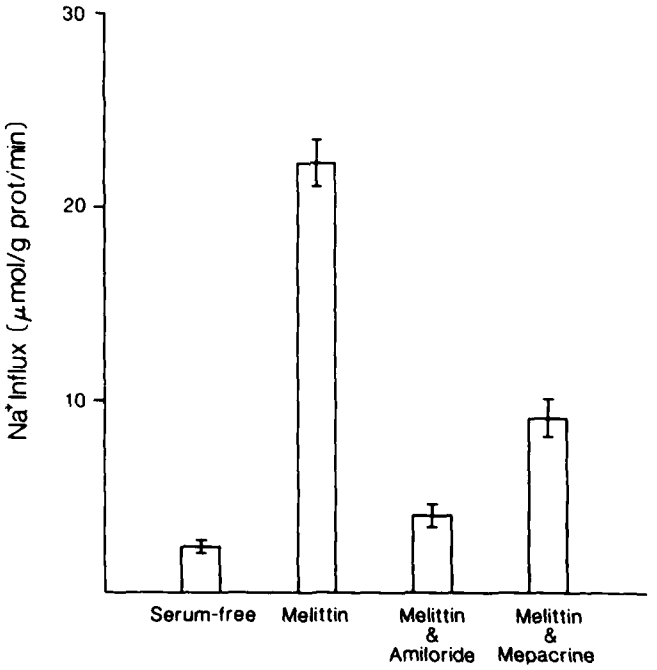

Figure 2.11. Effect of melittin on Na^+ influx in serum-free medium. Cells were serum deprived as described in the legend of Fig. 2.1. Initial Na^+ influx was measured over a 5-min period in serum-free medium containing 20 μM digitoxin. Melittin, amiloride, and mepacrine were used at concentrations of 800 ng/ml, 3 mM and 100 μM respectively. Values represent means ± S.E.M. for five determinations.

argue strongly that melittin is activating the amiloride-sensitive, Na^+/H^+ exchange system. Second, we find that preincubation of cells in melittin leads to a desensitization phenomenon similar to that seen with serum stimulation of Na^+ influx (see below). The Na^+ flux desensitizes to melittin with a similar time course and to the same extent as seen with serum. This observation argues that the melittin stimulation of Na^+ flux occurs by a mechanism quite similar to the one by which serum stimulates Na^+ influx.

11. EFFECT OF DEXAMETHASONE ON THE SERUM STIMULATION OF Na^+ INFLUX

In recent studies, Hirata and co-workers have shown that a number of cell types (including human fibroblasts) synthesize a 40,000-dalton molecular weight protein in response to chronic treatment with dexamethasone (7). This protein, called lipomodulin, acts as an endogenous phospholipase inhibitor. Thus one would predict that treatment of human fibroblasts with dexamethasone would result in an inhibition of serum-stimulated phospholipase activity and thereby an inhibition of the serum stimulation of Na^+ influx. In

this regard, we found that chronic (24-h) treatment of HSWP cells with 1 μM dexamethasone had no significant effect on either basal Na^+ influx or on the basal release of [^{3}H]arachidonic acid. However, chronic treatment of cells with dexamethasone reduced the serum stimulation of phospholipase activity by 45 ± 8% and reduced the serum-stimulated Na^+ influx by 50 ± 5% in three separate experiments. Acute treatment (up to 4 h) with dexamethasone had no effect on either the Na^+ influx or [^{3}H]arachidonic release in the presence of serum. These observations are consistent with the contention that stimulation of phospholipase activity is an important step in the activation of Na^+ influx by serum.

12. DESENSITIZATION OF THE SERUM EFFECT ON Na^+ INFLUX

In assessing the mechanism for serum stimulation of Na^+ influx, it is important to know whether the stimulation is stable or declines with time. Thus we investigated the effect of preincubating cells in the presence of serum prior to the measurement of net Na^+ influx. As shown in Fig. 2.12, the direct addition of serum to serum-deprived cells produced a six-fold stimulation over the level of basal Na^+ influx. However, when cells were preincubated in serum, their response to a subsequent addition of fresh serum declined with a half-time of 15 min. This desensitization is not an artifact of the Tris-

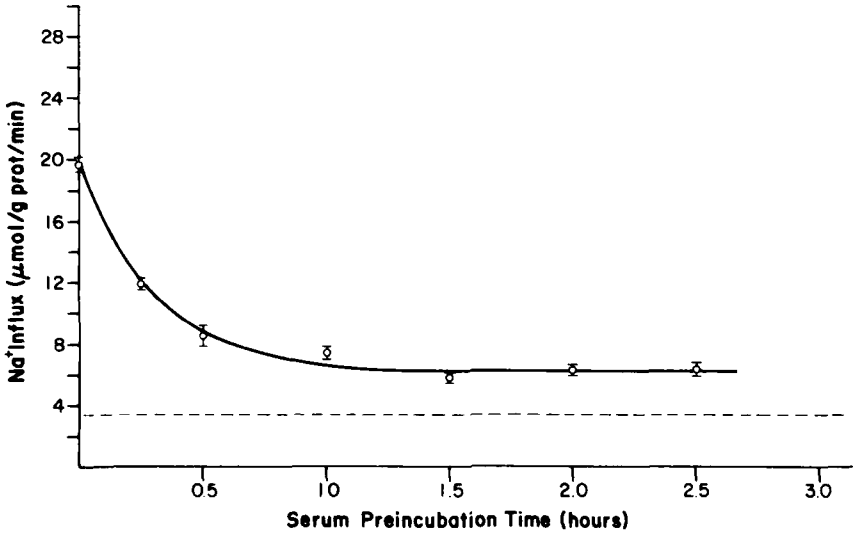

Figure 2.12. Desensitization of serum-stimulated Na^+ influx. Cells were serum deprived for 4 h in Tris-buffered, amino acid–free EMEM + 0.1% FBS. Cells were then preincubated in identical medium containing 10% FBS for varying lengths of time. Following serum pretreatment, Na^+ influx was assayed in fresh medium containing 10% FBS and 20 μM digitoxin over a 5-min time course. Values represent means ± S.E.M. for five determinations. Dashed line represents the level of serum-deprived flux for this series of experiments.

buffered assay medium as a similar response occurs in Hepes- or CO_2-buffered medium (42). Desensitized cells rapidly ($t_{1/2}$ = 20′) regain their sensitivity to serum when incubated in a serum-free medium; thus de novo synthesis of proteins is an unlikely mechanism for reversal of desensitization. The desensitization is not unique to serum since the bradykinin and vasopressin stimulation of Na^+ influx also decline with preincubation time.

Although the mechanism for desensitization is not clear, we have been able to eliminate some possible mechanisms. The desensitization process is not dependent on mitogen receptor down-regulation since we find that A23187-activation of Na^+ influx also desensitizes with time (42). In addition, the desensitization does not appear to be due to a negative feedback process at the Na^+/H^+ transporter by way of a rise in intracellular Na^+ or a rise in intracellular pH. We find that desensitization to serum occurs when cells are preincubated with serum in a low-Na^+ medium, which blocks the serum-stimulated rise in intracellular Na^+, or when cells are preincubated with serum in a low-pH medium, which blocks the serum-stimulated rise in intracellular pH (42).

13. SUMMARY OF REGULATION OF Na^+/H^+ EXCHANGE

The addition of mitogens to serum-deprived human fibroblasts rapidly stimulates Na^+ influx by means of an amiloride-sensitive Na^+/H^+ exchange system. The Na^+/H^+ exchange system appears to be virtually inactive under basal conditions and thus must be rapidly activated. Based on the evidence presented, we propose the model shown in Fig. 2.13 to explain the activation of Na^+ influx. The initial step in the activation sequence is the binding of

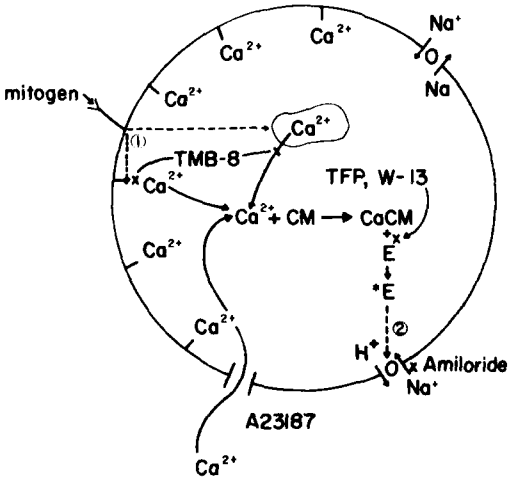

Figure 2.13. Schematic representation of the mechanism for activation of the amiloride-sensitive Na^+/H^+ exchange pathway by mitogens. Possible sites for involvement of phospholipase activity are designated by 1 and 2.

mitogens to their surface receptors. This leads to a mobilization of intracellular Ca^{2+} which may occur from membrane-bound stores or from intracellular organelles. This contention is supported by the observation that A23187 can activate Na^+ influx in serum-free medium, that the serum stimulation of Na^+ flux is blocked by the intracellular Ca^{2+} antagonist TMB-8, and that mitogens stimulate $^{45}Ca^{2+}$ efflux that is blocked by TMB-8.

The next step in the activation sequence appears to be the interaction of Ca^{2+} with the Ca^{2+}-dependent regulatory protein calmodulin. This contention is supported by data for two classes of calmodulin antagonists that show an excellent correlation between a drug's ability to interact with calmodulin and its ability to block the activation of Na^+ flux. We have depicted the action of calmodulin to be the activation of an enzyme system that leads to a biochemical modification of the transport system. For example, the calmodulin-dependent enzyme could be a protein kinase that activates the Na^+ transport system by means of a phosphorylation reaction. Although not depicted, it is also possible that the calmodulin-stimulated process is the fusion of submembrane vesicles, containing Na^+/H^+ transport systems, into the plasma membrane thereby leading to incorporation of active transports in a manner similar to that seen with insulin stimulation of glucose transport in rat adipocytes (31).

Although there is considerable evidence for the stimulation of phospholipase activity as an important step in the activation sequence, at present the temporal relationship between Ca^{2+} mobilization and activation of PLase activity is not clear. There are two key places (labeled 1 and 2 in Fig. 2.13) in the activation scheme where an increase in phospholipase activity could be important. First, the mitogen receptor could be coupled to the phospholipase enzyme so that binding of mitogen causes an increase in phospholipase activity as an initial event. This could lead to the mobilization of intracellular Ca^{2+} through direct effects on phospholipid pools, which could serve as membrane-binding sites for Ca^{2+}, or through release of by-products of phospholipase action (e.g., arachidonic acid metabolites or inositol triphosphate), which have recently been suggested to mobilize intracellular Ca^{2+} (35). The second possibility is that the activation of phospholipid is secondary to the mobilization of intracellular Ca^{2+}. In this scheme binding of mitogen to its receptor would lead to mobilization of Ca^{2+} and formation of a Ca^{2+}–calmodulin complex. This could result in an increase in phospholipase activity, perhaps by inactivating lipomodulin by way of a phosphorylation reaction (7). The phospholipase action could modify the environment of the Na^+/H^+ transporters in the membrane or could enhance the fusion of submembrane vesicles containing Na^+/H^+ transporters into the plasma membrane. Recent evidence for arachidonic acid as a fusigen in the exocytosis process is consistent with the enhanced incorporation theory (3). We are currently investigating the temporal relationship between Ca^{2+} mobilization and stimulation of phospholipase activity so that the activation scheme can be more clearly defined.

REFERENCES

1. Chafouleas, J. G., Bolton, W. E., Hidaka, H., Boyd, A. E., and Means, A. R. (1982) *Cell*, **28**, 41–50.
2. Cone, C. D. (1980) *Ann. N.Y. Acad. Sci.*, **339**, 115–131.
3. Creutz, C. E. (1981) *J. Cell Biol.*, **91**, 247–256.
4. Dise, C. A., Burch, J. W., and Goodman, D. B. P. (1982) *J. Biol. Chem.*, **257**, 4701–4704.
5. Epel, D. (1980) *Ann. N.Y. Acad. Sci.*, **339**, 74–85.
6. Hirata, F., Schiffmann, E., Venkatasubramanian, K., Salomon, D., and Axelrod, J. (1980) *J. Biol. Chem.*, **77**, 2533–2536.
7. Hirata, F. (1981) *J. Biol. Chem.*, **256**, 7730–7733.
8. Hong, S. L., and Deykin, D. (1981) *J. Biol. Chem.*, **256**, 5215–5219.
9. Johnson, J. D., Epel, D., and Paul, M. (1976) *Nature*, **262**, 661–664.
10. Kinesella, J. L. and Aronson, P. S. (1981) *Am. J. Physiol.*, **241**, F374–F379.
11. Koch, K. S. and Leffert, H. L. (1979) *Cell*, **18**, 153–163.
12. Levin, R. M. and Weiss, B. (1979) *J. Pharm. Exp. Ther.*, **208**, 454–459.
13. Malagodi, M. H. and Chiou, C. Y. (1974) *Eur. J. Pharmacol.*, **27**, 25–33.
14. Mix, L. and Villereal, M. L. (manuscript in preparation).
15. Moolenaar, W. H., Boonstra, J., van der Saag, P. T., and de Laat, S. W. (1981) *J. Biol. Chem.*, **256**, 12883–12887.
16. Moolenaar, W. H., Mummery, C. L., van der Saag, P. T., and de Laat, S. W. (1981) *Cell*, **23**, 789–798.
17. Moolenaar, W. H., Tsien, R. Y., van der Saag, P. T., and de Laat, S. W. (1983) *Nature*, **304**, 645–648.
18. O'Donnell, M. E., Cragoe, Jr., E., and Villereal, M. L. (1983) *J. Pharm. Exp. Ther.*, **226**, 368–372.
19. Owen, N. E. and Villereal, M. L. (1982) *Proc. Natl. Acad. Sci. USA*, **79**, 3537–3541.
20. Owen, N. E. and Villereal, M. L. (1983) *Cell*, **32**, 977–985.
21. Owen, N. E. and Villereal, M. L. (1983) *J. Cell. Physiol.*, **117**, 23–29.
22. Owen, N. E. and Villereal, M. L. (unpublished observations).
23. Pouysségur, J., Chambard, J. C., Franchi, A., Paris, S., and van Obberghen-Schilling, E. (1982) *Proc. Natl. Acad. Sci. USA*, **79**, 3935–3939.
24. Rindler, M. J., Taub, M., and Saier, Jr., M. H. (1979) *J. Biol. Chem.*, **254**, 11431–11439.
25. Rindler, M. J. and Saier, M. H. (1981) *J. Biol. Chem.*, **256**, 10820–10825.
26. Rittenhouse-Simmons, S. and Deykin, D. (1978) *Biochim. Biophys. Acta*, **543**, 409–422.
27. Rozengurt, E. and Mendoza, S. (1980) *Ann. N.Y. Acad. Sci.*, **339**, 175–179.
28. Rozengurt, E., Gelehrter, T. D., Legg, A., and Pettican, P. (1981) *Cell*, **23**, 781–788.
29. Schuldiner, S. and Rozengurt, E. (1982) *Proc. Natl. Acad. Sci. USA*, **79**, 7778–7782.
30. Seeman, P. and Weinstein, J. (1966) *Biochem. Pharmacol.*, **15**, 1737–1752.
31. Simpson, I. A. and Cushman, S. W., et al., Chapter 3, this book.
32. Smith, J. B. and Rozengurt, E. (1978) *Proc. Natl. Acad. Sci. USA*, **75**, 5560–5564.
33. Smith, J. B. and Rozengurt, E. (1978) *J. Cell. Physiol.* **97**, 441–450.
34. Smith, R. J. and Iden, S. S. (1979) *Biochem. Biophys. Res. Comm.*, **91**, 263–271.
35. Streb, H., Irvine, R. F., Berridge, M. J., and Schulz, I. (1983) *Nature*, **306**, 67–69.
36. Uchikawa, T. and Borle, A. B. (1978) *Am. J. Physiol.*, **234**, R29–R33.
37. Vicentini, L. M., Miller, R. J., and Villereal, M. L. (1984) *J. Biol. Chem.* **259**, 6912–6919.

38. Villereal, M. L. (1981) *J. Cell. Physiol.*, **107**, 359–369.
39. Villereal, M. L. (1981) *J. Cell. Physiol.*, **108**, 251–259.
40. Villereal, M. L. (1982) *J. Cell. Physiol.*, **111**, 163–170.
41. Villereal, M. L. (unpublished observations).
42. Villereal, M. L. and Owen, N. E., *J. Cell. Physiol.* (in press).
43. Wallach, D. P. and Brown, V. J. R. (1981) *Biochem. Pharmacol.*, **30**, 1315–1324.

CHAPTER 3

MECHANISM OF INSULIN'S STIMULATORY ACTION ON GLUCOSE TRANSPORT IN THE ISOLATED RAT ADIPOSE CELL

IAN B. SIMPSON
EDDY KARNIELI
PAUL J. HISSIN
ULF SMITH
SAMUEL W. CUSHMAN
Cellular Metabolism and Obesity Section
National Institute of Arthritis, Diabetes, and Digestive and Kidney Diseases
National Institutes of Health
Bethesda, Maryland

Dr. Karnieli's present address: Metabolic Unit, Endocrine Institute, Rambam Medical Center, Haifa, Israel. Dr. Hissin's present address: Department of Chemistry, Mount Sinai Hospital, New York. Dr. Smith's present address: Department of Medicine, University of Göteborg, Göteborg, Sweden.

Early studies demonstrated that insulin stimulates glucose transport in the rat adipose cell by a mechanism that increases the maximum transport velocity without changing the affinity of the transporters for glucose (2, 3). The question still remained, however, as to whether this increase in transport velocity is the result of a change in the intrinsic activity of the transporter or an increase in the number of functional transporters.

Independently, our group at the National Institutes of Health (4, 13, 25) and Dr. Kono's group (14, 15, 22) at Vanderbilt University proposed a translocation mechanism to account for insulin's stimulatory action on glucose transport whereby glucose transporters are reversibly translocated from an intracellular pool to the adipose cell's plasma membrane. The aim of this chapter is to discuss the basis for this hypothesis and to consider some of the individual steps involved.

1. QUANTITATION AND SUBCELLULAR DISTRIBUTION OF GLUCOSE TRANSPORTERS

The assay we used to measure the number of glucose transporters in a particular subcellular fraction is based on the equilibrium binding of cytochalasin B, a potent competitive inhibitor of glucose transport. Specificity is achieved by performing the binding assay in the presence of 2 μM cytochalasin E, at which concentration it inhibits the specific binding of cytochalasin B to several proteins but has no effect on the binding to the transporters. Further specificity is attained by measuring only that fraction of the total bound cytochalasin B that is inhibited by the natural substrate D-glucose (4, 13, 25).

Figures 3.1 and 3.2 show the distributions of marker enzyme activities and glucose transporters, respectively, in subcellular fractions prepared from adipose cells incubated in the absence or presence of insulin. In these experiments isolated adipose cells (13), suspended in a Krebs–Ringer bicarbonate (10 mM)/HEPES (30 mM) buffer supplemented with 1% BSA, were incubated for 30 min at 37°C in the absence or presence of 7 nM insulin. The cells were washed in a TRIS : EDTA : sucrose (20 : 1 : 225 mM) buffer, pH 7.4, and homogenized. Three major subcellular fractions were then isolated by differential ultracentrifugation: a plasma membrane fraction (PM); a high-density microsomal membrane fraction (HDM); and a low-density microsomal membrane fraction (LDM). The marker enzyme activities 5′-nucleotidase for plasma membranes, rotenone-insensitive NADH : cytochrome c reductase for endoplasmic reticulum, and UDP-galactose : N-acetylglucosamine galactosyltransferase for the Golgi apparatus were measured in each of the isolated fractions. Figure 3.1 clearly demonstrates that the plasma membrane fraction is enriched in the plasma membrane marker enzyme activity, and, similarly, the high- and low-density microsomal membranes are enriched in the marker enzyme activities characteristic of the endoplas-

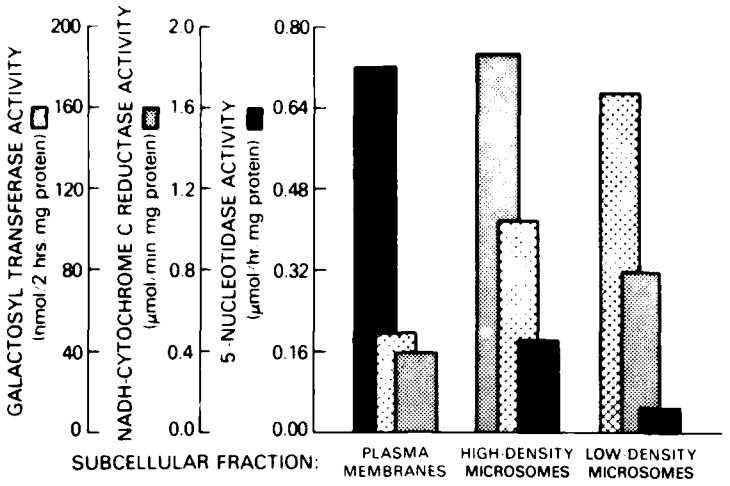

Figure 3.1. Distribution of marker enzyme activities among subcellular membrane fractions of the isolated rat adipose cell. Isolated adipose cells were incubated in the absence or presence of insulin (7 n*M*) for 30 min at 37°C. The cells were then washed and homogenized, and plasma membrane and high- and low-density microsomal membrane fractions prepared by the method described by Hissin et al. (10). The marker enzyme activities 5'-nucleotidase (1) for plasma membranes, NADH : cytochrome c reductase (7) for endoplasmic reticulum, and UDP-galactose : *N*-acetylglucosamine galactosyltransferase (8) for the Golgi apparatus were assayed using the indicated published procedures as described by Simpson et al. (20).

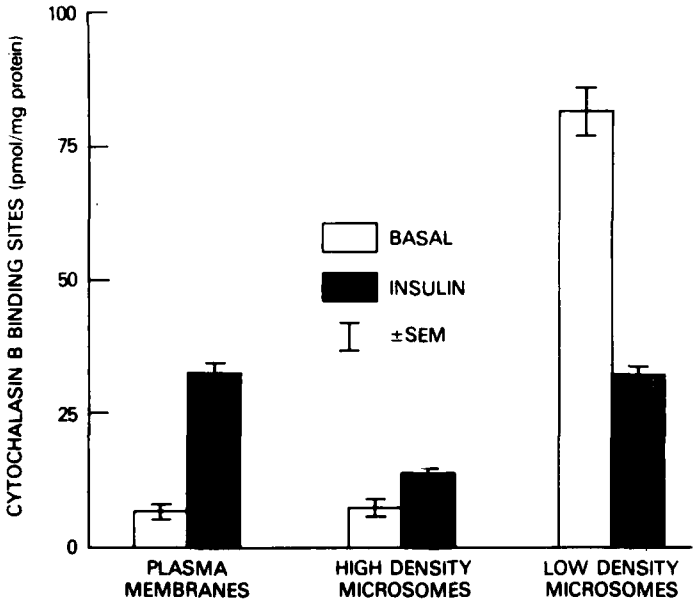

Figure 3.2. The effect of insulin on the distribution of glucose transporters among subcellular membrane fractions of the isolated rat adipose cell. Adipose cells were incubated in the absence or presence of insulin (7 n*M*) for 30 min at 37°C. The cells were then washed and fractionated as described for Figure 3.1. D-Glucose-inhibitable cytochalasin B binding to the isolated fractions was determined as previously described (13, 20). The data represent the mean values ± S.E.M. observed in 8–10 experiments.

mic reticulum and Golgi apparatus, respectively. In addition, incubation of the adipose cells with insulin is without effect on the distribution of these marker enzyne activities among the three subcellular fractions studied here. However, the membrane fractions are far from pure and contain significant organelle cross-contamination.

Figure 3.2 shows the distribution of glucose transporters as assessed by D-glucose-inhibitable cytochalasin B binding. In membranes prepared from basal cells, the vast majority of glucose transporters (~90%) resides in the low-density microsomal membrane fraction enriched in marker enzymes of the Golgi apparatus, and the remainder is associated with the plasma and endoplasmic reticulum-enriched membranes. However, the distribution of glucose transporters in the latter two fractions is not in proportion to the galactosyltransferase activity found in the same fractions, suggesting that the intracellular pool of transporters may be localized to a unique membrane species or a specialized fraction of the Golgi apparatus. Insulin induces a profound change in the subcellular distribution of glucose transporters. The plasma membranes prepared from insulin-treated cells show a five-fold increase in the number of transporters compared to the plasma membranes from basal cells. Similarly, the number of glucose transporters in the high-density microsomal membranes is increased two-fold while that present in the low-density microsomal membranes is decreased by 50%. Attempts to quantitate the recovery of transporters are complicated by the inability to determine the total number of transporters in either the intact cell or the initial homogenate owing to the hydrophobic nature of cytochalasin B and the amount of lipid associated with the cells. However, in a detailed study (20) using marker enzyme recoveries and based on the assumption that the glucose transporters in the low-density microsomal fraction are recovered in the same proportion as the galactosyltransferase activity in that fraction, we have concluded that the total number of transporters is approximately 6 amol per cell, corresponding to approximately 3.6×10^6 transporters per cell, and is unaltered by exposure of the cell to insulin despite the marked change in their subcellular distribution.

The data discussed so far provide a static view of how insulin may induce a translocation of glucose transporters from an intracellular pool to the plasma membrane and thus give rise to an increase in transport. However, it is equally important to establish that this mechanism is compatible with the rapidity with which insulin is known to stimulate glucose transport activity.

2. KINETICS OF THE TRANSLOCATION PROCESS

Figure 3.3 illustrates the time course of the translocation process both in response to insulin and during its reversal induced by anti-insulin antibody. In these experiments, the adipose cells prepared from 96 rats were divided into six samples and incubated with either insulin or insulin followed by anti-

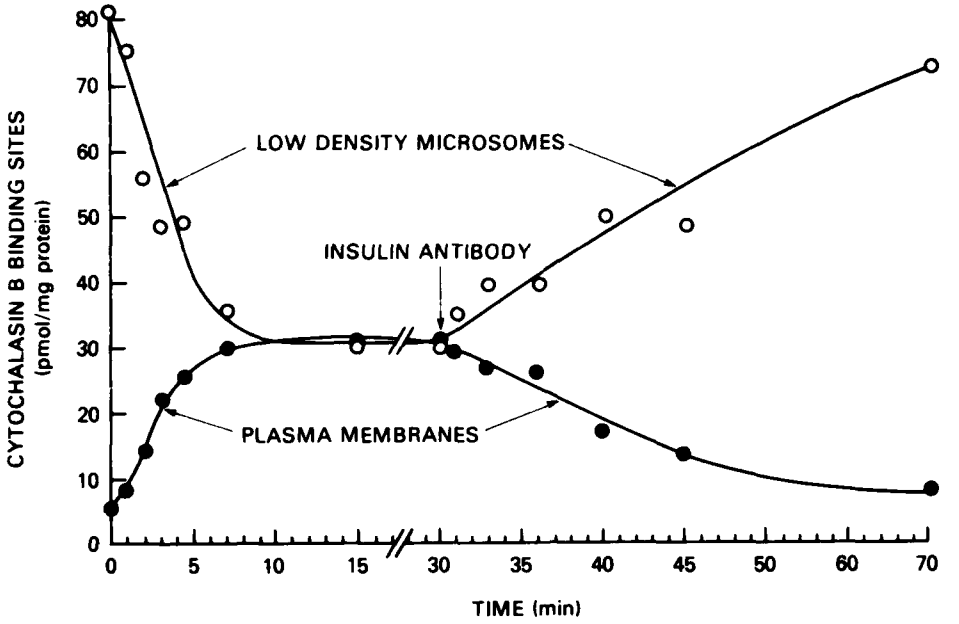

Figure 3.3. Time course of insulin's action on the distribution of glucose transporters and the reversal of insulin's action by anti-insulin antibody. Adipose cells from 96 rats were divided into six samples and incubated with insulin (0.7 n*M*) for the indicated times. The cells were then washed and homogenized, and plasma membrane and low-density microsomal membrane fractions were prepared (13). The numbers of D-glucose-inhibitable cytochalasin B binding sites in both fractions were determined as previously described (13, 20). In a separate series of experiments, adipose cells were incubated first with insulin (0.7 n*M*) for 30 min at 37°C to maximally stimulate glucose transport. A 300-fold excess of anti-insulin antibody was then added, and at the indicated times samples were removed and fractionated, and D-glucose-inhibitable cytochalasin B binding to the plasma membrane and low-density microsomal membrane fraction was determined.

insulin antibody for the indicated times. The cells were then fractionated and the cytochalasin B binding assessed in both the plasma membranes and low-density microsomes as described. The results demonstrate that the increase in the number of transporters seen in the plasma membranes with time after the addition of insulin is precisely paralleled by a decrease in the number of transporters in the low-density microsomal membranes. The half-times for these events are approximately 2.5 min. It should be pointed out that the data in these figures are expressed per milligram of membrane protein and that, at the time these experiments were performed, the ratio of recovered plasma membranes to recovered low-density microsomes was approximately 2:1. Hence the decrease in transporters in the low-density microsomal membrane fraction appears to be greater than the increase in the plasma membranes.

To demonstrate that this translocation process is reversible, we stimulated glucose transport with the minimum concentration of insulin required

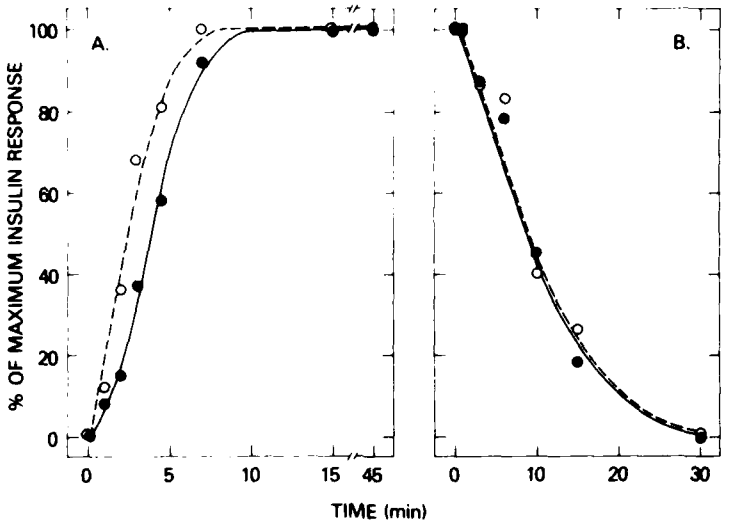

Figure 3.4. Comparison of the time courses of (A) insulin's action and (B) its reversal by anti-insulin antibody on the number of glucose transporters in the plasma membranes and the rate of 3-O-methylglucose transport in the intact rat adipose cell. The data shown in Fig. 3.3 are compared with the rates of 3-O-methylglucose transport (closed circles) measured in the isolated adipose cells immediately prior to homogenization (13). The results are expressed as percentages of the maximal insulin response.

for full stimulation over a 30-min period, added an approximately 300-fold excess of anti-insulin antibody to remove the insulin, and assessed the re-translocation of transporters with time (13). As seen in the forward direction, the loss of transporters from the plasma membranes closely parallels the increase in the number of transporters in the low-density microsomes, the half-times for both events being approximately 10 min.

A comparison of the changes in glucose transport activity measured in the intact cell with the appearance or removal of transporters from the plasma membranes is shown in Fig. 3.4. Upon stimulation of the cells with insulin, the appearance of glucose transporters in the plasma membranes precedes the increase in glucose transport activity, suggesting that the transporters are associated with the plasma membranes for a finite time before becoming functional. In contrast, upon removal of insulin with anti-insulin antibody, the decrease in transport activity directly corresponds to the decrease in the number of transporters in the plasma membranes, suggesting that the reverse translocation may proceed by means of a different mechanism.

3. PROPOSED MECHANISM OF INSULIN ACTION

Based on the data so far described, we have proposed the working model shown in Fig. 3.5 (13). Here, we envisage the stimulation of glucose trans-

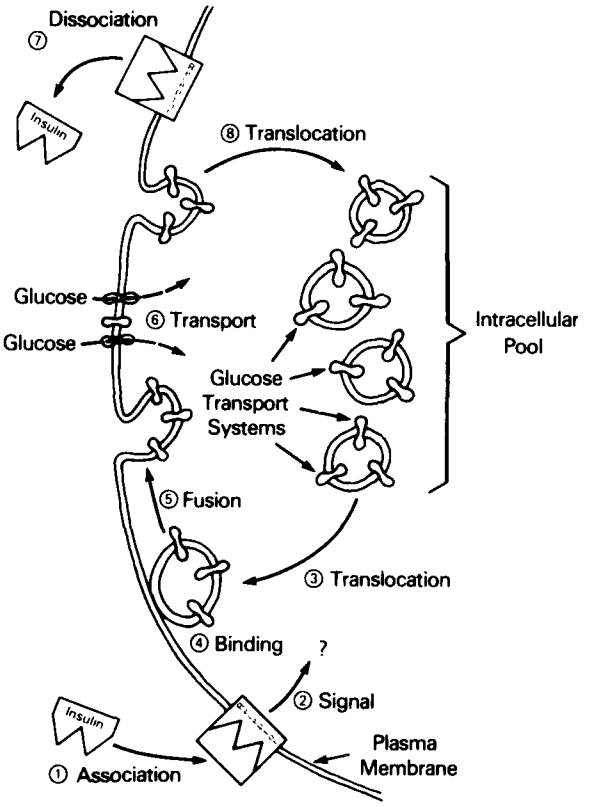

Figure 3.5. Schematic representation of a hypothetical mechanism of insulin's stimulatory action on glucose transport in the isolated rat adipose cell.

port to be initiated by the binding of insulin to its receptor (step 1), which in turn leads to the generation of a signal (step 2). We have represented the signal by a question mark since its precise nature remains unclear despite several theories and intensive investigation. In response to this signal, intracellular vesicles containing glucose transporters are translocated to (step 3) and become associated with (step 4) the plasma membrane of the cell, before their activity is expressed. The inclusion of this step was initially based on the kinetic data described in Fig. 3.4; however, more recent data, discussed later, have confirmed the existence of this intermediate step. Step 5, which we have depicted here as a membrane fusion, represents the point at which active glucose transporters are exposed to the extracellular medium and increased glucose transport activity can be observed (step 6). Finally, upon removal of insulin from its receptor (step 7), transporters are retranslocated to their intracellular location (step 8), apparently without passing through an intermediate complex comparable to that depicted at step 4.

Based on a completely different subcellular fractionation procedure and methodology for monitoring the translocation of the transporters, Dr. Kono

and his co-workers have proposed a translocation model very similar to that suggested in Fig. 3.5 (22). Using a continuous linear sucrose gradient to isolate the subcellular fractions, they directly assessed the distribution of glucose transporters by glucose transport measurements made in artificial liposomes reconstituted from the various subcellular fractions. Through this approach, they have demonstrated that neither the insulin-induced translocation of glucose transporters nor its reversal is protein synthesis-dependent (15). However, the movement of vesicles in either direction is energy-dependent, and both processes can be blocked by agents such as KCN or 2,4-dinitrophenol (15). They have further shown that insulinomimetic agents such as H_2O_2, concanavalin A, or vitamin K_5 stimulate glucose transport in the rat adipose cell by a mechanism identical to that of insulin (14).

Thus the basic translocation mechanism is quite well established. Other techniques used to confirm it include the use of antibodies against the human erythrocyte glucose transporter which cross-react with the rat adipose cell transporter (16, 26) and experiments that cross-link cytochalasin B directly to the glucose transporter (17). Both approaches have provided an estimate of a molecular weight of approximately 45,000, which is directly comparable to that observed for the human erythrocyte glucose transporter whose activity is not regulated by insulin. Additional recent studies have extended the cell types in which an insulin-induced translocation of glucose transporters is observed to include the rat diaphragm (23, 24) and the isolated human (6) and guinea pig (11) adipose cells, suggesting that this mechanism may well be ubiquitous.

In the remainder of this chapter, we discuss some of the approaches we are currently using to dissect the individual steps of the translocation mechanism.

4. EFFECTS OF TEMPERATURE ON THE TRANSLOCATION PROCESS

The first is an investigation of the effects of temperature on both the insulin-stimulated translocation of glucose transporters and its reversal (19). Figure 3.6A illustrates the time course of the stimulation of glucose transport in the intact cell at 16°C. The data are expressed as percentages of the maximal rate of insulin-stimulated transport seen at 37°C. At the indicated times, the stimulatory process at 16°C was rapidly stopped by the addition of KCN to 1 m*M*, and 3-O-methylglucose transport activity subsequently was assessed at 37°C. At this reduced temperature, insulin is clearly capable of stimulating glucose transport with a half-time for full stimulation only approximately double (~5 min) that observed at 37°C. Insulin is still able to stimulate glucose transport at temperatures below 16°C; however, the half-times for full stimulation become considerably longer. These data should now be contrasted with the data in Fig. 3.6B which shows the reversal of insulin-stimu-

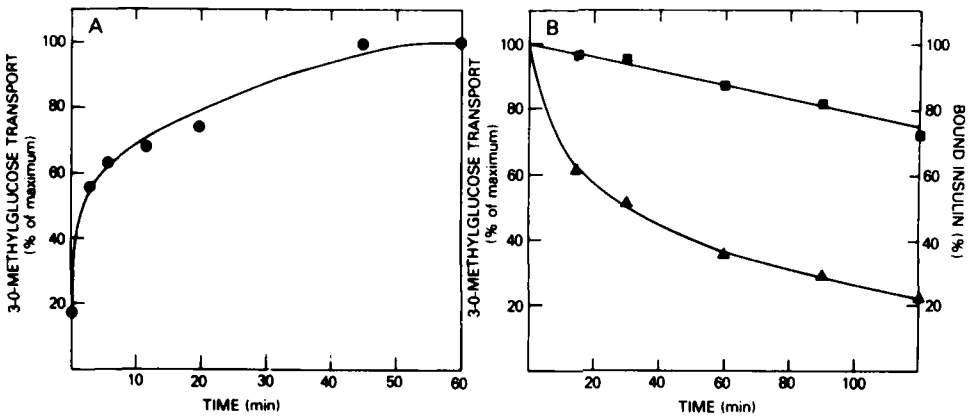

Figure 3.6. Time course at 16°C of (A) insulin's action and (B) its reversal by collagenase on the rate of 3-O-methylglucose transport in the isolated rat adipose cell. (A) Adipose cells were incubated at 16°C for the indicated times with 0.7 n*M* insulin. Stimulation was stopped by the addition of KCN to 1 m*M* before 3-O-methylglucose transport activity was assessed at 37°C. (B) Adipose cells were incubated with insulin (0.7 n*M*) for 1 h at 16°C to fully stimulate 3-O-methylglucose transport. Collagenase (3.3 mg/ml) was then added, and, at the indicated times, samples were removed for 3-O-methylglucose transport activity determination. In parallel experiments, tracer [^{125}I]insulin was mixed with cold insulin and specific insulin binding determined as previously described (5). The results are expressed as percentages of the maximal insulin response.

lated glucose transport at 16°C. In this case we have used collagenase to remove the bound insulin and the same KCN technique to arrest translocation. With this protocol, the reversal of insulin binding, which at 100% represents the amount of insulin bound at the minimum insulin concentration required to elicit a full response (0.7 n*M*), can be clearly distinguished from the reversal of glucose transport activity. The latter has a half-time on the order of 4–5 h. These data provide more conclusive evidence for the distinct nature of the steps involved in the incorporation of the glucose transporters into the plasma membrane and the steps involved in the retranslocation of glucose transporters to the intracellular pool.

Studies of the effects of temperature have also provided insight into the site of insulin action. By reducing the incubation temperature to 10°C (19) we have demonstrated a translocation of glucose transporters from the intracellular pool to the plasma membranes in the absence of a concomittant increase in glucose transport activity in the intact cell. However, upon the addition of insulin, the stimulation of glucose transport activity is observed with essentially no further translocation. A similar phenomenon is observed by incubating cells at 37°C in the presence of TRIS, a buffering agent that markedly promotes the insulin-induced down-regulation of the insulin receptor in this cell type (18). These observations raise the possibility that at least one of the major sites of insulin action is the promotion of the fusion step depicted by step 5 in Fig. 3.5.

5. EFFECTS OF ISOPROTERENOL ON THE TRANSLOCATION PROCESS

The counterregulatory actions of insulin on catecholamine-stimulated lypolysis in the rat adipose cell are well documented. However, the counterregulatory effects of catecholamines on insulin-stimulated glucose transport have not been observed until very recently (21). Figure 3.7A demonstrates the effects of isoproterenol on basal and insulin-stimulated glucose transport. The enzyme adenosine deaminase (ADA) has been included with the isoproterenol to remove any exogenous adenosine which is capable of inhibiting the actions of isoproterenol. The results show that incubation of cells with isoproterenol and ADA in combination leads to a 70% decrease in both basal and insulin-stimulated glucose transport activity as compared to the equivalent control cells. Furthermore, kinetic studies attribute this inhibition to a change in the maximum transport velocity and not to a change in the transporter's affinity for 3-O-methylglucose.

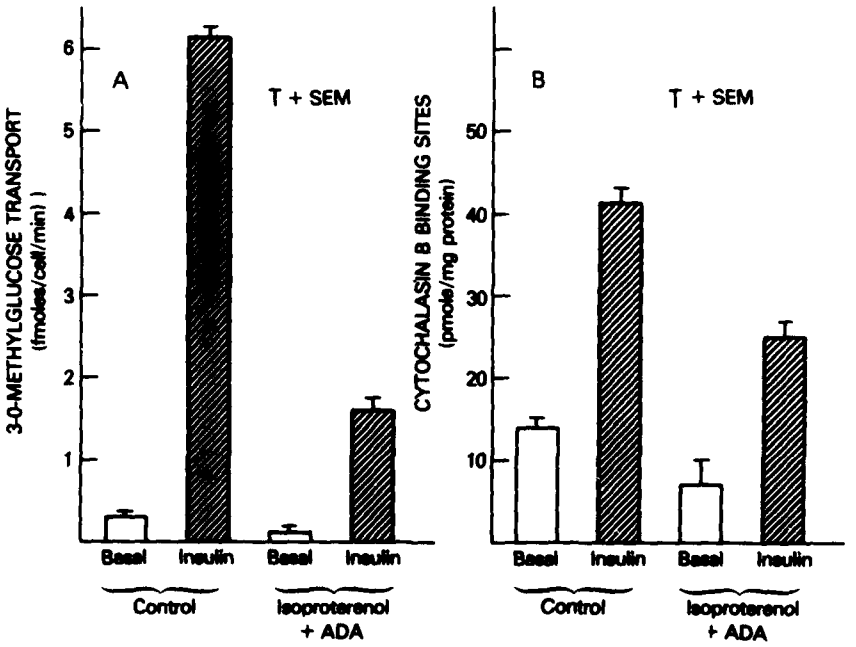

Figure 3.7. The effects of isoproterenol and adenosine deaminase on (A) basal and insulin-stimulated 3-O-methylglucose transport and (B) the distribution of glucose transporters in membranes from basal and insulin-treated cells. Isolated rat adipose cells were incubated in the absence or presence of insulin (7.0 n*M*) and in either the absence or presence of isoproterenol (1 μM) + adenosine deaminase (1 unit per milliliter) for 30 min at 37°C in a Krebs–Ringer bicarbonate buffer supplemented with 4% untreated bovine serum albumin. Following incubation, samples were removed to determine 3-O-methylglucose transport activity, and the remaining cells were washed and fractionated as previously described (20). D-glucose-inhibitable cytochalasin B binding to the plasma membranes was determined as previously described (13, 20).

Also shown in Fig. 3.7B are the effects of isoproterenol/ADA on the distribution of glucose transporters in plasma membranes prepared from basal and insulin-stimulated cells. Qualitatively, the effects are similar to those seen for transport. Quantitatively, however, the decrease in the number of transporters in the plasma membranes from both basal and insulin-treated cells with exposure to isoproterenol and ADA is significantly smaller than would be predicted from the inhibition of glucose transport. These data suggest the existence of another level of regulation capable of modulating both translocation and the intrinsic activity of the transporter. Alternatively, this cAMP-mediated effect could be counterregulating insulin's action at the fusion step (step 5 in Fig. 3.5), thus effectively preventing the exposure of functional transporters.

6. EFFECTS OF INSULIN-RESISTANT METABOLIC STATES ON THE TRANSLOCATION PROCESS

One aspect of our recent studies not yet discussed in this chapter is the link between the translocation mechanism and certain altered metabolic states in the rat that are associated with insulin resistance. We have ascertained in three such conditions, the aged, obese rat (10), the streptozotocin diabetic rat (12), and rats fed a high fat diet (9), that the inability of insulin to induce a full stimulation of glucose transport comparable to that seen in adipose cells from control rats can be directly attributed to a reduction in the number of glucose transporters in the intracellular pool. Under these circumstances, the translocation mechanism appears fully operational; however, fewer transporters are translocated to the plasma membrane with a consequent diminished glucose transport activity. Thus a third level of control of insulin-stimulated glucose transport activity that modulates the biosynthesis and/or degradation of glucose transporters can clearly be identified in the rat adipose cell. The interrelationship among these various levels of control and the mechanisms through which these controls alter individual steps within the overall translocation process remain to be elucidated. The mechanism we have proposed does, however, appear to be the first of a growing number of analogous systems in which expression of specific protein activities in the plasma membrane can be modulated by their subcellular distribution. It will, therefore, be of considerable future interest to examine whether these systems share common mechanisms with each other and/or with other endocytic/exocytic processes.

7. SUMMARY

The mechanism by which insulin stimulates glucose transport in the rat adipose cell has been shown to be a rapid, reversible, and energy-dependent

process. Stimulation is achieved by the translocation of glucose transporters from an intracellular pool to the plasma membrane where their insertion is ultimately responsible for the increase in transport activity. The reversal of this process also occurs rapidly at 37°C, with the transporters reappearing in the intracellular pool. The overall cycle thus appears as a reversible endocytic-exocytic process with the endocytic and exocytic steps showing markedly different kinetic properties. Studies of the effects of incubation temperature and TRIS confirm the existence of an intermediate state in which transporters are associated with the plasma membrane but incapable of transporting extracellular glucose. This suggests that insulin may act at the level of the plasma membrane at the step that results in the exposure of functional glucose transporters. The existence of a cAMP-mediated process capable of overriding the actions of insulin raises the possibility of a second level of control of glucose transport activity the significance of which remains to be assessed. Finally, a third control mechanism exists for regulating the absolute number of glucose transporters per cell that appears to be specifically affected in certain pathophysiological conditions in the rat.

ACKNOWLEDGMENTS

The authors wish to thank Mary Jane Zarnowski and Dena R. Yver for their expert technical assistance during this work and Louie Zalc for her typing of the manuscript. These investigations were supported in part by a research grant from The Kroc Foundation.

REFERENCES

1. Avruch, J. and Hoelzl-Wallach, D. F. (1971) *Biochim. Biophys. Acta*, **233**, 334–347.
2. Crofford, O. B. and Renold, A. E. (1965) *J. Biol. Chem.*, **240**, 14–21.
3. Crofford, O. B. and Renold, A. E. (1965) *J. Biol. Chem.*, **240**, 3237–3244.
4. Cushman, S. W. and Wardzala, L. B. (1980) *J. Biol. Chem.*, **255**, 4758–4762.
5. Cushman, S. W., Noda, D., and Salans, L. B. (1981) *Am. J. Physiol.*, **240**, E166–E174.
6. Cushman, S. W., Karnieli, E., Foley, J. E., Hissin, P. J., Simpson, I. A., and Salans, L. B. (1982) *Clin. Res.*, **30**, 388A (abstr).
7. Dallner, G., Siekevitz, G., and Palade, G. E. (1966) *J. Cell Biol.*, **30**, 97–117.
8. Fleischer, B. (1974) *Methods Enzymol.*, **31**, 180–191.
9. Hissin, P. J., Karnieli, E., Simpson, I. A., Salans, L. B., and Cushman, S. W. (1982) *Diabetes*, **31**, 589–592.
10. Hissin, P. J., Foley, J. E., Wardzala, L. J., Karnieli, E., Simpson, I.A., Salans, L. B., and Cushman, S. W. (1982) *J. Clin. Invest.*, **70**, 780–790.
11. Horuk, R., Rodbell, M., Cushman, S. W., and Wardzala, L. J. (1983) *J. Biol. Chem.*, **258**, 7425–7429.
12. Karnieli, E., Hissin, P. J., Simpson, I. A., Salans, L. B., and Cushman, S. W. (1981) *J. Clin. Invest.*, **68**, 811–814.

13. Karnieli, E., Zarnowski, M. J., Hissin, P. J., Simpson, I. A., Salans, L. B., and Cushman, S. W. (1981) *J. Biol. Chem.*, **256,** 4772–4777.

14. Kono, T., Robinson, F. W., Blevins, T. L., and Ezaki, O. (1982) *J. Biol. Chem.*, **257,** 10942–10947.

15. Kono, T., Suzuki, K., Dansey, L. E., Robinson, F. W., and Blevins, T. L. (1981) *J. Biol. Chem.*, **256,** 6400–6407.

16. Lienhard, G. E., Kim, H. K., Ranson, K. T., and Gorga, J. C. (1982) *Biochem. Biophys. Res. Commun.*, **105,** 1150–1156.

17. Shanahan, M. F., Olson, S. A., Weber, M. J., Lienhard, G. E., and Gorga, J. C. (1983) *Biochem. Biophys. Res. Commun.* **107,** 38–43.

18. Simpson, I. A., Martin, M. L., and Cushman, S. W. (1982) *Diabetes*, **31,** (Suppl. 2), 2A (abstr.).

19. Simpson, I. A., Zarnowski, M. J., and Cushman, S. W. (1983) *Fed. Proc.*, **42,** 1790 (abstr.).

20. Simpson, I. A., Yver, D. R., Hissin, P. J., Wardzala, L. J., Karnieli, E., Salans, L. B., and Cushman, S. W. (1983) *Biochim. Biophys. Acta*, **763,** 393–407.

21. Smith, U., Kuroda, M., and Simpson, I. A. (1984) *J. Biol. Chem.* **259,** in press.

22. Suzuki, K. and Kono, T. (1980) *Proc. Natl. Acad. Sci. USA*, **77,** 2542–2546.

23. Wardzala, L. J. and Jeanrenaud, B. (1981) *J. Biol. Chem.*, **256,** 7090–7093.

24. Wardzala, L. J. and Jeanrenaud, B. (1983) *Biochim. Biophys. Acta*, **730,** 49–56.

25. Wardzala, L. J., Cushman, S. W., and Salans, L. B. (1978) *J. Biol. Chem.*, **253,** 8002–8005.

26. Wheeler, T. J., Simpson, I. A., Sogin, D. C., Hinkle, P. C., and Cushman, S. W. (1982) *Biochem. Biophys. Res. Commun.*, **105,** 89–95.

CHAPTER 4

THE REGULATION OF THE Ca^{2+} TRANSPORT ACTIVITY OF SARCOPLASMIC RETICULUM

A. MARTONOSI
G. KRACKE
Department of Biochemistry
SUNY Upstate Medical Center
Syracuse, New York

K. A. TAYLOR
Department of Anatomy
Duke University Medical Center
Durham, North Carolina

L. DUX
Institute of Biochemistry
School of Medicine
University of Szeged
Szeged, Hungary

C. PERACCHIA
Department of Physiology
University of Rochester
Rochester, New York

The cytoplasmic Ca^{2+} concentration of skeletal muscle is regulated by an elaborate system of ATP-dependent Ca^{2+} pumps, $Na^{+}:Ca^{2+}$ exchangers, Ca^{2+} channels, and Ca^{2+}-binding proteins located in the surface membranes, transverse tubules, sarcoplasmic reticulum, mitochondria, and cytoplasm (56). Although the Ca^{2+} transport ATPase of sarcoplasmic reticulum is usually viewed as the dominant element in this hierarchy; in reality the various components of the system are tightly integrated and form an indivisible unit.

Kinetic studies provide a clear picture of the concentration, Ca^{2+} affinity, and mechanism of action of the individual components, but the principles and mechanisms that govern their integration are almost entirely unknown.

This chapter summarizes recent observations on the structure and regulation of the Ca^{2+} transport ATPase of sarcoplasmic reticulum, and speculates about the mechanisms that regulate its cellular concentration in response to physiological requirements.

1. THE STRUCTURE OF THE Ca^{2+} TRANSPORT ATPase OF SARCOPLASMIC RETICULUM

The Ca^{2+} transport ATPase is an intrinsic membrane protein of about 100,000 molecular weight (52, 59); (for review see ref. 58) that constitutes 60–70% of the protein content of sarcoplasmic reticulum membranes isolated from fast-twitch skeletal muscle (32). The amino acid sequence of five major hydrophilic segments amounting to nearly two-thirds of the total mass of the protein has been determined (1, 2, 4, 5). One of these segments contains the active site aspartyl residue that serves as phosphate acceptor for ATP during Ca^{2+} transport (3). The structure of the interposed hydrophobic sequences is unknown.

The hydrophilic regions of the protein are exposed on the cytoplasmic surface of the membrane, giving rise to 40-Å-diameter surface particles (Fig. 4.1) that can be visualized by negative staining (51). The density of the 40-Å particles ($\approx$16,000–20,000/μ^2, ref. 45) is close to the calculated density of ATPase polypeptide chains in the membrane; therefore we assume that each 40-Å particle corresponds to one ATPase molecule. High-resolution electron microscopy of negatively stained or rotary shadowed sarcoplasmic reticulum preparations reveals a substructure within the 40-Å particles that may reflect two major structural "domains" within the ATPase molecule (72, 87).

The intramembranous regions of the protein are seen by freeze-fracture electron microscopy as 85-Å diameter particles (Fig. 4.1) that are more numerous in the cytoplasmic than in the luminal fracture face (21); this is consistent with an asymmetric distribution of protein mass within the bilayer. The density of 85-Å intramembranous particles is about 4000/μ^2 (45). The 4 : 1 ratio of the density of 40-Å surface/85-Å intramembranous particles

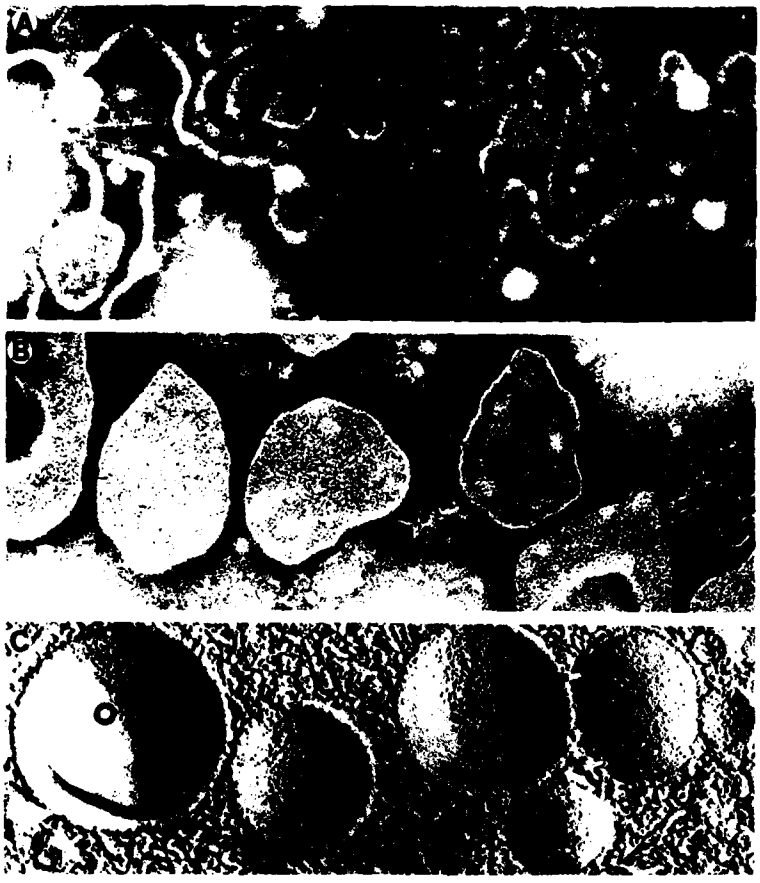

Figure 4.1. Electron microscopy of sarcoplasmic reticulum. (*A*) Mouse microsome preparations isolated from leg muscles of 40–50-day-old mice, negatively stained with 0.5% K-phosphotungstate. Magnification: ×88,000. (*B*) Reconstituted vesicles of the Ca^{2+} transport ATPase. Ca^{2+} transport ATPase isolated from rabbit skeletal muscle was reconstituted with soybean phospholipids. Negative staining with 1% K-phosphotungstate. Magnification: ×105,000. (*C*) Freeze-etch replicas of sarcoplasmic reticulum from muscles of 25-day-old chicken. Magnification: ×45,000. (Reproduced with permission from Tillack, et al., ref. 89.)

led to the proposition that the 85-Å particles represent clusters of several (probably four) ATPase molecules. The oligomer structure of Ca^{2+}-ATPase in phospholipid membranes is supported by ultracentrifuge, chromatography, and fluorescence energy transfer data obtained on detergent-solubilized and reconstituted Ca^{2+}-ATPase preparations (for a review see refs. 58, 66). The disposition of the hydrophobic segments within the membrane is entirely hypothetical. Although there is no physical evidence for the exposure of significant protein mass on the luminal surface of sarcoplasmic reticulum, transient penetration of structures involved in Ca^{2+} translocation is possible during some steps of the Ca^{2+} transport cycle.

2. THE MECHANISM OF Ca^{2+} TRANSPORT BY SARCOPLASMIC RETICULUM

The active accumulation of Ca^{2+} by sarcoplasmic reticulum is coupled to the hydrolysis of ATP by the Ca^{2+} transport ATPase. For each mole of ATP cleaved, two Ca^{2+} ions are translocated across the membrane (39, 58). The kinetics of Ca^{2+}-dependent ATP hydrolysis was extensively analyzed in several laboratories, and the scheme of Fig. 4.2 accounts for much of the observations (24).

The enzyme E_1 interacts with $2Ca^{2+}$ and 1ATP in a sequential reaction forming the $E_1{}^{2Ca}_{1ATP}$ complex (steps 1 and 2). The ATP is cleaved with transfer of terminal phosphate to the active site aspartyl group $\left(E_1{}^{P}_{2Ca}\right)$ followed by the release of ADP (step 3). The enzyme-bound Ca^{2+} is occluded in a form that is not released in the presence of EGTA. The free energy change connected with ATP cleavage is surprisingly small, and the ATP cleavage step is rapidly reversible, leading to ATP–ADP exchange. In step 4 the phosphorylated enzyme intermediate changes its conformation

$$E_1{}^{P}_{2Ca} \rightarrow E_2{}^{P}_{2Ca}$$

with a decrease of its affinity for Ca^{2+}. The release of Ca^{2+} on the membrane interior (step 5) is followed by the Mg^{2+}-catalyzed hydrolysis of $E_2{}^{P}$ intermediate (step 6) and the release of inorganic phosphate on the cytoplasmic side of the membrane (step 7). The cycle is completed by the return of the carrier from the E_2 to the E_1 conformation.

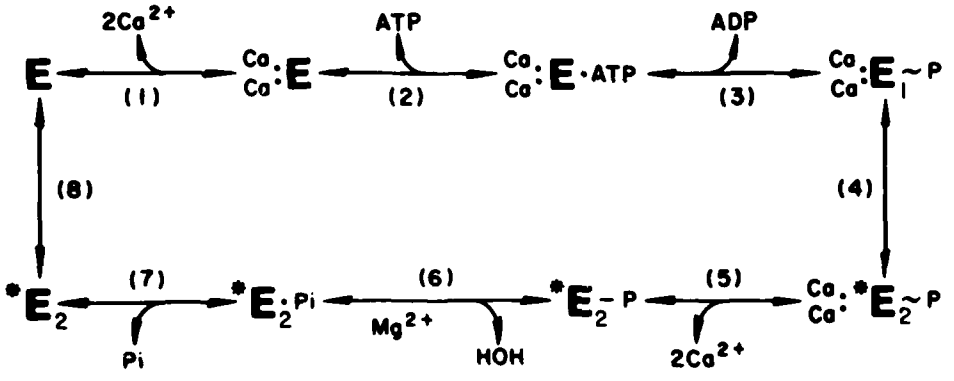

Figure 4.2. Reaction scheme of the Ca^{2+} transport ATPase. (Reproduced from De Meis and Vianna, ref. 24.)

The $2Ca^{2+}/1ATP$ stoichiometry of ATP-dependent active Ca^{2+} transport is preserved over Ca^{2+} gradients $[Ca_i]/[Ca_o]$ ranging from 1, at the beginning of the Ca^{2+} accumulation into microsomes, to approximately 1000, when the system approaches equilibrium. At first glance this would imply that the thermodynamic efficiency of the conversion of the free energy of ATP hydrolysis into the electrochemical Ca^{2+} gradient is less at the beginning of the Ca^{2+} transport ($[Ca_i]/[Ca_o] \simeq 1$) than near equilibrium ($[Ca_i]/[Ca_o] \simeq 1000$); therefore, if not obscured by heat changes connected with the binding of Ca^{2+} and other ions to the membranes, the heat liberation per mole of ATP hydrolyzed should decrease as $[Ca_i]/[Ca_o]$ increases. This prediction would not hold if osmotic work, like the mechanical work of muscle (Fenn effect), results in extra heat liberation or if the free energy change of ATP hydrolysis changes as the function of Ca^{2+} gradient. Calorimetric studies of this problem could shed new light on the energetic aspects of the transport process.

The Ca^{2+} transport is fully reversible. Release of accumulated Ca^{2+} in the presence of ADP and Pi leads first to a Mg^{2+}-dependent phosphorylation of the enzyme by inorganic phosphate, followed by Ca^{2+}-dependent transfer of the enzyme-bound Pi to ADP forming ATP. The net result is the formation of one mole of ATP for each two Ca^{2+} ions released across the membrane (38). Ca^{2+} release by reversal of Ca^{2+} transport requires low external $[Ca^{2+}]$, high external [ADP], $[Mg^{2+}]$ and [Pi], and the virtual absence of ATP, that is, conditions that do not exist in the cell. Therefore reversal of Ca^{2+} transport is not likely to play a significant role in Ca^{2+} release during muscle activation (57).

3. THE REGULATION OF ATPase–ATPase INTERACTIONS IN SARCOPLASMIC RETICULUM

Crystalline arrays of Ca^{2+}-ATPase develop in sarcoplasmic reticulum membranes exposed to vanadate (27, 28), phosphate (29), or lanthanide (31) ions.

3.1. Ca^{2+}-ATPase Crystals Induced by Na_3VO_4

The Ca^{2+}-ATPase crystals induced by vanadate contain ATPase dimers as structural units (86, 87). The ATPase dimers interact to form right-handed helical dimer chains on the surface of the crystalline tubules that associate with neighboring dimer chains into an extended cylindrical lattice (Fig. 4.3). Na_3VO_4 induces crystallization by acting as an analog of inorganic phosphate. Based on the generally accepted mechanism of Ca^{2+} transport, the vanadate-induced crystallization is presumed to arise from the stabilization of the E_2 conformation of Ca^{2+}-ATPase owing to the formation of a stable E_2-vanadate intermediate by reversal of reaction step 7 (Fig. 4.2). Inorganic phosphate induces crystallization by a similar mechanism, but the ATPase

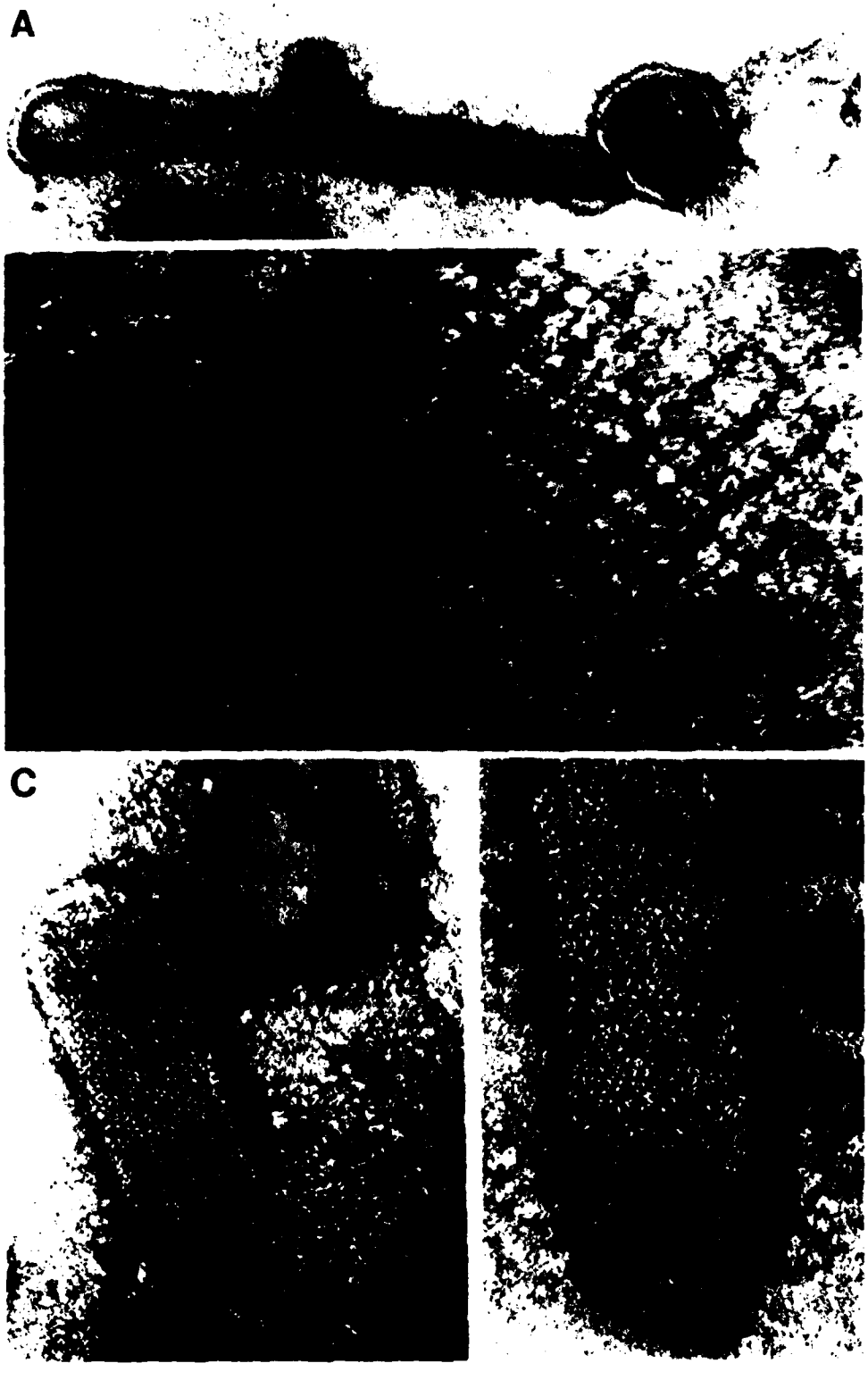
A
C

crystals formed with inorganic phosphate are less frequent and are disordered compared with the vanadate-induced crystals (29).

The crystallization of Ca^{2+}-ATPase by vanadate or inorganic phosphate is optimal at a medium Ca^{2+} concentration of 10^{-8} *M* or less. Raising the free $[Ca^{2+}]$ of the medium to 10^{-6}–10^{-5} *M* inhibits crystallization and disrupts preformed Ca^{2+}-ATPase crystals (29); we presume that Ca^{2+} shifts the conformational equilibrium of Ca^{2+}-ATPase in favor of the E_1 form by interaction with the high-affinity Ca^{2+}-binding site of the enzyme. ATP (5 m*M*) interferes with crystallization, presumably by the same mechanism.

The rate of crystallization is markedly influenced by membrane potential induced by ion substitution (11, 30). Under standard conditions several

Figure 4.3. Electron micrographs of crystalline arrays of Ca^{2+}-ATPase in rabbit sarcoplasmic reticulum. (*A*–*C*) Crystalline arrays of Ca^{2+}-ATPase formed in the presence of 0.1 *M* KCl, 10 m*M* imidazole pH 7.4, 5 m*M* $MgCl_2$, 0.5 m*M* EGTA, and 5 m*M* Na_3VO_4 at 2°C for 48 h, followed by negative staining with 1% uranyl acetate. The crystals are usually observed on the surface of elongated tubules that are close to 700 Å in diameter. In some cases the crystalline tubules emerge from spherical profiles, suggesting that formation of Ca^{2+}-ATPase crystals imparts the cylindrical shape on the vesicles. On spherical surfaces the arrays are less regular and occasionally absent. In early phases of crystallization, ATPase dimer chains are occasionally seen in the form of isolated strands that gradually enter into more regular lattice. In some cases (*B*, *C*) the crystalline arrays unravel, revealing dimer chains that adhere to the support film. Magnification: (*A*) 79,500; (*B*) 780,000; (*C*) 159,148. (*D*) Ca^{2+}-ATPase crystals induced by $GdCl_3$. Sarcoplasmic reticulum vesicles were incubated in 0.1 *M* KCl, 10 m*M* imidazole pH 7.2, 5 m*M* $MgCl_2$, and 10^{-6} *M* $GdCl_3$ at 2°C for 48 h, and samples were taken for negative staining with 1% uranyl acetate. Magnification: ×311,248. (*E*) Freeze-etched, rotary shadowed image of a crystalline array of Ca^{2+}-ATPase in rabbit sarcoplasmic reticulum. The crystals were induced with 5 m*M* Na_3VO_4, under conditions similar to those described in Fig. 4.3, (A–C). The micrograph is printed with reverse contrast. The ATPase dimers are arranged in chains oriented obliquely (arrow) to the long axis of the SR tubule. The inset shows an averaged image of ATPase dimer obtained by photographic superimposition of several dimers; each monomer of a dimer appears to contain two domains. The two arrows (in the inset) indicate the orientation of the long axis of the chain. Magnification: ×260,000; inset ×1,500,000.

hours are required for the formation of crystalline arrays of Ca^{2+}-ATPase over the surface of 50% of the vesicles. Inside positive potential produced by transfer of vesicles from choline–chloride into K-glutamate medium or from Na-methanesulfonate into K-methanesulfonate + valinomycin increases the rate of vanadate-induced crystallization to such extent that within one minute crystals form in about one-half of the vesicle population (30). Inside negative potential disrupts preformed Ca^{2+}-ATPase crystals (30). The effects of Ca^{2+}, ATP, and membrane potential on the vanadate-induced crystallization indicate that the interaction of ATPase molecules in the membrane depends on enzyme conformation and sensitively responds to physiologically important effectors.

Analysis of digital Fourier transforms calculated from images of the negatively stained crystalline arrays yielded the averaged electron density map shown in Fig. 4.4. The unit cell dimensions derived from low-dose electron micrographs are a = 65.9 Å, b = 114.4 Å, and γ = 77.9° (87). The space group of the crystal is P2. The space group and unit cell dimensions are consistent with ATPase dimers as structural units and lead to the proposition that the crystalline tubules are formed through lateral aggregation of right-handed helical chains made up of dimers of Ca^{2+}-ATPase molecules. The diameter of the crystalline tubules is about 600–700 Å; this implies that a lateral array of 9–10 dimer chains is required to cover the surface of the cylinder. The striking regularity of the shape of crystalline tubules implies that the curvature of the membrane surface is an important determinant of the stability of crystal lattice. So far we have not been able to produce flat crystalline "sheets" of the Ca^{2+}-ATPase, although such sheets are the preferred forms of two-dimensional crystals for most other membrane enzymes (47), including the Na^+,K^+-ATPase (40, 80).

3.2. Characterization of Bonds Involved in ATPase–ATPase Interactions

The formation of crystalline Ca^{2+}-ATPase arrays requires at least three types of ATPase–ATPase interactions. These bonds involve distinct regions of the ATPase molecules and are characterized by unique stabilities under various experimental conditions.

Ca^{2+}-ATPase Dimers (Site A). Excimers are defined as dimers that exist only within the lifetime of excited electronic states. Covalent labeling of the Ca^{2+} transport ATPase in sarcoplasmic reticulum vesicles with pyrenemaleimide at a dye/ATPase mole ratio of 1 : 2 gives rise to an excimer fluorescence with an emission maximum of about 460 nm (48). Since each ATPase molecule on the average contains less than 1 mole covalently bound pyrenemaleimide, the excimer fluorescence was taken to indicate interaction between ATPase molecules in the native membrane (48). Such interactions were inferred earlier from (1) Förster-type fluorescence energy transfer be-

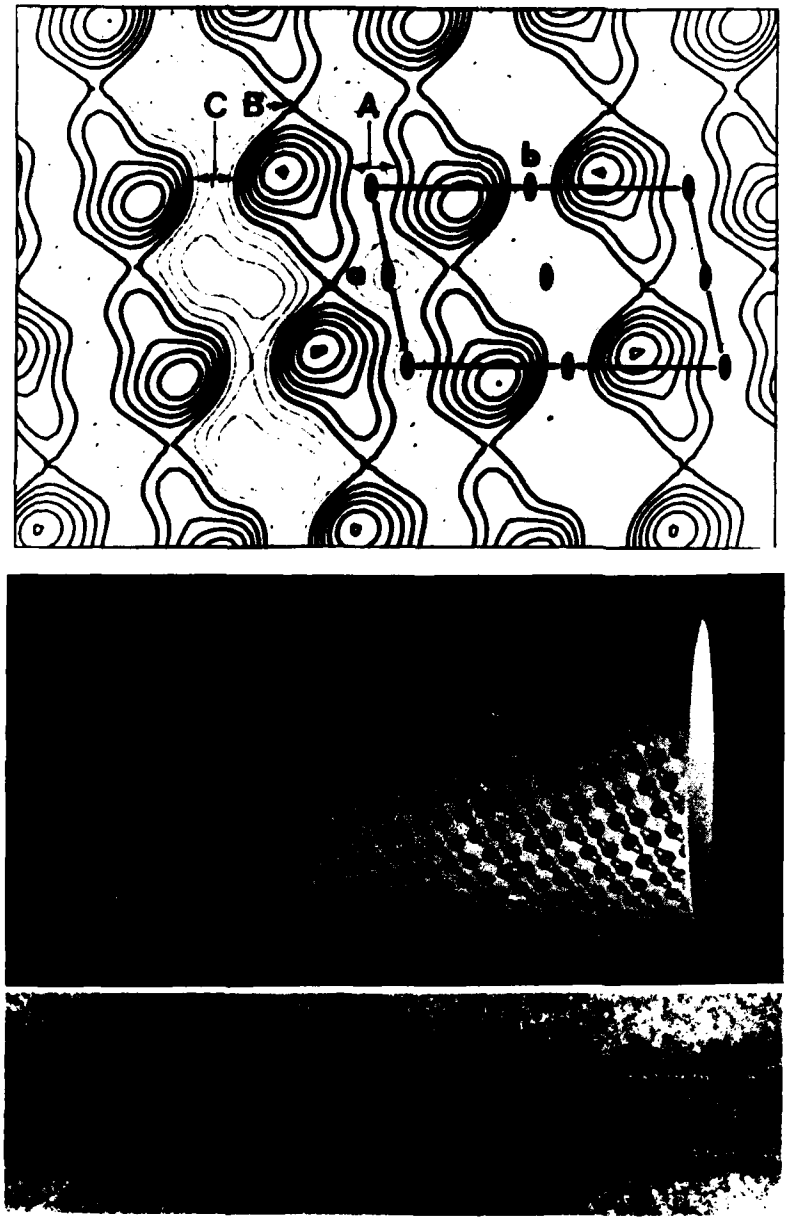

Figure 4.4. Electron density maps of Ca^{2+}-ATPase crystals. The density map (top figure) was calculated in space group P1 using the averaged structure factors of the low-dose data from electron micrographs. Heavy contours represent stain-excluding regions (protein), lighter contours represent negative stain. The unit cell as drawn contains ATPase dimers clustered around two-fold rotation axes at the corner of the unit cell. The ribbons of dimers that run parallel to the a axis of the crystal correspond to the right-handed helices in the electron micrograph (bottom figure) and in the computer-reconstructed density map folded into a cylinder (middle figure). The observer is looking at the outer surface of the tubule. The bonding regions involved in the formation of dimers (A), dimer chains (B) and extended lattice (C) are indicated. Top figure map scale: 0.306 mm/Å. Middle figure map scale: 0.0457 mm/Å. Bottom figure magnification: ×137,892. (For details see Taylor et al., ref. 87.)

tween ATPase molecules labeled with donor or acceptor fluorophores in reconstituted membranes (90, 94); (2) electron spin resonance studies (6); and (3) ultracentrifuge sedimentation and gel exclusion chromatography data on detergent-solubilized ATPase preparation (for review see ref. 66).

The excimer fluorescence of covalently bound pyrenemaleimide is insensitive to moderate concentrations of neutral detergents (Brij 35, Triton X-100, octylglucoside, $C_{12}E_8$; Fig. 4.5); to zwitterionic detergents of short alkyl chain length (Zwittergent 3-08; Fig. 4.6); to Ca^{2+} (10^{-5} *M*), and ATP (5 m*M*), that is, conditions that disrupt the vanadate-induced crystals of Ca^{2+}-ATPase. The pyrenemaleimide excimer fluorescence is inhibited by more powerful detergents (sodium dodecylsulfate, lysolecithin, sodium deoxycholate (Fig. 4.5), zwittergents 3-12 through 3-16 (Fig. 4.6), or brief heat treatment of microsomes (5 min at 70°C), together with inhibition of ATPase activity. The inhibition of excimer fluorescence in the presence of detergents is accompanied by an increase in the fluorescence of covalently bound pyrenemaleimide monomers measured at 375 and 395 nm (Fig. 4.5*A*, *B*; Fig. 4.6*A*, *B*).

The validity of pyrenemaleimide (PMI) excimer fluorescence as an indicator of ATPase-ATPase interactions depends to a large extent upon the presumed selective labeling of one SH group per ATPase molecule by pyrenemaleimide, under the conditions described by Ludi and Hasselbach (48).

Exhaustive peptic digestion of ATPase labeled with pyrenemaleimide at a mole ratio of 1 : 1 did not yield a distinct fluorescent PMI-peptide after separation by thin layer chromatography on silica-gel (Sil G-25, Macherey-Nagel and Co.) or on cellulose MN 300 (Cel 300-10, Macherey-Nagel and Co.) plates using the following solvent systems: *N*-butanol : acetic acid : H_2O, 400 : 100 : 100 (v/v), *n*-butanol : pyridine : acetic acid : H_2O, 244 : 378 : 76 : 302 (v/v), and isoamylalcohol : acetic acid : H_2O (v/v) 350 : 350 : 280 as solvents. These observations imply that the covalently bound PMI was distributed more or less evenly among several peptide bands and therefore reacts with several distinct SH groups within each ATPase molecule. Should this conclusion be confirmed by direct labeling of the ATPase with ^{14}C-pyrenemaleimide, the excimer fluorescence of PMI-labeled sarcoplasmic reticulum may have to be viewed as an *intramolecular* probe of conformational changes rather than an *intermolecular* indicator of interactions between ATPase molecules. The significance of the observations of Ludi and Hasselbach (48) and of the data presented in Fig. 4.5 and 4.6 with respect to the problem of ATPase-ATPase interactions thus depends upon the identification of the site(s) of reaction of PMI with the Ca-ATPase.

The functional significance of ATPase oligomers is still debated (66). Conditions that permit interaction between ATPase molecules increase the stability of the enzyme against inactivation by EGTA to the extent observed in native membranes and exert major influence upon the reactivity of SH groups with dithionitrobenzoate (DTNB). Comparative kinetic analysis of detergent-solubilized ATPase monomers, oligomers, and native sarcoplas-

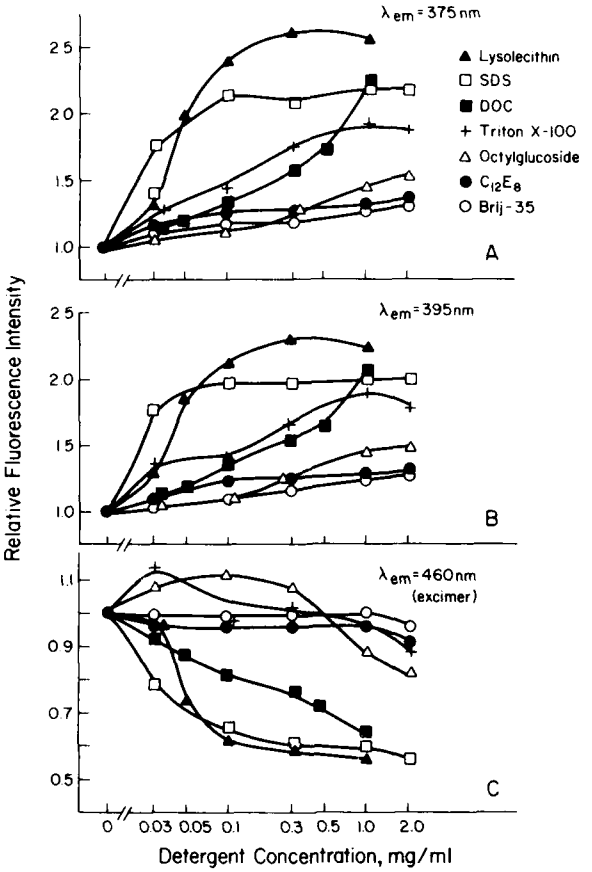

Figure 4.5. Effect of various detergents on the monomer and excimer fluorescence of *N*-(1-pyrene)maleimide labeled sarcoplasmic reticulum. To 0.1 mg of pyrenemaleimide labeled SR, suspended in 50-μl solution A (80 m*M* KCl, 5 m*M* $MgCl_2$, 0.5 m*M* Ca Cl_2, 0.45 m*M* EGTA, and 20 m*M* MOPS buffer, pH 7.0), 0–4 mg of detergents were added from a 10 mg/ml stock solution in 10 m*M* Tris-maleate pH 7.0. After 10-min incubation at 23°C, the mixture was diluted to 2.0 ml final volume with solution A, and the spectra were recorded. The final protein concentration was 0.050 mg/ml. The final detergent concentration ranged between 0.03 and 2 mg/ml. The emission spectra were recorded at an excitation wavelength of 342 nm. Excitation and emission slits were both 4 nm, and the temperature was 23°C. The relative fluorescence intensities at emission wavelengths of (*A*) 375 (*B*) 395, and (*C*) 460 nm were calculated from emission spectra. The emission maximum of the excimer band is at 460 nm (*c*); the fluorescence intensities of the detergent-containing solutions were normalized to the corresponding spectra recorded in the absence of detergents and plotted as the function of detergent concentration. Symbols: ▲, lysolecithin; □, sodium dodecylsulfate (SDS); ■, K-deoxycholate (DOC); +, Triton X-100; △, octylglucoside; ●, $C_{12}E_8$; ○, Brij-35.

For experiments with SDS, solution A was replaced with a K-free solution containing 0.15 *M* chlorine chloride, 5 m*M* $MgCl_2$, 0.5 m*M* EGTA, 0.45 m*M* $CaCl_2$, 10 m*M* histidine, pH 6.8. (G. Kracke and A. Martonosi, in preparation.)

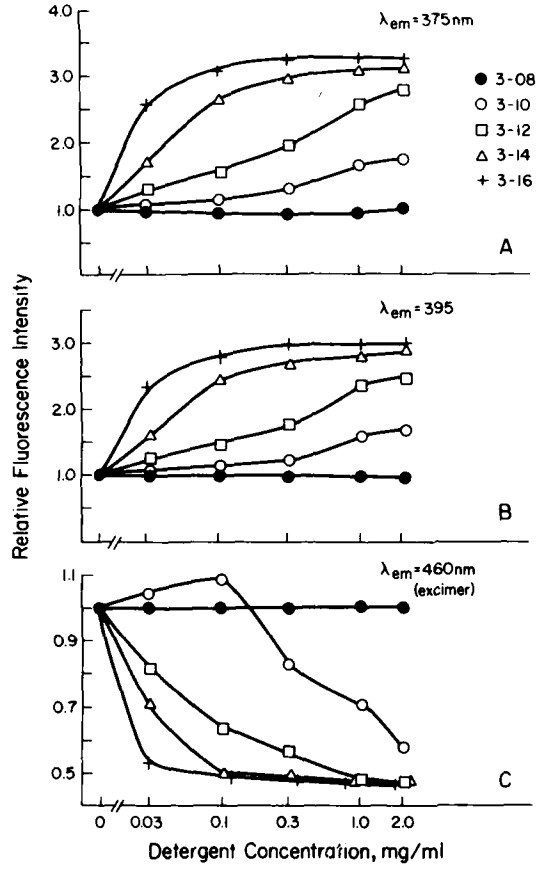

Figure 4.6. Effect of zwitterionic detergents on the monomer and excimer fluorescence of the *N*-(1-pyrene)maleimide labeled sarcoplasmic reticulum. The relative fluorescence intensities of the detergent-containing solutions measured at (*A*) 375 nm, (*B*) 395 nm, and (*C*) 460 nm were normalized to the corresponding spectra taken in the absence of detergent and plotted against the final concentration of the detergent. The emission maximum of the excimer fluorescence is at 460 nm (*C*). Symbols (Zwittergent alkyl chain length) ●, 3–08; ○, 3–10; □, 3–12; △, 3–14; +, 3–16. (G. Kracke and A. Martonosi, in preparation.)

mic reticulum membranes reveals only minor differences between them, suggesting that most elementary reaction steps of the Ca^{2+}-activated ATP hydrolysis can be performed by ATPase monomers. It remains to be determined whether the ATP-energized Ca^{2+} translocation across the membrane can also be catalyzed by ATPase monomers.

The Formation of Dimer Chains (Site B). Isolated chains of ATPase dimers were frequently observed during early phases of the vanadate-induced crystallization followed by lateral association into the extended crystal lattice (29). These observations imply that Ca^{2+}-ATPase dimer chains represent kinetically significant intermediates that accumulate during early phases of the crystallization.

The bonds that link the ATPase dimers into dimer chains (site B) are presumed to be located at the two ends of the pear-shaped ATPase profiles, where the electron density map reveals close contact between ATPase molecules (Fig. 4.4). Dimer chains of considerable length occur only in the presence of vanadate and EGTA, suggesting that stable interactions by way of site B are only possible between ATPase molecules of identical (E_2) conformation. Dimer chains were not observed even in the presence of vanadate if the medium contained 10^{-5} *M* Ca^{2+} or 5 m*M* ATP. The unique geometry of bond B is likely to contribute to the right-handed helical turn of the dimer chains on the surface of cylinders. Preferential association of dimers into tetramers may occur under the conditions of freeze-fracture electron microscopy (71, 72). This would account for the size of the 85-Å diameter intramembranous particles seen by freeze-etch electron microscopy and for the approximately 4 : 1 ratio of surface to intramembranous particles (45).

Separation of dimer chains was observed during hypotonic lysis of crystalline vesicles (29), suggesting that the bonds that stabilize the dimer chains (bonds A and B) are mechanically stronger than the bonds that link them into lateral register. Treatment of crystalline vesicles with 0.1–0.5 mg of Triton X-100 per milligram of protein disrupted the dimer chains, although it was insufficient to cause lysis of the vesicles and had little effect on the excimer fluorescence of pyrenemaleimide covalently attached to the Ca^{2+}-ATPase. These observations suggest that the interactions at bond B are influenced by the properties of the lipid phase of the membrane. The formation of dimer chains is probably governed by the mechanism of fibrous condensation (70) with a critical protein concentration significantly below the concentration of Ca^{2+}-ATPase in the membrane.

Formation of Crystal Lattice (Site C). Extended crystalline arrays form by lateral association of dimer chains (27, 86, 87), through contacts established by the contiguous regions of ATPase molecules depicted in Fig. 4.4 as the probable location of binding site C. The formation of dimer chains may create the necessary conditions for their subsequent association into crystalline arrays by proper orientation of the ATPase molecules. In line with this suggestion, isolated dimer chains are transient features during crystallization, and conditions that interfere with the formation of bonds at site B (Ca^{2+}, ATP, inside negative membrane potential, detergents, etc.) also inhibit lattice development. The existence of large amounts of isolated dimer chains observed during osmotic lysis of crystalline vesicles (Fig. 4.3) may be due to stabilization by the support film *in statu nascendi* (Fig. 4.3).

3.3. Crystallization of Ca^{2+}-ATPase by Lanthanide Ions

The lanthanide ions—gadolinium and lanthanum—effectively compete with Ca^{2+} for the high-affinity binding sites of Ca^{2+}-ATPase (36) and induce the

formation of a crystal lattice in sarcoplasmic reticulum that appears to be different visually from the vanadate-induced ATPase crystals (Fig. 4.3). Based on the reaction scheme of Ca^{2+} transport (Fig. 4.2), we assume that the Ca^{2+}-ATPase crystals induced by lanthanide ions reflect the stabilization of the E_1 conformation of the enzyme. If this assumption is correct, comparison of the Ca^{2+}-ATPase structures derived from the lanthanide E_1 and vanadate E_2 crystals should give detailed molecular information about the conformation change of the enzyme connected with Ca^{2+} translocation.

4. THE CONTROL OF CYTOPLASMIC [Ca^{2+}] BY SARCOPLASMIC RETICULUM

Sarcoplasmic reticulum alternates between two functional states during the contraction-relaxation cycle.

1. Contraction is initiated by Ca^{2+} release from sarcoplasmic reticulum, triggered by the depolarization of T tubules (for review see ref. 57). The details of the process are not clear, but a voltage-dependent charge movement during muscle activation indicates the involvement of a gated Ca^{2+} channel.
2. Muscle relaxation is caused by the active accumulation of Ca^{2+} into the sarcoplasmic reticulum. The rate of Ca^{2+} transport is regulated at several levels:
   a. Control of the activity of Ca^{2+}-ATPase by Ca^{2+} and pH.
   b. Ca^{2+}-ATPase isoenzymes.
   c. The effect of membrane lipid composition.
   d. The effect of membrane potential.
   e. The regulation of the cellular concentration of Ca^{2+}-ATPase.

The various mechanisms of regulation are discussed in turn.

4.1. Kinetic Regulation of Ca^{2+} Transport: The Effect of Substrates and pH

The Effects of Calcium. The concentrations of Mg and ATP are relatively constant during the contraction-relaxation cycle, and the short-term regulation of the Ca^{2+} transport activity of sarcoplasmic reticulum depends largely on the sarcoplasmic and intravesicular Ca^{2+} concentration. The sarcoplasmic Ca^{2+} concentration in resting skeletal muscle is about 10^{-8} *M* and may rise during muscle contraction to 10^{-6}–10^{-5} *M*. The Ca^{2+}-dependent ATPase activity of sarcoplasmic reticulum vesicles or solubilized ATPase preparations has an apparent Km_{Ca} of about 10^{-7} *M*, which reflects the affinity of the enzyme for Ca^{2+} in the E_1 conformation. The Ca^{2+} dependences of ATP

hydrolysis, enzyme phosphorylation, ATP : ADP exchange, and Ca^{2+} transport are similar and show positive cooperativity with a Hill coefficient close to 2; this is consistent with the $2Ca^{2+}$/1ATP stoichiometry of Ca^{2+} transport. As the Ca^{2+} concentration is increased above 10^{-4} *M*, an inhibition of ATPase activity is observed in solubilized or leaky vesicles, which is nearly complete at 10^{-2} *M* Ca^{2+}. The $Ki_{Ca} \simeq 10^{-3}$ *M* is assumed to reflect the affinity of the enzyme for Ca^{2+} in the E_2 conformation. These data were rationalized in terms of three sets of Ca^{2+} binding sites (43). The α sites ($K_{diss} \simeq 10^{-7}$ *M*) are involved in the recognition of Ca^{2+} on the cytoplasmic side of the membrane, whereas the γ sites ($K_{diss} \simeq 10^{-3}$ *M*) are the internal binding sites instrumental in the inhibition of the enzyme at high intravesicular Ca^{2+} concentration. The functional assignment of β sites is unclear. The inhibition of ATPase activity and Ca^{2+} transport at a [Ca^{2+}] of several millimolar reflects the shift of the equilibrium of step 5 in the reaction scheme shown in Fig. 4.2 in favor of the $E_2 \sim \overset{2Ca}{P}$ form.

In resting muscle essentially all the Ca^{2+} content is sequestered in the sarcoplasmic reticulum (83). Assuming a sarcoplasmic reticulum content of 5–10 mg SR protein per gram muscle, an SR volume of 5 μl/mg protein (25), and a total calcium content of approximately 2 μmol calcium per gram muscle, the estimated intravesicular Ca^{2+} concentration in sarcoplasmic reticulum of resting muscle is of the order of 10–20 m*M*. This implies that in resting muscle with a cytoplasmic Ca^{2+} concentration of 10^{-8} *M* and an intravesicular [Ca^{2+}] of 10–20 m*M* the [Ca^{2+}] pump is completely inhibited, and the dominant enzyme form is probably the $E_2 \sim \overset{2Ca}{P}$.

During activation of muscle contraction, Ca^{2+} is released from the sarcoplasmic reticulum. The amount of Ca^{2+} released during a single twitch is probably of the order of 0.5 μmol/g muscle. The rise in cytoplasmic [Ca^{2+}] and the corresponding decrease in intravesicular [Ca^{2+}] activate the Ca^{2+} pump. The activation is likely to involve a complex reaction sequence. As the Ca^{2+} pump in the resting muscle is probably trapped in the $E_2 \sim \overset{2Ca}{P}$ form, the decrease in intravesicular [Ca^{2+}] should first promote Ca^{2+} release from the $E_2 \sim \overset{2Ca}{P}$ (step 5) followed by the Mg^{2+}-catalyzed cleavage of $E_2 \sim P$ yielding inorganic phosphate (steps 6–7) and the return of the enzyme to the E_1 form (step 8). Only after the completion of these reactions can a new cycle of Ca^{2+} uptake begin. As isomerization of the E_2 into E_1 enzyme form (step 8) is usually viewed as a slow reaction (23), completion of steps 5–8 may introduce a significant lag between Ca^{2+} release and the initiation of the

reabsorption of Ca^{2+}. The reaccumulation of 0.5 μmol calcium per gram muscle with a Ca^{2+} pump content of 0.08 μmol/g muscle (i.e., about 10 mg SR protein per gram muscle) would require about three cycles of Ca^{2+} transport.

Posttranslational Modification of Ca^{2+}-ATPase. Ca^{2+}-calmodulin-dependent phosphorylation of Ca^{2+}-ATPase may alter the kinetics of Ca^{2+} transport (for review see ref. 34), but the significance of this process is not fully established.

The Effects of ATP. The complex dependence of Ca^{2+} transport and ATP hydrolysis on ATP concentration suggests that in addition to its role as substrate ($Km \approx 1\ \mu M$), ATP at higher concentration interacts with a regulatory site on the enzyme ($Km \approx 1$ mM) and activates ATP hydrolysis and Ca^{2+} transport (26, 91, 96). Since significant changes in ATP concentration do not accompany muscle contraction, and at a cytoplasmic ATP concentration of approximately 5 mM the regulatory site of ATP is near saturation, the regulatory significance of the low-affinity ATP-binding site is unclear.

The Effects of pH. The Ca^{2+} transport activity of sarcoplasmic reticulum is characterized by a pH optimum around pH 7.0 and a sharp decline of Ca^{2+} transport at mildly alkaline pH. The decrease in transport activity at alkaline pH is accompanied by an increase in the Ca^{2+} permeability of the membrane (25). Contrary to earlier suggestions (68, 82), the pH-induced changes in the transport activity and Ca^{2+} permeability of the membrane are not likely to play a physiological regulatory role in Ca^{2+} release, since the cytoplasmic pH during muscle contraction changes only by 0.004 pH units (8).

4.2. "Isoenzymes" of Ca^{2+}-ATPase in Muscles of Different Fiber Types and in Nonmuscle Cells

The ATP-dependent Ca^{2+} pump is present in the endoplasmic reticulum of all animal and plant cells that have been tested (56). The cellular concentration of the Ca^{2+} pump varies widely, depending on physiological requirements. In smooth, slow-twitch skeletal and cardiac muscles the sarcoplasmic reticulum is sparsely developed, compared with fast-twitch skeletal muscles, where it may constitute 90% of the total membrane mass of the cell.

Corresponding differences were observed in the Ca^{2+} transport activity of crude microsome preparations isolated from slow- or fast-twitch skeletal and cardiac muscles. In general there is good correlation between twitch velocity and the extent of development of sarcoplasmic reticulum. Particularly extensive development of sarcoplasmic reticulum is observed in the toadfish swim

bladder muscle that can perform 200–300 contractions per second (33), and in the fast-acting motor muscle of the lobster second antenna which must operate at high speed at low temperature (75).

The differences in Ca^{2+} transport activity are largely due to a higher concentration of Ca^{2+} pump molecules in fast-twitch as compared with slow-twitch muscles. There are two possible explanations of these findings:

1. Differences in Ca^{2+} pump density in the "sarcoplasmic reticulum" membranes of slow-twitch and fast-twitch muscles. In fact, the density of 85-Å intramembranous particles, usually associated with the Ca^{2+}-ATPase, differs only by a factor of 2 between sarcoplasmic reticulum membranes of slow and fast skeletal muscles (16), although the Ca^{2+} transport activity of isolated membranes differs by an order of magnitude.
2. Differences in the relative amount of sarcoplasmic reticulum as compared with other membrane elements in microsomes isolated from slow- as compared with fast-twitch muscle.

The second explanation is supported by the observation that the proportion of vesicles containing Ca^{2+}-ATPase crystals in microsome preparations isolated from rat muscles of different fiber types (semimembranosus, levator ani, extensor digitorum longus, diaphragm, soleus, heart) correlates well with the Ca^{2+}-ATPase content and Ca^{2+}-modulated ATPase activity (Table 4.1; ref. 32). This implies that the concentration of Ca^{2+}-ATPase in sarcoplasmic reticulum membranes of fast and slow skeletal and cardiac muscles differs only slightly. The low Ca^{2+} transport activity of crude microsome preparations isolated from red skeletal and cardiac muscles is due to the presence of large amount of contaminating non-SR membrane elements.

Since the crystalline arrays of Ca^{2+}-ATPase extend over much of the surface of the vesicles, the ATPase content of sarcoplasmic reticulum membranes in adult muscles of diverse fiber composition is close to physical saturation. Therefore the sarcoplasmic reticulum content of a given muscle in adult animals is probably regulated by changing the total amount of sarcoplasmic reticulum of relatively constant ATPase content, rather than by changing the concentration of Ca^{2+}-ATPase in the membrane. As the Ca^{2+} transport ATPase is cotranslationally synthesized on polysomes bound to the surface of the sarcoplasmic reticulum (for review see ref. 54), its synthesis and insertion may be inhibited when the membrane is fully saturated by the enzyme. The average distance between ATPase molecules in the membrane is only about 100–200 Å; therefore it is possible that the hydrophilic head portions of the ATPase molecules interfere with the attachment of the polysomes to the membrane, which causes the inhibition of ATPase synthesis when the ATPase concentration rises above a certain level. If this hypothesis is correct, the sarcoplasmic reticulum content of a muscle may be largely determined by the availability of relatively phospholipid-rich and

TABLE 4.1. COMPARISON OF CRYSTALLIZATION INDEX, Ca^{2+}-ATPASE CONTENT AND ATPase ACTIVITIES IN MICROSOMES FROM DIFFERENT MUSCLES

Muscle	Type	Crystallization Index[a]	ATPase Content (%)[b]	Ca^{2+}-Activated ATPase[c] (μmolPi/mg/min)	Vanadate-Inhibited ATPase[d] (μmolPi/mg/min)
Rat semimembr.	Fast glycolytic	36.22 ± 2.92 (3)	48.20	1.93	1.56
Rat lev. ani	Fast glycolytic	44.45 ± 4.90 (4)	59.27	2.30	2.24
Rat ext. dig. long.	Fast oxidative	40.45 ± 10.25 (4)	47.00	1.29	0.97
Rat diaphragm	Mixed oxidative	32.77 ± 8.10 (4)	30.68	1.68	1.74
Rat soleus	Slow oxidative	10.71 ± 6.28 (4)	16.30	0.36	0.45
Rat heart	—	6.01 ± 3.01 (5)	8.49	0.30	0.21
Rabbit longiss. dorsi and quadr. fem.	Fast glycolytic	65.87 ± 10.80 (3)	61.1	—	—
Rabbit soleus	Slow oxidative	6.32 ± 3.39(15)	18.3	—	—

[a] The crystallization of Ca^{2+}-ATPase was induced by Na_3VO_4 as described in Fig. 4.3. The crystallization index gives the number of vesicles with crystalline regions on portions of their surface expressed as percent of the total number of vesicles. The presence of clearly identifiable crystalline regions on the surface of a vesicle implies that it is derived from the sarcoplasmic reticulum. The number of experiments is in parentheses.

[b] The ATPase content was determined by computerized densitometry of SDS gel electrophoretic patterns of solubilized microsomes from various sources.

[c] The Ca^{2+}-activated ATPase activity was measured as described earlier (14) in a medium of 0.1 *M* KCl, 10 m*M* imidazole pH 7.4, 5 m*M* $MgCl_2$, 0.5 m*M* EGTA, 5 μ*M* A23187, 0.45 m*M* $CaCl_2$, and 5 m*M* ATP at 25°C. Fore measurement of the Ca^{2+}-insensitive ATPase the $CaCl_2$ was omitted.

[d] The vanadate inhibition of ATPase activity was tested in the presence of 1 m*M* Na_3VO_4 (32).

ATPase-poor membrane surfaces with attachment sites for Ca^{2+}-ATPase polysomes.

The dimensions of the Ca^{2+}-ATPase crystal lattice are similar in SR membranes of different types; therefore if structural differences exist between "isoenzymes" of Ca^{2+}-ATPase, these are not reflected in the crystal lattice. Although the existence of Ca^{2+}-ATPase isoenzymes in different fiber types remains a distinct possibility, the kinetic (85, 93) and immunological (19, 22, 92), evidence now available does not prove their existence conclusively. The relatively small kinetic differences between Ca^{2+} pumps of fast and slow skeletal or cardiac muscles may arise entirely from differences in lipid composition (15). The observed immunological differences pose a dilemma in view of the strong cross-reaction between antibodies against the Ca^{2+} transport ATPase of rabbit sarcoplasmic reticulum and the Ca^{2+} pump isolated

from the slime mold (99). Clearly, data are needed on the amino acid sequence of Ca^{2+}-ATPases isolated from muscles of different fiber types within a given species to substantiate the claim of the existence of structurally distinct Ca^{2+}-ATPase isoenzymes. Similarly, the interpretation of the observed changes in the Ca^{2+} transport activity of sarcoplasmic reticulum after cross-innervation or chronic stimulation (46) requires clear demonstration that, in addition to changes in the cellular concentration of pump molecules, changes in "isoenzyme" composition also occur.

4.3. The Effect of Membrane Lipid Composition

The Ca^{2+} transport activity of sarcoplasmic reticulum is absolutely dependent on membrane phospholipids (50, 58, 61, 62). Based on reconstitution experiments with phospholipids of known fatty acid composition, optimum Ca^{2+} transport activity is defined largely by the chain length and unsaturation of the fatty acyl residues, without evidence for unique requirement for specific phospholipids (for reviews see refs. 12, 58). These observations suggest that the "microviscosity" of lipids in the environment of the protein exerts influence upon the motion of polypeptide chains involved in ATP hydrolysis and Ca^{2+} transport. Therefore it is conceivable that dietary changes in lipid composition could influence the Ca^{2+} transport activity. There is no convincing evidence that this is indeed the case. Although alterations in the fatty acid composition of sarcoplasmic reticulum have been detected in animals maintained on special diets (81, 97), the changes in Ca^{2+} transport activity, if any, were only marginal. Similarly, the massive rearrangement of fatty acid composition that occurs during development of chicken embryos *in ovo* leaves the specific Ca^{2+} transport activity of pump molecules essentially unaffected (14, 53).

In reconstituted ATPase preparations after complete replacement of membrane phospholipids with dipalmitoylphosphatidylcholine or dioleoylphosphatidylcholine, the specific ATPase and Ca^{2+} transport activities assayed at 37°C changed only slightly (69); sharp reduction in these activities was observed in reconstituted dipalmitoylphosphatidylcholine-ATPase vesicles only at temperatures below 30°C (69).

These observations suggest that, within the range encountered under physiological conditions, changes in the fatty acid composition of membrane phospholipids are not expected to have significant influence on the Ca^{2+} transport activity of sarcoplasmic reticulum. Adaptive changes in lipid composition may be more important in the maintenance of Ca^{2+} pump activity during hibernation or in the adjustment to seasonal temperature changes in poikilotherm animals (fishes, frogs, etc.) and plants, but there is no conclusive evidence that this is indeed the case.

The lipid composition of microsome preparations isolated from red, white, and cardiac muscles are significantly different (15). It remains to be determined whether some of the kinetic differences in Ca^{2+} transport activ-

ity between these preparations (93) are attributable to the differences in lipid composition.

4.4. The Effect of Membrane Potential

Ca^{2+} transport into sarcoplasmic reticulum vesicles generates inside-positive membrane potential (9, 10, 98). Inside-positive potential generated by ion substitution inhibits whereas inside-negative potential accelerates (Fig. 4.7) the rate of Ca^{2+} transport and Ca^{2+}-dependent ATP hydrolysis (9, 10). Dilution of vesicles equilibrated in K-glutamate into a medium of Na-glutamate

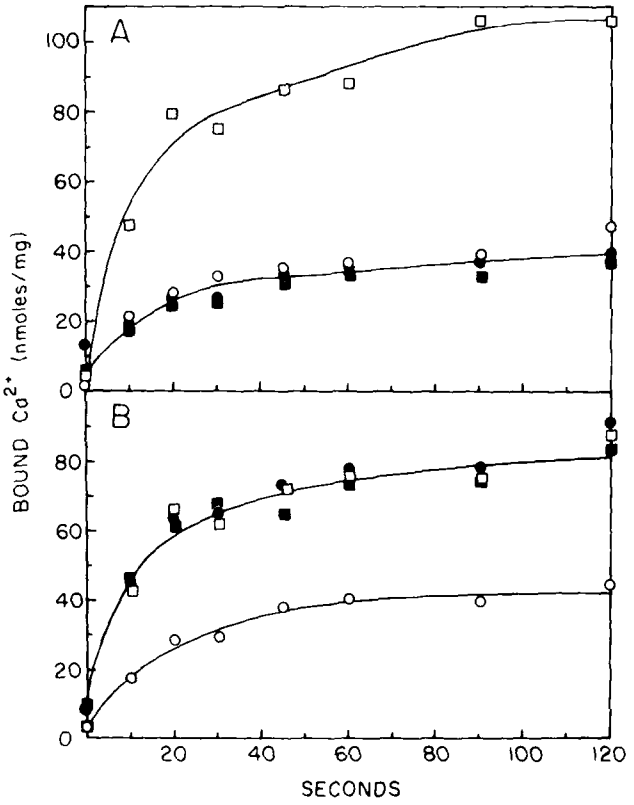

Figure 4.7. Effect of membrane potential on calcium transport by sarcoplasmic reticulum vesicles (*A*) Sarcoplasmic reticulum vesicles (32 mg protein per milliliter) equilibrated in 0.15 *M* choline-Cl (○, ●) or 0.15 *M* K-glutamate (□, ■), 10 m*M* imidazole (pH 6.6) and 1 m*M* Mg-maleate were diluted 100-fold into 0.15 *M* choline-Cl, 10 m*M* imidazole (pH 6.6), 1 m*M* Mg-maleate, and 120 μM ^{45}Ca-maleate (1 μCi/ml) at 15°C. Ca^{2+} uptake was initiated with 1.0 m*M* ATP at the time of dilution (○, □) or 1 h later (●, ■) after the microsomes had equilibrated with the dilution medium. Aliquots (200 μl) were removed at various times after initiation of Ca^{2+} uptake and passed through Millipore filters. The filters were washed with dilution medium containing 5 m*M* EGTA in place of ^{45}Ca maleate. (*B*) Similar to the foregoing experiment, but the dilution medium contained 0.15 *M* K-glutamate instead of choline-Cl. (Reproduced with permission from Beeler et al., ref. 10.)

plus valinomycin gives rise to negative potential that is rapidly abolished by Ca^{2+} transport initiated with the addition of ATP (10). These observations clearly establish that the ATP-dependent Ca^{2+} transport by sarcoplasmic reticulum is electrogenic and that pump-mediated Ca^{2+} fluxes are influenced in a predictable manner by membrane potential.

The positive potential generated during Ca^{2+} transport is much smaller than would be expected considering the electrical properties of biological membranes and the transfer of four positive charges per transport cycle. The small magnitude and transient nature of the pump-generated potential is the result of compensating ion fluxes through cation and anion channels in sarcoplasmic reticulum (25, 45, 58).

A fluorescence change of the voltage-sensitive dye Nile Blue A accompanies Ca^{2+} release from sarcoplasmic reticulum during muscle activation (13); the direction of the signal is consistent with the development of a negative potential in the sarcoplasmic reticulum. The subsequent Ca^{2+} uptake begins while the negative potential is still present. The negative potential generated by Ca^{2+} release is expected to speed up the reaccumulation of calcium into the sarcoplasmic reticulum that, in turn, will abolish the negative potential. Such interaction between membrane potential and Ca^{2+} fluxes may in part explain that the calculated rate of Ca^{2+} uptake during relaxation of living muscle is faster than the maximum rate of Ca^{2+} uptake measured in isolated vesicles *in vitro*. In resting muscle there is no demonstrable transmembrane potential across the sarcoplasmic reticulum (83).

The effect of membrane potential upon Ca^{2+} pump activity suggests that the conformation of the Ca^{2+}-ATPase in the membrane is influenced by the electrical field. A particularly striking demonstration of such an effect is the marked acceleration of the vanadate-induced crystallization of Ca^{2+}-ATPase in sarcoplasmic reticulum membrane by inside-positive membrane potential induced by ion substitution (30) (Fig. 4.8). Inside-negative membrane potential caused disruption of preformed Ca^{2+}-ATPase crystals within seconds (Fig. 4.8). The effects of membrane potential on the rate of Ca^{2+} transport imply that the rate-limiting step of the process is potential sensitive. The identification of this reaction step is in progress using stopped-flow fluorescence techniques.

4.5. The Regulation of the Cellular Concentration of Ca^{2+}-ATPase

The Ca^{2+} transport ATPase of sarcoplasmic reticulum is synthesized on membrane-bound polysomes (18, 35, 74), and it is inserted cotranslationally into the membrane without glycosylation or the cleavage of a signal peptide (18, 67). The NH_2-terminal methionine group of the ATPase, derived from initiator methionyl tRNA, is acetylated during translation (74).

The regulation of the concentration of Ca^{2+}-ATPase in the muscle cells has been extensively investigated during embryonic development *in vivo* and

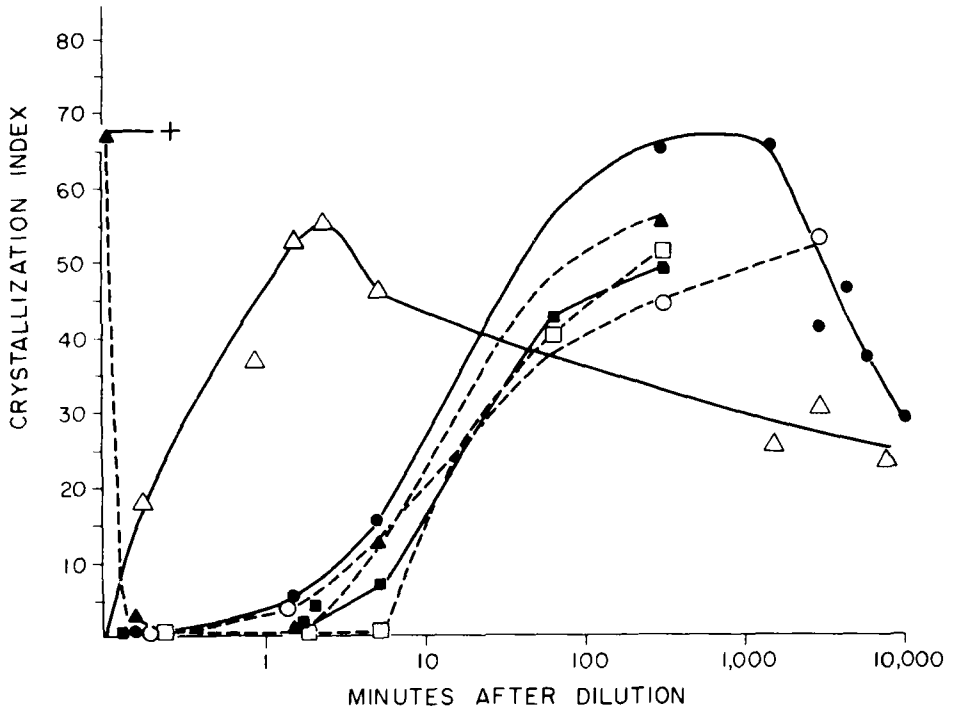

Figure 4.8. Effect of potential on the rate of crystallization of Ca^{2+}-ATPase. Sarcoplasmic reticulum vesicles (10 mg of protein per milliliter) were equilibrated for 16 h at 2°C in solutions of the following composition: solution A, KG, 0.15 *M* K-glutamate, 10 m*M* imidazole, 5 m*M* $MgCl_2$, 0.5 m*M* EGTA, without Na_3VO_4 (○, ■) or with 5 m*M* Na_3V_4 (+, ▲); solution B, CCl, 0.15 *M* choline chloride, 10 m*M* imidazole, pH 7.4, 5 m*M* $MgCl_2$, 0.5 m*M* EGTA without vanadate (△, □). The preequilibrated suspensions were diluted tenfold in solution A, containing 5 m*M* Na_3VO_4 (+, △, ■) or in solution B containing 5 m*M* Na_3VO_4 (▲, ○, □). The crystallization index was determined at indicated intervals after dilution. Dilution of vesicles from KG into CCl medium is expected to generate inside-negative membrane potential, whereas dilution from CCl into KG medium, inside-positive potential. Dilution of vesicles from KG into KG or from CCl into CCl medium does not generate diffusion potential; therefore these systems serve as control. For measurement of the rate of crystallization under standard conditions (●) sarcoplasmic reticulum vesicles (25 mg of protein/per milliliter) in 0.25 *M* sucrose, 10 m*M* Tris-Cl, pH 8.0, and 0.3 m*M* dithiothreitol were diluted 25-fold into a medium of 0.1 *M* KCl, 10 m*M* imidazole, pH 7.4, 5 m*M* $MgCl_2$, 0.5 m*M* EGTA, and 5 m*M* Na_3VO_4. The crystallization index is defined as the number of vesicles with crystalline regions on their surface expressed as percent of the total number of vesicles counted by four independent observers in randomly selected electron micrographs. The rate of crystallization was not affected by increasing the EGTA concentration of the dilution medium from 0.5 to 1 or 5 m*M*. The Ca^{2+} ionophore A23187 only slightly increased the rate of crystallization under standard conditions and did not significantly influence the accelerating effect of positive potential on the crystallization rate. (Reproduced with permission from Dux and Martonosi, ref. 30.)

in tissue culture (for review see refs. 54, 65). In the last week of development *in ovo* the rates of contraction and relaxation of chicken skeletal muscles increase severalfold (73), accompanied by changes in the electrical properties of the surface membrane (84), in the Ca^{2+} sensitivity of actomyosin (41), and a 10–20 fold increase in the Ca^{2+} transport activity of sarcoplasmic reticulum (14, 53, 54). The increase in Ca^{2+} transport activity (Table 4.2) is due to an increase in the concentration of Ca^{2+}-ATPase in the membrane, shown by SDS polyacrylamide gel electrophoresis, active-site labeling with ^{32}P-ATP, and by the increase in the density of surface and intramembranous particles seen by negative staining and freeze-etch electron microscopy (7, 14, 64, 89). In spite of marked changes in the ATPase/lipid ratio and in the fatty acid composition of membrane lipids (14), the specific Ca^{2+} transport activity of pump molecules remains constant throughout development (53). Essentially similar observations were made in developing rabbit muscle (77, 78, 92, 99).

The gradual increase in the Ca^{2+}-ATPase content of sarcoplasmic reticulum during embryonic development is consistent with the hypothesis (14, 53, 54, 65) that the phospholipid-rich rough endoplasmic reticulum of embryonic muscle is gradually converted during development into Ca^{2+}-transporting

TABLE 4.2. DEVELOPMENTAL CHANGES IN THE STRUCTURE AND COMPOSITION OF SARCOPLASMIC RETICULUM IN CHICKEN PECTORALIS MUSCLE[a]

Days of Development	Ca^{2+} Transport Activity (μmol Ca^{2+}/mg min)	Ca^{2+}-Modulated ATPase (μmol P_i/mg min)	Phosphorylated Intermediate E ~ P (nmol/mg protein)	ATPase Content from Gel Electrophoresis, Total Protein (%)	85-Å-Diameter Freeze-Etch Particle Density (per μm surface area)	
					In Isolated Microsome	In Whole Muscle
10	0.015	0.02	0.12	2	186	212
12	0.025	0.03	0.18			
14	0.034		0.22	6	352	462
16	0.060	0.08	0.31		405	
18	0.089			12		826
21 (hatching)	0.120	0.15	0.50			
22	0.200	0.19	0.87		1257	
26	0.32	0.35	1.35	55		3800
33	0.41	0.42	1.86	62		
46	0.60	0.70	2.20	65	2750	4330

[a] For technical details see refs. 14 and 89.

sarcoplasmic reticulum by stepwise insertion of the Ca^{2+}-ATPase and other components into the membrane. The symmetrical disposition of sarcoplasmic reticulum in the two halves of the sarcomere in mature muscle may imply the existence of central growth regions located in the middle of the A zone, where preferential insertion of ATPase molecules may take place during later phases of development. The relatively even distribution of Ca^{2+}-ATPase in the longitudinal tubules and the terminal cisternae is presumably achieved by lateral diffusion of ATPase molecules. The cotranslational insertion of Ca^{2+}-ATPase molecules is expected to proceed until the membrane approaches physical saturation. In mature sarcoplasmic reticulum the average distance between ATPase molecules is only 100–200 Å; that may prevent further attachment of bound polysomes and inhibit the synthesis and/or insertion of ATPase molecules. Therefore the synthesis of Ca^{2+}-ATPase required for the slow turnover of the enzyme in adult muscle (60) may be largely confined either to special growth regions of adult muscle fibers (49, 54) or to young, relatively immature muscle cells that are present even in fully developed muscle tissues. The coexistence of muscle fibers of different maturity may also explain the observation that the density of 85-Å intramembranous particles in sarcoplasmic reticulum vesicle populations isolated at different stages of development varies over a relatively wide range (89).

The major conclusions derived from studies on SR development *in vivo* were confirmed in tissue culture, with some further insight into the mechanism of regulation of the synthesis of Ca^{2+} transport ATPase. The accumulation of Ca^{2+}-ATPase begins during the fusion of myoblasts into myotubes and continues during the next 10 days of development accompanied by a large increase in the amount of contractile proteins (37, 42, 64). The accumulation of Ca^{2+}-ATPase did not occur in chicken muscle cultures grown in low-Ca^{2+} medium ($\simeq 100\ \mu M\ Ca^{2+}$) that inhibited fusion (37). As inhibition of the fusion of rat muscle cells with cytochalasin B did not interfere with the development of sarcotubular elements (17) the inhibition observed in low-Ca^{2+} medium is probably the direct consequence of Ca^{2+} deficiency. It is reasonable to assume that medium Ca^{2+} concentration regulates the synthesis and/or degradation of intracellular enzymes, including the Ca^{2+}-ATPase, by means of changes in the cytoplasmic free Ca^{2+} concentration.

Differential gene expression may imply regulation at the following levels: (1) gene transcription; (2) gene loss or amplification; (3) DNA transposition or modification; (4) RNA processing and transport; (5) mRNA translation; (6) mRNA stability and turnover; (7) posttranslational modification, intracellular transport, and insertion of proteins into membranes; (8) activation, inhibition, or modification of proteins as a result of interaction with other proteins or lipids in the membrane; (9) recycling and degradation of proteins. The regulation of Ca^{2+} transport ATPase utilizes several of these control mechanisms.

A hypothesis was proposed in which changes in intracellular free Ca^{2+}

concentrations are assumed to influence the rate of synthesis of Ca^{2+}-ATPase and other Ca^{2+}-modulated proteins by Ca^{2+}-dependent regulation of the synthesis or processing of relevant classes of mRNA (63). If this hypothesis is correct, an increase in cytoplasmic free [Ca^{2+}] should influence the expression of Ca^{2+}-ATPase. There are several indications that such feedback regulation by Ca^{2+} may in fact occur:

1. Continuous exposure of cultured muscle cells to 10^{-8} *M* A23187 increases the steady state level of Ca^{2+}-sensitive, hydroxylamine labile phosphoprotein that is assumed to reflect the concentration of Ca^{2+}-ATPase (64).
2. Brief exposure of cultured muscle cells to ionomycin or A23187 (1–4 μM for 1–3 h) increases severalfold the rate of [^{35}S]methionine incorporation into two membrane proteins—one of 100 KD and one of 80 KD—that sediment in the microsomal fraction. The 100-KD protein is assumed to represent the Ca^{2+}-ATPase, although chemical evidence is still required. The identity of the 80-KD protein is unknown (54, 55, 76).
3. Treatment with ionomycin or A23187 causes an increase in cytoplasmic [Ca^{2+}] (44).
4. Increased synthesis of the 80-KD and 100-KD proteins was observed upon cell-free translation of poly A enriched RNA isolated from ionomycin-treated as compared with control cultures (63, 95). Therefore ionomycin selectively increases the cellular concentration of mRNA-s that code for the 80-KD and 100-KD proteins.
5. The total Ca^{2+} content of embryonic muscle cells is high before the accumulation of Ca^{2+}-ATPase begins and decreases with age as development proceeds (64). The high cellular Ca in early stages of development may be due to Ca^{2+} channels in the surface membrane (84) or to increased Ca^{2+} influx into muscle cells during fusion into myotubes (20).
6. Ca^{2+}-binding proteins with a broad range of Ca^{2+} affinities were observed among the nonhistone chromosomal proteins and in the insoluble protein fraction of nuclei isolated from skeletal muscles of embryonic and adult chicken or rabbits (79). The possible role of these proteins in Ca^{2+}-dependent gene regulation is under study.

These observations are consistent with the hypothesis that increased cytoplasmic-free Ca^{2+} in early phases of development induces the expression of Ca^{2+}-ATPase mRNA by acting on one or more pretranslational step(s) in the protein synthesis. The participation of nuclear Ca^{2+}-binding proteins as inducers or repressors of gene expression is an exciting but unproven possibility.

In addition to a control of protein synthesis, regulation of the turnover of

AD-A166 003 REGULATION & DEVELOPMENT OF MEMBRANE TRANSPORT PROCESSES(U) MEDICAL UNIV OF SOUTH CAROLINA CHARLESTON J S GRAVES 15 MAY 85 AFOSR-TR-86-0142 2/4

UNCLASSIFIED F/G 6/16 NL

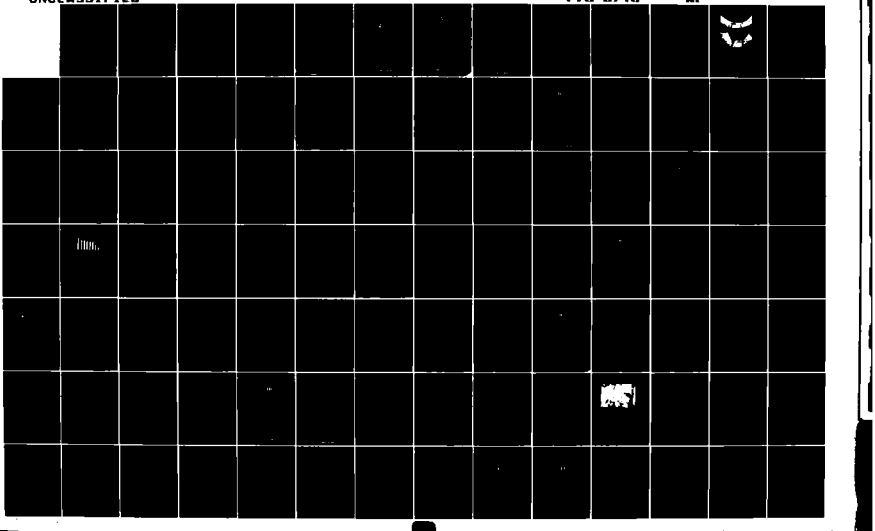

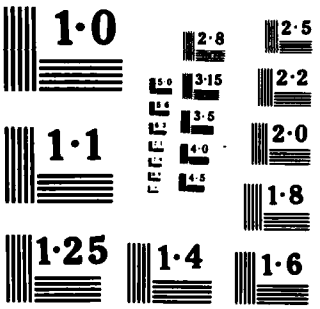
1·0
1·1
1·25
1·4
1·6
1·8
2·0
2·2
2·5
2·8
3·15
3·5
4·0
4·5
5·0

Ca^{2+}-ATPase is indicated by the fact that the half-life of the Ca^{2+}-ATPase in cultured rat muscle cells is only 20 h (42), whereas in adult rat muscle it is 10–14 days (60). Analysis of the rate of degradation of Ca^{2+}-ATPase in muscle cells during various phases of development, with particular attention to Ca^{2+}-activated proteases, could provide the explanation of this difference.

It is likely that the principles of membrane assembly and regulation derived from the foregoing studies on developing systems also govern the adaptation of SR structure and function to physiological requirements in the adult animals. Examples of this adaptation are the changes in Ca^{2+} transport activity observed after cross-innervation or chronic electric stimulation of muscle (46), which suggest neural control of the Ca^{2+} pump density in mature muscle cells.

5. SUMMARY AND PERSPECTIVES

The Ca^{2+} transport activity of sarcoplasmic reticulum is regulated at several levels:

1. Control of enzyme concentration is achieved by regulation of the rate of synthesis and degradation of Ca^{2+}-ATPase. Ca^{2+} is expected to play a feedback regulatory role in both processes.
2. In the control of enzyme activity cytoplasmic Ca^{2+} concentration and membrane potential play a dominant role, but phosphorylation of Ca^{2+}-ATPase or its interaction with regulatory proteins (phospholamban) could contribute to fine control of transport activity.

Further work is needed to assess the significance of ATPase-ATPase interactions in sarcoplasmic reticulum function. While the Ca^{2+}-ATPase monomer is competent to catalyze the elementary steps of Ca^{2+}-activated ATP hydrolysis, the enzyme is present in the native sarcoplasmic reticulum largely in an oligomeric form, presumably as dimer. A requirement for ATPase dimers in active Ca^{2+} translocation across the membrane has not been excluded. ATPase dimers were suggested to control the stability of the Ca-ATPase in the membrane and could contribute to regulation of the passive permeability of the sarcoplasmic reticulum to calcium and other ions.

REFERENCES

1. Allen, G. (1980a) *Biochem. J.*, **187**, 545–563.
2. Allen, G. (1980b) *Biochem. J.*, **187**, 565–575.
3. Allen, G. and Green, N. M. (1976) *FEBS Lett.*, **63**, 188–192.
4. Allen, G., Bottomley, R. C., and Trinnaman, B. J. (1980a) *Biochem. J.*, **187**, 577–589.
5. Allen, G., Trinnaman, B. J., and Green, N. M. (1980b) *Biochem. J.*, **187**, 591–616.

6. Andersen, J. P., Fellmann, P., Møller, J. V., and Devaux, P. F. (1981) *Biochemistry*, **20**, 4928–4936.
7. Baskin, R. J. (1974) *J. Ultrastruct. Res.*, **49**, 348–371.
8. Baylor, S. M., Chandler, W. K., and Marshall, M. W. (1982) *J. Physiol.*, **331**, 105–137.
9. Beeler, T. J. (1980) *J. Biol. Chem.*, **255**, 9156–9161.
10. Beeler, T. J., Farmen, R. H., and Martonosi, A. (1981) *J. Membrane Biol.*, **62**, 113–137.
11. Beeler, T. J., Dux, L., and Martonosi, A. (1984) *J. Membrane Biol.* **78**, 73–75.
12. Bennett, J. P., McGill, K. A., and Warren, G. B. (1980) *Curr. Top. Membrane Transp.*, **14**, 127–164.
13. Bezanilla, F. and Horowicz, P. (1975) *J. Physiol. (Lond.)*, **246**, 709–735.
14. Boland, R., Martonosi, A., and Tillack, T. W. (1974) *J. Biol. Chem.*, **249**, 612–623.
15. Borchman, D., Simon, R., and Bicknell-Brown, E. (1982) *J. Biol. Chem.*, **257**, 14136–14139.
16. Bray, D. F. and Rayns, D. G. (1976) *J. Ultrastruct. Res.*, **57**, 251–259.
17. Cantini, M., Sartore, S., Vitadello, M., and Schiaffino, S. (1979) *Cell Biol. Int. Rep.* **3**, 151–156.
18. Chyn, T. L., Martonosi, A. N., Morimoto, T., and Sabatini, D. (1979) *Proc. Natl. Acad. Sci. USA*, **76**, 1241–1245.
19. Damiani, E., Betto, R., Salvatori, S., Volpe, P., Salviati, G., and Margreth, A. (1981) *Biochem. J.*, **197**, 245–248.
20. David, J. D., See, W. M., and Higginbotham, C. A. (1981) *Dev. Biol.*, **82**, 297–307.
21. Deamer, D. W. and Baskin, R. J. (1969) *J. Cell Biol.*, **42**, 296–307.
22. DeFoor, P. H., Levitsky, D., Biryukova, T., and Fleischer, S. (1980) *Arch. Biochem. Biophys.*, **200**, 196–205.
23. de Meis, L. (1981) *The Sarcoplasmic Reticulum. Transport and Energy Transduction*, Wiley, New York.
24. de Meis, L. and Vianna, A. L. (1979) *Ann. Rev. Biochem.*, **48**, 275–292.
25. Duggan, P. F. and Martonosi, A. (1970) *J. Gen. Physiol.*, **56**, 147–167.
26. Dupont, Y. (1977) *Eur. J. Biochem.*, **72**, 185–190.
27. Dux, L. and Martonosi, A. (1983a) *J. Biol. Chem.*, **258**, 2599–2603.
28. Dux, L. and Martonosi, A. (1983b) *J. Biol. Chem.*, **258**, 10111–10115.
29. Dux, L. and Martonosi, A. (1983c) *J. Biol. Chem.*, **258**, 11896–11902.
30. Dux, L. and Martonosi, A. (1983d) *J. Biol. Chem.*, **258**, 11903–11907.
31. Dux, L., Taylor K. A. and Martonosi, A. (1984a) *Fed. Proc.* **43**, 1700.
32. Dux, L. and Martonosi, A. (1984b) *Eur. J. Biochem.* **141**, 43–49.
33. Fawcett, D. W. and Revel, J. P. (1961) *J. Biophys. Biochem. Cytol.*, **10:** 4 Supp. 89–109.
34. Galani-Kranias, E., Bick, R., and Schwartz, A. (1980) *Biochim. Biophys. Acta*, **628**, 438–450.
35. Greenway, D. C. and MacLennan, D. H. (1978) *Can. J. Biochem.*, **56**, 452–456.
36. Grisham, C. M. (1982) in Martonosi, A., *Membranes and Transport*, Vol. 1, Plenum, New York, pp. 585–592.
37. Ha, D. B., Boland, R., and Martonosi, A. (1979) *Biochim. Biophys. Acta*, **585**, 165–187.
38. Hasselbach, W. (1978) *Biochim. Biophys. Acta*, **515**, 23–53.
39. Hasselbach, W. (1979) *Top. Curr. Chem.*, **78**, 1–56.
40. Hebert, H., Jorgensen, P. L., Skriver, E., and Maunsbach, A. B. (1982) *Biochim. Biophys. Acta*, **689**, 571–574.
41. Hitchcock, S. E. (1970) *Dev. Biol.* **23**, 399–423.

42. Holland, P. C. and MacLennan, D. H. (1976) *J. Biol. Chem.*, **251,** 2030–2036.
43. Ikemoto, N. (1974) *J. Biol. Chem.*, **249,** 649–651.
44. James-Kracke, M. R. and Martonosi, A. (1983) *Fed. Proc.*, **42,** 996.
45. Jilka, R. L., Martonosi, A., and Tillack, T. W. (1975) *J. Biol. Chem.*, **250,** 7511–7524.
46. Jolesz, F. and Sreter, F. A. (1981) *Ann. Rev. Physiol.*, **43,** 531–552.
47. Leonard, K. R. and Weiss, H. (1982) in Martonosi, A., Ed., *Membranes and Transport*, Vol. 1, Plenum, New York, pp. 105–108.
48. Ludi, H. and Hasselbach, W. (1983) *Eur. J. Biochem.*, **130,** 5–8.
49. MacLennan, D. H., Zubrzycka, E., Jorgensen, A. O., and Kalnins, V. I. (1978) in Fleischer, S., Hatefi, Y., MacLennan, D. H., and Tzagoloff, A. Eds., *The Molecular Biology of Membranes*, Plenum, New York, pp. 309–320.
50. Martonosi, A. (1964) *Fed. Proc.*, **23,** 913–921.
51. Martonosi, A. (1968) *Biochim. Biophys. Acta*, **150,** 694–704.
52. Martonosi, A. (1969) *Biochem. Biophys. Res. Commun.*, **36,** 1039–1044.
53. Martonosi, A. (1975) *Biochim. Biophys. Acta*, **415,** 311–333.
54. Martonosi, A. (1982a) *Ann. Rev. Physiol.*, **44,** 337–355.
55. Martonosi, A. (1982b) in Schmitt, F. O., Bird, S. J., and Bloom, F. E. Eds., *Molecular Genetic Neuroscience*, Raven Press, New York, pp. 445–456.
56. Martonosi, A. (1983) in Stracher, A., Ed., *Muscle and Nonmuscle Motility*, Vol. 1, Academic, New York, pp. 233–357.
57. Martonosi, A. (1985) in Engel, A. G. and Banker, B. Q., Eds., *Myology*, McGraw-Hill, New York, in press.
58. Martonosi, A. and Beeler, T. J. (1983) in Peachey, L. D. and Adrian, R. H., Eds., *Handbook of Physiology. Skeletal Muscle*, American Physiological Society, Bethesda, pp. 417–485.
59. Martonosi, A. and Halpin, R. A. (1971) *Arch. Biochem. Biophys.*, **144,** 66–77.
60. Martonosi, A. and Halpin, R. A. (1972) *Arch. Biochem. Biophys.*, **152,** 440–450.
61. Martonosi, A., Donley, J., and Halpin, R. A. (1968) *J. Biol. Chem.*, **243,** 61–70.
62. Martonosi, A., Donley, J. R., Pucell, A. G., and Halpin, R. A. (1971) *Arch. Biochem. Biophys.*, **144,** 529–540.
63. Martonosi, A. N., Dux, L., Terjung, R. L., and Roufa, D. (1982) *Ann. N.Y. Acad. Sci.*, **402,** 485–514.
64. Martonosi, A. N., Roufa, D., Boland, R., Reyes, E., and Tillack, T. W. (1977) *J. Biol. Chem.*, **252,** 318–332.
65. Martonosi, A., Roufa, D., Ha, D. B., and Boland, R. (1980) *Fed. Proc.*, **39,** 2415–2421.
66. Møller, J. V., Andersen, J. P., and le Maire, M. (1982) *Mol. Cell Biochem.*, **42,** 83–107.
67. Mostov, K. E., DeFoor, P., Fleischer, S., and Blobel, G. (1981) *Nature*, **292,** 87–88.
68. Nakamaru, Y. and Schwartz, A. (1972) *J. Gen. Physiol.*, **59,** 22–32.
69. Nakamura, H., Jilka, R. L., Boland, R., and Martonosi, A. (1976) *J. Biol. Chem.*, **251,** 5414–5423.
70. Oosawa, F. and Asakura, S. (1975) *Thermodynamics of the polymerization of protein*, Academic, New York.
71. Peracchia, C., Dux, L., and Martonosi, A. (1983a) *Biophys. J.*, **41,** 172a.
72. Peracchia, C., Dux, L., and Martonosi, A. (1984) *J. Muscle Res. Cell Motility* 5, in press.
73. Reiser, P. J. and Stokes, B. T. (1982) *Am. J. Physiol.*, **242,** C52–C58.
74. Reithmeier, R. A. F., de Leon, S., and MacLennan, D. H. (1980) *J. Biol. Chem.*, **255,** 11839–11846.

75. Rosenbluth, J. (1969) *J. Cell Biol.*, **42,** 534–547.

76. Roufa, D., Wu, F. S., and Martonosi, A. (1981) *Biochim. Biophys. Acta,* **674,** 225–237.

77. Sarzala, M. G., Pilarska, M., Zubrzycka, E., and Michalak, M. (1975) *Eur. J. Biochem.*, **57,** 25–34.

78. Sarzala, M. G. and Pilarska, M. (1976) *Biochim. Biophys. Acta,* **441,** 81–92.

79. Schibeci, A. and Martonosi, A. (1980) *Eur. J. Biochem.*, **113,** 5–14.

80. Skriver, E., Maunsbach, A. B., and Jorgensen, P. L. (1981) *FEBS Lett.*, **131,** 219–222.

81. Seiler, D. and Hasselbach, W. (1971) *Eur. J. Biochem.*, **21,** 385–387.

82. Shoshan, V., MacLennan, D. H., and Wood, D. S. (1981) *Proc. Natl. Acad. Sci.*, **78,** 4828–4832.

83. Somlyo, A. V., Gonzalez-Serratos, H., Shuman, H., McClellan, G., and Somlyo, A. P. (1981) *J. Cell Biol.*, **90,** 577–594.

84. Spitzer, N. C. (1979) *Ann. Rev. Neurosci.*, **2,** 363–397.

85. Sumida, M., Wang, T., Mandel, F., Froehlich, J. P., and Schwartz, A. (1978) *J. Biol. Chem.*, **253,** 8772–8777.

86. Taylor, K. A., Dux, L., and Martonosi, A. (1983a) *Fed. Proc.*, **42,** 1933.

87. Taylor, K. A., Dux, L., and Martonosi, A. (1984) *J. Mol. Biol.* **174,** 193–204.

88. Taylor, K. A., Dux, L., and Martonosi, A. (1985) in preparation.

89. Tillack, T. W., Boland, R., and Martonosi, A. (1974) *J. Biol. Chem.* **249,** 624–633.

90. Vanderkooi, J. M., Ierokomos, A., Nakamura, H., and Martonosi, A. (1977) *Biochemistry,* **16,** 1262–1267.

91. Verjovski-Almeida, S. and Inesi, G. (1979) *J. Biol. Chem.*, **254,** 18–21.

92. Volpe, P., Damiani, E., Salviati, G., and Margreth, A. (1982) *J. Muscle Res. Cell Motility,* **3,** 213–230.

93. Wang, T., Grassi de Gende, A. O., and Schwartz, A. (1979) *J. Biol. Chem.*, **254,** 10675–10678.

94. Watanabe, T. and Inesi, G. (1982) *Biochemistry,* **21,** 3254–3259.

95. Wu, F. S., Park, Y. C., Roufa, D., and Martonosi, A. (1981) *J. Biol. Chem.*, **256,** 5309–5312.

96. Yamamoto, T. and Tonomura, Y. (1967) *J. Biochem. (Tokyo)*, **62,** 558–575.

97. Yu, B. P., DeMartinis, F. D., and Masoro, E. J. (1968) *J. Lipid Res.*, **9,** 492–500.

98. Zimniak, P. and Racker, E. (1978) *J. Biol. Chem.*, **253,** 4631–4637.

99. Zubrzycka-Gaarn, E., Korczak, B., and Osinska, H. E. (1979) *FEBS Lett.*, **107,** 335–339.

100. Zubrzycka, E., Michalak, M., Kosk-Kosicka, D., and Sarzala, M. G. (1979) *Eur. J. Biochem.*, **93,** 113–121.

PART 2

REGULATION OF EPITHELIAL TRANSPORT

CHAPTER 5

MINERALOCORTICOID REGULATION OF SODIUM AND POTASSIUM TRANSPORT BY THE CORTICAL COLLECTING DUCT

BRUCE M. KOEPPEN
Departments of Medicine and Physiology
University of Connecticut Health Center
Farmington, Connecticut

GERHARD H. GIEBISCH
Department of Physiology
Yale University School of Medicine
New Haven, Connecticut

Portions of this study have been published previously: B. M. Koeppen, B. A. Biagi, G. H. Giebisch, (1983). Intracellular microelectrode characterization of the rabbit cortical collecting duct, *Am. J. Physiol.*, **244**, F35–F47.

The collecting duct of the mammalian kidney plays an important role in fluid and electrolyte excretion. Along its length the transport of the many ions is regulated to meet the homeostatic need of the animal. Mineralocorticoid hormones have long been recognized as being essential for the maintenance of Na^+ and K^+ balance. Studies of single collecting duct segments from the rabbit have identified the cortical portion as a major site where these hormones influence the transport of Na^+ and K^+ (5, 12, 14, 26).

Although much is known about the effects of mineralocorticoid hormone deficit and excess on the transepithelial transport properties of the rabbit cortical collecting duct (2, 5–7, 9, 11, 13, 15, 18. 19, 21, 26, 30) our understanding of the cellular mechanism(s) reponsible for the observed changes in ion transport remains incomplete. With the recent adaptation of intracellular microelectrode techniques to the study of single cells of the rabbit cortical collecting duct (11), it is possible to examine directly the electrical properties of the individual cell membranes and thereby define the electrochemical driving forces and membrane conductances for transcellular and paracellular ion movement. Accordingly, the cellular sites at which mineralocorticoid hormones act to regulate the transport of Na^+ and K^+ can be determined.

In this chapter the effects of chronic, high-dose mineralocorticoid hormone treatment on the transport of Na^+ and K^+ by the rabbit cortical collecting duct are reviewed. In addition, the results of intracellular microelectrode studies obtained under similar experimental conditions are examined, and a model for the regulation of Na^+ and K^+ transport is presented.

1. CHARACTERISTICS AND CELLULAR MECHANISM OF Na^+ and K^+ TRANSPORT

The cortical collecting duct reabsorbs Na^+ from and secretes K^+ into the tubule lumen (4, 9, 18, 21, 24, 25). Both ions are distributed across the tubule epithelium against their respective electrochemical gradients, and therefore are actively transported (4, 9, 18, 24, 25).

Under most conditions the transepithelial voltage V_T of the cortical collecting duct is oriented lumen negative and depends on the active reabsorption of Na^+ (4, 13, 18, 24, 25). Inhibition of Na^+ transport, either by removal of Na^+ from or addition of amiloride to the luminal perfusate (12, 17, 22, 23) or by the addition of ouabain to the peritubular bathing solution (4, 13) abolishes the lumen negative V_T.*

The active secretion of K^+ also depends on the reabsorption of Na^+. Net K^+ secretion J_K^{net} varies linearly with net Na^+ reabsorption J_{Na}^{net} and the magnitude of the lumen-negative V_T (25). Moreover, agents that inhibit Na^+ transport result in a parallel reduction in K^+ secretion (4, 18, 24, 25).

* Frequently inhibition of Na^+ transport causes the V_T to reverse polarity, becoming lumen positive. This lumen-positive V_T appears to reflect active electrogenic H^+ secretion (13).

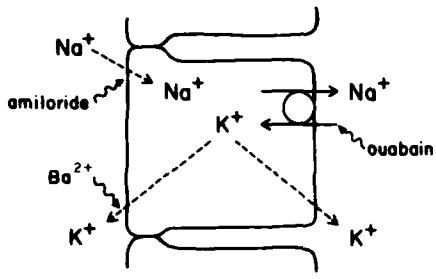

Figure 5.1. Cellular model for Na^+ and K^+ transport by the cortical collecting duct. Although not shown, the basolateral cell membrane also contains a conductive pathway for Cl^-. (From ref. 11 with permission of the publisher.)

Taken together, the features of Na^+ and K^+ transport just outlined can be attributed to the cellular mechanism shown in Fig. 5.1 (3, 16, 25). Recent microelectrode studies have provided direct confirmation of this scheme (11), which likely represents the properties of the principal cell.*

The active reabsorption of Na^+ as well as the active secretion of K^+ is driven by the Na^+,K^+-ATPase located in the basolateral cell membrane. Na^+ enters and K^+ exits the cell across the apical (luminal) cell membrane by way of separate conductive pathways and passively down their respective electrochemical gradients. The conductive movement of Na^+ across the apical cell membrane is blocked specifically by amiloride, while $BaCl_2$ inhibits the K^+ conductive pathway in this membrane (11). The basolateral cell membrane also contains a conductive pathway for K^+ (11), thus allowing the K^+ brought into the cell by the Na^+,K^+-ATPase to recycle in part across this membrane. Although Na^+ and K^+ appear to be the major if not only conductive ion species across the luminal cell membrane (11; see below), the basolateral cell membrane is not, under most conditions, selective only to K^+ (11, 17, 20). In particular, a variable yet significant Cl^- conductive pathway has been identified and shown to contribute to the electrical properties of this membrane (17, 20).

By this scheme the coupling of K^+ secretion to Na^+ reabsorption is direct by way of the Na^+,K^+-ATPase and also is secondary to the potential profile across the individual cell membranes. Accordingly, three general mechanisms could operate to regulate the transepithelial transport of Na^+ and K^+. First, cellular uptake of K^+ and extrusion of Na^+ could be altered by a change in the activity of the Na^+,K^+-ATPase. This could occur either by a change in the number of functional enzyme units in the basolateral cell membrane and/or by a change in the activity of each enzyme unit. Second, the electrochemical gradients for passive ion movement across both the apical and basolateral cell membranes could be altered. This would be espe-

* The principal cell is the majority cell type of the cortical collecting duct comprising 65–75% of the total cell population. The remaining cells are the intercalated cells (10). Structure-function studies suggest that the principal cell reabsorbs Na^+ and secretes K^+ whereas the intercalated cell is responsible for urinary acidification (10, 22, 23). In addition, the intercalated cell may be involved in K^+ reabsorption under conditions of prolonged K^+ depletion (23).

cially important when considering the transport of K^+, since both membranes contain conductive pathways for this ion. Finally, the specific ion conductances of the individual cell membranes could be modified. As will be shown, regulation of Na^+ and K^+ transport by mineralocorticoid hormones appears to involve all three mechanisms.

2. MINERALOCORTICOID HORMONE EFFECTS ON TRANSEPITHELIAL PROPERTIES

Administration of high doses of mineralocorticoid hormones to rabbits for extended periods of time results in marked alterations in the morphology, transport properties, and electrophysiology of the cortical collecting duct. Table 5.1 summarizes some of these reported effects. In most studies animals received daily injections of 5 mg of deoxycorticosterone acetate (DOCA) or its analog. Typically, the treatment period ranged from several days to several weeks and on the average lasted for 7–10 days. It is important to note that during this period the rabbits become polyuric and polydipsic (18), and usually develop a hypokalemic metabolic alkalosis (2, and unpublished observations). Thus, even though the observed changes in the properties of the cortical collecting duct are attributed to direct effects of mineralocorticoid hormone, an important influence of the associated changes in potassium and/or acid-base balance cannot be ruled out. Moreover, DOCA possesses both mineralocorticoid and glucocorticoid activity, especially at the doses commonly employed (14). Consequently some of the observed effects of DOCA could be related to the glucocorticoid properties of the hormone. In this regard, chronic high-dose dexamethasone treatment of rabbits (5 mg/day for 11–18 days) results in hyperpolarization of the lumen-negative V_T and an increase in the area of the basolateral cell membrane of the cortical collecting duct (27). Lower doses (0.8 mg/day for 12–31 days) do not, however, alter the V_T or Na^+ and K^+ transport rates (21).

Several of the effects of DOCA treatment listed in Table 5.1 have particular importance for interpretation of the results of the microelectrode studies reported later and require special note. First, the morphologic alterations of the tubule are limited to the basolateral cell membrane of the principal cell (27). As shown in Fig. 5.2 and summarized in Table 5.1, there is a two- to threefold increase in the area of this membrane, whereas all other cellular dimensions are essentially unchanged. Second, the enzymatic activity of the Na^+,K^+-ATPase increases dramatically (2). Third, the rates of net Na^+ reabsorption and net K^+ secretion are increased with the increase in K^+ secretion being proportionately larger than the increase in Na^+ reabsorption, such that the ratio J_{Na}^{net}/J_K^{net} decreases (9, 18, 21, 25, 26). Fourth, the increased transport of Na^+ and K^+ is associated with an increase in the transepithelial equivalent conductances for these ions (9, 18). Finally, the Cl^- permeability (6), and equivalent Cl^- conductance of the epithelium (9, 18), thought to

TABLE 5.1. EFFECT OF CHRONIC HIGH-DOSE MINERALOCORTICOID HORMONE TREATMENT ON RABBIT CORTICAL COLLECTING DUCT[a]

	Control	*DOCA*	*Reference*
I. *Morphology*			
Inner diameter (μm)	19	17	27
Outer diameter (μm)	27	29	27
Number of cells/mm	511	507	2
Cell volume (μm^3/mm)			
Principal cell	2.02×10^5	2.67×10^5	27
Intercalated cell	0.62×10^5	0.61×10^5	27
Membrane area (μm^2/mm)			
Principal cell			
Luminal membrane	0.77×10^5	0.93×10^5	27
Basolateral membrane	6.35×10^5	15.61×10^5	27
Intercalated cell			
Luminal membrane	0.20×10^5	0.30×10^5	27
Basolateral membrane	1.35×10^5	1.40×10^5	27
II. *Ion Transport*			
J_{Na}^{l-b} (pmol/cm sec)	7.3	14.8	21, 25
J_{Na}^{b-l} (pmol/cm sec)	2.6	2.8	21, 25
J_{Na}^{net} (pmol/cm sec)	4.1	10.2	18, 21, 25
J_{K}^{net} (pmol/cm sec)	−1.7	−6.4	18, 21, 25
J_{Na}/J_{K}	2.4	1.6	18, 21, 25
J_{Cl}^{l-b} (pmol/cm sec)	13.9	9.2	6
J_{Cl}^{b-l} (pmol/cm sec)	14.2	7.2	6
J_{Cl}^{net} (pmol/cm sec)	−0.3	2.0	6
Lumen pH	5.93	5.43	13
Na^+,K^+-ATPase (pmol/mm min)	23	143	2
III. *Electrophysiology*			
V_T (mV)	−14.2	−47.9	5, 6, 7, 11, 13, 18, 21, 25, 26, 27
R_T (k$\Omega \cdot$ cm)	21.0	29.5	9, 11, 18
G_{Na}^{te} (μS/cm)	2.4	9.9	9, 18
G_{K}^{te} (μS/cm)	0.9	3.1	9, 18
(G_{Cl}^{te} (μS/cm)	25.7	5.3	9, 18

[a] The values reported are from studies in which control and DOCA-treated tubules were studied using the same protocol. Where more than one study is referenced, the summarized value represents the mean of each study. No distinction is made between tubules studied at 25°C and at 37°C. Negative values of net fluxes represent secretion of the ion species indicated. G_{Na}^{te}, G_{K}^{te}, and G_{Cl}^{te} represent transepithelial equivalent conductances for Na^+, K^+, and Cl respectively.

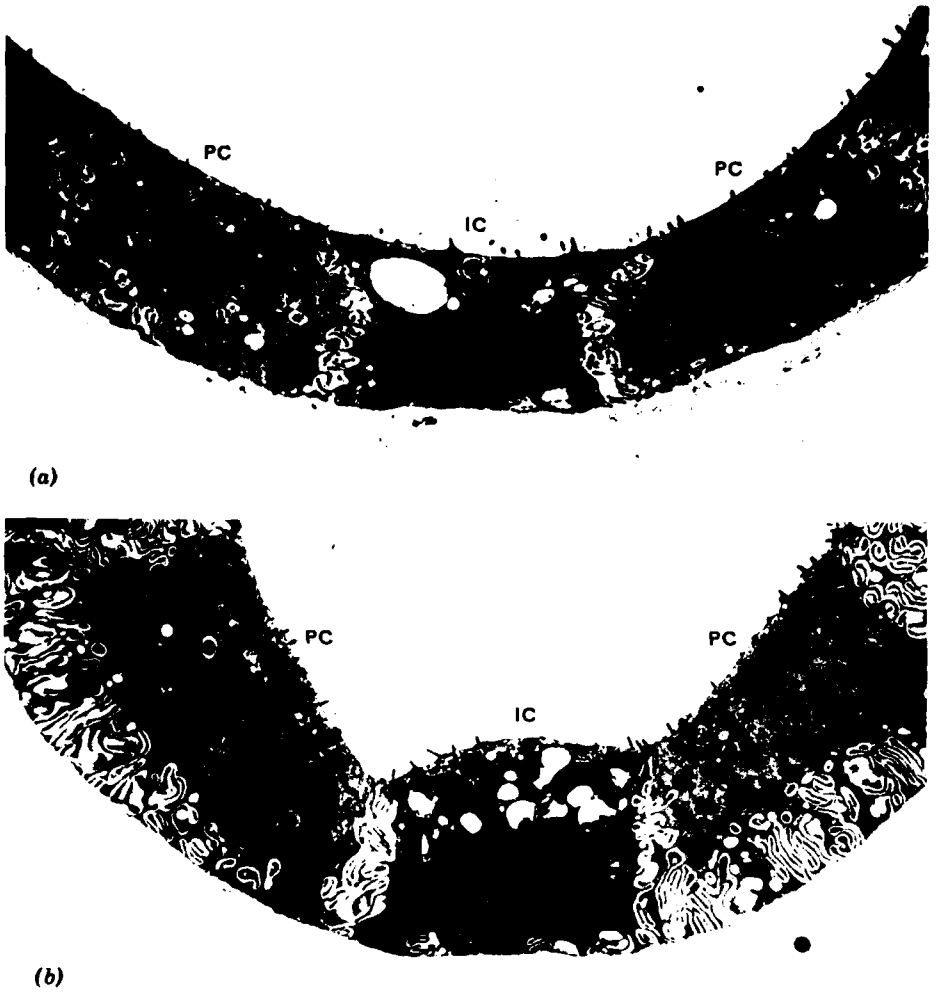

Figure 5.2. Transmission electronmicrograph of isolated cortical collecting ducts showing principal cells (PC) and intercalated cells (IC). (*a*) Tubule from control rabbits. (*b*) Tubule from DOCA-treated rabbit. Magnification: × 6500. (From ref. 27, courtesy of the authors.)

reflect in large part the properties of the paracellular pathway (9), are markedly reduced.*

These DOCA-related changes in the transepithelial properties of the cortical collecting duct, when viewed within the context of the model for Na^+ and

* The paracellular (shunt) pathway is broadly defined here as any transepithelial route for conductive ion movement that is in parallel with the cells responsible for Na^+ and K^+ transport. Although the paracellular pathway in the cortical collecting duct is thought to be Cl^- selective (9, 18), there is no direct evidence that all Cl^- movement is restricted to a paracellular route. As already noted, the basolateral cell membrane does contain a Cl^- conductive pathway (17, 20). Also, Cl^- reabsorption by DOCA pretreated tubules can occur against a transepithelial electrochemical gradient (6). Thus some fraction of Cl^- transport must occur by a transcellular route.

K^+ transport depicted in Fig. 5.1, allow several predictions as to the mechanism(s) involved in the regulation of Na^+ and K^+ transport. In addition, and perhaps more important, they provide a framework for interpretation of the results of microelectrode studies. For example, following DOCA treatment the transepithelial properties of the cortical collecting duct epithelium would be expected to reflect to a greater degree the electrical properties of the cellular rather than the paracellular pathway. Specifically, the increased equivalent conductance of Na^+ and K^+ would be consistent with changes in the properties of the luminal and/or basolateral cell membranes, whereas the reduced Cl^- conductance would reflect an increase in the resistance of the paracellular pathway. Accordingly, regulation of Na^+ and K^+ transport by DOCA could result from the increased activity of the Na^+,K^+-ATPase in association with increases in the Na^+ and K^+ conductances of the luminal cell membrane.

3. MICROELECTRODE STUDIES OF DOCA-TREATED TUBULES

Microelectrode studies were done on cortical collecting ducts isolated from kidneys of rabbits maintained on a standard laboratory diet (control tubules) and from rabbits which in addition received daily injections of 5 mg of DOCA for 7–10 days (DOCA tubules). All tubules were perfused as shown in Fig. 5.3 and as described in detail elsewhere (11). In brief, tubules were perfused and bathed with artificial Ringer solutions containing 150 m*M* Na^+ and 5 m*M* K^+, and which were equilibrated with 95% O_2/5% CO_2 at 37°C (pH = 7.4–7.5).

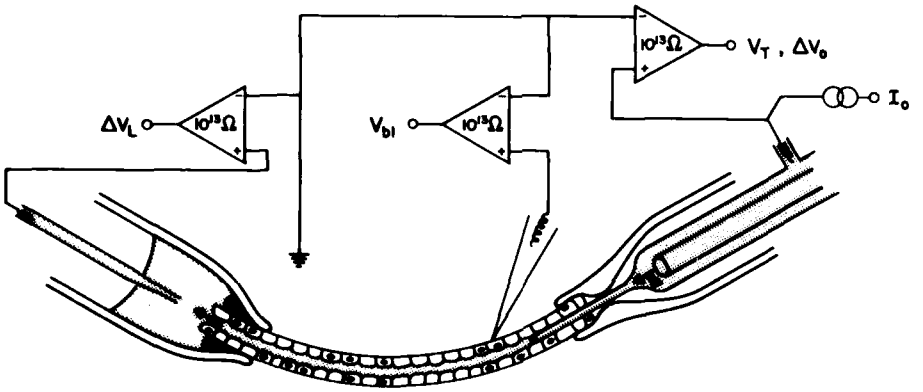

Figure 5.3. Arrangement of pipettes and electrical schematic for microelectrode studies of single cortical collecting ducts. The perfusion pipette (right) was fitted with an exchange pipette to change the luminal composition. The perfusion pipette was also used to inject pulses of constant current I_0 into the tubule lumen for the determination of membrane resistances. The transepithelial voltage V_T and the basolateral membrane voltage V_{bl} were referenced to the grounded bath solution. (From ref. 11 with permission of the publisher.)

The transepithelial voltage V_T was measured through the perfusion pipette and referenced to the bath solution. The perfusion pipette was also used to inject pulses of constant current into the tubule lumen. From the resultant voltage deflections at each end of the tubule ΔV_O and ΔV_L and with use of cable analysis, the transepithelial resistance of the tubule R_T was calculated (11).

The voltage across the basolateral cell membrane V_{bl} was measured using microelectrodes filled with 1*M* KCl (90–180 MΩ), and referenced to the bath. From the measured values of V_{bl} and V_T the voltage across the apical cell membrane V_a was calculated.

$$V_a = V_T - V_{bl} \tag{1}$$

During luminal current injection the voltage divider ratio was measured and the fractional membrane resistance calculated as

$$fRa = 1 - \frac{\Delta V_{bl}}{\Delta V_x} = \frac{R_a}{R_a + R_{bl}} \tag{2}$$

where ΔV_x and ΔV_{bl} are the voltage responses to luminal current injection across the tubule epithelium and basolateral cell membrane, and R_a and R_{bl} are the resistances of the apical and basolateral cell membranes.

A summary of the baseline electrical parameters of control and DOCA-treated tubules is shown in Fig. 5.4. As can be seen, with DOCA treatment V_T and V_{bl} hyperpolarized by 32.4 and 21.8 mV, respectively, while V_a depolarized by 10.6 mV. The mechanism(s) that underlie these changes in membrane voltage, as well as their influence on transcellular Na^+ and K^+ transport, are considered later.

Both the transepithelial resistance and the fractional membrane resistance fell slightly with DOCA treatment; R_T from 14.7 ± 1.4 kΩ · cm to 12.2 ± 2.3 kΩ · cm and fR_a from 0.40 ± 0.03 to 0.35 ± 0.04. However, these

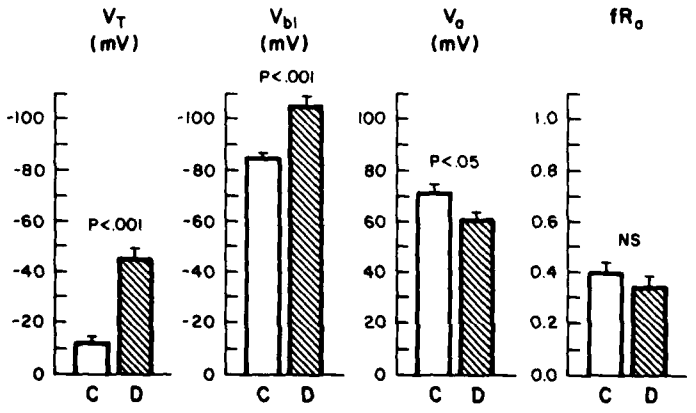

Figure 5.4. Cellular electrical properties of cortical collecting ducts obtained from control (C) and DOCA-treated rabbits (D).

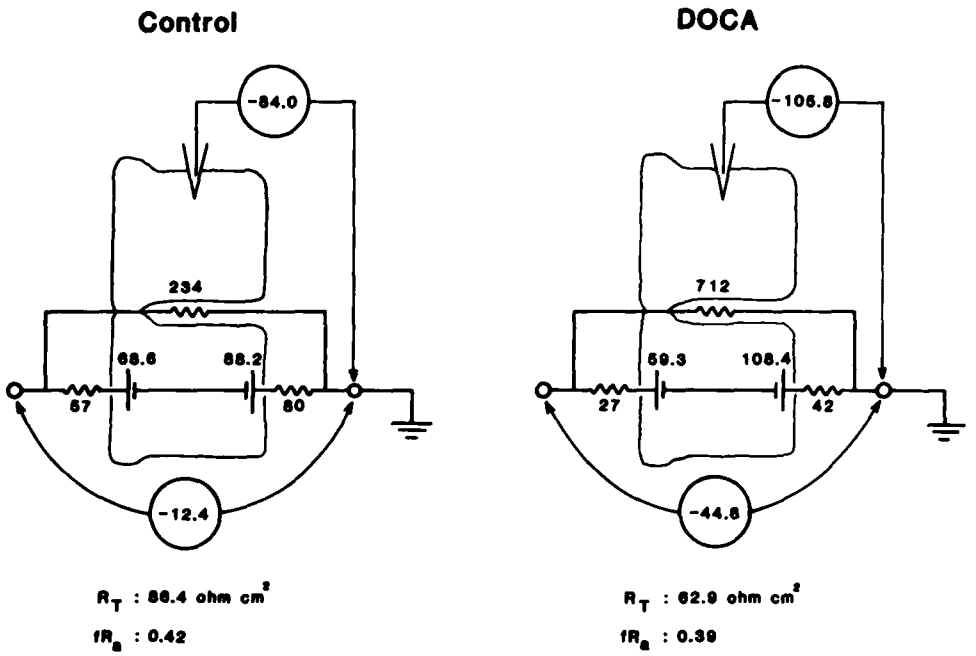

Figure 5.5. Electrical equivalent circuit of the cortical collecting duct. The measured values of V_T and V_{bl} are indicated and referenced to the peritubular solution. The values of membrane resistance are expressed as ohms times square centimeters ($\Omega \cdot cm^2$) of luminal membrane area. The values of R_T and fR_a are calculated from the equivalent circuit and are not different from the measured values summarized in Fig. 5.4.

changes were not statistically significant. The fact that fR_a did not change was surprising since the area of the basolateral cell membrane is amplified 2–3 fold under these conditions (27). Thus an increase in the area of this membrane would be expected to increase fR_a, whereas a small decrease in its value was actually observed. One possible explanation for the lack of an effect of DOCA treatment on fR_a is that the resistances of both the apical and basolateral cell membranes changed proportionally under these conditions. To examine more directly the effect of DOCA treatment on the conductive properties of the tubule, the data were analyzed within the framework of the simple equivalent circuit shown in Fig. 5.5. The individual values of apical R_a and basolateral R_{bl} membrane resistances and the shunt resistance R_s were calculated as

$$R_a = \frac{\alpha(\alpha - \alpha')R_T R_{T'}}{(1 + \alpha)(1 + \alpha')(R_T - R_{T'})} \tag{3}$$

$$R_{bl} = \frac{(\alpha - \alpha')R_T R_{T'}}{(1 + \alpha)(1 + \alpha')(R_T - R_{T'})} \tag{4}$$

$$R_s = \frac{R_T(R_a + R_{bl})}{R_a + R_{bl} - R_T} \tag{5}$$

where α and α' are the ratios of apical to basolateral membrane resistance (R_a/R_{bl}) in the absence and presence of agent(s) that specifically alter the conductance of the apical cell membrane (1). Similarly, R_T, represents the transepithelial resistance in the presence of these same agents. Since amiloride and $BaCl_2$ appear to be specific inhibitors of the apical membrane Na^+ and K^+ conductances (11), these drugs were used for the determination of the equivalent resistances.* The results of this analysis are summarized in Fig. 5.5.

As can be seen, the resistance of both the basolateral and apical cell membranes was reduced in proportion; R_a from 57 to 27 $\Omega \cdot cm^2$ and R_{bl} from 80 to 42$\Omega \cdot cm^2$. As a result, the value of fR_a was unchanged. In addition, the resistance of the shunt pathway was increased markedly with DOCA treatment, a finding in accordance with the equivalent circuit analysis of Helman and O'Neil, and consistent with their observed decrease in G_{Cl}^{te} (9).

3.1 Properties of the Apical Cell Membrane

Since the values of R_a, R_{bl}, and R_s, as calculated by this analysis, were normalized to the luminal surface area (inner diameter of the tubule = 20 μm), the twofold decrease in R_{bl} parallels the measured amplification in the surface area of this membrane (27), and as such would be consistent with the altered cellular geometry. In contrast, the reduction in R_a must reflect a change in the conductive properties of the apical cell membrane, as its area is not modified by DOCA treatment (27). To determine if this reduction in R_a was the result of a change in conductance of the Na^+ and/or K^+ pathways of this membrane, the effect of luminal addition of amiloride and $BaCl_2$ on fR_a was examined. Assuming that these drugs alter fR_a by effecting only the conductance of the apical cell membrane (11), it is possible to determine the fractional Na^+ and K^+ conductances of this membrane. Fig. 5.6 summarizes the effects of these drugs alone and in combination on fR_a.

As expected, both amiloride and $BaCl_2$ increased fR_a. More important, within the experimental error of these measurements, the change in the value of fR_a was not different between control and DOCA treated tubules. It would seem therefore, that the fractional Na^+ and K^+ conductances of the apical cell membrane were unchanged by DOCA treatment, and that the reduction in R_a was the result of an increase in the conductance of both the Na^+ and K^+ pathways. It is of interest to note in this regard that mineralocorticoid-mediated changes in the Na^+ and K^+ conductances of the luminal membrane of late distal tubules in the rat have been reported (28, 29). The importance of this correlation is underscored by the realization in recent

* This analysis assumes that the effects of amiloride and $BaCl_2$ are limited to changes in R_a. Preliminary studies suggest that for the collecting duct this asumption is valid, since plots of G_t versus $(1 + R_a/R_b)^{-1}$ generated with addition of $BaCl_2$ to the luminal perfusate are linear. O'Neil has recently obtained similar results (personal communication).

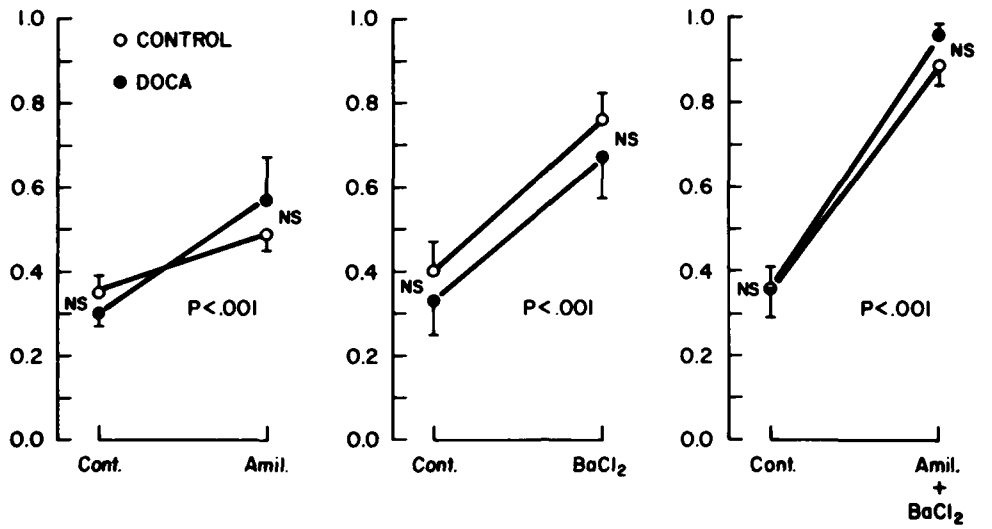

Figure 5.6. Effect of 10^{-5} M amiloride and 2×10^{-3} M $BaCl_2$ on fR_a in control (open circles) and DOCA treated (solid circles) tubules. Both drugs alone and in combination significantly increased fR_a. However, the change in fR_a was not different between the two groups of tubules.

years that this portion of the rat distal tubule comprises the initial collecting duct (22), and resembles the cortical collecting duct both structurally and functionally (3, 10, 22). The increased conductance of the apical membrane Na^+ and K^+ pathways is also consistent with the equivalent circuit analysis of Helman and O'Neil (9, 18), where both G^{te}_{Na} and G^{te}_{K} were found to increase with DOCA treatment.

When amiloride and $BaCl_2$ were added in combination to the luminal perfusate fR_a approached 1.0. This was true in both control and DOCA-treated tubules. From this it can be concluded that Na^+ and K^+ are the major if not only conductive ion species across the apical cell membrane and that other ion conductive pathways are not induced by DOCA treatment.

Because of the scatter inherent in the data, the only conclusion that can be drawn from the effects of amiloride and $BaCl_2$ on fR_a (Fig. 5.6) is that both the Na^+ and K^+ conductances of the apical cell membrane are increased with DOCA treatment. However, there is some indication that these conductances do not increase in exact proportion, but rather that the Na^+ conductance is increased to a slightly larger degree than K^+ conductance. For example, although not statistically different, the amiloride-induced increase in fR_a was slightly greater in DOCA-treated tubules ($\Delta fR_a = 0.27$) than in control tubules ($\Delta fR_a = 0.14$). Also, the equivalent EMF of the apical membrane E_a was reduced by approximately 10 mV in DOCA-treated tubules (see Fig. 5.5). Since E_a is determined by the opposing equivalent EMF and conductance of the Na^+ (E_{Na}, G_{Na}) and K^+ (E_K, G_K) pathways,

$$E_a = \frac{E_{Na} \cdot G_{Na}}{G_{Na} + G_K} + \frac{E_K \cdot G_K}{G_{Na} + G_K} \tag{6}$$

a decrease in its value would be consistent with a greater increase in G_{Na} as compared to G_K. This of course assumes that neither E_{Na} nor E_K are appreciably altered by DOCA treatment. Finally, a tenfold increase in the luminal $[K^+]$ resulted in a 38.2-mV depolarization of E_a in DOCA-treated tubules, while in control tubules the same K^+ step depolarized E_a by 51.9 mV.

3.2 Properties of the Basolateral Cell Membrane

As summarized in Fig. 5.5, the equivalent EMF of the basolateral cell membrane E_{bl} is increased by approximately 20 mV in DOCA-treated tubules. Since in control tubules the basolateral cell membrane contains conductive pathways for K^+ and Cl^- (11, 17, 20), an increase in E_{bl} would be consistent with either an increase in G_K and/or a decrease in G_{Cl}. This assumes, as before, that the K^+ and Cl^- equivalent EMFs are not altered by DOCA treatment. Recent studies by Natke and Stoner (15) would support the idea that with DOCA treatment G_K is increased. In their study the animals did not receive exogenous hormone, but rather endogenous aldosterone levels were increased by feeding the rabbits a low Na^+ diet. Under these conditions the apparent K^+ permeability of the basolateral cell membrane increased threefold. Regardless of the mechanism involved, it is clear that in DOCA-treated tubules the basolateral cell membrane is predominantly K^+ selective. This is evident from the effect of a ten-fold increase in the peritubular $[K^+]$ on E_{bl}. In control tubules this K^+ step resulted in a 36.5-mV depolarization of E_{bl}, whereas in DOCA-treated tubules a 52.2-mV depolarization was observed.

As shown in Fig. 5.4, V_{bl} hyperpolarized from -84 to -105 mV with DOCA treatment. As a result of these high values of V_{bl} it is likely that K^+ may enter the cell passively across the basolateral membrane. Although intracellular K^+ activity measurements have not been made under these conditions, the intracellular $[K^+]$ would have to be near 290 m*M* if K^+ was in electrochemical equilibrium across this membrane (extracellular $[K^+] = 5.0$ m*M*). Intracellular K^+ levels of this magnitude seem unlikely from osmotic considerations. Furthermore, the highest reported values of total cellular K^+ content are approximately 150 m*M* (15).

If it is assumed that the intracellular $[K^+]$ is 150 m*M*, and not apreciably altered by DOCA treatment, then the Nernst equilibrium potential for K^+ (E_K) would be -90 mV, or 15 mV below the value of V_{bl}. Accordingly, it can be argued that the Na^+,K^+-ATPase is electrogenic. In support of this is the observation that addition of ouabain to the peritubular bathing solution results in a two-phase depolarization of V_{bl} (see Fig. 5.7), with an initial rapid depolarization (10–15 mV) followed by a slower and more prolonged phase. A similar response has been observed in other epithelial tissues (8, 31), and attributed to inhibition of an electrogenic pump and subsequent dissipation of the cellular ion gradients.

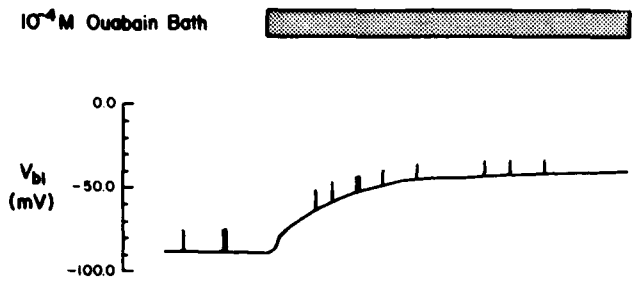

Figure 5.7. Effect of ouabain on V_{bl}. A two-phase depolarization in V_{bl} is clearly visible. The vertical lines represent changes in V_{bl} during luminal current injection. (Adapted from ref. 11, with permission of the publisher.)

4. MODEL FOR DOCA REGULATION OF Na^+ AND K^+ TRANSPORT

The changes in the electrical properties of the cortical collecting duct with chronic high- dose DOCA treatment, and the consequences of these changes for the regulation of Na^+ reabsorption and K^+ secretion are summarized in Fig. 5.8.

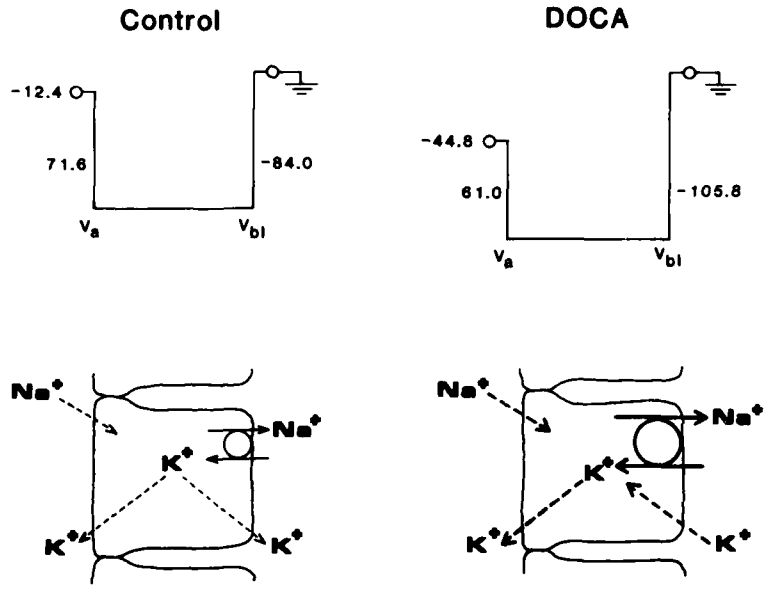

Figure 5.8. Potential profile of cells and model for regulation of Na^+ and K^+ transport by DOCA. Na^+ reabsorption would be increased with DOCA treatment by an increase in Na^+,K^+-ATPase activity and an increase in the apical membrane Na^+ conductance. Increased secretion of K^+ would result from increased cellular uptake across the basolateral membrane, both by the increased activity of the Na^+,K^+-ATPase and the favorable electrical gradient for passive K^+ entry. Exit of K^+ from the cell into the tubule lumen would be facilitated by a more favorable electrical gradient and by an increase in the K^+ conductance of this membrane.

4.1. Na^+ Reabsorption

The increased Na^+ reabsorption that occurs with DOCA treatment can be attributed to enhanced uptake across the apical cell membrane, secondary to an increase in the conductance of this membrane to Na^+, together with increased extrusion across the basolateral cell membrane by way of the Na^+,K^+-ATPase. Recent studies using more physiologic doses of mineralocorticoid hormones indicate that the Na^+,K^+-ATPase activity increases only after the Na^+ conductance of the apical membrane is altered (19). Thus it appears that the increased Na^+ conductance of the apical membrane results in changes in intracellular $[Na^+]$ (or other secondary changes in cellular composition), which in turn modulate Na^+,K^+-ATPase activity by the synthesis and/or insertion of additional enzyme units into the basolateral cell membrane. The long-term morphologic consequence of pump insertion into the basolateral cell membrane is that the area of this membrane is dramatically increased.

4.2 K^+ Secretion

Several mechanisms appear to be involved in increasing net K^+ secretion during DOCA treatment. The increased activity of the Na^+,K^+-ATPase would serve to increase cellular K^+ uptake. In addition, the hyperpolarization of V_{bl} above E_K would further augment cellular K^+ uptake by bringing K^+ passively into the cell. The exit of K^+ from the cell into the tubule lumen would be facilitated by the increased conductance of the apical cell membrane to K^+ and by a more favorable electrochemical gradient resulting from the altered potential profile across the individual cell membranes.

It should be recalled that with chronic DOCA treatment the ratio J_{Na}^{net}/J_K^{net} decreases, reflecting a larger increase in net K^+ secretion compared to the increase in net Na^+ reabsorption (see Table 5.1). This can be attributed to the DOCA-induced changes in the cellular electrical profile. Under control conditions K^+ is brought into the cell by the action of the Na^+,K^+-ATPase. This K^+ can then exit the cell across the apical cell membrane resulting in transcellular K^+ secretion, or recycle across the basolateral cell membrane. Under these conditions J_{Na}^{net} could exceed J_K^{net} by severalfold depending on the amount of K^+ that is recycled across the basolateral cell membrane. With DOCA treatment the potential profile across the cell is altered so that the movement of K^+ from the cell across the apical membrane is facilitated, while K^+ recycling across the basolateral is inhibited. Indeed, recycling would not be expected to occur since the electrochemical gradient for K^+ movement across this membrane is reversed. Under these conditions J_{Na}^{net}/J_K^{net} should be less than the coupling ratio of the Na^+,K^+-ATPase. If it is assumed that the only pathways for transepithelial Na^+ and K^+ transport are as indicated in Fig. 5.1 and that the Na^+,K^+-ATPase exchanges $3Na^+$ for

$2K^+$, then a ratio of J_{Na}^{net}/J_K^{net} less than 1.5 should be observed. In fact ratios as low as 1.26 have been reported (9, 18).

4.3 Electrophysiology

A well-described and easily measured effect of DOCA treatment is a marked hyperpolarization of the lumen negative V_T. From the results of the equivalent circuit analysis (see Fig. 5.5) it is clear that this reflects in part the increased resistance of the shunt pathway R_s. Thus

$$V_T = iR_s \tag{7}$$

where i is the current flow across the epithelium and is calculated as $(E_b - E_a)/(R_a + R_{bl} + R_s)$. Despite the increase in R_s, R_T was not appreciably altered by DOCA treatment (9, 11, 18, and see above). R_s increased three-fold with DOCA treatment, while the transcellular resistance $(R_a + R_{bl})$ decreased by approximately one-half. Since R_T is the parallel sum of the transcellular and paracellular pathways,

$$R_T = \frac{(R_a + R_{bl})R_s}{R_a + R_{bl} + R_s} \tag{8}$$

the net result is that the transepithelial resistance is not appreciably altered (9, 11, 18, and see above). Thus with DOCA treatment the conductive properties of the epithelium reflect to a greater degree the properties of the transcellular rather than the paracellular pathway.

5. SUMMARY

Chronic high-dose mineralocorticoid hormone treatment of rabbits results in marked alterations of the structure and function of the cortical collecting duct. Most importantly, the reabsorption of Na^+ and the secretion of K^+ are increased. Intracellular microelectrode measurements provide evidence consistent with the idea that the increased transport of these ions is a result of changes in the membrane conductances and electrochemical driving forces for passive ion movement and of the activity of the Na^+,K^+-ATPase. Specifically, the Na^+ and K^+ conductances of the apical membrane are increased, and the cellular potential profile is altered to promote transcellular movement of K^+ from the peritubular to the luminal fluid compartments. The associated increase in the activity of the Na^+,K^+-ATPase facilitates extrusion of Na^+ from and accumulation of K^+ into the cell.

The resistance of both the apical and basolateral cell membranes are reduced with DOCA treatment, while the resistance of the paracellular pathway is increased. Consequently, the electrophysiological properties of the tubule epithelium reflect to a greater degree the properties of the transcellular pathway.

ACKNOWLEDGMENTS

The authors thank Dr. Bruce A. Stanton for his critical review of the manuscript. This work was supported by the Connecticut Affiliate of the American Heart Association and by National Institutes of Health, grant AM-17433-07.

REFERENCES

1. Frömter, E., and Gebler, B. (1977) *Pflugers Arch.*, **371,** 99–108.
2. Garg, L. C., Knepper, M. A., and Burg, M. (1981) *Am. J. Physiol.*, **240,** F536–F544.
3. Giebisch, G. (1981) *Jap. J. Physiol.*, **23,** 859–871.
4. Grantham, J. J., Burg, M. B., and Orloff, J. (1970), *J. Clin. Invest.*, **49,** 1815–1826.
5. Gross, J. B., Imai, M., and Kokko, J. P. (1975) *J. Clin. Invest.*, **55,** 1284–1294.
6. Hanley, M. J. and Kokko, J. P. (1978) *J. Clin. Invest.*, **62,** 39–44.
7. Hanley, M. J., Kokko, J. P., Gross, J. B., and Jacobson, H. R. (1980) *Kidney Inter.*, **17,** 74–81.
8. Helman, S. I., Nagel, W., and Fisher, R. S. (1979) *J. Gen. Physiol.*, **74,** 105–127.
9. Helman, S. I. and O'Neil, R. G. (1977) *Am. J. Physiol.*, **233,** F559–F571.
10. Kaissling, B. and Kriz, W. (1979) *Adv. Anat. Embryol. Cell Biol.*, **56,** 1–123.
11. Koeppen, B. M., Biagi, B. A., and Giebisch, G. H. (1983) *Am. J. Physiol.*, **244,** F35–F47.
12. Koeppen, B. M., Biagi, B. A., and Giebisch, G. (1983) *Ann. Rev. Physiol.*, **45,** 497–517.
13. Koeppen, B. M. and Helman, S. I. (1982) *Am. J. Physiol.*, **242,** F521–F531.
14. Marver, D. and Kokko, J. P. (1983) *Miner. Elec. Metab.*, **9,** 1–18.
15. Natke, E. and Stoner, L. C. (1982) *Am. J. Physiol.*, **242,** F664–F671.
16. O'Neil, R. G. and Boulpaep, E. L. (1979) *J. Membrane Biol.*, **50,** 365–387.
17. O'Neil, R. G. and Boulpaep, E. L. (1982) *Am. J. Physiol.*, **243,** F81–F95.
18. O'Neil, R. G. and Helman, S. I. (1977) *Am. J. Physiol.*, **233,** F544–F558.
19. Petty, K. J., Kokko, J. P., and Marver, D. (1978) *J. Clin. Invest.*, **68,** 1514–1521.
20. Sansom, S. C., Weinman, E. J., and O'Neil, R. G. (1982) *Fed. Proc.*, **42,** 305.
21. Schwartz, G. J. and Burg, M. B. (1978) *Am. J. Physiol.*, **235,** F576–F585.
22. Stanton, B. A., Biemesderfer, D., Wade, J. B., and Giebisch, G. (1981) *Kidney Inter.*, **19,** 36–48.
23. Stetson, D. L., Wade, J. B., and Giebisch, G. (1980) *Kidney Inter.*, **17,** 45–56.
24. Stoner, L. C., Burg, M. B., and Orloff, J. (1974) *Am. J. Physiol.*, **227,** 453–459.
25. Stokes, J. B. (1981) *Am. J. Physiol.*, **241,** F395–F402.
26. Stokes, J. B., Ingram, M. J., Williams, A. D., and Ingram, D. (1981) *Kidney Inter.*, **20,** 340–347.
27. Wade, J. B., O'Neil, R. G., Pryor, J. L., and Boulpaep, E. L. (1979) *J. Cell Biol.*, **81,** 439–445.
28. Wiederholt, M., Schoormans, W., Fischer, F., and Behn, C. (1973) *Pflugers Arch.*, **345,** 159–178.
29. Wiederholt, M., Schoormans, W., Hansen, L., and Behn, C. (1974) *Pflugers Arch.*, **348,** 155–165.
30. Wingo, C. S., Seldin, D. W., and Kokko, J. P. (1982) *J. Clin. Invest.*, **70,** 579–586.
31. Zeuthen, T. and Wright, E. M. (1981) *J. Membrane Biol.*, **60,** 105–128.

CHAPTER 6

HORMONAL REGULATION OF Na^+ CHANNELS IN TIGHT EPITHELIA

HAIM GARTY
Department of Membrane Research,
The Weizmann Institute, Rehovot, Israel

ISIDORE S. EDELMAN
Department of Biochemistry,
College of Physicians and Surgeons
Columbia University, New York

Sodium ion transport across the toad urinary bladder is considered to be a two-step process as suggested by Koefed-Johnson and Ussing for frog skin (22). According to this scheme, Na^+ enters epithelial cells passively from the mucosal (or apical) side and is then pumped into the interstitial space by the basolateral Na^+/K^+ pump (i.e., Na^+,K^+-ATPase*). Entry of Na^+ from the mucosal side is known to occur through apical Na^+ specific channels which can be blocked by the diuretic amiloride (2, 6, 28, 35).

The flow of Na^+ across this and related epithelia is regulated by two classes of hormones: mineralcorticoids, such as aldosterone, and antidiuretic peptide hormones (ADH) such as vasopressin and oxytocin. Aldosterone diffuses into the epithelial cells and combines with a receptor in the cytoplasm. The active complex is then translocated to the nucleus and induces RNA and protein synthesis (8, 9). ADH, on the other hand, binds to a receptor on the basolateral membrane and mediates its action on Na transport by activating adenylate cyclase (20).

Although the initial stages of the hormone-cell interaction are fairly well understood both for aldosterone and ADH, the mechanisms by which Na^+ transport is augmented by these hormones are under current investigation. Accumulating data indicate that a critical step in the stimulation of Na^+ transport by aldosterone and ADH is augmentation of apical Na^+ permeability (1, 5, 12, 13, 24, 40). For aldosterone, however, effects (direct or indirect) on the Na^+,K^+-ATPase are also under consideration (17, 29, 39).

In recent studies amiloride-induced fluctuations in I_{sc} were used to analyze the nature of hormonal effects on apical Na^+ permeability (27, 35). The increases in I_{sc} induced by both aldosterone and ADH were proportionate to increases in the density of Na^+-conducting channels in the apical membrane, without appreciable changes in the single-channel currents. These findings indicate the existence of mechanism(s) capable of activating a pool of silent (not conductive) channels, and also raise the possibility that the two hormones share the same activation process, that is, a single pool of silent channels is activated as a consequence of the addition of either aldosterone or ADH.

It is also well documented that the Na^+ transport response to aldosterone depends on the availability of metabolic substrates (8, 11). The dependence of the aldosterone effect on cellular metabolism has been attributed to one of two possible pathways: either an increase in the supply of energy to the Na^+ pump or to effects on cellular Na^+ activity (determined by the pumping rate), which in turn regulates apical Na^+ permeability (13, 25, 40).

* Abbreviations: ADH, antidiuretic hormone, in this study vasopressin; TAME, *p*-toluene sulfonyl-L-arginine methyl ester; 2DG, 2-deoxy-glucose; I_{sc}, the transepithelial short circuit current; G, the transepithelial slope conductance; I_{Na}, the Na^+-specific (amiloride blockable) current; J_{Na} the initial rate of amiloride-sensitive ^{22}Na uptake measured in epithelial membrane vesicles; Na^+,K^+-activated adenosine triphosphatase (Na^+,K^+-ATPase).

In a recent study we obtained evidence of direct metabolic regulation of apical Na^+ permeability (15). This mechanism was also operative in ouabain-blocked bladders maintained in Na^+-free solutions. It is therefore independent of the pumping rate or the internal Na^+ activity. Reversible energy-dependent changes in apical Na^+ permeability in aldosterone-depleted bladders were also evident. Thus the apical Na^+ channels appear to be regulated by some energy-dependent process.

Previous studies on the regulation of Na^+ transport in tight epithelia provided indications of the existence of three types of processes:

1. Insertion of new channels in the apical membrane as a result of either *de novo* synthesis of channel proteins (8) or fusion of channel-containing vesicles with the apical membrane (26, 32, 36).
2. Activation of a preexisting, nonconductive pool of channels in the apical membrane by means of chemical modification of membrane components. Such processes may involve dephosphorylation of channel proteins (7, 30), or changes in the composition of the lipids surrounding the channels (19, 24, 45). Although not well documented with respect to the actions of aldosterone or ADH, other possible effects such as reducing S-S groups, methylation of lipids or proteins, or other covalent modifications, may have to be considered in the future.
3. Activation of silent, preexisting channels in the membrane mediated by a cytoplasmic effector which interacts noncovalently with the Na^+ channels, such as Na^+ (13, 25), Ca^{2+} (3, 4, 44), protons, or nucleotides.

In this chapter we summarize recent experiments designed to distinguish between the preceding possibilities and, specifically, whether regulation of Na^+ transport by ADH, aldosterone, and metabolism are mediated by the same pool of reservoir channels. Evidence is provided for the existence of two distinct processes: The first, which is triggered by aldosterone and is dependent on cellular metabolism, involves the opening of nonconductive channels that are resident in the apical surface. The second, triggered by ADH, involves recruitment of Na^+-conducting channels from another pool of channels, possibly subapical, and neither of these processes involves a stable, covalent chemical modification of a membrane component.

1. AMILORIDE-SENSITIVE TRYPSINIZATION OF Na^+ CHANNELS

A possible approach to the study of mechanisms involved in the regulation of Na^+ channels is to block irreversibly at least part of the channels present in the membrane at a given time, and assess if such blockage also impairs hormonal effects on I_{sc}. Such irreversible inactivation of apical Na^+ channels was achieved by amiloride-sensitive proteolytic digestion of the muco-

sal surface (14). In these experiments bladders were mounted in Ussing-type chambers, and the changes induced in apical Na^+ permeability by trypsin, amiloride, hormones, and metabolism were assessed by monitoring I_{sc} and G (14, 43).

As described previously (14), the application of trypsin (1 mg/ml) to the mucosal surface of toad bladders evoked substantial decreases in I_{sc}, to about 50% of the initial values (Fig. 6.1*A*). Removing the proteolytic enzyme by extensive perfusion with trypsin-free Ringers (Fig. 6.1*A*) or inhibiting its action (Fig. 1 in ref. 14) aborted the current decrease but did not significantly reverse it. The residual current was not decreased further by a second application of trypsin after the washout. The addition of amiloride (80 μM), however, completely inhibited this residual current, implying that the Na^+-conducting channels retained the amiloride-binding site. The effects of trypsin on I_{sc} were prevented if trypsin inhibitor (0.5 mg/ml) was added together with the enzyme. In these experiments the mucosal and serosal solutions (NaCl Ringers) were identical. Thus the decrease in I_{sc} must represent a decrease in Na^+ flux across the epithelium, presumably due to proteolytic digestion of a component of the apical Na^+ channels.

The specificity of the proteolytic attack on the Na^+ channels was assessed by evaluating the degree of protection afforded by pretreatment with amiloride (Fig. 6.1*B*). In this experiment, paired quarter bladders were challenged with amiloride (80 μM added mucosally), and 5 min later one of them received trypsin. Amiloride and trypsin were then removed by perfusing the mucosal side with NaCl Ringers. This wash restored the initial current in the quarter bladder that was trypsinized in the presence of amiloride in contrast to the quarter bladder that received trypsin alone (compare Fig. 6.1*A* and

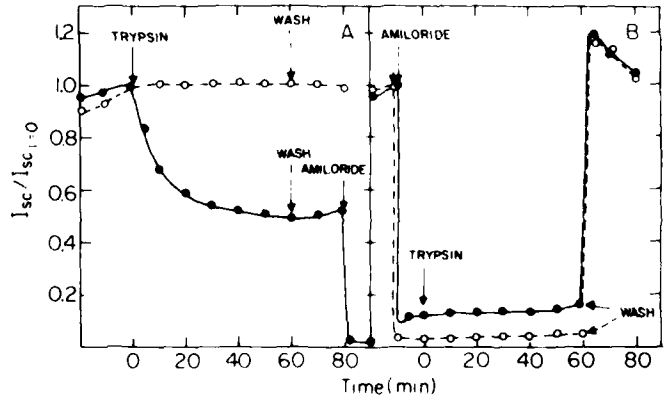

Figure 6.1. Trypsin effects on I_{sc} in the presence and absence of amiloride. Paired hemibladders were mounted in double chambers and incubated for several hours in NaCl Ringer's. I_{sc} was measured in the quarter bladders as described previously (14, 43). At the times indicated by arrows, trypsin (1 mg/ml) and amiloride (80 μM) were added to the mucosal solutions. The washout was performed by perfusing the musocal compartment with trypsin- and amiloride-free Ringer's for 5 min. Experimental quarter bladders (●) are compared to controls (○).

Fig. 6.1*B*), that is, amiloride prevented the irreversible decrease in current induced by trypsin. The same conclusion was derived from experiments in which one of two paired quarter bladders received amiloride and both tissues were exposed to trypsin (14). The possibility that amiloride inactivates trypsin directly was ruled out by assaying the proteolytic potency of the two mucosal solutions. The enzymatic activity was 80–90 TAME units per milligram trypsin with or without amiloride in the solution.

Table 6.1 summarizes eight experiments in which the protocol of Fig. 6.1 was used: Proteolytic digestion decreased I_{sc} to 0.52 ± 0.06 of the initial value, and no significant effect on the postwashout I_{sc} was found when trypsin was added to amiloride-blocked quarter bladders. We suggest that binding of amiloride to the Na^+ channels either itself masks the cleavage site or induces conformational changes that mask the cleavage site from the proteolytic enzyme.

In contrast to the marked trypsin-induced change in I_{sc} no significant decrease of G was detected (Table 6.1). The transepithelial conductance is of course made up of three components, the apical membrane, the basolateral membrane, and the paracellular shunt (31). It is possible that changes in G are small because only one of these components, the apical membrane, is affected by trypsinization. To estimate the effect of trypsinization on the apical conductance, we measured the changes in I_{sc} and G in K^+-depolarized bladders in the presence and absence of amiloride. The high serosal K^+ in this preparation causes a large increase in the conductance of the basolateral membrane (34). Under these conditions, total transcellular conductance is nearly equal to the conductance of the apical membrane alone. In addition, amiloride was used to evaluate the paracellular (amiloride–insensitive) contribution to the transepithelial conductance. With this protocol we found that the trypsin-induced decrease in I_{sc} to 0.4 ± 0.04 of the initial value was accompanied by a proportionate decrease in apical conductance

TABLE 6.1. EFFECTS OF TRYPSIN ON I_{sc} AND G IN THE PRESENCE AND ABSENCE OF AMILORIDE[a]

	Initial Values		Fractional Change	
	$I_{sc}(\mu A/cm^2)$	$G(mS/cm^2)$	I_{sc}	G
Trypsin	27.3 ± 6.7	0.75 ± 0.09	0.52 ± 0.06	0.95 ± 0.10
Trypsin + amiloride	28.5 ± 11.3	0.77 ± 0.13	1.02 ± 0.13	1.10 ± 0.10
Amiloride	39.8 ± 13.9	0.72 ± 0.20	1.14 ± 0.10	1.12 ± 0.06
Diluent	15.8 ± 3.0	0.8 ± 0.15	1.00 ± 0.10	0.98 ± 0.07

[a] The experimental protocol is as described in Fig. 6.1. The fractional changes of I_{sc} and G are the ratios between the values measured after the washout (at $t \sim 90$ min) and the values measured before the addition of amiloride and/or trypsin ($t \sim -15$ min). Measurements in eight toads were averaged, and the data are expressed as mean ± S.E.M. (14).

to 0.38 ± 0.05 of the initial value (14). In contrast, proteolytic digestion had no significant effect on the paracellular conductance (1.1 ± 0.07). The finding that trypsinization decreases I_{sc} and apical conductance to the same extent lends support to the conclusion that the changes in I_{sc} reflect irreversible closure of Na^+ channels.

The ability of trypsin to block, irreversibly, part of the Na^+-conducting channels that are present in the membrane at a given time was used to investigate and distinguish between two possible mechanisms in hormonal activation of Na^+ channels. The experimental protocol utilized in this study is illustrated in Fig. 6.2 and involved comparisons of the responses of control and trypsin-treated quarter bladders to ADH, aldosterone, and pyruvate (added to a substrate-depleted, aldosterone-treated bladder). For this comparison two parameters were calculated: (1) The fractional hormone-induced increase in current, that is, I_{sc2}/I_{sc1}*; (2) the normalized incremental increase in current, defined as $(I_{sc2} - I_{sc1})/I_{sc0}$.

Two possible mechanisms were considered. In the first, denoted Model I, it was assumed that the hormone-induced channels are present in the membrane in a silent form prior to exposure to the hormone and are subject to the same degree of trypsin inactivation as the base-line channels. In this case fewer channels will be opened by the hormone in the trypsin-inactivated bladder, that is, $(I_{sc2} - I_{sc1})I_{sc0}$ will be smaller, but I_{sc2}/I_{sc1} should have the same value for both quarter bladders.† The second possibility, denoted Model II, assumed that the hormone-induced channels are completely protected from trypsin inactivation prior to the addition of hormone, that is, they are either not exposed to the mucosal solution or have a trypsin-insensitive conformation. In this case, the same number of channels will be induced by ADH and/or aldosterone in the control and trypsinized bladders, that is, $(I_{sc2} - I_{sc1})/I_{sc0}$ will have the same value in both cases. I_{sc2}/I_{sc1}, in contrast, will be larger for the trypsinized hemibladder by a factor of I_{sc0}/I_{sc1}. Thus by performing the foregoing analysis one may be able to distinguish between two principal mechanisms for Na^+ channel activation (14).

Table 6.2 summarizes the fractional and normalized incremental current changes measured in control and trypsin-treated bladders, stimulated by ADH, aldosterone, and pyruvate (applied to substrate-depleted, aldosterone-repleted bladders). In addition to the experimental values, the values predicted by the models are also included in the table. These predictions were made from the response of the control quarter bladders to ADH, aldosterone, or pyruvate, and the trypsin-induced decrease of the baseline currents (I_{sc1}/I_{sc0}).

* I_{sc0} denotes the short-circuit current just before the addition of trypsin or the diluent, I_{sc1} the value just before the addition of hormone, I_{sc2} the value at the peak of the response to hormone.
† Note that ADH and aldosterone are added to the serosal compartment only, whereas trypsin is applied from the mucosal side. Thus interaction between the proteolytic enzyme and these hormones or their receptors is highly unlikely.

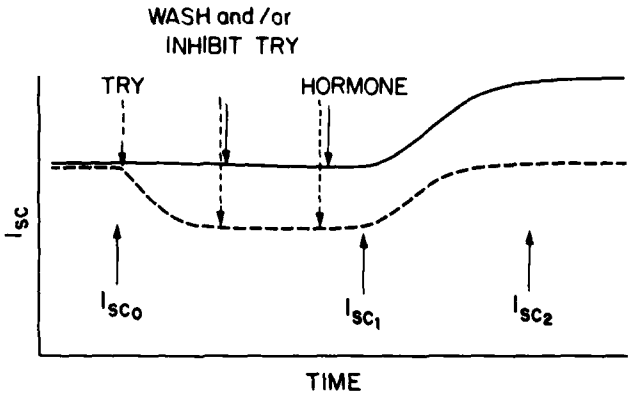

Figure 6.2. Schematic representation of the protocol used to assess the effects of pretrypsinization on the response to hormones.

Preexposure to trypsin increased the fractional change in I_{sc} induced by ADH from 2.2 ± 0.1 to 3.4 ± 0.3 and had no effect on the normalized incremental current change (Table 6.2). This result is in full agreement with the predictions made by Model II and indicates that exposing the mucosal surface to trypsin did not impair the ability of ADH to activate apical Na^+ channels, that is, the ADH-induced channels were either not present in the apical membrane or were in a tryspin-insensitive conformation prior to the addition of ADH.

TABLE 6.2. ANALYSIS OF HORMONAL AND METABOLIC AUGMENTATION OF I_{sc}[a]

		Measured Values		Predicted Values		
Additions	Parameter	Control	Trypsin Treated	Model I	Model II	Quarters (n)
	I_{sc0} (μA/cm^2)	26.7 ± 9.3	25.9 ± 10.6			
ADH	I_{sc2}/I_{sc1}	2.2 ± 0.1	3.4 ± 0.3	2.2	3.5	12
	$(I_{sc2} - I_{sc1}/I_{sc0}$	1.1 ± 0.1	1.2 ± 0.2	0.5	1.1	
	I_{sc0} (μA/cm^2)	21.7 ± 4.5	17.1 ± 4.8			
Aldosterone	I_{sc2}/I_{sc1}	2.4 ± 0.4	1.9 ± 0.3	2.4	3.5	12
	$(I_{sc2} - I_{sc1}/I_{sc0}$	1.45 ± 0.4	0.8 ± 0.2	0.8	1.45	
	I_{sc0} (μA/cm^2)	12.5 ± 2.1	18.3 ± 2.7			
Pyruvate	I_{sc2}/I_{sc1}	1.9 ± 0.2	1.85 ± 0.15	1.9	2.9	9
	$(I_{sc2} - I_{sc1}/I_{sc0}$	1.2 ± 0.2	0.65 ± 1.5	0.6	1.2	

[a] The fractional and incremental responses to ADH (50 mU/ml), aldosterone (0.5 uM) and pyruvate (5 mM) were determined as described in the text. The experimental procedures are given in ref. 14.

The opposite result was obtained when the same analysis was carried out for bladders activated by aldosterone (Table 6.2). In this case similar fractional changes in current were measured for the control and trypsinized quarter bladders, but the normalized incremental increase in I_{sc} of the trypsinized quarter bladders (0.8 ± 0.2) was significantly lower than that obtained for the control (1.45 ± 0.4). This result fits Model I but not Model II. Thus, in contrast to ADH, the action of aldosterone is impaired by proteolytic digestion. The magnitude of this impairment fits the possibility that aldosterone inducible silent channels in the apical membrane are inactivated by the enzyme exactly to the same extent as the baseline, conductive, channels. A similar conclusion was derived from the response of substrate-depleted bladders to pyruvate. As for aldosterone, the trypsin-treated quarter bladders exhibit a "Model I type" current change in response to pyruvate. Thus the increase in Na^+ permeability induced by substrates appears to involve a set of preexisting nonconductive apical channels.

An alternative possibility, however, is that the impairment in the response to aldosterone and pyruvate is due to the lysis of membrane proteins other than the Na^+ channels. To assess this possibility, we took advantage of the ability of amiloride to "protect" the Na^+ channels from enzymatic digestion. As shown in Fig. 6.1 and Table 6.1, amiloride prevented the inactivation of Na^+ channels by trypsin but presumably had no effect on the cleavage of other "non amiloride-binding" proteins. Thus, impairment of the response to aldosterone by trypsinization of membrane proteins, other than silent Na^+ channels, should not be prevented by exposure to trypsin in the presence of amiloride. If the hypothetical closed channels, however, happen to interact with amiloride in the same way as the baseline (open) channels, trypsin should have no effect on the ability of aldosterone to stimulate I_{sc}. In eight pairs of quarter bladders we saw no difference in the response to aldosterone between the quarter bladders trypsinized in the presence of amiloride and the control quarter bladders that were not exposed to trypsin. This finding indicates not only that the channels activated by aldosterone were indeed exposed to the proteolytic enzyme prior to the hormonal stimulation, but also the amiloride binds to these silent channels in a way similar to the baseline channels.

In summary, the data described in this section provide evidence of the existence of two spatially distinct precursors of Na^+ channels which are under differential control by ADH and aldosterone. At least one of these precursors is continuously present in the apical membrane; it can be inactivated by trypsin and is capable of binding amiloride. The other could be present in a submembranal compartment or have a trypsin-insensitive conformation. The conclusion that ADH and aldosterone do not draw on the same pool of inactive channels is supported by the finding that ADH added to aldosterone-treated bladders increased I_{sc} even more than in bladders that did not receive aldosterone (18). In two previous studies an approach similar to ours was used to investigate hormonal effects on I_{sc}. Palmer and

Edelman (33), and Park and Fanestil (37) used diazosulfanilic acid (DSA) and tyrosine-reactive reagents, respectively, to inhibit the baseline current irreversibly. In both studies the response to ADH was inhibited as well. A possible explanation for the discrepancy between these results and ours is that DSA and the tyrosine-reactive reagent impair the ability of ADH to insert Na^+ channels in the apical membrane by modifying sites other than silent Na^+ channels, which are not modified by trypsin. Alternatively, it is possible that the ADH-induced channels are present in the apical membrane in a conformation that is sensitive to the foregoing reagents but insensitive to trypsin.

2. AMILORIDE-INHIBITABLE Na^+ FLUXES IN APICAL MEMBRANE VESICLES

Another system we used to explore possible mechanisms of hormonal activation of Na^+ channels was a vesicle preparation, isolated from the toad bladder epithelium, in which amiloride inhibitable $^{22}Na^+$ fluxes were measured. These measurements, however, are subject to two major difficulties common to many other vesicle preparations that contain ion channels. First, Na^+ flux through a single Na^+ channel is of the order of 10^6 ions per sec (28, 35). Thus the equilibration time of a tracer added to a suspension of small vesicles will be of the order of seconds, that is, inaccessible to manual techniques. Second, the density of Na^+-conducting channels in the apical membrane is as low as $0.5/\mu m^2$ (35). The mean diameter of a membrane vesicle, which we estimated from the electron micrographs of Rodriguez and Edelman (38), is 0.4 μm. Accordingly only part of the apical vesicles are expected to contain a channel. In addition, the preparation is invariably contaminated by basolateral and mitochondrial membranes. One is therefore faced with the problem of measuring a very fast flux in a small fraction of the total vesicular volume. Indeed, previous measurements of Na^+ fluxes in toad bladder membrane vesicles either failed to show sensitivity to amiloride or required a fast reaction apparatus (4, 23). To overcome these difficulties, Garty et al (16) developed a simple and sensitive flux assay which enabled us to detect conveniently amiloride-sensitive $^{22}Na^+$ fluxes in a crude microsomal preparation. This assay proved to be useful in a number of other similar systems, such as gramicidin D incorporated into lipid vesicles and the veratridine-activated, tetrodotoxin-inhibitable Na^+ channels in rat brain synaptic membranes (16).

The principle of the assay is as follows: vesicles are prepared to contain a relatively high concentration of NaCl (55 m*M*), and shortly before the assay the external Na^+ is replaced by $K^+$and/or Tris. As a consequence of the imposed ion gradients an electrical diffusion potential is set up across each membrane, the magnitude of which is determined by the relative permeabilities of Na^+, K^+, Cl^-, and Tris. In those vesicles that are highly permeable to

Na^+ and impermeable to K^+, Cl^-, and Tris (i.e., of apical origin and containing Na^+ channels), a maximal, negative inside potential will be formed. $^{22}Na^+$, added to the external solution, will tend to equilibrate with the electrical potential (without itself significantly affecting it) and therefore accumulate selectively in those vesicles containing Na^+ channels. In time, the ion gradients will slowly dissipate, and $^{22}Na^+$ will leave the vesicles, until chemical equilibrium is reached. The advantages of measuring $^{22}Na^+$ uptake by this method are the following:

1. At the peak of the uptake the tracer will accumulate inside the vesicles at least 100-fold. Therefore, the sensitivity of this transport assay should be much greater than the conventional measurements of tracer equilibration.
2. As a result of this accumulation the time course of $^{22}Na^+$ uptake is relatively slow, that is, in minutes rather than in seconds (4, 16, 18).
3. The "functional discrimination" between vesicles with different permeability characteristics enables the detection of amiloride-sensitive fluxes even in very crude cell homogenates. This is particularly important if the time delay between the disruption of the cells and the assay of Na channels must be kept as brief as possible.

Figure 6.3 illustrates the time course of $^{22}Na^+$ uptake measured in toad bladder microsomes that contain 55 m*M* NaCl and were suspended in isotonic solution that contained sucrose and either 10 m*M* NaCl or 10 m*M* KCl. In the absence of external Na^+, $^{22}Na^+$ was accumulated to a peak concentra-

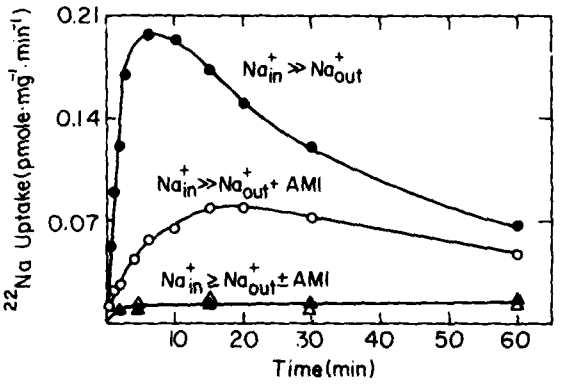

Figure 6.3. Time course of $^{22}Na^+$ uptake in cell membrane vesicles. Vesicles were prepared from two hemibladders as described in ref. 16 and suspended in 0.5 ml homogenizing medium (final concentration ~ 1 mg protein per milliliter). Aliquots of 150 μl were applied on shorter Dowex 50 × 8 columns (Tris form) and eluted with 175 m*M* sucrose. The eluted vesicles (1 ml) were mixed at $t = 0$ with 100 μl reaction mixture which contained 5 μCi ^{22}NaCl plus one of the following mixtures: (●—●) 110 m*M* KCl; (○—○) 110 m*M* KCl and 1 m*M* amiloride: (▲—▲) 110 m*M* NaCl; (△—△) 110 m*M* NaCl + 1 m*M* amiloride. Aliquots of 100 μl were sampled at the times indicated in the figure as described in ref. 16.

tion in 6 min (upper curve) and then leaked out slowly. The initial uptake represents the accumulation of $^{22}Na^+$ in the vesicles, driven by the potential established across the apical membrane vesicles. The secondary decrease of radioactivity is due to the slow dissipation of the NaCl gradient (Na^+/K^+ exchange and NaCl efflux). Most of the $^{22}Na^+$ uptake was blocked by amiloride (100 μM) added to the vesicle suspension at $t = 0$ (middle curve). Amiloride decreased the initial rate of uptake of $^{22}Na^+$ and shifted the peak radioactivity level to longer times. This behavior is as expected for a reagent that decreases the Na^+ permeability of the vesicles (compare Figure 5 in ref. 16). When 10 mM NaCl was included in the external medium $^{22}Na^+$ uptake was minimal, and sensitivity to amiloride could not be detected (lower curve in Fig. 6.3). Similarly, $^{22}Na^+$ uptake was abolished if LiCl was used instead of NaCl in the external medium. Thus the ^{22}Na fluxes shown in Fig. 6.3 occur in vesicles that are highly permeable to Na^+ and Li^+ but relatively impermeable to K^+ and Cl^-, that is, as predicted for apical Na^+-channel-containing vesicles (21, 42).

To confirm that in these vesicles the amiloride-sensitive flux is mediated by apical Na^+ channels, we measured the dose-response relations of this diuretic (Fig. 6.4). About 35% of $^{22}Na^+$ uptake was insensitive to amiloride (up to 200 μM). The mean amiloride concentration that produced 50% inhibition was 4.6 ± 0.2 μM ($N = 5$ vesicle preparations). This value is substantially higher than that usually obtained in intact bladder (2, 35), yet low enough to exclude nonspecific amiloride effects. The decreased sensitivity to amiloride, compared to the intact bladder may be a result of the high internal Na^+ activity (as compared to the usual cytoplasmic Na^+ activity), the low external Na^+ activity (as compared to the usual mucosal Na^+ con-

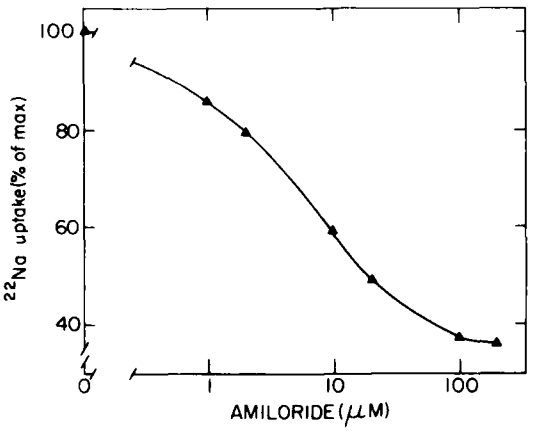

Figure 6.4. The sensitivity of $^{22}Na^+$ uptake to amiloride in vesicles. Tracer uptake was measured as described in the legend to Fig. 6.3 and ref. 16 using a reaction mixture that contained KCl and various concentrations of amiloride. The initial rate of ^{22}Na uptake was calculated, for each amiloride concentration, from four time points taken during the first 3 min after adding $^{22}Na^+$. These rates are presented as percent of the rate in the absence of amiloride.

centrations), or the magnitude of the electrical potential imposed across the apical membrane in our preparations. Indeed, Shum and Fanelli (41) found that in frog skin substitution of high internal and zero external Na^+ concentrations for the standard solutions increased the K_i of amiloride from 0.44 μM to 2.3 mM.

We used the vesicle preparation to determine if activation of Na^+ channels in intact bladders by ADH and aldosterone is preserved in the isolated membranes obtained from these bladders. In these experiments, one of each pair of hemibladders was treated with ADH or aldosterone and the other served as a control. After the full hormonal effect on I_{sc} had been developed, membrane vesicles were prepared, and $^{22}Na^+$ uptake was measured in the presence and absence of amiloride, as described previously (16).

As observed in many previous studies, aldosterone and ADH both induced two-fold increases in I_{sc} (Table 6.3), but no significant increases were detected in J_{Na} measured in vesicles isolated from the hormone-treated hemibladders (Table 6.3). The ratio of the fluxes measured in the control and hormone-treated vesicles did not differ significantly from one. The J_{Na} values obtained in the experiments with aldosterone, however, were about half of the values obtained in the experiments with ADH (both control and hor-

TABLE 6.3. COMPARISON OF HORMONAL EFFECTS ON I_{sc} IN ISOLATED TOAD BLADDERS AND J_{Na} IN EPITHELIAL VESICLES[a]

I_{sc}(μA/mg Protein)	Treated Hemibladder	Control Hemibladder	Paired Ratio
I Aldosterone	181.7 ± 47.2	120.3 ± 20.6	1.8 ± 0.5
II ADH	308 ± 48.5	147.7 ± 47.2	2.7 ± 0.9
III 2-DG	48.3 ± 21.1	203 ± 54.6	0.29 ± 0.13
J_{Na}(pmol $^{22}Na^+$/mg min)			
I Aldosterone	0.68 ± 0.07	0.65 ± 0.1	1.07 ± 0.08
II ADH	1.13 ± 0.18	1.35 ± 0.18	0.85 ± 0.1
III 2-DG	1.3 ± 0.07	1.22 ± 0.11	1.1 ± 0.15

[a] Paired hemibladders were mounted and treated as follows:

I. One hemibladder (treated) received aldosterone (0.5 μM serosal side only) and the other (control) an equal volume of diluent. The hemibladders were incubated in NaCl Ringers for 14–18 h. Then I_{sc} was measured, vesicles prepared, and J_{Na} measured as described in ref. 16.

II. The treated hemibladder received ADH (50 mU/ml added serosally) and the control diluent. I_{sc} was recorded continuously, and when maximal stimulation was obtained (15–20 min) the cells were scraped and treated as described.

III. The treated hemibladder received 2-deoxyglucose (10 mM, added serosally) and the control glucose (10 mM, added serosally). Two hours later I_{sc} was measured, the cells were scraped, and treated as before. For each treatment four experiments were averaged, and the data are expressed as mean ± S.E.M.

mone-treated vesicles). This difference probably is a result of overnight incubation of the mounted bladders in the aldosterone experiments, whereas in the case of ADH cells were scraped from freshly mounted tissues. Overnight incubation of the mounted bladders did indeed reduce I_{sc} to 0.43 ± 0.1 (N = 4 hemibladders) of the initial value, that is, this treatment, unlike the application of ADH or aldosterone, induced a proportionate change of I_{sc} and J_{Na}.

The foregoing protocol was also used to examine whether the decrease of apical Na^+ permeability induced by metabolic inhibitors such as 2-deoxyglucose and oxythamine is reflected in the vesicles isolated from the inhibited bladders. A 2-h incubation with 2-deoxyglucose (10 mM) reduced I_{sc} to 0.29 ± 0.13 of the control value measured in a paired hemibladder that received 10 mM glucose (Table 6.3). This decrease, however, was not associated with a significant change of J_{Na} (Table 6.3). Thus, as for aldosterone and ADH, the changes induced in apical Na^+ permeability by 2-deoxyglucose in intact bladders are not retained by the vesicles isolated from these bladders.

The fact that the hormonal and metabolic effects on I_{sc} were not preserved in the vesicles isolated from the treated bladders may serve as a criterion for distinguishing among some of the possible mechanisms responsible for the activation of apical Na^+ channels. For instance, the possibility that aldosterone stimulates Na^+ transport by enhancing the synthesis of new channel proteins (8) or by modifying apical membrane lipid composition (19, 24) now seems unlikely. In both cases, stable, covalent modification of the apical surface should be preserved in the membrane vesicles.

These data, however, are in agreement with other possible mechanisms that involve noncovalent interactions between channels and cytoplasmic effectors such as Ca^{2+} or Na^+ (3, 4, 13, 25, 44) or mechanisms that assume covalent but unstable modification of the channel protein (e.g., cAMP-dependent dephosphorylation) (7, 30). In these cases the hormonal effect is expected to reverse shortly after the cell is ruptured and the cytoplasm is replaced by the external medium. In previous studies special consideration has been given to the possibility that ADH stimulates Na^+ transport by inducing the fusion of channel-containing vesicles with the apical membrane (26, 32, 36). This model is supported by the finding that the ADH-induced channels are inaccessible to trypsin prior to the addition of this hormone (14). The fact that the ADH-induced increase in Na^+ permeability is not retained by the vesicles isolated from ADH-treated bladders was somewhat unexpected. The interpretation of this result, however, is complicated because:

1. It is well documented that the ADH effect on Na^+ transport is transient and I_{sc} decays to the pre-ADH values within 1–3 h. Since the nature of this reversibility is not understood it is difficult to predict whether or not disruption of the cell membrane will "freeze" the high-permeability state of the apical membrane.

2. Fusion of cytoplasmic vesicles with the plasma membrane could in principle be either facilitated or reversed by homogenizing the cells. In this case the distribution of Na^+ channels between plasma membrane and cytoplasmic vesicles will be unrelated to their distribution in the intact cells.

3. Cytoplasmic Na^+ channel-containing vesicles may contribute to the measured amiloride-sensitive flux in the isolated microsomes. Thus the flux assay may not distinguish between channels in plasma membrane and cytoplasmic vesicles.

3. CONCLUSION

Our results and studies by others led to the construction of the scheme illustrated in Fig. 6.5. The main features of this scheme are as follows: (1) Na^+ channels exist in the apical membrane in at least two conformations, closed (nonconductive) and open (conductive). Both conformations can be cleaved by trypsin and bind amiloride (upper illustration). (2) As suggested by others (3, 4, 44) Ca^{2+} can block Na^+ channels from the cytoplasmic side. The target for Ca^{2+} ions will be either the cytoplasmic side of the open channel or the reaction that activates closed channels (upper illustration). It has been suggested that cellular Na^+ may have similar functions (13, 25). However, no convincing evidence in favor of this model has been presented thus far. (3) Aldosterone acts by shifting the equilibrium between the two conformations toward the open state by an as yet unknown process. This process, however, does not involve a stable covalent modification of the apical membrane proteins or lipids. The aldosterone effect is mediated by some energy-dependent pathway (lower illustration). (4) Cellular metabolism can reversibly modulate the equilibrium between the closed and open

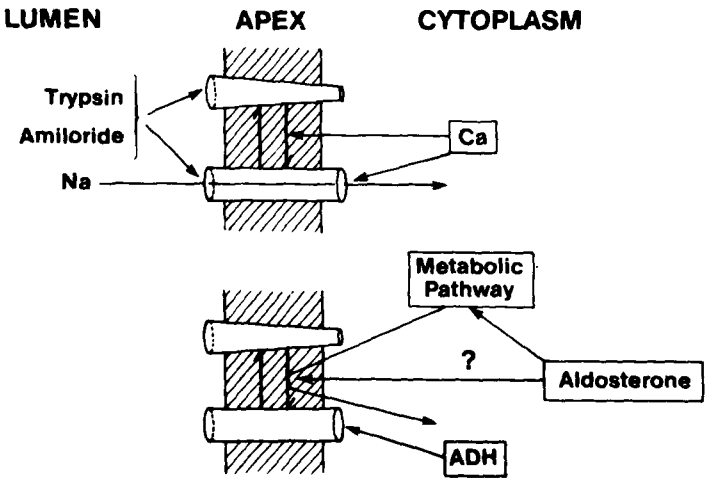

Figure 6.5. Model of the pathways for the regulation of apical Na channels in toad bladder.

states. This effect is not mediated by metabolic effects on the basal-lateral Na^+ pump or the cytoplasmic Na^+ activity (15). (5) ADH affects the apical Na^+ permeability through another pathway which does not involve the previously postulated equilibrium between closed and open channels. This hormone may either induce the fusion of channel-containing vesicles with the apical membrane or recruit another trypsin-insensitive pool of apical channels (lower illustration).

REFERENCES

1. Andreoli, T. E., and Schafer, J. A. (1976) *Ann. Rev. Physiol.*, **38**, 451–500.
2. Bentley, P. J. (1968) *J. Physiol. (Lond.)*, **195**, 317–330.
3. Chase, H. S. and Al-Awqati, Q. (1981) *J. Gen. Physiol.*, **77**, 693–712.
4. Chase, H. S. and Al-Awqati, Q. (1983) *J. Gen. Physiol.*, **81**, 643–665.
5. Crabbe, J. (1972) *J. Steroid Biochem.*, **3**, 229–235.
6. Crabbe, J. and Ehrlich, E. N. (1968) *Pfluegers Arch.*, **304**, 284–296.
7. DeLorenzo, R. J., Walton, K. G., Curran, P. F., and Greengard, P. (1973) *Proc. Natl. Acad. Sci. USA*, **70**, 880–884.
8. Edelman, I. S., Bogoroch, R., and Porter, G. A., (1963) *Proc. Natl. Acad. Sci. USA*, **50**, 1169–1177.
9. Edelman, I. S. and Marver, D. (1980) *J. Steroid. Biochem.*, **12**, 219–224.
10. Fanestil, D. D., Porter, G. A., and Edelman, I. S. (1967) *Biochim. Biophys. Acta*, **135**, 74–88.
11. Fimognari, G. M., Porter, G. A., and Edelman, I. S. (1967) *Biochim. Biophys. Acta*, **135**, 89–99.
12. Frazier, H. S., Dempsey, E. F., and Leaf, A. (1962) *J. Gen. Physiol.*, **45**, 529–543.
13. Frizzell, R. A. and Schultz, S. G. (1978) *J. Membrane Biol.*, **39**, 1–26.
14. Garty, H. and Edelman, I. S. (1983) *J. Gen. Physiol.*, **81**, 785–803.
15. Garty, H., Edelman, I. S., and Lindemann, B. (1983) *J. Membrane Biol.*, **74**, 15–24.
16. Garty, H., Rudy, B., and Karlish, S. J. D. (1983) *J. Biol. Chem.*, **258**, 13094–13099.
17. Geering, K., Girardet, M., Bron, G., Kraehenbuhl, J. P., and Rossier, B. C. (1982) *J. Biol. Chem.*, **257**, 10338–10343.
18. Glynn, I. M. and Warner, A. E. (1972) *Br. J. Pharmacol.*, **44**, 271–278.
19. Goodman, D. B. P., Wong, M., and Rasmussen, H. (1975) *Biochemistry*, **14**, 2803–2809.
20. Handler, J. S. and Orloff, J. (1973) in *Handbook of Physiology. Renal Physiology*, *Am. Physiol. Soc.*, 791–814.
21. Herrera, F. C. (1972) *Am. J. Physiol.*, **222**, 499–502.
22. Koefoed-Johnsen, V. and Ussing, H. H. (1958) *Acta Physiol. Scand.*, **42**, 298–308.
23. Labelle, E. F. and Valentine, M. E. (1980) *Biochim. Biophys. Acta*, **601**, 195–205.
24. Lein, E. L., Goodman, D. B. P., and Rasmussen, H. (1975) *Biochemistry*, **14**, 2749–2754.
25. Lewis, S. A., Eaton, D. C., and Diamond, J. M. (1976) *J. Membrane Biol.*, **28**, 41–70.
26. Lewis, S. A. and Moura, J. L. C. (1982) *Nature*, **297**, 685–688.
27. Li, J. H. Y., Palmer, L. G., Edelman, I. S., and Lindemann, B. (1982) *J. Membrane Biol.*, **64**, 77–89.
28. Lindemann, B. and Van Driessche, W. (1977) *Science*, **195**, 292–294.

29. Lipton, P. and Edelman, I. S. (1971) *Am. J. Physiol.*, **221,** 733–741.
30. Liu, A. Y. C. and Greengard, P. (1974) *Proc. Natl. Acad. Sci. USA*, **71,** 3869–3873.
31. MacKnight, A. D. C., DiBona, D. R., and Leaf, A. (1980) *Physiol. Rev.*, **60,** 615–715.
32. Masur, S. K., Holtzman, E., and Walter, R. (1972) *J. Cell. Biol.*, **52,** 211–219.
33. Palmer, L. G. and Edelman, I. S. (1981) *Ann. N.Y. Acad. Sci.*, **372,** 1–14.
34. Palmer, L. G., Edelman, I. S., and Lindemann, B. (1980) *J. Membrane Biol.*, **57,** 59–71.
35. Palmer, L. G., Li, J. H. Y., Lindeman, B., and Edelman, I. S. (1982) *J. Membrane Biol.*, **64,** 91–102.
36. Palmer, L. G. and Lorenzen, M. (1983) *Am. J. Physiol.*, **244,** F195–F205.
37. Park, C. S. and Fanestil, D. D. (1980) *Am. J. Physiol.*, **239,** F299–F306.
38. Rodriquez, H. J. and Edelman, I. S. (1979) *J. Membrane Biol.*, **45,** 215–232.
39. Saito, T., Essig, A., and Caplan, S. R. (1973) *Biochim. Biophys. Acta*, **318,** 371–382.
40. Sharp, G. W. G. and Leaf, A. (1966) *Physiol. Rev.*, **46,** 593–633.
41. Shum, W. K. and Fanelli, J. M., Jr. (1978) *Biochim. Biophys. Acta*, **512,** 593–597.
42. Singer, I. and Civan, M. M. (1971) *Am. J. Physiol.*, **221,** 1019–1026.
43. Spooner, P. M. and Edelman, I. S. (1975) *Biochem. Biophys. Acta*, **406,** 304–314.
44. Windhager, E. E. and Taylor, A. (1983) *Ann. Rev. Physiol.*, **45,** 519–532.
45. Yorio, T. and Bentley, P. J. (1978) *Nature*, **271,** 79–81.

CHAPTER 7

STUDIES OF THE KALLIKREIN–KININ SYSTEM AND PROSTAGLANDINS IN EPITHELIAL ION TRANSPORT

H. S. MARGOLIUS
P. V. HALUSHKA
J. CHAO
D. H. MILLER
Departments of Pharmacology and Medicine
Medical University of South Carolina
Charleston, South Carolina

A. W. CUTHBERT
J. A. SPAYNE
Department of Pharmacology
University of Cambridge
Cambridge, United Kingdom

Segments of intestinal epithelia serve as convenient model tissues for the study of the mechanisms responsible for peptide hormone effects on transport (8, 9, 31). The recent observations that the kinin peptides are among the most potent stimuli of intestinal chloride secretion (6, 7, 17), allow the addition of these agents to the list of peptides with a potential physiological or pathophysiological role in epithelial ion transport. The intestinal epithelium is also known to contain significant quantities of tissue kallikreins (10), specific serine proteinases capable of attacking kininogen substrates to liberate either lysyl bradykinin (kallidin) or bradykinin. The functional responsibilities of endogenous tissue kallikreins (and their kinin products) are still uncertain despite decades of study. However, recent evidence suggests some sort of kallikrein involvement in membrane transporting processes in kidney as well as in intestine. Some of the work described here represents a review of findings concerned predominantly with relations between tissue kallikrein and transepithelial electrolyte transport. The rest covers very recent studies of kinin effects upon epithelial ion transport events and some of the mechanisms involved in these events.

1. TISSUE KALLIKREINS AND ELECTROLYTE HOMEOSTASIS

The first association of tissue kallikreins with electrolyte homeostasis was the finding that the urinary excretion of human or rat renal kallikrein was increased markedly by low dietary sodium intake (12, 20). These observations, in conjuction with abnormally elevated kallikrein excretion in diseases of aldosterone excess (e.g., primary aldosteronism, Bartter's syndrome) (13, 21) led to many additional efforts which have established close correlations between urinary kallikrein excretion and/or renal kallikrein levels and sodium-retaining steroid activity (18). With the development of a method to measure tissue kallikrein synthesis (22), it is now possible to state that increased renal tissue kallikrein levels, or excretion in response to low dietary sodium, signify increased kallikrein synthesis (Table 7.1). Whether this represents a direct effect of sodium-retaining steroid upon the rate of synthesis of this constituitive enzyme of renal tubular cells (2, 24, 37) or an indirect response to other renal cellular events remains to be determined. However, renal kallikrein is localized in portions of the nephron long considered to be aldosterone sensitive, namely, the cortical distal convoluted tubule and collecting duct (27, 28, 33). Recently, the kininogen substrate from which the tissue kallikreins liberate kallidin has been localized to the same tubular segments (29). Studies of isolated renal cortical cells in suspension or of renal cortical subcellular fractions have established that tissue kallikreins are enriched in plasma membranes, with evidence for both apical and basolateral distributions (15, 27, 28, 33, 39). The enzyme behaves as a membrane-bound ectoprotein with active sites accessible to kallikrein inhibitors, anti-

TABLE 7.1. EFFECT OF LOW DIETARY SODIUM ON KALLIKREIN CONTENT AND SYNTHESIS RATE IN RAT KIDNEY AND SUBMAXILLARY GLAND[a]

	Kidney Kallikrein		Submaxillary Gland Kallikrein	
	Content (ng/mg protein)	Synthesis Rate (kallikrein CPM/ protein CPM)	Content (μg/mg protein)	Synthesis Rate (kallikrein CPM/ protein CPM)
Control	20.3 ± 1.3	$7.3 \pm 0.4 \times 10^{-4}$	39.3 ± 3.3	$3.0 \pm 0.2 \times 10^{-2}$
Low Na^+	36.7 ± 3.0	$13.5 \pm 1.7 \times 10^{-4}$	46.1 ± 4.4	$3.2 \pm 0.3 \times 10^{-2}$
	($P < 0.001$)	($P < 0.003$)	(NS)	(NS)

[a] Male Sprague-Dawley rats were kept on either a control or low sodium diet then injected with [^{35}S]methionine three to four weeks later. Kallikrein content and incorporation of [^{35}S]methionine were measured as described in ref. 22. All values are means ± S.E. ($n = 8$).

bodies, and substrates (2). These findings led to studies of kallikrein interactions with amiloride (19) and monovalent cations (3) which have shown that both are capable of inhibiting the purified enzyme *in vitro* but that only the former is equally effective in inhibiting membrane-bound enzyme (Figs. 7.1 and 7.2). It must be emphasized that the concentrations of amiloride

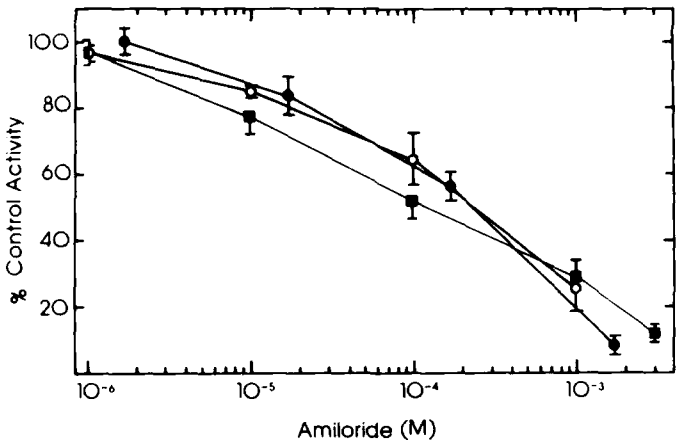

Figure 7.1. Inhibition of rat or human urinary kallikrein or of renal cortical cell suspension Tos-Arg-O[^{3}H]Me esterase activity by amiloride. Ten microliters (11 n*M*) of either rat (●) or human (○) urinary kallikrein, 10 μl of water or water plus amiloride (final concentrations as indicated), and 30 μl of 0.2 *M* Tris-HCl buffer, pH 8 were mixed and allowed to stand for 30 min at 25°C. Twenty microliters of freshly prepared rat renal cortical cells (■) (5.0×10^6 cells per milliliter) in phosphate-buffered saline containing 2 m*M* Ca^{2+}, 20 μl of 0.2 *M* Tris-HCl buffer, pH 8, and 10 μl of water or water containing amiloride (final concentrations as indicated) were mixed and allowed to stand for 30 min at 25°C. Tos-Arg-O[^{3}H]Me (3.0×10^4 cpm, 10 μl) was added, mixed, and allowed to incubate for 30 min. The reaction was stopped, and the [^{3}H] methanol released was measured as described in ref. 20. Activity is expressed as the percent of control esterase activity in the absence of amiloride. Each value represents the mean ± S.E. of from 6–12 experiments in duplicate. (Reprinted with permission from ref. 19.)

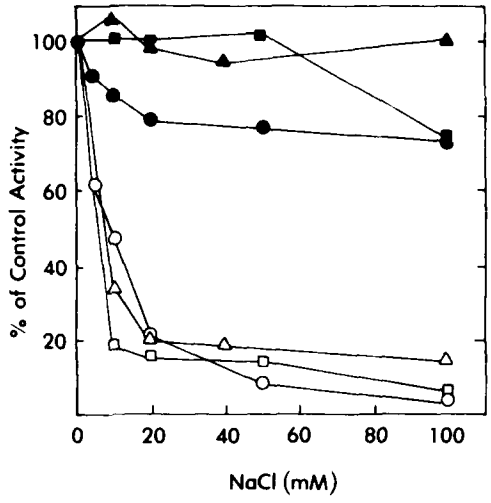

Figure 7.2. Effect of NaCl on soluble versus membrane-bound renal kallikreins. Esterase, kininogenase, and immunoreactivity of rat urinary kallikrein and rat renal cortical microsomal fractions were measured. Purified rat urinary kallikrein or amounts of rat renal microsomal fractions of comparable activity were mixed with NaCl (preincubation mixture concentration as indicated) at 37°C for 30 min. Subsequent kallikrein assay procedures are described in ref. 31. Open symbols represent purified enzyme and closed symbols represent membrane-bound enzyme. ○, ●, esterase activity; △, ▲, kininogenase activity; □, ■, immunoreactivity. (Reprinted with permission from ref. 3.)

required to inhibit all tested activities of human or rat tissue kallikreins 50% range from 85 to 230 μM, depending upon substrate, enzyme preparation, or assay system. These concentrations are far above those required for inhibition of amiloride-sensitive sodium channels, but are lower than required to inhibit other sodium entry pathways or Na^+,K^+-ATPase activity (1, 34). Recently, amiloride infused intravenously into rats was found to reduce significantly both urinary kallikrein activity as well as kinin excretion, along with the expected diuresis and increased urinary osmolar concentration (32).

An attempt to extend these inferential findings to a convenient, aldosterone- and amiloride-sensitive epithelium that contained tissue kallikrein was made and we focused upon the urinary bladder and skin of *Bufo marinus* toads where a high concentration of kallikrein-like enzyme(s) was found. This membrane-bound activity could be inhibited by amiloride with significant inhibition appearing with a low drug concentration ($\sim 10^{-8}$ M) but major inhibition at about 10^{-4} M (Fig. 7.3). Initial attempts to determine whether this enzymatic activity could be related to any ion transport events examined the effects of known inhibitors of kallikreins on urinary bladder short circuit current (SCC) measured in the usual fashion (25). A reversible inhibitor (aprotinin) and an irreversible inhibitor (D-phe-D-phe-L-arg-chloromethylketone, DPPA) of tissue kallikreins inhibit SCC at this site, but only partially (Fig. 7.4). Aprotinin effects on SCC were reversible and DPPA effects were irreversible. Both were effective more promptly and with lower doses after mucosal addition than after serosal addition. The soya bean trypsin inhibitor (SBTI) is an effective and potent inhibitor of trypsin-like serine proteinases, including the enzymes known as plasma kallikreins. This reagent had no effect on urinary bladder SCC (25), and this lack of efficacy is notable because SBTI is not an inhibitor of tissue kallikreins (36). Experiments carried out to assess the effects of aprotinin or DPPA on the amphotericin B-induced SCC after bladder exposure to a high concentration of

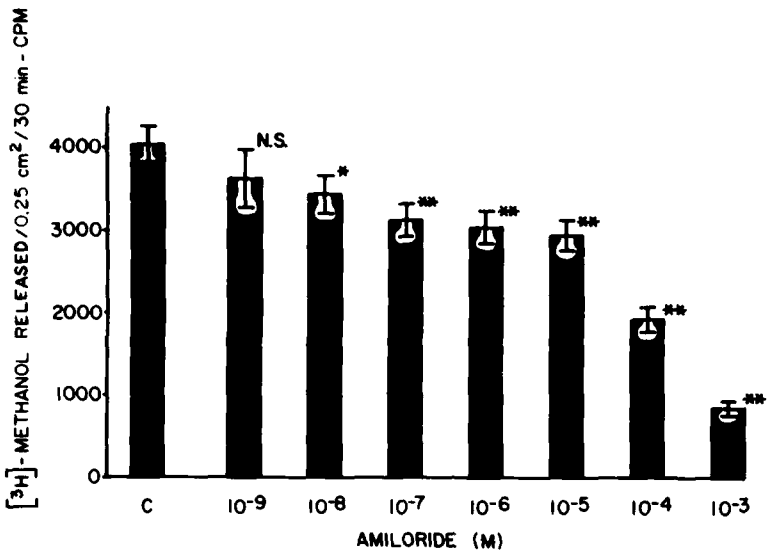

Figure 7.3. Tos-Arg-O[^{3}H]Me esterase (kallikrein-like) activity of toad bladder pieces in the absence (C) or the presence of amiloride. Each box represents the mean ± S.E. of the esterase activity (expressed as counts per minute of [^{3}H]methanol released per 0.25 cm^2/30 min) of no less than 45 separate pieces from 15 to 20 hemibladders. NS, not significantly different from control. *, **, differ from control with $P < 0.05$ or 0.001, respectively. (Reprinted with permission from ref. 19.)

amiloride disclosed no reduction in the induced SCC (26). This was in contrast to the observed reduction with ouabain and, together with the available localization data, suggests that tissue kallikrein inhibitors reduce SCC at this site by some action(s) at or near the mucosal surface. Clearly, the further characterization of this amphibian kallikreinlike enzymatic activity and the availability of antibodies to it will be of help in determining its relation to ion transport events in these amphibian tissues.

An examination of the effects of the mammalian kinin products of kallikreins upon ion transport processes in the amphibian bladder or skin was unsuccessful because neither tissue showed changes in SCC in response to bradykinin or kallidin (Orce, Cuthbert, and Margolius, unpublished observations). This negative finding, perhaps related to the observation that the amphibian bladder kinin known as bufokinin is probably structurally dissimilar from its mammalian counterparts (11), along with recent evidence showing that the mammalian intestine contained quantities of a predominantly inactive tissue kallikrein characterized as being identical to the urinary enzyme (41), suggested the rat colon might be a fruitful site for further efforts. This notion was reinforced to some extent by the studies of Will et al. (38), who showed that the descending colon of rats eating a chronic low dietary sodium intake or given sodium-retaining steroids exhibited increased basal SCC, sodium reabsorption, and amiloride sensitivity. In addition, we had found that the rate of tissue kallikrein synthesis by rat descending colon is

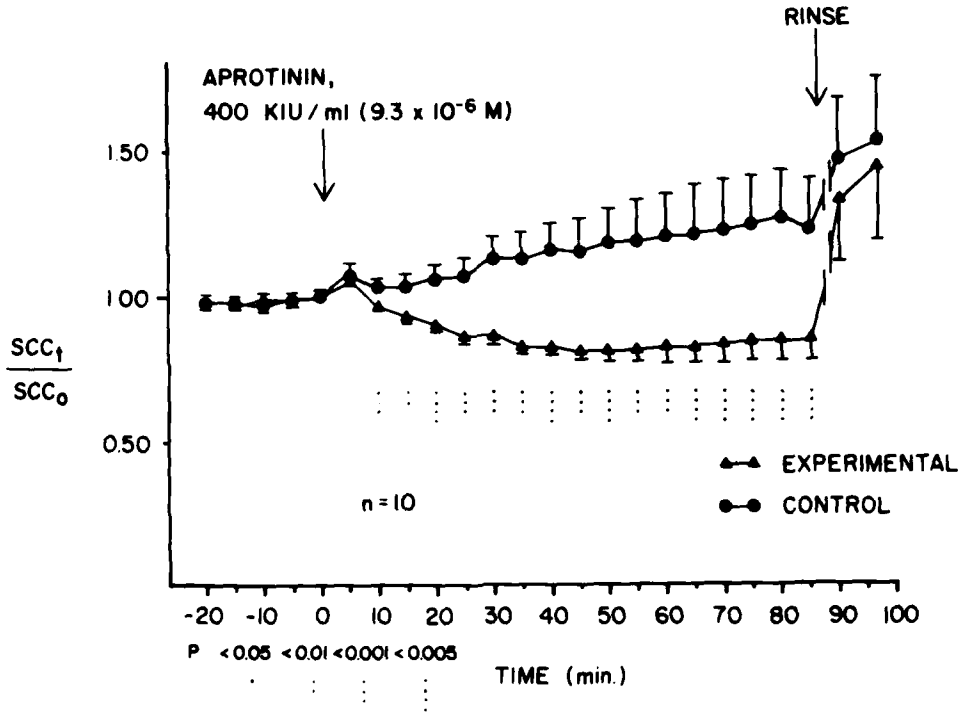

Figure 7.4. Effect of mucosal aprotinin on baseline SCC in *Bufo marinus* urinary bladder. Aprotinin was added to the mucosal bath of one quarter bladder (▲), the control quarter bladder (●) receiving an equal volume of vehicle. Both quarter bladders were rinsed three times with inhibitor-free Ringer solution 90 min later and SCC again recorded. SCC at 0 time was 154.1 ± 29.7 and 149.2 ± 33.2 μA/3.3 cm^2 for the aprotinin-treated versus control quarter bladders, respectively (NS). (Data from ref. 25.)

comparable to that in kidney, and is very rapid (Table 7.2). The seemingly reasonable notion that mucosally applied kinins would affect cation movement at this site was then examined.

2. KININS AND INTESTINAL ION TRANSPORT

Bradykinin or kallidin was found to be totally ineffective in changing SCC when added to the mucosal bath of Ussing chambers in which pieces of stripped rat descending colon are mounted. However, both increased SCC immediately after addition to the medium bathing serosal surfaces of the descending colon (Fig. 7.5). This response was unaffected by mucosal amiloride. Threshold kinin concentration is about 500 p*M*, and maximal responses (ΔSCC ~ 70 μA/cm^2) are seen with 50–100 n*M* kinin. Kinin responses were often transient for unknown reasons. Both a highly purified rat urinary kallikrein or mellitin, a potent activator of membrane-bound kallikreins, also increased SCC after addition to the serosal bath (7). The changes

TABLE 7.2. TISSUE CONTENT AND LABELING OF TISSUE KALLIKREIN[a]

		[^{35}S]Methionine Labeling				
	Content (ng/mg protein)	(1) Kallikrein CPM (per mg protein)	(2) Total Protein CPM (per mg protein)	Ratio[b] (1)/(2)	(3) Kallikrein CPM (per mg protein)	Ratio[c] (3)
Descending colon	47.1 ± 6.2	839,795 ±240,250	9210 ± 699	87.4 ±13.0	40.2 ±11.7	4.14 ± 1.12 ($\times 10^{-3}$)
Kidney	20.3 ± 1.4	532,523 ± 55,066	5964 ± 565	89.5 ± 4.9	10.5 ± 0.9	1.78 ± 0.09 ($\times 10^{-3}$)

[a] Male rats on a normal lab chow diet were labeled with [^{35}S]methionine for a period of 20 min prior to being killed. Kallikrein content and incorporation of [^{35}S]methionine were measured as described in ref. 22. All values are means ± S.E. (n = 8).

[b] Ratio of kallikrein-specific radioactivity to total protein radioactivity.

[c] Rate of kallikrein synthesis relative to total protein synthesis.

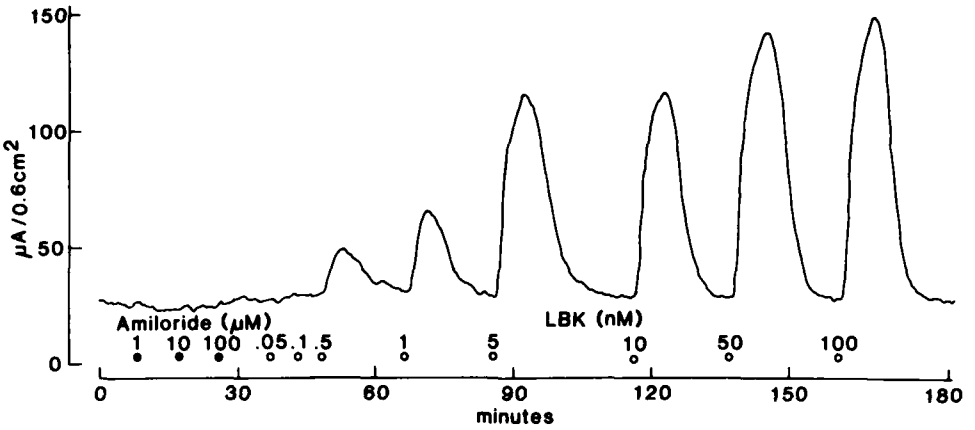

Figure 7.5. Typical effects of kallidin on rat colon SCC. The peptide was added cumulatively to the serosal bath of an Ussing-type chamber. Added amounts of amiloride (up to 111 μM cumulatively added to the mucosa) did not affect basal SCC in this or nine other experiments. The SCC response to kinins was generally transient for unknown reasons. (Reproduced with permission from ref. 7.)

in SCC were accompanied by significant increases in transepithelial conductance from 12.1 ± 2.7 to 13.6 ± 2.8 mmhos/cm² ($p < 0.001$). With replacement of serosal medium chloride by gluconate and sulphate, kinin responses were almost completely abolished, but could be reinstituted when chloride-containing medium was again present. Serosal furosemide significantly attenuated the SCC response to kallidin. In nine preparations, the response to kallidin (0.1 μM) was 58.9 ± 15.1 μA/cm² before, and 19.8 ± 6.2 μA/cm² after furosemide (100 μM) ($p < 0.05$). In these earliest studies of kinin effects on SCC, indomethacin (50 μM) or mepacrine (10 μM) added to the serosal bath abolished or attenuated SCC responses. However, some subsequent studies (discussed later) suggest that the conclusion reached by us (7) and others (16) on the basis of such results, namely, that the kinin-induced SCC response was by way of a prostaglandin-dependent pathway, was not a fully accurate one.

Regardless of the mechanistic elements involved in the kinin-induced intestinal SCC response, it is now clearly established that net chloride secretion accounts for the major portion of kinin-induced charge movement. This effect is shown in Table 7.3. In the control periods there was net chloride movement from mucosa to serosa (4.32 μEq/cm² hr). The mean current in these tissues before kallidin was 25.2 ± 6.1 μA/cm² ($n = 14$), which corresponds to an outward (toward the lumen) chloride movement of 0.94 μEq/cm² hr, which clearly cannot be equated to the resting current. Kallidin (1 μM) reduced net chloride absorption to 0.23 μEq/cm² hr, a value not significantly different from zero. This change in chloride movement caused

TABLE 7.3. EFFECTS OF KALLIDIN ON CHLORIDE FLUXES[a]

Control	*Kallidin*		
J_{sm} (0–30)	J_{sm} (32–62)	ΔJ_{sm}	ΔSCC
16.95 ± 1.35	19.08 ± 1.57	2.13 ± 0.41	3.20 ± 0.40
	$P < 0.0025$		
Control	*Kallidin*		
J_{ms} (0–30)	J_{ms} (32–62)	ΔJ_{ms}	ΔSCC
21.17 ± 1.36	19.31 ± 1.64	−1.96 ± 0.57	2.73 ± 0.56
	$P < 0.05$		

[a] All values are expressed in micro equivalents per square centimeter per hour. Each measurement is the mean value ± S.E. ($n = 7$). J_{sm} and J_{ms} refer, respectively, to the serosal-to-mucosal and to the mucosal-to-serosal unidirectional chloride flux. Kallidin (1 μM) was present in the serosal bathing solution during the period 32–62 min, while 0–30 min was the control period. The Δ values refer to the changes in flux or in SCC caused by kallidin. Experimental details appear in ref. 7, from which this data is reproduced, with permission.

by the kinin is equal to 4.09 μEq/cm^2 hr, equivalent to approximately 137% of the current change caused by the kinin. The effects of kallidin are both to reduce chloride movement inward from the lumen and to increase chloride efflux to similar extents. It should be noted that the average values in Table 7.3 obscure the variability among different tissues. In some cases, augmented serosal to mucosal chloride flux could account for more than 80% of the increment in current induced by kallidin; in others almost all of the increment could result from a decrease in J_{MS}Cl.

Similar sets of flux studies were carried out to examine movements of sodium or potassium (using $^{86}Rb^+$). Kallidin caused small, but statistically significant, decreases in both J_{SM}Na and J_{MS}Na (7). These changes in sodium transport induced by kallidin can have little importance for the effects of the peptide on SCC in this tissue, except insofar as the direction of the changes would reduce by approximately 10% the discrepancy between the kallidin-induced net chloride flux and SCC. No physiologically significant changes in Rb^+ fluxes were noted in response to kallidin.

The foregoing results and those of Manning et al. (17), clearly establish that kinins are among the most potent stimuli discovered to the process of net chloride secretion in the intestine. These findings are in accord with an earlier prediction by Hardcastle and associates (14) based on their preliminary studies of kinin effects on rat transintestinal potential differences using both *in vivo* and *in vitro* preparations.

3. MEDIATORS OF KININ-INDUCED INTESTINAL CHLORIDE SECRETION

One question now arising concerns the mediators of this secretory response. Many previous studies carried out using a variety of cellular, tissue, or whole animal systems have suggested that arachadonic acid metabolites are crucially involved in kinin-induced ion transport and hemodynamic events (23), although reports have appeared that are inconsistent with this general notion (30, 35). Our further studies of kinin-induced chloride secretion have revealed that at least a portion of this response occurs independently of eicosanoid production (4). First, although kallidin is capable of stimulating eicosanoid synthesis and release into media bathing isolated, short-circuited intestinal epithelia, the SCC response and eicosanoid output are not proportional, with more eicosanoid output at lower than at higher kinin concentrations. Second, indomethacin (5 μM) was able to abolish eicosanoid output by such tissues in response to kinin while part of the SCC response remained (Fig. 7.6). Third, it was found that kinin-induced increases in SCC were dependent on the presence of calcium in the serosal medium, but circum-

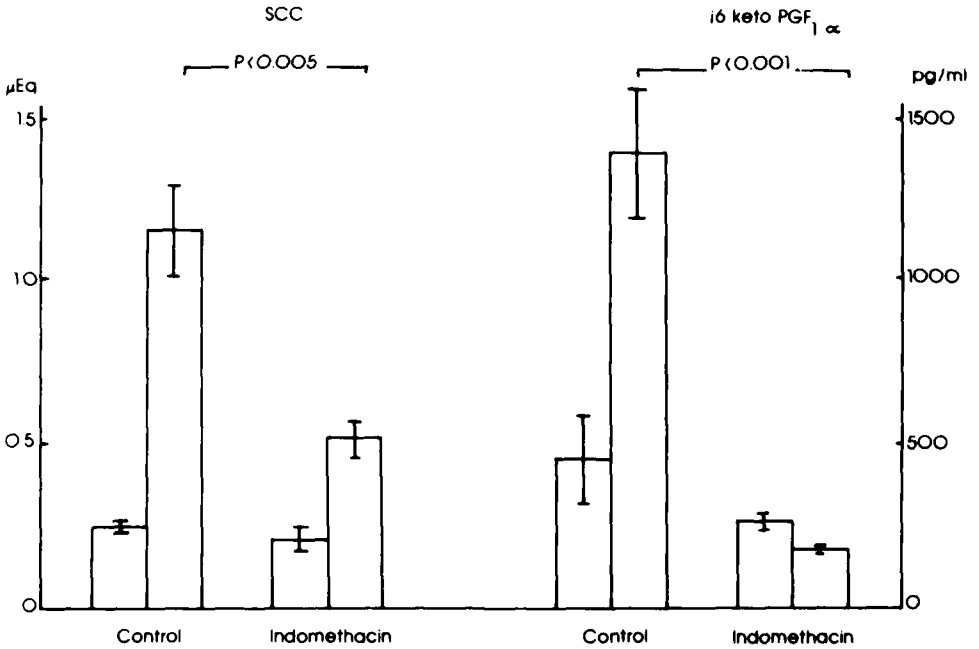

Figure 7.6. Effect of indomethacin (5 μM) on the SCC response and the simultaneous serosal output of i6-keto-$PGF_{1\alpha}$ in response to kallidin (1 μM) added to the serosal bath of six paired preparations of rat descending colon. Values on the left of each pair of columns represent the basal condition, where those on the right are after addition of kallidin. The SCC responses (in microequivalents) and i6-keto-$PGF_{1\alpha}$ output (in picograms per milliliter) are for tissues of 0.6 cm^2, during 20 min, with 10 ml nutrient fluid bathing each side of the tissue. Indomethacin caused a significant, but only partial, reduction in the SCC response and abolished the increase in i6-keto-$PGF_{1\alpha}$ due to kallidin. (Data from ref. 5.)

stances that effectively removed serosal calcium (and prevented the kinin-induced increases in SCC) did not significantly reduce the output of iPGE-like material by the tissue. These and other more recent findings suggest that extracellular calcium is the proximal requirement for kinin-induced net chloride secretion (5). It is suggested that a kinin-induced calcium influx at the basolateral surfaces of this epithelium is necessary for not only efficient production of eicosanoids but also of cAMP, which is then involved in the ultimate increase in apical chloride permeability.

Further studies of the mechanisms involved in local generation of endogenous kinin, presumably secondary to the action of activated local prokallikrein, are required. The subsequent role of this enzyme-product system in electrolyte and water secretory and/or absorptive processes in normal intestine or in intestinal diseases is of interest for several reasons. Among these are: (1) the known significant concentrations of tissue prokallikrein in intestinal mucosa; (2) the extreme potency of kinins in provoking both eicosanoid synthesis and net chloride secretion; (3) several earlier studies which suggest abnormalities in kallikrein levels and activity in disorders of intestinal function such as human ulcerative colitis (40); and (4) the seemingly paradoxical decreases in SCC and sodium absorption with inhibitors of tissue kallikreins in amphibian bladder and amiloride inhibition of kallikrein—versus the fact that the kinin products of this enzyme promote a net chloride secretion.

4. SUMMARY

Tissue kallikrein of colon mucosa is synthesized rapidly, and this synthetic process can now be examined in relation to hormonal or dietary manipulations or pathological circumstances that affect intestinal ion transport. Although the identical renal tissue enzyme is known to be enriched in membranes of distal convoluted tubular epithelial cells, the precise localization of the intestinal enzyme is uncertain. An understanding of the intestinal cellular locale of kallikrein will help in defining its local role. That tissue kallikreins can be inhibited by monovalent cations and some drugs (e.g., amiloride) and that kallikrein inhibitors affect cation transport across epithelial surfaces containing such enzymes must be reconciled with the new observations of kinin-induced chloride secretion. Extracellular calcium, eicosanoid synthesis, and cyclic nucleotide production are involved in the secretory response to kinins, although an absolute requirement for intact eicosanoid synthesis may not exist.

ACKNOWLEDGMENT

This paper was supported in part by grants HL 17705 and HL 29566 from the National Institutes of Health.

REFERENCES

1. Benos, D. J. and Sapirstein, V. S. (1983) *J. Cell. Physiol.*, **116,** 213–220.
2. Chao, J. and Margolius, H. S. (1979) *Biochim. Biophys. Acta*, **570,** 330–340.
3. Chao, J., Tanaka, S., and Margolius, H. S. (1983) *J. Biol. Chem.*, **258,** 6461–6465.
4. Cuthbert, A. W., Halushka, P. V., Margolius, H. S., and Spayne, J. A. (1984) *Brit. J. Pharmacol.*, in press.
5. Cuthbert, A. W., Halushka, P. V., Margolius, H. S., and Spayne, J. A. (1984) *Brit. J. Pharmacol.*, in press.
6. Cuthbert, A. W. and Margolius, H. S. (1981) *J. Physiol.*, **319,** 45P.
7. Cuthbert, A. W. and Margolius, H. S. (1982) *Brit. J. Pharmacol.*, **75,** 587–598.
8. Dharmsathaphorn, K., Racusen, K., and Dobbins, J. W. (1980) *J. Clin. Invest.*, **66,** 813–820.
9. Field, M. (1980) in: Field, M., Fordtran, J. S., Schultz, S. G., Eds., *Secretory Diarrhea*, American Physiological Society, Bethesda, Maryland, pp. 21–30.
10. Frankish, N. H. and Zeitlin, I. J. (1980) *J. Physiol.*, **298,** 361–370.
11. Furtado, M. R. F. (1972) *Biochem. Pharmacol.*, **21,** 118–124.
12. Geller, R. G., Margolius, H. S., Pisano, J. J., and Keiser, H. R. (1972) *Circulation Res.*, **31,** 857–861.
13. Halushka, P. V., Wohltmann, H., Privitera, P. J., Hurwitz, G., and Margolius, H. S. (1977) *Ann. Int. Med.*, **87,** 281–286.
14. Hardcastle, J., Hardcastle, P. T., Flower, R. J., and Sanford, P. A. (1978) *Experientia*, **34,** 617–618.
15. Heidrich, H. G. and Geiger, R. (1980) *Kidney Int.*, **18,** 77–85.
16. Hojvat, S. A., Musch, M. W., and Miller, R. J. (1983) *J. Pharmacol. Exp. Ther.*, **226,** 749–755.
17. Manning, D. C., Snyder, S. H., Kachur, J. F., Miller, R. J., and Field, M. (1982) *Nature*, **299,** 256–259.
18. Margolius, H. S. (1984) *Ann. Rev. Physiol.*, **46,** 309–326.
19. Margolius, H. S. and Chao, J. (1980) *J. Clin. Invest.*, **65,** 1343–1350.
20. Margolius, H. S., Horwitz, D., Geller, R. G., Alexander, R. W., Jr., Gill, J. R., Jr., Pisano, J. J., and Keiser, H. R. (1974) *Circulation Res.*, **35,** 812–819.
21. Margolius, H. S., Horwitz, D., Pisano, J. J., and Keiser, H. R. (1974) *Circulation Res.*, **35,** 820–825.
22. Miller, D. H., Chao, J., and Margolius, H. S. (1984) *Biochem. J.*, **218,** 37–43.
23. Nasjletti, A. and Malik, K. U. (1981) *Kidney Int.*, **19,** 860–868.
24. Omata, K., Carretero, O. A., Scicli, A. G., and Jackson, B. A. (1982) *Kidney Int.*, **22,** 602–607.
25. Orce, G. G., Castillo, G. A., and Margolius, H. S. (1980) *Am. J. Physiol.*, **239,** F459–F465.
26. Orce, G. G., Castillo, G. A., and Margolius, H. S. (1981) *Hypertension*, **3**(Suppl. II), 92–95.
27. Ørstavik, T. B., Nustad, K., Brandtzaeg, P., and Pierce, J. V. (1976) *J. Histochem. Cytochem.*, **24,** 1037–1039.
28. Pinkus, G. S., Ole-Moi Yoi, O., Austen, K. F., and Spragg, J. (1981) *J. Histochem. Cytochem.*, **29,** 38–44.
29. Proud, D., Perkins, M., Pierce, J. V., Yates, K. N., Highet, P. F., Herring, P. L., Mangkornkanok/Mark, M., Bahu, R., Carone, F., and Pisano, J. J. (1984) *J. Biol. Chem.*, **256,** 10634–10639.

30. Schrör, K., Metz, U., and Krebs, R. (1979) *Naunyn-Schmiedeberg's Arch. Pharmacol.*, **307,** 213–221.

31. Schwartz, C. J., Kimberg, D. V., Sheerin, H. E., Field, M., and Said, S. I. (1974) *J. Clin. Invest.*, **54,** 536–544.

32. Scicli, A. G., Diaz, M., and Carretero, O. A. (1983) *Am. J. Physiol.*, **245,** F198–F203.

33. Simson, J. A. V., Spicer, S. S., Chao, J., Grimm, S., and Margolius, H. S. (1979) *J. Histochem. Cytochem.*, **27,** 1567–1576.

34. Soltoff, S. P. and Mandel, L. J. (1983) *Science*, **220,** 957–959.

35. Strand, J. C. and Gilmore, J. P. (1982) *Renal Physiol., Basel*, **5,** 286–296.

36. Vogel, R. (1979) in Erdös, E. G., Ed., *Bradykinin, Kallidin and Kallikrein (Handbook of Experimental Pharmacology, XXV Supplement)*, Springer-Verlag, Berlin-Heidelberg-New York, pp. 163–225.

37. Ward, P. E., Erdös, E. G., Gedney, C. D., Dowben, R. M., and Reynolds, R. C. (1976) *Biochem. J.*, **157,** 642–650.

38. Will, P. C., Lebowitz, J. L., and Hopfer, U. (1980) *Am. J. Physiol.*, **238,** F261–F268.

39. Yamada, K. and Erdös, E. G. (1982) *J. Clin. Invest.*, **65,** 1343–1350.

40. Zeitlin, I. J. and Smith, A. N. (1973) *Gut*, **14,** 133–138.

41. Zimmerman, A., Geiger, R., and Kortmann, H. (1979) *Hoppe-Seyler's Z. Physiol. Chem.*, **360,** 1767–1773.

CHAPTER 8

PROPERTIES OF OUABAIN-RESISTANT VARIANTS ON A POLARIZED ESTABLISHED CELL LINE

B. ROSSI
Laboratory of Molecular Biology
Division of Cancer Biology and Diagnosis
National Cancer Institute
National Institutes of Health
Bethesda, Maryland

K. SODERBERG
Howard Hughes Medical Institute
University of Utah
Salt Lake City, Utah

D. LOUVARD
Institut Pasteur
Department de Biologie Moleculaire
Paris, France

The epithelial cells that perform transport function in various secretory and absorptive epithelia display a striking structural and functional polarity. The cell surface is comprised of two specialized domains: 1) the apical surface which is amplified by microvilli; 2) the basolateral surface which may be amplified by convolutions but not microvilli. These surface domains are separated by the tight junctional complex. Each domain possesses a characteristic set of proteins (10), detected functionally as enzymes or antigens (18).

The existence of such highly specialized surface domains raises important questions concerning plasma membrane biogenesis. How is such specificity in membrane structures generated, and where during their intracellular transport are different pools of membrane protein sorted out? It has been clearly demonstrated that aminopeptidase and Na^+,K^+-ATPase have the same asymmetric distribution on the cell surface of the established cell line MDCK* grown in monolayers as that observed in many epithelial tissues; the aminopeptidase is associated with apical surface, whereas the Na^+,K^+-ATPase is on the basolateral surface (17). Therefore, MDCK cells provide a useful model system to study the molecular mechanisms leading to the formation of domains on the surface of polarized epithelial cells.

We have focused our attention on Na^+,K^+-ATPase, an integral membrane protein, because of the important role it plays in controlling the intracellular ionic environment in eukaryotic cells. This cation pump drives Na^+ efflux coupled to K^+ influx with energy derived from ATP hydrolysis. The enzyme consists of one or more heterodimers containing a small, richly glycosylated subunit (β), $M_r \simeq 55{,}000$, and a larger subunit (α), $M_r \simeq 100{,}000$ (15). Both ATP hydrolysis and cation pumping are specifically inhibited by cardiac glycosides such as ouabain. It has been shown by the use of covalent probes that the α subunit is the polypeptide principally involved in the interaction with the cardiac glycosides (8, 22, 24).

Because of its asymmetric distribution in epithelial cells, studies on the genetic aspect of biosynthesis of Na^+,K^+-ATPase can be directed toward understanding the basolateral localization of this transport enzyme. Thus we have used a genetic approach to study the appearance of altered forms of this membrane protein. Ouabain-resistant variants of MDCK have been selected to progressively higher concentrations of the drug, and we have studied the membrane proteins of these variants in an attempt to understand the modification leading to ouabain resistance.

1. ISOLATION OF MDCK OUABAIN-RESISTANT CELLS

MDCK cells were tested at several ouabain concentrations to determine the lethal dose for this canine cell line. We found that plating efficiency and

* "MDCK" refers to Madin-Darby Canine Kidney cell established as an immortal cell line in 1969.

growth were normal at 20 nM ouabain but decreased with increasing drug concentration to 100 nM. With 200 nM ouabain present in the growth medium, plating efficiency was zero for 10^4 cells tested. This dose-response closely resembles that measured by Mankovitz et al. (19) for normal human fibroblasts and by Baker (2) for the human cell line HeLa.

Ouabain resistance behaves as a codominant marker. Only one allele for a gene in a diploid cell need be altered for manifestation of the phenotype. Therefore mutants with altered ouabain sensitivity are normally derived from unmutagenized cell populations at a frequency of 10^{-7}–10^{-8} per cell per generation (3).

Selection protocols published for human cells have shown that it is possible to obtain mutants resistant to 200 times the lethal dose for wild-typed cells (2, 19). We used as our selection medium 2 μM ouabain, which is about 100 times the lethal dose for MDCK. With this selection medium we were unable to obtain survivors from unmutagenized populations of MDCK cells, even with 10^6 cells tested. These results suggest that a single genetic alteration would not confer resistance to this high a concentration of the drug. We then attempted the same selection with cells that had been treated with the mutagen ethyl methanesulfonate (EMS). The concentration of EMS used effected the death of greater than 90% of cells treated, which is a fairly harsh level of mutagenesis in the methodology of somatic cell genetics. After mutagen treatment, cells were grown for six generations before transfer to ouabain-containing medium. Of a total of 1.8×10^8 survivors of mutagenesis, one clone was obtained which was able to grow in 2 μM ouabain. This frequency, by analogy with the reported frequencies of isolation of thymidine kinase mutants (6, 14, 23) and adenine phosphoribosyl transferase deficient mutants (5, 12), is consistent with two genetic alterations having contributed to the phenotypic change selected. Care should be taken in this interpretation, however, because with only one variant obtained, it is possible that this is an underestimate of the number of alterations necessary.

The single clone obtained from these mutagenesis and selection experiments was tested against increased concentrations of ouabain. We found that the cell type could plate efficiently in 2 or 4 μM ouabain and that a significant fraction grew in 8 μM ouabain. At 16 μM ouabain the majority of cells died. This concentration of drug was then used to select hyper-resistant variants from the 2 μM ouabain-resistant population.

Hyper-resistant variants arose at a frequency of approximately 4×10^{-7} per cell per generation without further mutagen treatment. This rate would be explained above for alteration at a single genetic locus. Selected for growth in 16 μM ouabain, the cells were resistant to twice this concentration of drug, but plating efficiency was severely reduced in 60 μM ouabain. Variants able to grow in 64 μM ouabain arose at a frequency of 1×10^{-6} per cell per generation from the 16 μM ouabain-resistant line, indicating that only with spontaneous mutation had the cells acquired the ability to survive in this higher concentration of drug. Further tests proved that the cells

selected with 64 μM ouabain could plate efficiently in concentrations of ouabain up to 4 mM.

Through sequential alteration of the cells and imposition of increasingly severe selection conditions, we have isolated a series of three variant MDCK types resistant to 2–4 μM ouabain, 16–32 μM ouabain, and up to 4 mM ouabain. These cell types are referred to as low Ou^r, mid Ou^r, and high Ou^r, respectively, and Ou^s is the ouabain-sensitive wild type.

2. STABILITY OF THE OUABAIN-RESISTANT PHENOTYPES

In the initial selection experiment we found that pretreatment with a mutagen greatly increased the frequency of recovery of cells able to grow in 2 μM ouabain. This result in itself supports the premise that genetic alteration rather than epigenetic adaptation was necessary for growth in this concentration of drug. However, for the mid Ou^r and high Ou^r lines it was possible that a nonheritable adaptive response rather than genetic alteration was being monitored. To test this possibility, all three classes of variants, low, mid, and high Ou^r, were grown for six weeks in normal medium and then back-tested against the appropriate concentrations of drug. In each case, the plating efficiency in drug-containing medium was very near 100%. This result demonstrates that the phenotypes are stable in the absence of selection and indicates that genetic alterations are responsible for the observed drug resistance.

3. METABOLIC LABELING OF WILD-TYPE VERSUS MUTANT CELLS

To assess whether the rate of synthesis of Na^+,K^+-ATPase is greatly altered in mutant cells, newly synthesized proteins of wild-type and high Ou^r cells were compared. Cultures were metabolically labeled with ^{35}[S]methionine for 1 h, the membrane fraction collected, and proteins of these fractions separated by SDS-gel electrophoresis. The results are shown in Fig. 8.1. The band at 94,000 daltons indicates the α subunit of the Na^+,K^+-ATPase as demonstrated by immunoprecipitation of a protein species of this size with antibody against the subunit (lanes B and B′). The β subunit of the ATPase is reported to have an apparent molecular weight of approximately 55,000 daltons on SDS-gels (13, 15). We therefore assume that the β subunit is at least a component of the prominent band seen in this region of our gel.

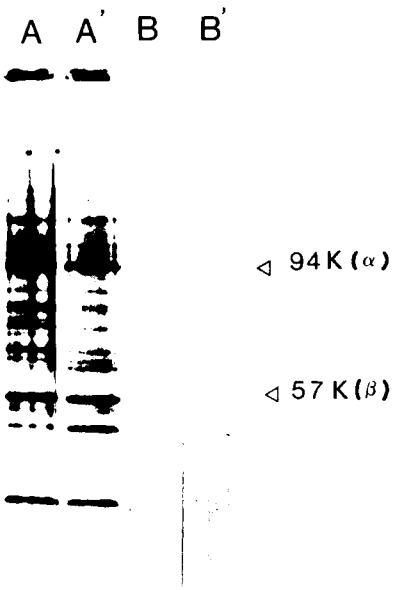

Figure 8.1. Autoradiogram of [^{35}S]labeled polypeptides of wild-type versus Ou^r mutant cells. Mutant and wild-type cells were incubated with 0.5 m*M* of [^{35}S]methionine (200 μCi/ml) for 1 h at 37°C followed by 30 min chase. A, crude membrane preparation of wild-type cells. A', crude membrane preparation of ouabain-resistant cells (a clone able to grow in 2 μM ouabain). B, immunoprecipitation pattern obtained after incubation of antialpha antibody with a crude membrane preparation of wild-type cells. B', immunoprecipitation pattern obtained using a crude membrane preparation of ouabain-resistant cells.

There is no significant difference in the proportion of total label distributed to the 55 K, or 94 K bands for wild-type versus mutant cell (lanes A and A'). In fact, no significant difference for any size class of proteins is apparent. A change in rate of synthesis able to make cells resistant to ouabain concentrations 10^2- to 10^5-fold higher than normal would surely have been visible as a dramatic increase by metabolic labeling. Such an increase was not seen, and we conclude that amplification of the genome with altered turnover of the enzyme is not the mode by which cells have acquired ouabain resistance.

It should also be noted that in the immunoprecipitation experiments use of equivalent amounts of antigen and antisubunit antibody in excess to this antigen resulted in similar amounts of protein being precipitated from wild-type and ouabain-resistant cells (lanes B and B'). Thus the ATPase of the mutants has not been altered to such a degree that it is no longer recognized by this antibody. It was therefore possible to compare the steady-state levels of α subunit in the two cell types by more sensitive immunoassay.

4. IMMUNOLOGICAL TITRATION OF THE Na^+,K^+-ATPase

The anti-α subunit antibody was used in an immunoradiometric assay to compare the amount of ATPase in wild-type versus mutant cells. A total membrane fraction from hyptonically lysed cells was used as the test antigen. Results are shown in Fig. 8.2. For a constant amount of antibody in solution, antibody binding increased with increasing membrane protein available on the plate until saturation was reached. Although high Ou^r cells showed a slightly greater amount of antibody binding, the saturating amount of antigen was equivalent for wild-type, low Ou^r and high Ou^r cells. If the Na^+,K^+-ATPase molecules have not been altered so as to disturb recognition by this antibody, these results can be taken as evidence that an equivalent amount of ATPase is present per unit membrane protein in each of these cell types. However, 1 mg protein of Ou^r cells corresponds to 4.4×10^6 cells instead of 2.2×10^6 cells for wild-type cells. These data taken together mean that the amount of Na^+,K^+-ATPase as measured by immunological titration is two-fold higher on Ou^r cells compared to wild-type cells.

5. MEASUREMENT OF Na^+,K^+-PUMP ACTIVITY AND OUABAIN-BINDING SITES

The cation pump activity of the fraction of Na^+,K^+-ATPase present at the plasma membrane can be measured using radioactive tracers. The potassium analog ^{86}Rb will be accumulated by cells in a manner dependent on intracellular sodium and ATP availability. Measurement of ^{86}Rb influx for MDCK cells in normal medium showed that cells took upon only small amounts of this cation and rapidly acquired an equilibrium concentration (data not shown). As reported by Cereijido et al. (4), the intracellular sodium pool of these cells limits cation pumping activity and makes measurement of flux rates difficult. To circumvent this problem, cells were preincubated in glucose-containing salt solution that lacked potassium for 4 h before assays were begun. After this preincubation a larger accumulation of ^{86}Rb could be measured, which for wild-type cells was still linear with time, was sodium and potassium dependent, and was 90% inhibitable by 10 m*M* ouabain (data not shown).

Figure 8.3 represents the results of ^{86}Rb influx assays for wild-type cells and cells of the three ouabain-resistant classes. The rate of accumulation of this cation in the absence of ouabain was two-fold higher in Ou^r cells than that observed in Ou^s cells. The ouabain sensitivity of this influx could be determined by including various concentrations of the inhibitor in the preincubation buffer. For wild-type cells, rubidium accumulation versus log of ouabain concentration gave the expected sigmoid curve, the ATPase behaving as a single species with a K_d of 10^{-7} *M* for ouabain. For each of the three

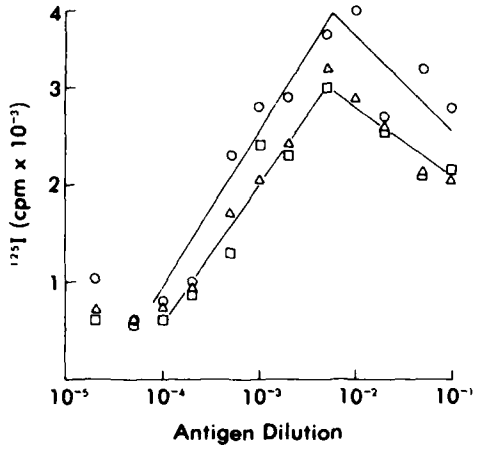

Figure 8.2. Immunological titration of the Na^+,K^+-ATPase in different cell types. Total membrane fractions were isolated from cells and adjusted to a protein concentration of 2 μg/ml. Further dilutions were prepared and aliquots of each dilution fixed to wells of a microtiter plate. The plates were incubated with antibody specific for the large subunit of the Na^+,K^+-ATPase. After washing, [^{125}I]protein A was added and allowed to bind to the antigen–antibody complexes that had formed. Individual wells were then cut from the plate, and the ^{125}I bound to each well was counted. All points are averages of measurements made in duplicate. The membranes tested were isolated from wild-type cells (□); low Ou^r mutants (△); and high Ou^r (○) mutants. (Reprinted by permission of *The Journal of Biological Chemistry*.)

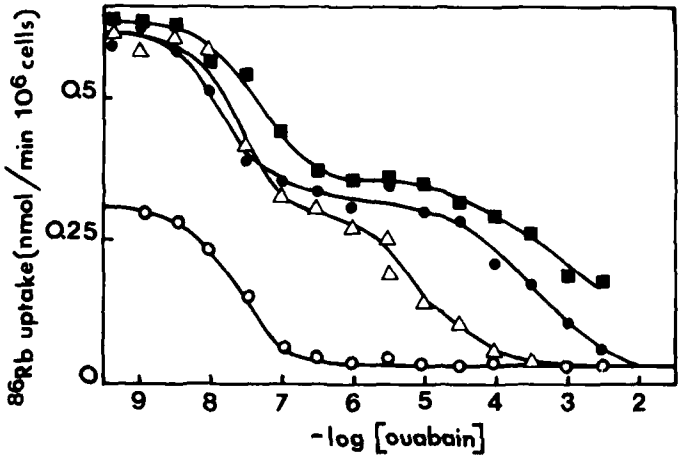

Figure 8.3. Oubain-sensitive ^{86}Rb uptake in wild-type cells (○) and ouabain-resistant clones selected on media containing ouabain at 2 μM (△), 10 μM (●) and 4 mM (■) concentrations. Cells were maintained in a K^+-free medium for 4 h at 37°C in the presence of increasing concentrations of ouabain before addition of ^{86}Rb at a final concentration of 5.5 mM (0.4 μCi/ml). Twenty minutes later each well was washed twice, and the cells were lysed in 0.1 N NaOH. (Reprinted by permission of *The Journal of Biological Chemistry*.)

mutant classes, 50% of the total rubidium uptake displayed wild-type sensitivity to ouabain inhibition. The remaining 50% of influx activity was relatively resistant to the drug. This second component demonstrated K_d's for ouabain of 10 μM, 300 μM, and 3 mM for cells of low Ou^r, mid Ou^r, and high Ou^r, respectively.

The altered ouabain inhibition of cation pumping activity presumably results from altered affinities of the ATPase molecules for ouabain. This can be measured directly using [^{3}H]ouabain. The amount of cell-associated radioactivity was determined for cultures exposed to radiolabeled ouabain for 2 h. MDCK cells are connected to one another by way of tight junctions which form an effective permeability barrier separating the tissue culture medium from the fluid bathing the basolateral surfaces. [^{3}H]Ouabain added to the buffer covering cells grown on plastic is immediately in contact with the apical surface of cells but requires a significant amount of time to reach the basolateral area. Na^+,K^+-ATPase is localized to the latter domain (15), and therefore a long period of incubation with the drug was necessary to achieve equilibrium binding. Wild-type cells bound ouabain with a K_d of 6×10^{-8} M and were saturated for binding at 8 pmol [^{3}H]ouabain per 10^6 cells (Fig. 8.4). For cells of the three mutant classes, incubation in the highest concentration of ouabain also resulted in 8 pmol of [^{3}H]ouabain being bound per 10^6 cells with a K_d of 6×10^{-8} M. This component represents that portion of rubidium influx activity inhibited by 10^{-6} M ouabain. The remaining 50% of the Na^+,K^+-ATPase in these mutants could not be seen to bind ouabain in this assay.

6. BIOCHEMICAL CHARACTERIZATION OF THE MUTANTS

We wished to determine the nature of the alteration in mutant cell lines that had conferred resistance to ouabain. The phenotypes could be derived by several mechanisms including: 1) alteration of the Na^+,K^+-ATPase, the target enzyme of the drug, such that it bound ouabain with a lower affinity; 2) increase in the amount of Na^+,K^+-ATPase present per cell; or (3) increase in the rate of turnover of the protein subunits of the ATPase such that ouabain-inhibited enzyme would be quickly replaced, although the total amount of ATPase per cell remained normal.

The last two mechanisms would result from mutations in regulatory regions of the genome or from amplification of genes for the ATPase. Amplification of genetic regions coding for sensitive enzymes has been shown to be one means of acquiring resistance to the drugs methotrexate (25) and PALA (20). However, the target enzymes (dihydrofolate reductase and aspartate transcarbamylase, respectively) for these drugs are soluble proteins of the cytosol, a compartment of the cell that may be under less stringent control of protein content than is the plasma membrane. In the cases where ouabain

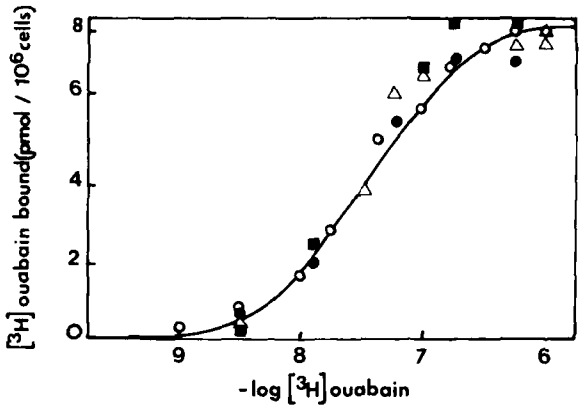

Figure 8.4. [^{3}H]Ouabain binding on the high-affinity classes of sites for wild-type (○) and ouabain-resistant mutants selected on media containing ouabain at 2 μM (△), 10 μM (●), and 4 mM (■) concentrations. Cells were incubated for 2 h in 140 mM NaCl, 10 mM Tris-HCl, 1.8 mM $CaCl_2$, 1 mM $MgCl_2$, and 5 mM glucose, pH 7.4, with increasing concentrations of [^{3}H]ouabain. Controls are performed by adding 1 μM unlabeled ouabain for each [^{3}H]ouabain concentration. (Reprinted by permission of *The Journal of Biological Chemistry*.)

resistance has been well studied, it has been shown to be associated with a loss in affinity of the ATPase for cardiac glycoside inhibitors (21), mechanism 1 in the foregoing list. However, since no group has reported a change in tolerance for ouabain as large as that demonstrated by wild-type versus high Ou^r MDCK, we thought that all three possible mechanisms should be investigated.

The last two hypotheses had been ruled out on the basis of data presented in Figs. 8.1 and 8.2. First, the two-fold increase in the level of Na^+,K^+-ATPase observed on Ou^r cells using an immunoradiometric assay cannot account for their ability to grow in ouabain concentration 10^2- to 10^5-fold higher than the IC_{50} for wild-type cells (Fig. 8.2). Second, no significant modification was observed on the rate of turnover of the subunits of Na^+,K^+-ATPase as visualized by metabolic labeling (Fig. 8.1).

Only the first hypothesis seems to be supported by our data. The preparations of the different ouabain-resistant clones for MDCK cells line present both ouabain-resistant and ouabain-sensitive populations of Na^+/K^+ pumps (Fig. 8.3). The ouabain-sensitive ^{86}Rb uptakes per milligram of protein on Ou^r mutants and Ou^s wild-type cells were identical (data not shown). However, when ^{86}Rb fluxes are normalized for the number of cells, a two-fold increase in the Na^+/K^+ pump activity on Ou^r variants is observed compared to Ou^s cells (Fig. 8.3).

The total ouabain-sensitive ^{86}Rb fluxes in Ou^r variants split into two categories of Na^+/K^+ pumps of equal importance presenting respectively high and low affinity for ouabain. Each pump family has the same level of activity, when normalized to cell protein, as that observed in the wild-type cells. Only the $K_{1/2}$ of the low-affinity population of sites increased with increasing

levels of resistance of the clone. Neither the affinity nor the maximal capacity was affected on the high-affinity sites of the Ou^r clones as measured by [^{3}H] ouabain binding (Fig. 8.4).

Recently Sweadner (26) reported the existence in the rat brain of two populations of ouabain-binding sites of different affinities. The α subunits of these two populations of Na^+,K^+-ATPase differ by 3000 daltons and can be separated by high-resolution electrophoresis. In parallel, different investigators claim the existence of two families of ouabain-binding sites in heart cells (1) and adipocytes (9). At the moment, no hypothesis has been proposed to explain the respective role of the two classes of sites. Our data suggest that the mutation that induces the ouabain resistance is linked to the expression of the gene coding for the low-affinity class of ouabain-binding site, which is not normally expressed in kidney cells.

7. METABOLIC COOPERATION IN COCULTURED Ou^r AND Ou^s MDCK CELLS

Wild-type MDCK are sensitive to low concentrations of ouabain and die rapidly after contact with the drug. After exposure to 2 μM ouabain for 25 h, no survivors could be detected starting from 10^6 cells. We wished to study whether protection from ouabain could be extended to the sensitive cell type by coculture with the ouabain-resistant variant. To carry out this study we first needed a test that would discriminate between Ou^r and Ou^s MDCK cells which are morphologically identical. For this purpose a subclone of the ouabain-resistant mutant was used that had been selected for a deficiency in hypoxanthine phosphoribosyl transferase activity ($HPRT^-$). Wild-type cells that display a typical ouabain sensitivity have a normal purine metabolism ($HPRT^+$) and are killed in a medium containing 6-thioguanine; conversely, the ouabain-resistant cells, which are deficient in HPRT, survive in this selective medium. The opposite situation is found when the two types of cells are grown in medium containing hypoxanthine, aminopterin, and thymidine (HAT), which is toxic for $HPRT^-$ cells (ouabain-resistant) but allows normal growth for $HPRT^+$ cells (ouabain-sensitive). This system provides a simple test to quantify the amount of each kind of cell present on a mixed Ou^r + Ou^s monolayer.

The metabolic cooperation has been tested as follows: The two types of MDCK cells, ouabain-sensitive ($HPRT^+$) and ouabain-resistant ($HPRT^-$) were mixed in a 1 : 1 ratio. The cultures were allowed to reach confluence and then were exposed to 2 μM ouabain for 24 h. Cultures were trypsinized, divided, and cells tested in HAT or 6-thioguanine-containing media. Under these conditions 46% of the drug-sensitive cells survived ouabain treatment, whereas no survivors could be seen on a control experiment containing only Ou^s cells. It is noteworthy that during the periods of time the cells were exposed to the drug, ouabain-resistant cells continued to grow in such a way

that the monolayer was confluent at the end of the ouabain treatment despite the loss of 56% of the ouabain-resistant cells.

8. DYE COUPLING

The question arises of how a ouabain-resistant cell can allow neighboring ouabain-sensitive cells to survive in the presence of toxic doses of ouabain. The lethal effect of ouabain results most probably from an unbalanced cytoplasmic Na^+/K^+ ratio resulting from the Na^+ pump inhibition. The first possibility we considered was that cells in monolayers shared the same pool of Na^+ and K^+ owing to intense communication between cells. In this hypothesis one can consider that in the presence of ouabain there are enough effective molecules of Na^+,K^+-ATPase on the surface of an Ou^r cell to pump out the Na^+ for itself and for several Ou^s neighboring cells. This implies that cations can diffuse easily between the cytoplasmic compartment of neighboring cells. The most common structures involved in cell–cell communication are gap junctions composed of nexons that form channels of approximately 20-Å in diameter spanning the plasma membrane (11, 27). Small molecules such as metabolites and electrolytes can diffuse through these channels (7, 16). One simple way to visualize the presence of gap junctions is to follow from one cell to its neighbor the diffusion of dyes, such as fluorescein or luciferin yellow, which have a size small enough to diffuse freely through these channels.

When we microinjected luciferin yellow in subconfluent MDCK cells, we could demonstrate the presence of such a communication. But, surprisingly, in a confluent monolayer (condition used under the ouabain treatment) we were unable to see any diffusion of the dye to neighboring cells after microinjection. This puzzling result raises the question of how Na^+ can diffuse from one cell to the other during ouabain treatment. Our data rule out the possibility of a diffusion of electrolytes through classic gap junction, challenging our original hypothesis. We are currently investigating two other possibilities: (1) gap junctions do exist in MDCK epithelium but have features different from those reported for other kinds of cells; or (2) epithelial cells can communicate through structures other than gap junctions, and in this regard the tight junctional complex, because it allows an intimate contact between epithelial cells, appears to us as a good candidate.

9. CONCLUSION

We have isolated ouabain-resistant variants of MDCK cells which express a population of Na^+,K^+-ATPase presenting a low affinity for ouabain. This new population comes in addition to a high-affinity class of sites which is normally expressed in canine kidney cells. Sweadner (26) reported the pres-

ence of two populations of Na^+,K^+-ATPase with different affinities for digitalis in the same tissue. The presence of two categories of Na^+,K^+-ATPase on a single type of cell has also been reported (1, 9). In the latter case, the low-affinity class of sites represents 90% of the total Na^+,K^+-ATPase present on the cell. Although no clear explanation has been proposed so far for the existence of two or more populations of Na^+,K^+-ATPase, these data suggest the presence of multiple genes coding for Na^+,K^+-ATPase in mammalian genomes.

The fact that our mutants express equally two populations of Na^+,K^+-ATPase makes them promising tools to study the mechanisms that lead to the turning off or on of a particular gene coding for Na^+,K^+-ATPase on a defined type of cell.

These variants can be used for purposes not directly correlated to the study of Na^+,K^+-ATPase. We have used them to visualize metabolic cooperation between ouabain-sensitive and ouabain-resistant MDCK cells grown in coculture when they are treated with ouabain. Preliminary results suggest that MDCK cells communicate through gap junctions when they are subconfluent but lose this type of communication when they reach confluency.

REFERENCES

1. Adams, R. J., Schwartz, A., Grupp, G., Grupp, I., Lee, S. W., Wallick, E. T., Powell, T., Twist, V. W., and Gathiram, R. (1982) *Nature*, **296**, 167–169.
2. Baker, R. M. (1976) in Cook, J. S., Ed., *Biogenesis and Turnover of Membrane Macromolecules*, Raven Press, New York, pp. 93–123.
3. Baker, R. M., Brunette, D. M., Mankovitz, R., Thompson, L. H., Whitmore, G. F., Siminovitch, L., and Till, J. E. (1974) *Cell*, **1**, 9–21.
4. Cerejido, M., Ehrenfeld, J., Meza, I., and Martenez-Palomo, A. (1980) *J. Membrane Biol.*, **52**, 147–159.
5. Chasin, L. (1974) *Cell*, **2**, 37–41.
6. Clive, D., Flamm, W., Marchesko, M., and Bernheim, N. (1972) *Mutat. Res.*, **16**, 77.
7. Corsaro, C. H. and Migeon, B. R. (1977) *Nature*, **268**, 737–739.
8. Forbush, B., Kaplan, J. H., and Hoffman, J. F. (1978) *Biochemistry*, **17**, 3667–3676.
9. Forest, C., Ponzio, G., Rossi, B., Lazdunski, M., and Ailhaud, G. (1982) *Biochem. Biophys. Res. Commun.*, **107**, 422–428.
10. Fujita, M., Ohta, H., Kawai, K., Matsui, H., Nakao, M. (1972) *Biochim. Biophys. Acta*, **274**, 336–347.
11. Gilula, N. B., Reeves, O. R., and Steinbach, A. (1972) *Nature*, **235**, 262–265.
12. Jones, G. and Sargent, R. (1974) *Cell*, **2**, 43–54.
13. Jorgensen, P. (1974) *Biochim. Biophys. Acta* **356**, 36–52.
14. Kit, S., Drubs, D., Peirkarski, L., and Hsu, T. (1963) *Exp. Cell Res.*, **31**, 297.
15. Kyte, J. (1971) *J. Biol. Chem.*, **246**, 4157–4165.
16. Ledbetter, M. L. S. and Lubin, M. (1979) *J. Cell Biol.*, **80**, 150–165.
17. Louvard, D. (1980) *Proc. Natl. Acad. Sci. USA* **77**, 4132–4136.

18. Louvard, D., Semeriva, M., Maroux, S. (1976) *Proc. Natl. Acad. Sci. USA*, **77,** 4132–4136.
19. Mankovitz, R., Buchwal, M., and Baker, R. M. (1973) *Cell*, **3,** 221–225.
20. Padgett, R. A., Wahl, G. M., Coleman, P. F., and Stark, G. R. (1979) *J. Biol. Chem.*, **254,** 974–980.
21. Robbins, A. and Baker, R. M. (1977) *Biochemistry*, **16,** 5163.
22. Rossi, B., Vuillemier, P., Gache, C., Balerna, M., and Lazdunski, M. (1980) *J. Biol. Chem.*, **255,** 9936–9941.
23. Routa, D., Sadow, B., and Caskey, C. (1973) *Genetics*, **75,** 515–530.
24. Ruoho, A. and Kyte, J. (1974) *Proc. Natl. Acad. Sci. USA*, **71,** 2352–2356.
25. Schimke, R. T., Kaufman, R. J., Alt, R. W., and Kellems, R. F. (1978) *Science*, **202,** 1051–1055.
26. Sweadner, K. J. (1979) *J. Biol. Chem.*, **254,** 6060–6067.
27. Unwin, P. N. T. and Zampighi, G. (1980) *Nature*, **283,** 543–549.

CHAPTER 9

RAPID INSERTION AND RETRIEVAL OF PUMPS AND CHANNELS INTO MEMBRANES BY EXOCYTOSIS AND ENDOCYTOSIS

QAIS AL-AWQATI
Departments of Medicine and Physiology
College of Physicians and Surgeons
Columbia University
New York, New York

Transport of solutes and water across biological membranes is a highly regulated process. Using patch clamps, reconstitution of membrane proteins into artificial membranes, as well as other more conventional methods, investigators have recently identified several mechanisms for the regulation of transport through these structures. Membrane potential of the appropriate size and orientation can open or close certain channels. Acetylcholine, by binding to its receptor, leads to a conformational change with consequent opening of a channel. Calcium binds to and blocks sodium channels and opens K^+ channels. Cyclic AMP, ultimately by inducing phosphorylation of a potassium channel, leads to its closure. Despite their diversity all these mechanisms have one property in common: regulation occurs by changes in the kinetic properties of an individual membrane protein. There is increasing evidence, however, that another general mechanism exists in which the regulating influence increases the *number* of channels or pumps in a membrane and that this is accomplished by rapid fusion of vesicles whose membranes are enriched in the specific transport protein. This process inserts these proteins into the membrane, and removal of the stimulus is accompanied by endocytotic internalization of these channels or pumps.

Of course, it is well known that membrane fusion is a major mechanism by which the cell surface is renewed. However, the process we are describing is much faster with half-times of at most a few minutes. In its time course it resembles more the exocytotic fusion of secretory vesicles than that responsible for the constitutive repair of cell membranes. Unlike secretory exocytosis, however, the content of the vesicles is of no significance in the regulatory process.

The first suggestion for a role of exocytotic insertion came from the studies of Masur et al. (10) who found that vasopressin stimulated fusion of vesicles and granules with the luminal membrane of toad urinary bladder. They suggested that this effect is related to the effect of vasopressin on increasing water permeability of this membrane. Subsequent studies by Bourguet, Kachadorian, and Wade (and their respective collaborators reviewed in ref. 16) showed that vasopressin caused fusion of vesicles whose membranes contained aggregates seen in freeze fracture. (Similar studies were also obtained in the collecting tubule of the kidney where vasopressin also increases water permeability). Based on correlation of the change in water permeability with the number of aggregates in the luminal membrane and the response of both to inhibitors, they suggested that these aggregates are the water channels. Because of the lack of a specific probe that either binds to the channel to alter its activity or measures some aspect of high water permeability in these vesicles in living cells, the relation of the aggregates to water channels remains at present tentative.

1. EXOCYTOTIC INSERTION OF THE H^+ PUMP

Direct evidence for the rapid insertion of pumps as a means of regulation was recently obtained in the H^+ transport system of the turtle urinary blad-

der. The surface cells of this membrane are of two types: the dominant type contains a large number of granules, whereas the minority are enriched in carbonic anhydrase and mitochondria. The latter are thought to be the cells that mediate H^+ secretion. Urinary acidification is produced by a proton-translocating ATPase located in the luminal membrane (2).

We investigated regulation of H^+ secretion in this epithelium using standard electrophysiological approaches as well as optical methods in living cells. Turtle bladders were mounted on the stage of a fluorescence microscope and stained with a number of dyes whose spectra were sensitive to concentration or pH. To identify mitochondria-rich cells we used the fluorescent, cationic carbocyanine compound, DiO-C_5(3). This dye will accumulate in mitochondria since their membrane potential is highly negative. We found that 10–20% of the surface cells of the bladder were enriched in mitochondria. When the turtle bladder was stained with acridine orange we found that these cells contained a large number of orange vesicles. The emission spectrum of this fluorescent weak base is quite sensitive to its concentration; at high concentration the dye aggregates and fluoresces in the red. The orange color was rapidly dissipated by proton ionophores, indicating that the accumulation of the dye was due to a low pH inside the vesicle. We found that CO_2, long known to be the major stimulus for H^+ secretion in urinary epithelia, induced fusion of these vesicles with the luminal membrane (6). This was demonstrated by superfusion of CO_2-containing media over the turtle bladder. When this was done we observed a dramatic change in the behavior of these vesicles. Whereas before CO_2 addition they appeared to be stationary, following the addition of CO_2 the vesicles exhibited rapid movement which was followed by fusion of the vesicles with the luminal membrane. One could tell that the vesicles fused with the luminal membrane since we saw discrete puffs of what looked like green smoke emanating from the luminal membrane simultaneously with the disappearance of a red vesicle.

Clearly what was happening was that the concentrated acridine orange was being discharged into the luminal medium thereby being diluted and causing its color to change rapidly from orange to green. There was also a suggestion that the vesicle swelled before bursting. This picture was mesmerizing, but unfortunately we were not able to capture it on film because the high-intensity light bleached the acridine orange and also rapidly killed the cells in our rather primitive optical set up.

Dr. Stephen Gluck and Christopher Cannon (then a Yale undergraduate), decided to develop a new assay for fusion and exocytosis (6). In this assay we reasoned that if CO_2 caused fusion, its removal should either cause endocytosis or at least allow the endocytic process to continue. Of course, the demonstration of exocytosis of necessity implies the presence of endocytosis. During removal of CO_2 we placed fluorescein isothiocyanate coupled to a high molecular weight dextran (FITC-dextran) in the luminal medium. We chose FITC because its excitation spectrum is sensitive to pH (11). When vesicles were induced to fuse with the luminal membrane by CO_2 in the

presence of FITC-dextran, subsequent removal of CO_2 caused internalization of FITC-dextran into the mitochondria-rich cells as well as a reduction in H^+ transport. Using appropriate calibration, we could measure the pH in these vesicles by spectral analysis in living cells; we found it to be near 5.0. Addition of proton conductors or metabolic poisons increased the pH, indicating that the low pH was due to a proton pump rather than to a Donnan effect. To measure the extent of exocytosis, bladders were loaded with FITC dextran and mounted in modified Ussing chambers. The mucosal loading solution was removed, and fresh medium was pumped through the luminal medium and the effluent passed through a flow-through cell of a fluorometer. In this chamber one can measure simultaneously the rate of H^+ secretion and the extent of exocytosis. CO_2 caused a measurable extrusion of fluorescent dye simultaneously with the increase in the proton current (Fig. 9.1). The response to CO_2 is quite variable, but we found that there was good correlation between the extent of exocytosis and the increase in H^+ secretion. Pretreatment of the bladders with colchicine prevented the exocytosis and the increase in H^+ transport. These results provide compelling evidence for the rapid insertion of proton pumps into the luminal membrane on stimulation by CO_2.

Exocytosis implies insertion of membrane into the luminal surface, which conceivably could expand that surface. Indeed, morphometric analysis of the effect of CO_2 on the turtle bladder by Stetson and Steinmetz (15) has shown that the luminal surface increases and the volume fraction of the vesicles in the mitochondria-rich cells decreases. Dixon and Clausen have recently performed impedance analysis of the turtle bladder and found that CO_2 rapidly increases the capacitance of the luminal membrane with a time course similar to its effect on H^+ transport (3). Removal of CO_2 then must have reduced the surface of the bladder.

Westley Reeves posed the question of the mechanism of the reduction in

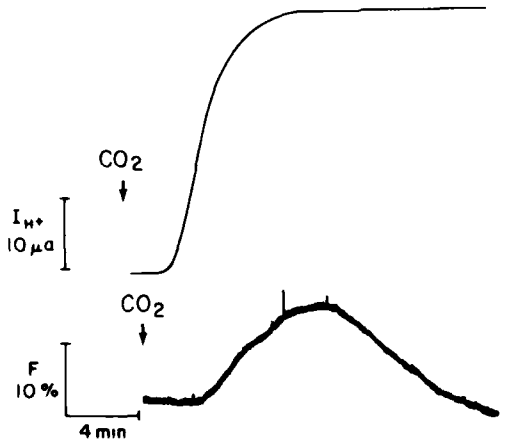

Figure 9.1. Simultaneous measurement of the H^+ current (I_{H+}; upper trace) and the rate of exocytosis of internalized fluorescent dextran (lower trace) in a turtle bladder mounted in a modified Ussing chamber. See text and ref. 6 for details.

the surface (13). In principle, one can conceive of two processes; one we can term constitutive endocytosis in which the cell surface is brought back to its original size by the continuous internalization of plasma membranes that occurs in all cells. A prediction here will be that addition of CO_2 or its removal will have no effect on the rate of endocytosis. Alternatively, removal of CO_2 could stimulate endocytosis, that is, the addition of CO_2 will inhibit this process.

To assay for endocytosis Reeves measured the uptake of FITC-dextran as a function of time into the turtle bladder. We had previously shown that this reagent is internalized only into the mitochondria-rich cells and that the endocytic vesicles that took them up contained proton pumps and fused with the luminal membrane. Hence this substance formed a particularly useful marker for the vesicles that contain the proton pumps. Reeves found that removal of CO_2 stimulated endocytosis.

Another issue that he addressed was whether all the proton pumps that are located on the luminal membrane can be internalized or whether there is one mobile pool that participates in this new regulatory process. He added the lectins concanavalin-A or wheat germ agglutinin and found that these lectins rapidly and completely inhibited H^+ secretion. Simultaneous measurement of endocytosis showed that these lectins stimulated endocytosis also. The lectins themselves were internalized into endocytic vesicles. These results suggest that all H^+ pumps in the luminal membrane can be internalized into vesicles in the cytoplasm of the mitochondria-rich cells (12). These vesicles were subsequently isolated by Gluck and found to contain an electrogenic proton translocating ATPase that was inhibited by dicyclohexyl carbodiimide and sulfhydryl reagents, but not by oligomycin (7).

The mechanism by which CO_2 causes the fusion of these vesicles remains unclear. It is very likely that CO_2 acidifies the cell. Cannon recently measured the intracellular pH of individual mitochondria-rich cells in bladders mounted on a fluorescence microscope and loaded with the permeant dye, 6-carboxy fluorescein diacetate. When this dye reaches the cytoplasm its acetate group is hydrolyzed by cytosolic esterases. The excitation spectrum of this dye is pH sensitive, and he was able to measure the cell pH using the same spectral method that Gluck used for measurement of the internalized FITC-dextran. He found that the cell pH in the mitochondria-rich cell is higher by 0.5–1.0 pH units than the cell pH of the granular cell. This pH difference in adjacent cells is remarkable since it implies that there is no cell-to-cell communication between these two cell types. Recall that the gap junction is a highly conductive channel that allows the penetration of molecules as large as 500 daltons. Further, recent studies by Spray and Bennett have shown that the gap junction is opened by alkaline pH's (14). Hence, if these cells contain gap junctions, they must be closed.

In tissue culture, cells of varying origin can develop gap junctions. The finding of the probable lack of communication between two cells in a single

epithelium raises a number of interesting developmental questions about the mitochondria-rich cells. For instance, are they cells of such completely different lineage that the other cells do not recognize them sufficiently to develop gap junctions? Are they invaders from some embryological past that have survived in the final adult tissue? In this regard it is interesting to recall that the development of the kidney of higher vertebrates occurs in three waves of tissues, only the last of them surviving as the adult metanephros. Could these cells be derived from the mesonephros or even pronephros? These and other questions of similar kind will be pursued in the near future.

Using the pH sensitivity of the spectrum to calculate cell pH we found in preliminary experiments that addition of CO_2 reduced the cell pH very rapidly by 0.2–0.5 pH units in a reversible manner. To test whether the signal for fusion is the cellular acidification, Cannon added weak acids such as butyric or acetic acids to the turtle bladder at different mucosal pH's. He found that these acids stimulated H^+ secretion and fusion of vesicles in bladders loaded with FITC-dextran. These acids as expected also reduced the cell pH in the mitochondria-rich cell.

Clearly, the first step in the cascade of events leading to fusion is cytosolic acidification. Since lowering cell pH can change cell calcium, which in turn can cause fusion, we used the permeant calcium buffer Maptam (Calbiochem). This buffer can be synthesized as an ester that is permeant, and when it reaches the cytosol it can be hydrolyzed to give the chelator. The unesterified form will complex calcium. We found that loading the bladder with Maptam reduced the rate of H^+ secretion in turtle bladders perfused with CO_2-free air. Addition of CO_2, caused no increase in H^+ secretion. The increase in H^+ secretion seen with addition of the weak acids was also prevented. However, there was no effect of Maptam on the cell pH—or on the effect of CO_2 or weak acid addition on acidifying the cell. Hence we propose that CO_2 acts by acidifying the cytosol, which in turn leads to a change in cell calcium that causes the fusion. Maptam prevents this increase by buffering the calcium.

The origin of the calcium is unknown at present, but $Ca^{2+}:H^+$ exchange processes are known to exist in a number of intracellular organelles. Whether the cellular acidification leads to an increase in cell calcium is not rigorously shown by the Maptam experiments, since if it caused a reduction in cell calcium, that chelator would also buffer that change. There is a large body of indirect evidence, based on the action of drugs whose mechanisms of action may or may not be known, which claims that the fusion event in epithelia induced by vasopressin is due to a decrease in cell calcium. As always, we await the direct measurement of cell calcium activity before any conclusions on this point can be made.

Forte et al. (5) suggested that histamine stimulated acid secretion in the stomach by causing the fusion of vesicles whose membranes contain the K^+, H^+-ATPase (5). However, DiBona and Sachs and their collaborators

have challenged this view, suggesting that histamine actually caused osmotic expansion of a tubular system already connected to the outside (1). The effect in the latter view is one of exposing the collapsed tubular system to the luminal medium rather than insertion of the ATPase into the luminal membrane.

2. EXOCYTOTIC INSERTION OF OTHER TRANSPORT SYSTEMS

Indirect evidence exists that other epithelial processes are regulated by rapid exocytotic insertion of pumps or channels. Electrophysiological analysis of membrane capacitance of the rabbit urinary bladder has shown that increased hydrostatic pressure increases the apparent capacitance of the luminal membrane. Since this procedure is not likely to have a significant effect on the dielectric constant of the membrane lipid, the change in the capacitance probably represents a change in membrane area. This change in capacitance was accompanied by an increase in sodium transport, suggesting that if vesicle fusion occurred then the vesicles might contain sodium channels. The change in capacitance and transport was prevented by pretreatment with cytochalasin (9). In the toad urinary bladder Garty and Edelman added trysin to the luminal membrane and were able to digest the sodium channels. They found that vasopressin appeared to increase the number of apical sodium channels following this digestion (this is discussed in detail in Chapter 6 of this book). Shorofsky et al. found that epinephrine increased the capacitance of the luminal membrane of the tracheal epithelium (13). This hormone also caused an increase in the chloride conductance of that membrane. One possible mechanism would be that the hormone induces fusion of vesicles enriched in chloride channels. More direct evidence of fusion events will be needed before any change in capacitance can be unequivocally interpreted as being due to fusion.

Lest it be thought that this process is limited to epithelia, it is now evident that insulin stimulates glucose transport in fat cells by causing fusion of vesicles whose membranes are rich in glucose carriers. Using cytochalasin B as a ligand for the glucose carrier, Cushman's group found a large intracellular reserve of microsomal membranes enriched in glucose carriers. Following insulin treatment these light vesicles changed their density to that typical of the plasma membrane (8). More recently, an antibody raised by Hinkle to the erythrocyte glucose carrier was found to bind specifically to the microsomal vesicles in resting cells and to the plasma membrane fraction in insulin-treated cells, confirming the view that the cytochalasin-binding site is indeed the sugar carrier (17). These results are discussed in more detail in Chapter 3 in this book. There is also circumstantial evidence that insulin stimulates K^+ transport into cells by exocytotic insertion of Na^+,K^+-

ATPase into membranes. Erlij found that insulin increases the number of ouabain-binding sites in frog skin and muscle; however, it is not clear at present whether the increase in ouabain binding is due to exocytotic insertion of sodium pumps or to a change in the affinity of binding for ouabain (4). Down- and up-regulation of many receptors is also known to occur by endocytosis and exocytosis and probably represents fundamentally the same process. There are probably other transport processes that are regulated by this mechanism.

The exocytosis mechanism does not have the biophysically elegant simplicity of ligand-receptor interaction which, as demonstrated for the case of the acetylcholine receptor, lends itself to rigorous electrophysiological and biochemical analysis. However, it increases the versatility of the cell in dealing, by a single mechanism, with different problems such as export of proteins and transmitters, cell surface renewal, and, now, regulation of transport. Resolution of this process in terms of chemical and physical details will have to await a more complete understanding of the role of the cytoskeleton and the various steps involved in membrane fusion, migration of proteins out into the bulk membrane, and, finally, the processes involved in the reversal of these processes on removal of the stimulus.

3. CONCLUSION

Regulation of transport by rapid fusion is likely to be a generalized phenomenon that will be detected in a variety of transport systems. The ability to detect a pH gradient by fluorescence methods in vesicles in a living cell, to trace their fusion as well as to isolate them and find that they contain a "label," in this case a proton translocating ATPase, provided the evidence needed to implicate exocytotic insertion of H^+ pumps as a mechanism of regulation of acid secretion in this epithelium. It would be important to develop similar kinds of evidence for each new system before one can conclude that a process is mediated by exocytotic fusion. Evidence based on the use of colchicine or other inhibitors without other more direct kinds of experiments serve only to confuse the issues. Because the ease of their use means that self-restraint by the investigator will be more difficult, we should remember that a large number of indirect results do not add up to direct evidence.

ACKNOWLEDGMENTS

The work described here was performed by Stephen Gluck, Christopher Cannon, and Westley Reeves. Not only did they perform the experiments, but also the ideas that emerged were a result of their combined efforts. I am grateful to all of them for their participation and especially to Steve Gluck

for his enthusiasm and penetrating insight into the problems investigated. The work was supported by grant AM20999 from the U.S. Public Health Service.

REFERENCES

1. DiBona, D. R., Ito, S., Berglindh, T., and Sachs, G. (1979) *Proc. Natl. Acad. Sci. USA*, **76**, 6689–6693.
2. Dixon, T. E. and Al-Awqati, Q. (1979) *Proc. Natl. Acad. Sci. USA*, **76**, 3135–3138.
3. Dixon, T. E. and Clausen, C. (1983) *Kidney Int.*, **23**, **231** (abstract).
4. Erlij, D. and Schoen, H. F. (1981) *Ann. N.Y. Acad. Sci.*, **372**, 272–290.
5. Forte, T. M., Machen, T. E., and Forte, J. G. (1977) *Gastroenterology*, **73**, 941–955.
6. Gluck, S., Cannon, C., and Al-Awqati, Q. (1983) *Proc. Natl. Acad. Sci. USA*, **79**, 4327–4331.
7. Gluck, S., Kelly, S., and Al-Awqati, Q. (1982) *J. Biol. Chem.*, **257**, 9230–9233.
8. Karniele, E., Zarnowski, M. J., Hissin, P. J., Simpson, I. A., Salama, L. B., and Cushman, S. W. (1982) *J. Biol. Chem.*, **256**, 4772–4777.
9. Lewis, S. A. and deMoura, J. I. C. (1982) *Nature*, **297**, 685–686.
10. Masur, S. K., Holtzman, E., and Walter, R. (1972) *J. Cell. Biol.*, **52**, 211–219.
11. Ohkuma, S. and Poole, B. (1978) *Proc. Natl. Acad. Sci. USA*, **75**, 3327–3331.
12. Reeves, W., Gluck, S., and Al-Awqati, Q. (1983). *Kidney Int.*, **23**, 237 (abstract).
13. Shorofsky, S. and Field, M. personal communication.
14. Spray, D. C., Stern, J. H., Harris, A. L., and Bennett, M. V. L. (1982) *Proc. Natl. Acad. Sci. USA*, **79**, 441–445.
15. Stetson, D. L. and Steinmetz, P. R. (1983) *Am. J. Physiol.*, **245**, C113–C120.
16. Wade, J. B. (1980) *Curr. Top. Membrane Transp.*, **13**, 123–147.
17. Wheeler, T. J., Simpson, I. A., Sogin, D. C., Hinkle, P. C., and Cushman, S. W. (1982) *Biochem. Biophys. Res. Comm.*, **105**, 89–95.

CHAPTER 10

VITAMIN D-DEPENDENT CALCIUM TRANSPORT

H. F. DELUCA

Department of Biochemistry
University of Wisconsin-Madison
Madison, Wisconsin

Vitamin D must be regarded as the major humoral substance involved in the regulation of calcium metabolism in all higher organisms. In the absence of vitamin D, bones fail to acquire the required mineral for structural function, resulting in the diseases rickets in the young and osteomalacia in the adult (13). Furthermore, insufficient levels of calcium and phosphorus are provided in the plasma resulting in failure of nerves and muscles to function properly giving rise to the overt convulsive state known as hypocalcemic tetany (13). In short, the supply of calcium and phosphorus to the organs of higher animals depends on the presence of vitamin D. Therefore, the essence of vitamin D function is the elevation of plasma calcium and phosphorus to levels that will support mineralization of bone and provide for adequate neuromuscular function. To carry out this basic function, vitamin D stimulates intestinal absorption of calcium and phosphorus (13). In addition, vitamin D plays a major role in the parathyroid-hormone-directed mobilization of calcium from bone. Furthermore, vitamin D may be involved in the parathyroid-hormone-dependent stimulation of calcium reabsorption in the distal renal tubule (70). These sites of action of vitamin D result in the transfer of calcium from the lumen of intestine, from the lumen of the distal renal tubule, and from the bone fluid compartment to the plasma compartment. Thus a primary function of vitamin D is to stimulate transport of calcium transcellularly across a membrane of cells. These functions are diagrammatically represented in Fig. 10.1. Please note that vitamin D is not involved in the actual transfer of calcium from the plasma compartment to the mineralizing sites of bone (75). This has recently been quite clearly excluded as a site of action of vitamin D.

For vitamin D to carry out the functions of stimulating the movements of

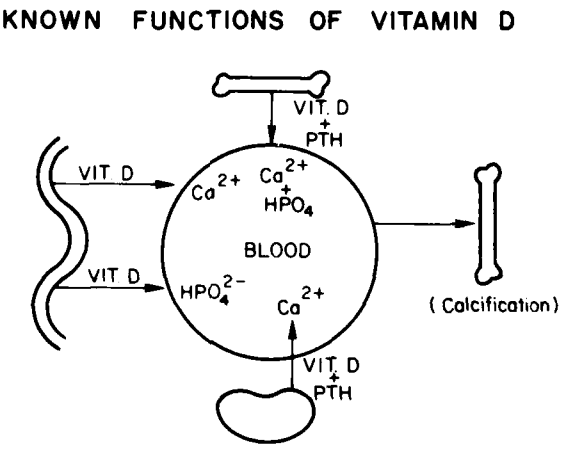

Figure 10.1. Diagrammatic representation of the sites of action of vitamin D in bringing about the elevation of plasma calcium and phosphorus concentrations. The sites of action are the small intestine, the bone membrane, and the distal renal tubule. In every instance vitamin D acts either by itself through its own hormonal form or together with the parathyroid hormone as indicated.

calcium and phosphorus indicated, it must be metabolized first in the liver to 25-hydroxyvitamin D_3 (25-OH-D_3) and subsequently in the kidney to 1,25-dihydroxyvitamin D_3 (1,25-$(OH)_2D_3$) (13, 14). 1,25-$(OH)_2D_3$ is regarded as the hormonal form of vitamin D that brings about the stimulation of calcium transfer reactions (13, 14). There is now little doubt that in the nonpregnant mammal the kidney is, for all practical purposes, the exclusive site of production of the vitamin D hormone, 1,25-$(OH)_2D_3$ or calcitriol (57). Furthermore, it is now well known that the production of calcitriol by the kidney is strongly regulated by the need for calcium or hypocalcemia (6, 51). Hypocalcemia stimulates secretion of the parathyroid hormone, and the parathyroid hormone stimulates the conversion of 25-OH-D_3 to 1,25-$(OH)_2D_3$ in the kidney (71). In addition, hypophosphatemia also stimulates conversion of 25-OH-D_3 to 1,25-$(OH)_2D_3$ (71). In true hormonal fashion, therefore, 1,25-$(OH)_2D_3$ stimulates active calcium and phosphorus transport in the small intestine and probably stimulates active transport at the other two sites as well (13). However, the other two sites are more complicated inasmuch as parathyroid hormone is also involved at these target sites. Figure 10.2 illustrates the metabolism of vitamin D required for function. Figure 10.3 presents the control of calcitriol or 1,25-$(OH)_2D_3$ production by plasma calcium concentration (12, 50).

Although the function of vitamin D in stimulating intestinal calcium transport has been known since the early part of the century (52), the molecular mechanism whereby it carries out this function has remained largely unknown. Furthermore, little investigation has taken place on the molecular mechanism whereby calcitriol functions to promote renal reabsorption of calcium or the mobilization of calcium from bone. For this reason the discussion here centers upon the role of the vitamin D hormone in the intestine. Finally, it should be noted that little is known concerning intestinal phosphate absorption as stimulated by calcitriol, and hence only a brief description of that system is provided.

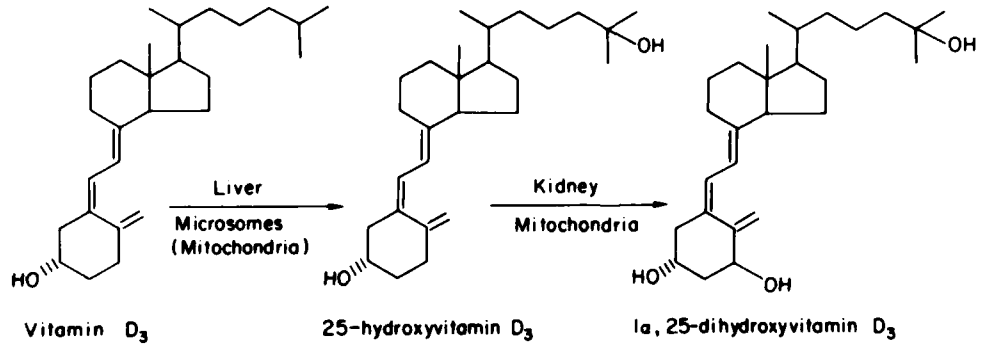

Figure 10.2. Metabolism of vitamin D required for function. In addition to the sites of 25-hydroxylation and 1-hydroxylation shown, intestine and kidney can carry out some 25-hydroxylation, and the placenta can carry out some 1-hydroxylation.

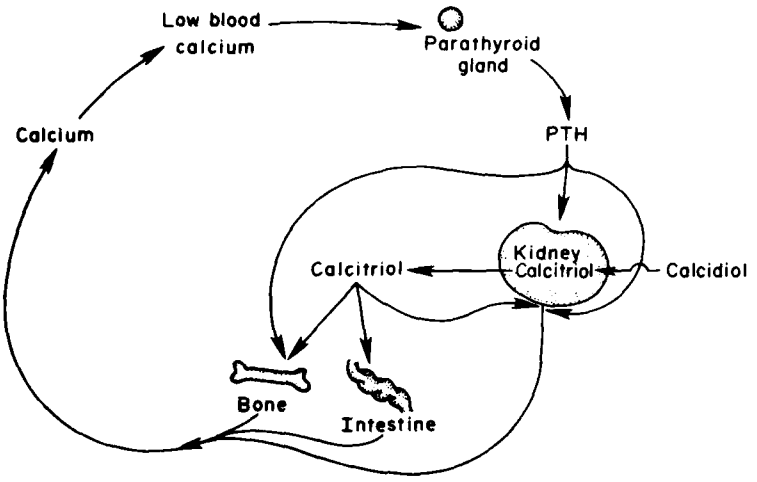

Figure 10.3. Diagrammatic representation of the regulation of $1,25\text{-}(OH)_2D_3$ (calcitriol) synthesis from $25\text{-}OH\text{-}D_3$ (calcidiol) involving the parathyroid hormone. Also shown are the sites of action of calcitriol and parathyroid hormone in bringing about elevation of plasma calcium concentration.

1. CHARACTERISTICS OF INTESTINAL CALCIUM TRANSPORT INDUCED BY VITAMIN D

Following the work of Orr in 1924 (52), Nicholaysen and his colleagues firmly established that vitamin D specifically stimulates intestinal absorption of calcium (48). This absorption did not require the presence of phosphate, but beyond that little new information was learned. In 1967 Schachter and Rosen (62) carried out the first *in vitro* experiments using the everted intestinal sac technique of Wilson and Wiseman (83) to show that calcium is transported against a concentration gradient and is specifically stimulated by vitamin D. This was subsequently followed by the demonstration in four laboratories that calcium is transported against an electrochemical potential gradient in response to vitamin D (41, 60, 76, 79). The characteristics of this calcium transport system are: (1) calcium is transported against an electrochemical potential gradient, (2) it has a K_m of 1 m*M* for calcium, and (3) metabolic energy is required for the transfer reaction. A thorough examination of the requirements of this transport system has revealed that an energy supply, usually glucose or fructose, and the presence of sodium ions are required (42). Sodium is required for calcium to be transported across the basal-lateral membrane of the small intestine, but little else is known about the mechanism for this transfer reaction. Cellular compartment levels of calcium measured during steady-state transport suggest that vitamin D functions at the brush-border surface and the basal-lateral surface in stimulating transport (61). The brush-border site has been confirmed using kinetic measurements (41, 76). Additionally, kinetics of calcium movements in isolated

villus cells suggest that vitamin D affects an intracellular compartment of calcium, perhaps mitochondria (5). Reports that brush-border vesicles from animals treated with vitamin D compounds show increased calcium transport (7, 55) and the polyene antibiotic experiments (1) offer further support to the idea that vitamin D affects the brush-border surface in effecting increased calcium transport. However, a clear description of the transport mechanism affected by vitamin D is lacking.

Of considerable interest was the discovery by Nicolaysen and his colleagues that animals fed a low-calcium diet but given adequate amounts of vitamin D had much higher rates of intestinal calcium absorption than animals fed a high-calcium diet given adequate amounts of vitamin D (49). This ability of the organism to adapt to the need for calcium led Nicolaysen to propose a factor released by bone that would instruct the intestine of the requirements for calcium. When it was learned that vitamin D must be converted to calcitriol (31) and the production of calcitriol is regulated by the need for calcium, it soon became clear that the Nicolaysen Endogenous Factor was nothing more than calcitriol appearing in response to parathyroid hormone secretion. Thus the increased rate of intestinal calcium absorption or transport that results from a dietary calcium lack is the result of a stimulation of production of the vitamin D hormone or calcitriol (58).

Phosphate transport in the intestine in response to calcitriol is now known to be independent of calcium in the medium (9), and an energy supply (35) is required as well as sodium ions (81). The sodium ions in the case of phosphate transport are required for entry of phosphate across the brush-border membrane of the mucosa. The K_m for phosphate is also about 1 m*M*, and phosphate is the active ion transported against an electrochemical potential gradient. So far, no carrier for this transport has been described. Since little more is known about the phosphate system, all remaining discussion focuses on the intestinal calcium transport mechanism.

2. TIME COURSE OF RESPONSE OF INTESTINAL CALCIUM TRANSPORT TO CALCITRIOL

Two techniques have been used to follow intestinal calcium transport in response to calcitriol. One is the everted intestinal sac technique (83), and the other is a measurement of oxygen-dependent calcium uptake by discrete discs (34) of intestinal mucosa taken from animals either vitamin D deficient or given vitamin D compounds. The results of these studies were identical regardless of the methods used.

Figure 10.4 illustrates the complex response observed in the duodenum of rats given a single injection of calcitriol (27). There is an initial rapid response in which calcium transport against a concentration gradient rises to a maximum value at 6 h after intravenous injection of a physiologic dose of calcitriol. This is followed by a fall in the transport ability to a low level

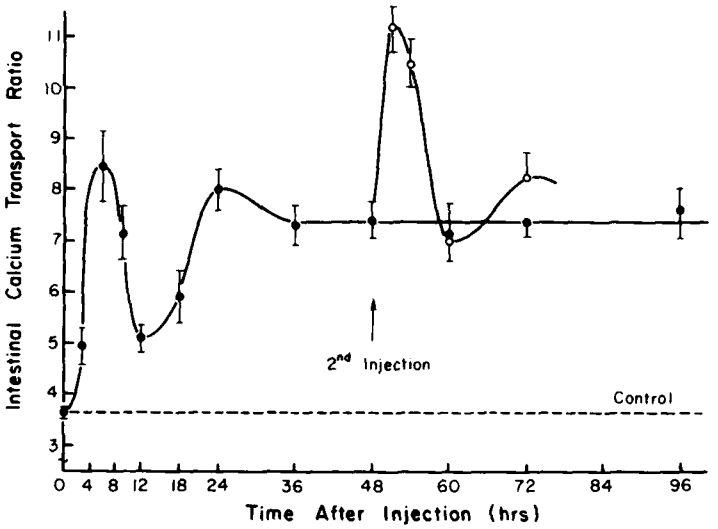

Figure 10.4. Time course of intestinal calcium transport response to the vitamin D hormone (calcitriol). At various times following a single intravenous injection of 325 pmol of calcitriol, duodena were removed and calcium transport measured by the everted gut sac technique. These values are to be compared with the everted intestinal sac transport ratios obtained in vitamin D-deficient or control animals (----).

observed at 18 h, only to have a resumption of transport reaching a maximum between 24–48 h. This transport response then remains for several days. These results illustrate that the first response is one of existent villus cells on the surface of the duodenum. It is clear that these villus cells are responding to the hormone. The second response is very likely a programmed response of the crypt cells as they migrate into the villus region where they begin calcium transport. Of particular importance is that at the 24-h period if a second injection of calcitriol is given, the initial rapid response is induced superimposed upon the slower or second response, but the second response from the second dose does not appear. These results suggest that there are two independent mechanisms.

With the synthesis of calcitriol labeled with tritium in the 26- and 27-positions (160 Ci/mmol), it was possible to carry out both biochemical-based cell fractionation and freeze-thaw autoradiography (10, 30, 40, 69, 84). Since biochemical fractionation of tissues carried with it the danger of redistribution of label following rupture of the cells, we relied almost entirely upon the freeze-thaw autoradiography approach to learn of the [illegible] of deposition of the calcitriol prior to the intestinal response (69, 84). It should be important to note that calcitriol is rapidly degraded in the small intestine by a side-chain oxidative-cleavage reaction that results in total loss of tritium (17, 39). Thus the label that appears arises from intact calcitriol. As shown in Fig. 10.5, calcitriol, within one-half hour postinjection, localizes in the villus cells of the small intestine and specifically in the nuclei (69). It is not found

Figure 10.5. Freeze-thaw autoradiography of rat small intestine one-half hour after *in vivo* injection of 325 pmol of 1,25-$(OH)_2$[26,27-^{3}H]D_3. Lumen of intestine is on the far right; submucosa is on the far left. Note the nuclear localization in the villus cells, with no other specific localization noted elsewhere in the same cells or in the goblet cell or in the submucosa.

concentrated in the brush border, in the Golgi apparatus, or in the basal-lateral membrane. Note there is no nuclear localization in the goblet cells or in the submucosa. Similar nuclear localization is found in the crypt cells but not in the smooth muscle cells of the small intestine (68). This label can be removed by competition with unlabeled calcitriol but not with calcidiol (25-hydroxyvitamin D_3) or other similar compounds, representing specific nuclear localization. This therefore suggests that a nuclear mechanism is involved in the expression of vitamin D action.

As might be expected from the fact that calcitriol is a steroid hormone and from the dogma of how steroid hormones act, a macromolecular receptor for calcitriol must exist. It is now quite clear that in chicks a 3.7S (8, 38) and in mammals a 3.2S macromolecule (18, 36, 47) is found in all target tissues which specifically binds calcitriol with high affinity and low capacity. Such a receptor molecule can be readily demonstrated either by Scatchard plot analysis or as shown in Fig. 10.6 by sucrose density-gradient analysis. In the small intestine of the chick and man, the K_d for calcitriol is 5×10^{-11} *M* (46, 82). The association and dissociation rate constants are known, and a ratio of the association and dissociation rate constants gives approximately the same K_d (46, 82). Therefore this represents a highly specific binder for calcitriol. In fact, experimental measurements using unlabeled analogs of calci-

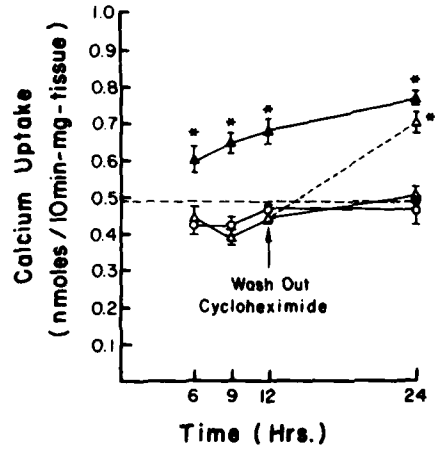

Figure 10.6. Inhibition of calcium uptake response of chick embryonic intestine in culture in response to 75 μM calcitriol. Solid triangles represent uninhibited calcium uptake response to the calcitriol. Open circles represent calcium uptake in embryonic intestine without addition of calcitriol. Open triangles represent intestinal responses to calcitriol in the presence of cycloheximide until 12 h, at which time one-half the cultures were continued in the presence of cycloheximide, whereas the other half were transferred to fresh medium without cycloheximide. This is represented by the dotted line. The * represents significant transport response with $p < 0.001$.

triol illustrate the high degree of selectivity (14, 16, 37). No metabolite of vitamin D approaches calcitriol in its ability to bind to this receptor molecule; the closest being 1,24R,25-trihydroxyvitamin D_3, a minor metabolite that shows a K_d of somewhere less than 10^{-9} M. 25-OH-D_3 or calcidiol, the precursor, will bind the receptor, but approximately a 1000-fold excess is required. It is unknown whether this macromolecule is located in the cytoplasm or is found in the nucleus prior to association with calcitriol (38, 77). Evidence from some cell fractionation experiments in low-salt medium suggest that it is nuclear, whereas fractionation experiments from high-salt media suggest that it is cytoplasmic. This cannot be resolved until frozen-section autoradiography is obtained with antibodies to the receptor molecule. Monoclonal antibodies to the chick receptor have been prepared (53), as has a pure preparation of the receptor (63). This will undoubtedly result in resolution of this dilemma.

3. IS TRANSCRIPTION INVOLVED IN THE EXPRESSION OF CALCITRIOL ACTION ON THE SMALL INTESTINE?

When calcitriol was first discovered, it could be demonstrated that the provision of actinomycin D to vitamin D-deficient animals did not prevent the

intestine from responding to physiologic amounts of calcitriol (72). This initial work has been repeated in subsequent years in which it has been concluded that calcitriol must act by a mechanism not involving transcription of DNA (3). Unfortunately, actinomycin D at 1 μg/g of body weight does not block the production of RNA in the small intestine by more than 30%. Addition of higher concentrations of actinomycin D brings about death of animals (74). In short, it is not possible to carry out *in vivo* experiments with actinomycin D that can be considered conclusive as to whether transcription is involved in the action of calcitriol on intestine or not. The best information available in this area has come from tissue culture experiments.

Corradino has developed a culture system in which intestine is excised from chick embryos at 20–21 days of incubation (11). These intestinal segments can be cultured conveniently for several days and show increasing calcium uptake following addition of saturating amounts of calcitriol (11, 21). This transport system has been quite thoroughly characterized; the K_m for calcium is of the order of 1–2 m*M*. It is a saturable transport process, but a requirement for energy supply could not be demonstrated. Thus blocking of glycolysis and oxidative phosphorylation did not block this calcium uptake process (21). This is unlike the process seen in intestine taken from intact animals. In any case, the addition of calcitriol at 75 n*M* produces a clear response at 6 h, and this response can be blocked by the addition of 5 μM cycloheximide or 5 μM of actinomycin D (20). To illustrate that this is not merely the result of death of the cells, if cycloheximide is washed away by transferring the cultures to fresh medium, the response to calcitriol immediately returns (Fig. 10.6). Similar but less dramatic results can be obtained with the actinomycin. Furthermore, other inhibitors of transcription block this *in vitro* response to calcitriol. If it can be accepted that this system represents at least a segment of the intestinal calcium transport mechanism found in young growing animals, then these results are consistent with the idea that calcitriol must function by interaction with a receptor followed by transcription of specific genes that code for calcium and phosphorus transport proteins.

Rasmussen and his colleagues have contended that calcitriol may function directly on the brush-border membrane by altering the lipid composition which thereby might affect calcium flux (56). To support these conclusions they have shown that there is a change in the phosphatidylcholine to phosphatidylethenolamine ratio in brush borders isolated from animals given calcitriol (56). They have also reported a change in the cholesterol ester to cholesterol content of the brush-border membranes (25). Finally, this group has provided evidence using membrane vesicles derived from animals given calcitriol to show increased calcium transfer across the brush-border membranes (45). In our experience, virtually all of the intestinal response is nuclear mediated, but it is indeed possible that other actions of calcitriol may exist in the small intestine.

4. PRODUCTS OF GENE EXPRESSION INDUCED BY CALCITRIOL

The nature and extent of the gene products that result from calcitriol stimulation of the enterocyte are not known. In 1967 Wasserman and Taylor described a calcium-binding protein found in the intestine that appeared dependent on vitamin D (80). Extensive work by this group and many other groups have shown that, in the chick, this protein has a molecular weight of 28,000 and, in mammals, of the order of 8000–12,000 (78). The amino acid sequence of the bovine calcium-binding protein is known (22), whereas the chick protein is still being characterized. Antibodies are available to this protein, and there is little doubt that the calcium-binding protein originally described by Wasserman is made in response to calcitriol (4). The site of localization of this protein appears to be cytoplasmic (73), and there is considerable debate as to whether this protein plays a role in calcium transport (29, 66). Of particular interest is the work of Spencer and Lawson, who could not find calcium-binding protein in the intestine at the time it responded (67), and furthermore, could find no evidence for the presence of messenger RNA for the calcium-binding protein at the time calcium transport appeared in response to calcitriol (65). Additionally, the calcium-binding protein remained in the intestine long after the response of the intestine to calcitriol had subsided (65, 67). Thus, on a temporal basis, it appeared that some other factor must be induced by calcitriol to carry out the transport function.

More recently we have developed a system of examining expression of genes in which intestinal mucosa explanted from vitamin D-deficient animals is incubated with ^{14}C amino acids, whereas mucosa explanted from animals given calcitriol 6 h before are incubated with the same amino acids but labeled with tritium (32, 33, Bishop, Thompson, Santek, and DeLuca, unpublished results). These two mucosal preparations are mixed, homogenized, and fractionated into a pellet fraction and a cytoplasmic fraction. Each of these fractions is then subjected to solubilization and two-dimensional gel electrophoretic separation. The gel is then exposed to film that is sensitive to ^{14}C only or other film to which a fluor is added, resulting in sensitivity to ^{14}C and tritium. The two records are subjected to a drum densitometer examination on line to a Man-computer Interactive Data Access System (McIDAS) that then locates, outlines the spots, and computes the tritium to ^{14}C ratio. The proteins that are specifically labeled with tritium in response to calcitriol are therefore highlighted by the computer, and the ratio is given (Bishop, Thompson, Santek, Kendrick, and DeLuca, in preparation). Furthermore, we have developed methods using computer analysis of these gels in which each spot of interest is subjected, because of internal standards, to computation of the amount of protein produced (4).

Two results have already come from this study. The first is shown in Fig.

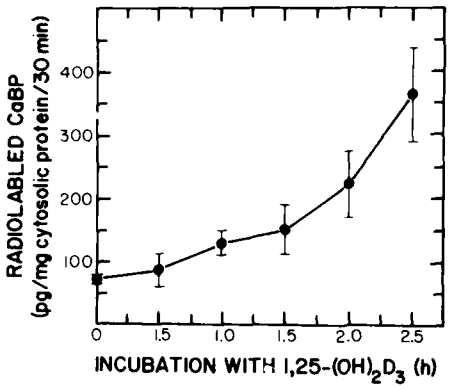

Figure 10.7. Time course of synthesis of calcium-binding protein in response to calcitriol in embryonic chick intestine. Tritium-labeled calcium-binding protein was detected by fluorography following two-dimensional gel electrophoresis separation from other proteins. With a drum densitometer on line with a McIDAS computer these spots were located, a program was used to define the areas in the spots, and the total incorporation was measured by comparison with internal standards using computer-based analysis. Significant increase in calcium-binding protein synthesis occurred within 1 h after addition of calcitriol, and calcium uptake was not altered until 6 h postincubation with calcitriol, leaving no doubt that calcium-binding protein is formed far in advance of calcium uptake by this tissue.

10.7 and demonstrates that the calcium-binding protein appears well in advance of calcium transport in the case of the *in vitro* chick intestinal organ cultures (4). This technique is about one order of magnitude more sensitive than immunoassay and supports the concept put forth by Wasserman that calcium-binding protein is present in sufficient time to play a role in calcium transport. The major question, however, is what are the other proteins that are synthesized in response to calcitriol and how can they be integrated into a molecular mechanism? So far, there are two such proteins that have made their appearance in our double-label profiles. Unfortunately, we have not thoroughly characterized these proteins and thus are unable to report at this time. Nevertheless, there are other gene products that appear in response to calcitriol besides the calcium-binding protein, and they must be integrated into a calcium transport mechanism. The suggested mechanism for calcium transport is diagrammatically illustrated in Fig. 10.8. Calcitriol must interact with the receptor that ultimately makes its appearance with the ligand in the nucleus bound to specific DNA sequences, which then causes transcription of specific genes that play a role in calcium and phosphate transport. One of these probably appears at the brush-border membrane that serves as a carrier for calcium. The calcium-binding protein may serve in the cytoplasm to bind the calcium and provide for selective expulsion of the calcium at the basal-lateral membrane. That process appears to be sodium dependent. Obviously, much remains to be learned about the molecular mechanism of calcium transport.

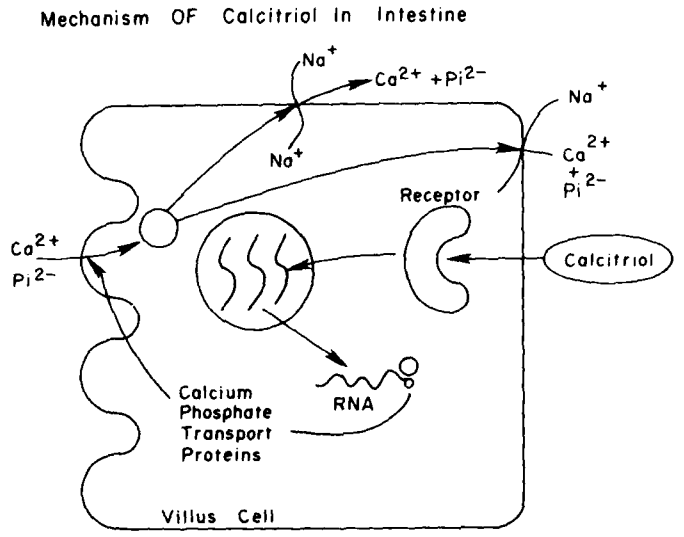

Figure 10.8. Diagrammatic representation of the probable molecular mechanism of action of calcitriol in stimulating intestinal calcium transport. Calcitriol must interact with the receptor, which in turn must interact with specific components of the nuclei. This results in transcription of specific genes that code for calcium and phosphorus transport proteins that are yet to be clearly defined. These act at the brush border, the cytosol, and probably at the basal-lateral membrane. Sodium is required for the final expulsion of calcium.

5. DEVELOPMENT OF THE INTESTINAL CALCIUM TRANSPORT IN NEONATAL ANIMALS

During the course of our investigation of the role of vitamin D in reproduction and lactation, we examined duodenal calcium transport in neonatal rats that were nursed by their mothers (26). It was surprising for us to learn, as shown in Fig. 10.9, that intestinal calcium transport did not make its appearance until shortly before weaning, and furthermore, the intestine seemed insensitive to vitamin D whether it was given to the mother or given directly to the rat pup prior to 14 days postpartum. At the same time we carried out these experiments, we learned that the vitamin D-dependent bone calcium mobilization had already developed during this period. In short, the intestinal calcium transport mechanism in response to vitamin D had specifically not developed in these animals while they were supported by milk from their mothers.

To illustrate that this lack of hormone sensitivity was not the result of a failure of development of metabolism of vitamin D, calcitriol given to animals during this neonatal period produced no response, illustrating that the intestine was insensitive to calcitriol until approximately 14–16 days postpartum (26). Upon examination of these intestines, it became clear that neonatal rat intestine has very little or no calcitriol receptor and that this

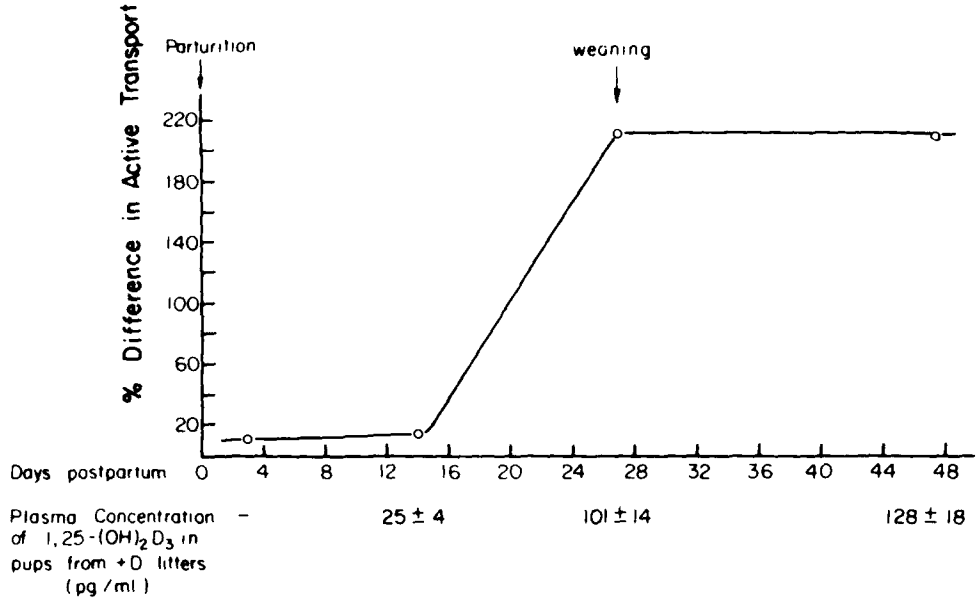

Figure 10.9. Time course of development of calcium transport in the intestines of neonatal rat pups given adequate amounts of vitamin D. Plasma concentrations of calcitriol are listed below the graph, and the percent difference in calcium transport between animals receiving vitamin D and those not receiving vitamin D is plotted. Note that responsiveness to vitamin D does not appear until 14 days postpartum.

receptor makes its appearance at precisely the time when active calcium transport and vitamin D sensitivity makes its appearance (Fig. 10.10) (28). To further support this observation, we examined the development of the receptor in adrenalectomized animals, since hydrocortisone is known to play an important role in the maturation of the small intestine (44). The results show quite clearly that adrenalectomy delays the onset of development of the receptor, whereas injection of hydrocortisone precociously brings about the appearance of the receptor (43). Finally, if the intestine is explanted at 14 days postpartum and incubated in culture with hydrocortisone, the receptor makes its appearance (Fig. 10.11), whereas if the intestine is incubated in the absence of hydrocortisone, the receptor does not appear (43). At later stages, however, hydrocortisone has no effect, and the receptor makes its appearance in culture in any case. These results provide two important facts: (1) interaction of calcitriol with a receptor is required for the intestinal calcium transport response; and (2) hydrocortisone plays an important role in maturation of the vitamin D calcium transport system in neonatal rats, probably by inducing the formation of the calcitriol receptor molecule.

To provide further evidence that the molecular mechanism of calcitriol action in the small intestine probably involves a nuclear mechanism, an experiment of nature can also be cited as further support. With three groups, we independently discovered a new type of vitamin D-resistant rickets,

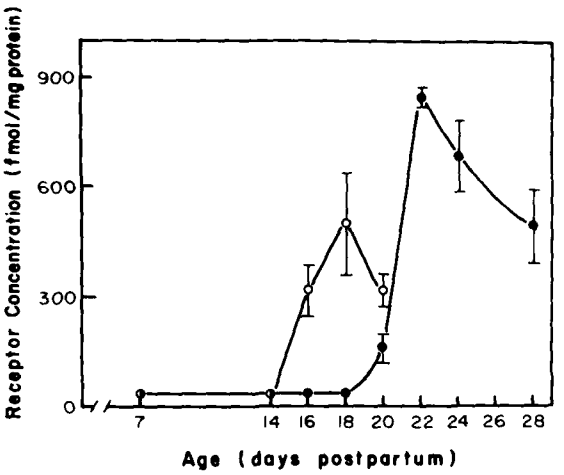

Figure 10.10. Time course of appearance of calcitriol intestinal receptor in the neonatal rat postpartum. Note that in the +D animals (○), the receptor makes its appearance between 14–16 days postpartum, whereas in the −D animals (●) the receptor does not appear until 20 days postpartum. This correlates with sensitivity of the intestine to calcitriol.

called vitamin D-dependency rickets Type II (2, 59, 64). Children born with this autosomal recessive defect show high circulating levels of calcitriol and an insensitivity of the intestine and other target organs to calcitriol administration. Thus these children become rachitic despite receiving the active form of vitamin D. Dr. Steve Marx at the National Institutes of Health has explanted skin cells from these subjects as well as skin cells taken from normal subjects (15, 19). In brief, he was able to show that in some of these patients there is a lack of calcitriol receptor, illustrating that at least a subgroup of this type of vitamin D-dependency rickets results from a lack of

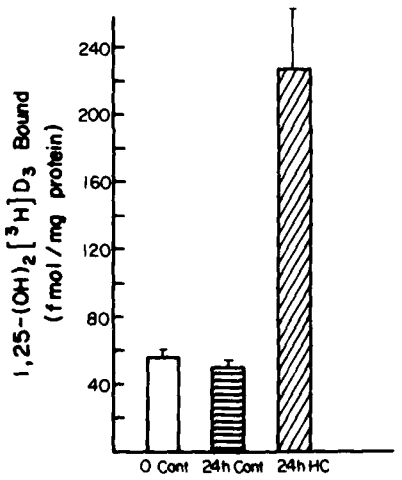

Figure 10.11. Response of calcitriol receptor to hydrocortisone. Intestinal tissue was explanted from neonatal rats at 14 days postpartum and incubated in the absence (parallel-marked graph) and in the presence of hydrocortisone (hatched bar) for 24 h. Following this the level of receptor present in the cultured tissue was measured. These results demonstrate that hydrocortisone brings about a maturation of the cells in culture and with it the calcitriol receptor makes its appearance.

receptor. Thus, in this experiment of nature it is clear that the intestine cannot respond unless calcitriol interacts with a receptor, again supporting the nuclear-mediated mechanism for calcitriol action in inducing intestinal calcium transport.

6. SUMMARY

Vitamin D must be metabolized to 25-OH-D_3 or calcidiol in the liver and subsequently to 1,25-$(OH)_2D_3$ (calcitriol) in the kidney to produce its physiological actions. Calcitriol stimulates calcium and phosphorus transport reactions in the small intestine and together with parathyroid hormone stimulates calcium transport reactions in bone and kidney. In the small intestine calcitriol brings about its response in a complex manner. It provides a very rapid response on existing villus cells, causing a rise in calcium transport within 6 h postadministration. This transport response subsides by 18 h, and a second response makes its appearance at 24–48 h. This second response is likely to be an action on crypt cells which then migrate into the villus region and bring about calcium transport. The molecular mechanism of calcium transport in the villus cells has been examined. Calcitriol localizes specifically in the nucleus within 0.5 h postadministration, and it does not localize in any of the other cell fractions. A receptor has been discovered for calcitriol, and interaction with this receptor is required for calcitriol to bring about its action in stimulating calcium transport. It is therefore believed that calcitriol, together with receptor, binds to specific portions of nuclear DNA to bring about transcription of specific genes that code for calcium and phosphorus transport proteins. Only one protein induced by calcitriol has been described. It is the calcium-binding protein found in the cytoplasm. Exactly how it functions in calcium transport is in debate, although the time sequence of its appearance appears to be consistent with a role in that system. It is likely that other gene products are induced by calcitriol, and they are currently being characterized.

In the neonatal rat, active calcium transport does not make its appearance until 14–16 days postpartum. The intestine is not sensitive to vitamin D or calcitriol prior to this time. This lack of sensitivity is because of the lack of a receptor for calcitriol. The receptor to calcitriol can be precociously induced by hydrocortisone injections, or it can be delayed by adrenalectomy. Incubation of intestine from neonatal rat pups at 14 days postpartum with hydrocortisone brings about *in vitro* appearance of the receptor molecule. These results and results of studies involving genetic vitamin D resistance strongly suggest that calcitriol must function by interaction with the receptor, presumably by a nuclear mechanism, to bring about intestinal calcium transport. The molecular mechanism, however, remains to be described.

ACKNOWLEDGMENTS

This work was supported by a Program Project Grant No. AM-14881 from the National Institutes of Health and by the Harry Steenbock Research Fund of the Wisconsin Alumni Research Foundation.

REFERENCES

1. Adams, T. H., Wong, R. G., and Norman, A. W. (1970) *J. Biol. Chem.*, **245,** 4432–4442.
2. Bell, N. H., Hamstra, A. J., and DeLuca, H. F. (1978) *N. Engl. J. Med.*, **298,** 996–999.
3. Bikle, D. D., Zolock, D. T., Morrissey, R. L., and Herman, R. H. (1978) *J. Biol. Chem.*, **253,** 484–488.
4. Bishop, C. W., Kendrick, N. C., and DeLuca, H. F. (1982) *J. Biol. Chem.*, **258,** 1305–1310.
5. Borle, A. B. (1974) *J. Membrane Biol.*, **16,** 207–220.
6. Boyle, I. T., Gray, R. W., and DeLuca, H. F. (1971) *Proc. Natl. Acad. Sci. USA*, **68,** 2131–2134.
7. Miller, A., III, and Bronner, F. (1981) *Biochem. J.*, **196,** 391–401.
8. Brumbaugh, P. F. and Haussler, M. R. (1975) *J. Biol. Chem.*, **250,** 1588–1594.
9. Chen, T. C., Castillo, L., Korycka-Dahl, M., and DeLuca, H. F. (1974) *J. Nutr.*, **104,** 1056–1060.
10. Chen, T. C., Weber, J. C., and DeLuca, H. F. (1970) *J. Biol. Chem.*, **245,** 3776–3780.
11. Corradino, R. A. (1973) *Science*, **179,** 402–404.
12. DeLuca, H. F. (1974) *Fed. Proc.*, **33,** 2211–2219.
13. DeLuca, H. F. (1981) in *The Harvey Lectures, Series 75*, Academic, New York pp. 333–379.
14. DeLuca, H. F. and Schones, H. K. (1983) *Ann. Rev. Biochem.*, **52,** 411–439.
15. Eil, C., Liberman, U. A., Rosen, J. F., and Marx, S. J. (1981) *N. Engl. J. Med.*, **304,** 1588–1591.
16. Eisman, J. A. and DeLuca, H. F. (1977) *Steroids*, **30,** 245–257.
17. Esvelt, R. P., Schnoes, H. K., and DeLuca, H. F. (1979) *Biochemistry*, **18,** 3977–3983.
18. Feldman, D., McCain, T. A., Hirst, M. A., Chen, T. L., and Colston, K. W. (1979) *J. Biol. Chem.*, **254,** 10378–10384.
19. Feldman, D., Chen, T., Cone, C., Hirst, M., Shani, S., Benderli, A., and Hochberg, Z. (1982) *J. Clin. Endocrinol. Metab.*, **55,** 1020–1023.
20. Franceschi, R. T. and DeLuca, H. F. (1981) *J. Biol. Chem.*, **256,** 3840–3847.
21. Franceschi, R. T. and DeLuca, H. F. (1981) *J. Biol. Chem.*, **256,** 3848–3852.
22. Fullmer, C. S. and Wasserman, R. H. (1979) *J. Biol. Chem.*, **254,** 7208–7212.
23. Garabedian, M., Holick, M. F., DeLuca, H. F., and Boyle, I. T. (1972) *Proc. Natl. Acad. Sci. USA*, **69,** 1673–1676.
24. Garabedian, M., Tanaka, Y., Holick, M. F., and DeLuca, H. F. (1974) *Endocrinology*, **94,** 1022–1027.
25. Goodman, D. B. P., Haussler, M. R., and Rasmussen, H. (1972) *Biochem. Biophys. Res. Commun.*, **46,** 80–84.

26. Halloran, B. P. and DeLuca, H. F. (1980) *Am. J. Physiol.*, **239,** G473–G479.
27. Halloran, B. P. and DeLuca, H. F. (1981) *Arch. Biochem. Biophys.*, **208,** 477–486.
28. Halloran, B. P. and DeLuca, H. F. (1981) *J. Biol. Chem.*, **256,** 7338–7342.
29. Harmeyer, J. and DeLuca, H. F. (1969) *Arch. Biochem. Biophys.*, **133,** 247–254.
30. Haussler, M. R., Myrtle, J. F., and Norman, A. W. (1968) *J. Biol. Chem.*, **243,** 4055–4064.
31. Holick, M. F., Schnoes, H. K., DeLuca, H. F., Suda, T., and Cousins, R. J. (1971) *Biochemistry*, **10,** 2799–2804.
32. Kendrick, N. C., Barr, C. R., Moriarity, D., and DeLuca, H. F. (1981) *Biochemistry*, **20,** 5288–5294.
33. Kendrick, N. C., Eakle, K., and DeLuca, H. F. (1982) *Electrophoresis*, **3,** 346–353.
34. Kendrick, N. C., Kabakoff, B., and DeLuca, H. F. (1981) *Biochem. J.*, **194,** 178–186.
35. Kowarski, S. and Schachter, D. (1969) *J. Biol. Chem.*, **244,** 211–217.
36. Kream, B. E. and DeLuca, H. F. (1977) *Biochem. Biophys. Res. Commun.*, **76,** 735–738.
37. Kream, B. E., Jose, M. J. L., and DeLuca, H. F. (1977) *Arch. Biochem. Biophys.*, **179,** 462–468.
38. Kream, B. E., Reynolds, R. D., Knutson, J. C., Eisman, J. A., and DeLuca, H. F. (1976) *Arch. Biochem. Biophys.*, **176,** 779–787.
39. Kumar, R., Harnden, D., and DeLuca, H. F. (1976) *Biochemistry*, **15,** 2420–2423.
40. Lawson, D. E. M., Wilson, P. W., and Kodicek, E. (1969) *Biochem. J.*, **115,** 269–277.
41. Martin, D. L. and DeLuca, H. F. (1969) *Arch. Biochem. Biophys.*, **134,** 139–148.
42. Martin, D. L. and DeLuca, H. F. (1969) *Am. J. Physiol.*, **216,** 1351–1359.
43. Massaro, E., Simpson, R. U., and DeLuca, H. F. (1982) *J. Biol. Chem.*, **257,** 13736–13739.
44. Massaro, E., Simpson, R. U., and DeLuca, H. F. (1983) *Am. J. Physiol.*, **244,** E230–E235.
45. Max, E. E., Goodman, D. B. P., and Rasmussen, H. (1978) *Biochim. Biophys. Acta*, **511,** 224–239.
46. Mellon, W. S. and DeLuca, H. F. (1979) *Arch. Biochem. Biophys.*, **197,** 90–95.
47. Mellon, W. S. and DeLuca, H. F. (1980) *J. Biol. Chem.*, **255,** 4081–4086.
48. Nicolaysen, R. and Eeg-Larsen, N. (1953) *Vitam. Horm.*, **11,** 29–60.
49. Nicolaysen, R., Eeg-Larsen, N., and Malm, O. J. (1953) *Physiol. Rev.*, **33,** 424–444.
50. Omdahl, J. L. and DeLuca, H. F. (1973) *Physiol. Rev.*, **53,** 327–372.
51. Omdahl, J. L., Gray, R. W., Boyle, I. T., Knutson, J., and DeLuca, H. F. (1972) *Nature*, **237,** 63–64.
52. Orr, W. J., Holt, L. E., Jr., Wilkins, L., and Boone, F. H. (1923) *Am. J. Dis. Child.*, **26,** 362–372.
53. Pike, J. W., Marion, S. L., Donaldson, C. A., and Haussler, M. R. (1983) *J. Biol. Chem.*, **258,** 1289–1296.
54. Rasmussen, H., DeLuca, H. F., Arnaud, C., Hawker, C., and von Stedingk, M. (1963) *J. Clin. Invest.*, **42,** 1940–1946.
55. Rasmussen, H., Fontaine, O., Max, E., and Goodman, D. B. P. (1979) *J. Biol. Chem.*, **254,** 2993–2999.
56. Rasmussen, H., Matsumoto, T., Fontaine, O., and Goodman, D. B. P. (1982) *Fed. Proc.*, **41,** 72–77.
57. Reeve, L., Tanaka, Y., and DeLuca, H. F. (1983) *J. Biol. Chem.*, **258,** 3615–3617.
58. Ribovich, M. L. and DeLuca, H. F. (1975) *Arch. Biochem. Biophys.*, **170,** 529–535.
59. Rosen, J. F., Fleischman, A. R., Finberg, L., Hamstra, A., and DeLuca, H. F. (1979) *J. Pediatr.*, **94,** 729–735.

60. Schachter, D. (1963) in R. H. Wasserman, Ed., *The Transfer of Calcium and Strontium Across Biological Membranes*, Academic, New York, pp. 197–210.

61. Schachter, D., Kowarski, S., Finkelstein, J. D., and Wang M. R. (1966) *Am. J. Physiol.*, **211,** 1131–1136.

62. Schachter, D. and Rosen, S. M. (1959) *Am. J. Physiol.*, **196,** 357–362.

63. Simpson, R. U., Hamstra, A., Kendrick, N. C., and DeLuca, H. F. (1983) *Biochemistry*, **22,** 2586–2594.

64. Sockalowsky, J. J., Ulstrom, R. A., DeLuca, H. F., and Brown, D. M. (1980) *J. Pediatr.*, **96,** 701–703.

65. Spencer, R., Charman, M., Emtage, J. S., and Lawson, D. E. M. (1976) *Eur. J. Biochem.*, **71,** 399–409.

66. Spencer, R., Charman, M., Wilson, P., and Lawson, E. (1976) *Nature*, **263,** 161–163.

67. Spencer, R., Charman, M., Wilson, P. W., and Lawson, D. E. M. (1978) *Biochem. J.*, **170,** 93–102.

68. Stumpf, W. E., Sar, M., and DeLuca, H. F. (1981) in Cohn, D. V., Talmage, R. V., and Matthews, J. L., Eds., *Hormonal Control of Calcium Metabolism*, Excerpta Medica, Amsterdam, pp. 222–229.

69. Stumpf, W. E., Sar, M., Reid, F. A., Tanaka, Y., and DeLuca, H. F. (1979) *Science*, **206,** 1188–1190.

70. Sutton, R. A. L. and Dirks, J. H. (1978) *Fed. Proc.*, **37,** 2112–2119.

71. Tanaka, Y. and DeLuca, H. F. (1973) *Arch. Biochem. Biophys.*, **154,** 566–574.

72. Tanaka, Y., DeLuca, H. F., Omdahl, J., and Holick, M. F. (1971) *Proc. Natl. Acad. Sci. USA*, **68,** 1286–1288.

73. Taylor, A. N. (1983) *J. Histochem. Cytochem.*, **31,** 426–429.

74. Tsai, H. C., Midgett, R. J., and Norman, A. W. (1973) *Arch. Biochem. Biophys.*, **157,** 339–347.

75. Underwood, J., Weinstein, R., and DeLuca, H. F. (1983) Abstract, American Society for Bone and Mineral Research, June 5–7, San Antonio, Texas.

76. Walling, M. W. and Rothman, S. S. (1969) *Am. J. Physiol.*, **217,** 1144–1148.

77. Walters, M. R., Hunziker, W., and Norman, A. W. (1980) *J. Biol. Chem.*, **255,** 6799–6805.

78. Wasserman, R. H. and Feher, J. J. (1977) in Wasserman, R. H., Corradino, R. A., Carafoli, E., Kretsinger, R. H., MacLennan, D. H., and Siegel, S. L., Eds., *Calcium Binding Proteins and Calcium Function*, Elsevier, New York, pp. 292–302.

79. Wasserman, R. H., Kallfelz, F. A., and Comar, C. L. (1961) *Science*, **133,** 883–884.

80. Wasserman, R. H. and Taylor, A. N. (1966) *Science*, **152,** 791–793.

81. Wasserman, R. H. and Taylor, A. N. (1973) *J. Nutr.*, **103,** 586–599.

82. Wecksler, W. R. and Norman, A. W. (1980) *J. Biol. Chem.*, **255,** 3571–3574.

83. Wilson, T. H. and Wiseman, G. (1954) *J. Physiol.*, **123,** 116–125.

84. Zile, M., Bunge, E. C., Barsness, L., Yamada, S., Schnoes, H. K., and DeLuca, H. F. (1978) *Arch. Biochem. Biophys.*, **186,** 15–24.

PART 3

MEMBRANE TRANSPORT DURING DIFFERENTIATION

CHAPTER 11

COORDINATED CHANGES IN POTASSIUM FLUXES AS EARLY EVENTS IN THE DIFFERENTIATION OF THE HUMAN PROMYELOCYTE LINE HL-60

J. J. GARGUS
Departments of Physiology and Pediatrics
Emory University School of Medicine
Atlanta, Georgia

E. A. ADELBERG
C. W. SLAYMAN
Departments of Human Genetics and Physiology
Yale University School of Medicine
New Haven, Connecticut

As presented in earlier chapters, there is increasingly compelling evidence for the importance of rapid changes in cation transport at the transition from G_0 to S phase of the cell cycle (24, 35, 36). It has long been suspected that mutually exclusive choices open to a G_0 cell are to reenter the cell cycle, replicate its DNA and divide, or to proceed out of G_0 along a path of increasing differentiation with restricted growth potential and the development of specialized functions. It has therefore seemed resonable to ask whether changes in cation flux corresponding to those seen in the transition from G_0 to S phase occur at the transition from G_0 to differentiation. To examine such a question one needs a system that faithfully reproduces the paradigm of differentiation. The model used very fruitfully by many investigators has been the Friend erythroleukemia cell, a virus-transformed mouse cell line that differentiates towards a red blood cell after exposure to dimethyl sulfoxide (DMSO) or any one of a number of other compounds (11, 28, 32).

There are, however, two serious criticisms that have been leveled against this cell as a model of differentiation. First, it fails to respond to the substance that controls differentiation *in vivo*, erythropoietin. Second, the Friend cell represents a precursor at an unknown stage of maturation, perhaps one already beyond the physiologically relevant step of commitment to differentiate, such that some more trivial process is being followed after DMSO induction (28, 32).

1. THE HL-60 MODEL

A newer model system without these difficulties and with several advantages is the human HL-60 leukemic cell line. The cell was isolated by Gallo and coworkers from a patient with promyelocytic leukemia (5, 13), and its characteristics are those of a promyelocyte, a step in the normal path of granulopoiesis (Fig. 11.1A).

HL-60 responds to colony stimulating factor (CSF), which is probably the *in vivo* granulopoietin, the hormone that stimulates proliferation and maturation of granulocyte precursors (21). Fortunately it does not have an absolute requirement for CSF, however, making culture far easier and cheaper. The HL-60 cell is human in origin, meaning to the clinician that it is a model of disease, and, even more important to the physiologist, that its sodium pump is highly ouabain-sensitive, which is a great help if transport systems are to be defined. Finally, like the normal promyelocyte, HL-60 can be directed to differentiate selectively down either of two paths, to neutrophils or to macrophages. It, therefore, cannot be already committed: some physiologically relevant switch is being thrown. This behavior is just like that of the normal promyelocyte which gives rise to neutrophils and macrophages. DMSO is the prototype inducer of differentiation toward the neutrophil in HL-60 (6); phorbol tumor promoters stimulate its differentiation toward the macrophage (18, 37) (Fig. 11.1B; Table 11.1).

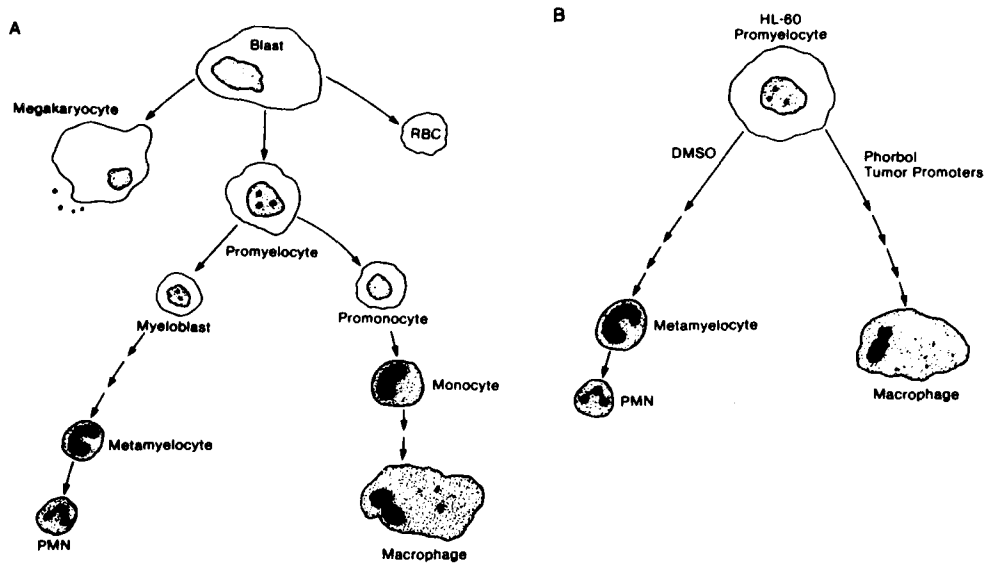

Figure 11.1. (*A*) Stages in myeloid maturation. (*B*) Pathways for HL-60 differentiation.

TABLE 11.1. INDUCERS OF HL-60 DIFFERENTIATION

Pathway	Inducer	Concentration	Reference
Granulocyte			
	DMSO	1.2–1.5%	6
	Dimethylformamide	60 m*M*	6
	Butyric acid	0.6 m*M*	6
	Retinoic acid	1 m*M*	4
	Hypoxanthine	5 m*M*	4
	Thymidine	2 m*M*	43
	Actinomycin D	5 ng/ml	4
	L-ethionine	2 m*M*	30
Macrophage			
	TPA	< 1 n*M*	18, 37, 38
	Phorbol-12,13-didecanoate	1.6 n*M*	18, 37
	Phorbol-12,13-dibenzoate	10 n*M*	37
	Mezerein	10 n*M*	37
	Phorbol-12,13-dibutyrate	10 n*M*	9, 18
	Phorbol-12,13-diacetate	100–1000 n*M*	18, 37

2. INDUCED NEUTROPHIL DIFFERENTIATION

Following exposure of HL-60 cells to DMSO at a concentration between 1.2 and 1.5% (v/v), the cells commence a series of pervasive changes in structure and function. A now quite extensive list of "neutrophil markers" have been found to appear, generally 2–3 days following initial exposure (Table 11.2). The cells look and behave like neutrophils, showing their characteristic morphology (6) and carrying out the functions of migration, chemotaxis, phagocytosis, and bacterial killing (6, 7, 31, 43). New proteins are synthesized, some identified functionally, such as the complement (7, 41, 42) and IgG receptors (34, 41, 42), and others by their new characteristic size on gels (12). There are also changes in metabolic pathways including increased activity of the hexose monophosphate shunt (31, 33), arachadonic acid metabo-

TABLE 11.2. NEUTROPHIL CHARACTERISTICS OF INDUCED HL-60 CELLS

	Reference
Morphology	6
Decreased cell volume	This paper
Loss of growth potential	6, 8, 10, 43
Migration and chemotaxis	7
Phagocytosis	6, 7, 31, 43
Oxidative metabolism	7, 31, 33, 43
Degranulation	31
Bacterial killing	31
Decreased myeloperoxidase activity	6, 33, 45
Increased arachadonic acid synthesis	3
Increased phopholipase and fatty acid cyclo-oxygenase	3
Increased hexose monophosphate shunt activity	31, 33
Increased polyamine synthesis and ornithine decarboxylase activity	19, 25
Increased cytochrome b	33
Increased acid phosphatase	44
Complement receptor	7, 41, 42
IgG receptor	34, 41, 42
Decreased synthesis of cholesterol and phospholipid	8
Hydrophobic cell surface	41, 42
Decreased membrane fluidity	20
New membrane glycoproteins	12
Decreased sodium pump activity	This paper
Decreased passive K^+ permeability	This paper

lism (3), and polyamine metabolism (19, 25), as well as increases in the activity of such enzymes as acid phosphatase (44) and cytochrome b (33). Myeloperoxidase decreases in activity (33, 45), perhaps by a change in isozyme (45). It has yet to be demonstrated that gene expression is being altered during any of these changes, which could all conceivably be at the post-translational level.

3. INDUCED MACROPHAGE DIFFERENTIATION

Following exposure of HL-60 to 12-O-tetradecanoyl-phorbol-13-acetate (TPA) or a number of other phorbol esters, all at submicromolar concentrations, the cells rapidly and progressively take on the characteristics of a macrophage (Table 11.3). In a matter of hours, the cells begin to attach and undergo nuclear condensation (9, 18, 37, 38); DNA synthesis and cell division halt after 1 day of exposure (18, 37). Over the next few days macrophage marker enzymes, such as NADase, acid phosphatase, and nonspecific esterase increase in activity (9, 38) while macrophage functions, such as latex phagocytosis and lysozyme release, develop (38). We do not consider this path of differentiation any further in this chapter.

4. THE UNINDUCED CELL

HL-60 is an immortal cell line which has been carried in culture for more than six years. Its doubling time when grown in αMEM medium (40) with 10% fetal bovine serum at 37°C in a 5% CO_2 atmosphere is 25 h. It is a large, irregularly spherical cell with a mean volume of 925 μm^3. It has a large reticular nucleus, multiple nucleoli, and a thin rim of cytoplasm (Fig. 11.2a). It has a high intracellular K^+ concentration (145 ± 25 mmol/l · cells) and a low intracellular Na^+ concentration (30 ± 16 mmol/l · cells).

TABLE 11.3. MACROPHAGE CHARACTERISTICS OF INDUCED HL-60 CELLS

	Reference
Morphology	18, 37
Attachment	18, 37
Loss of growth potential	18, 37
Phagocytosis of latex beads	38
Lysozyme release	38
Increased activity of NADase	38
Increased activity of acid phosphatase	38
Increased activity of nonspecific esterase	9, 38

AD-A166 003 REGULATION & DEVELOPMENT OF MEMBRANE TRANSPORT PROCESSES(U) MEDICAL UNIV OF SOUTH CAROLINA CHARLESTON J S GRAVES 15 MAY 85 AFOSR-TR-86-0142 3/4

UNCLASSIFIED F/G 6/16 NL

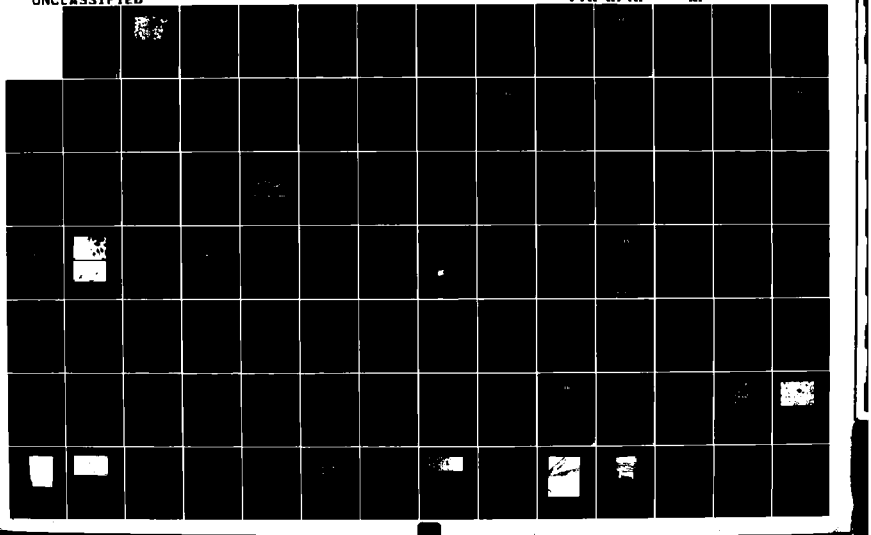

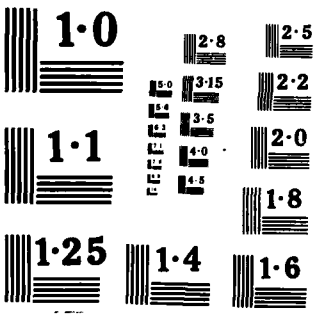
1·0
1·1
1·25
2·8
3·15
3·5
4·0
4·5
5·0
2·5
2·2
2·0
1·8
1·4
1·6

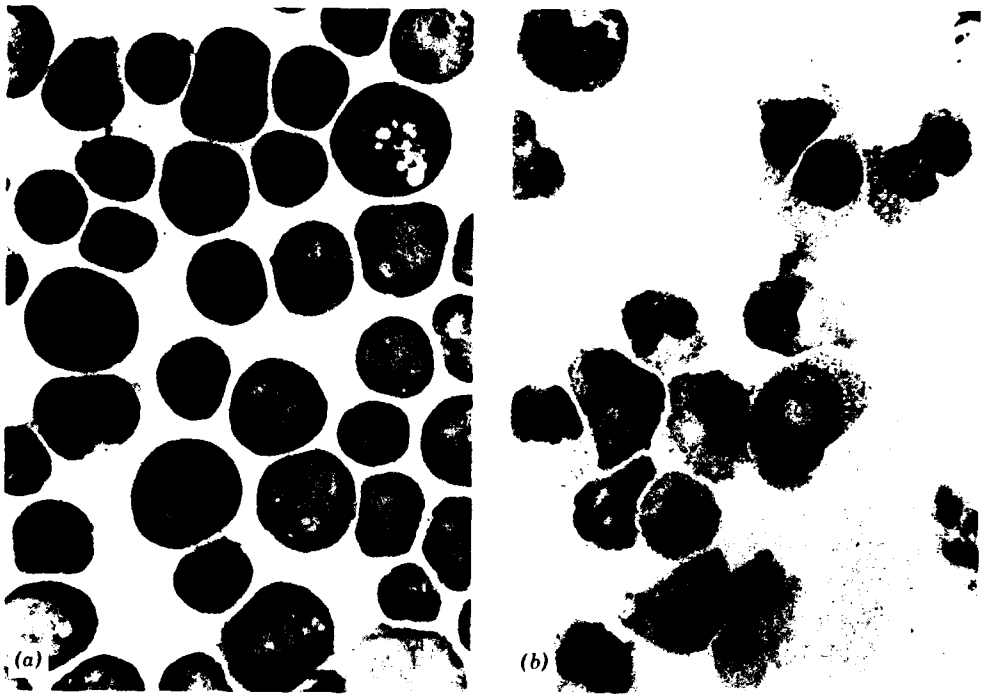

Figure 11.2. HL-60 cells, stained with Wright's stain. (*A*) Uninduced; (*B*) Induced with 1.5% DMSO. (Courtesy of Dr. Edward Benz and Mr. Jay Schneider.)

5. K^+ INFLUX

For influx studies, sodium-loaded cells were obtained by incubating cells in K^+-free medium at 37°C for 2.5 h. $^{42}K^+$ was added to a suspension of these cells at time zero, and uptake was stopped at various times by centrifuging samples in microcentrifuge tubes through a layer of silicone oil into a denser layer of 12% perchloric acid (14, 15). Ouabain inhibited 90% of unidirectional K^+ influx with a K_i of 5×10^{-8} *M* (Fig. 11.3). The ouabain-sensitive component of influx was a saturating function of extracelluar K^+. There was essentially no furosemide-sensitive influx. The ouabain-resistant influx was a linear function of extracellular K^+. Influx data for varied concentrations of K^+ (i.e., '*S*') were fitted to a two-system model of the form

$$v = \frac{V_{max}(S)}{K_{1/2} + S} + D(S)$$

with the use of a Marquardt fitting routine (29) kindly provided by Dr. C. L. Slayman. The parameter estimates for these systems are shown in Table 11.4.

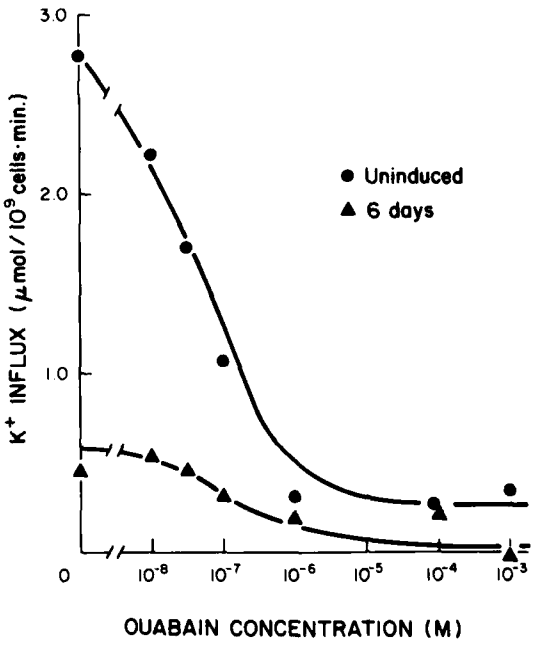

Figure 11.3. Inhibition of unidirectional $^{42}K^+$ influx by ouabain. The initial rate of $^{42}K^+$ uptake was determined at 20 m*M* K^+ in the presence of 0 to 10^{-3} *M* ouabain in cells that had been grown in the presence of 1.5% DMSO for 6 days (▲) and cells never exposed DMSO (●).

In both affinity for extracellular K^+ and ouabain, the ouabain-sensitive component is similar to that reported in a variety of human cells and identified with the activity of the Na^+,K^+-ATPase (1, 16, 23, 27). The linear ouabain-resistant component is consistent with a diffusional pathway.

TABLE 11.4. PROPERTIES OF K^+ TRANSPORT SYSTEMS IN HL-60[a]

	Uninduced Cells	Six-Day Induced Cells
V_{max} of ouabain-sensitive component (μmol $K^+/10^9$ cells per minute)	0.95 ± 0.07	0.09 ± 0.01
$K_{1/2}$ of ouabain-sensitive component for extracellular K^+ (m*M*)	0.85 ± 0.16	1.18 ± 0.41
Diffusional rate constant (D) (μmol $K^+/10^9$ cells per minute per m*M*)	0.003 ± 0.001	0.000 ± .001
Efflux rate constant (per minute)	−0.0127	−0.0033
Calculated efflux (μmol $K^+/10^9$ cells per minute)	1.70	0.30

[a] Influx experiments were performed at 20°C and efflux experiments at 37°C.

6. K^+ EFFLUX

For K^+ efflux studies cells were harvested from growth medium, blotted dry, and then resuspended in prewarmed K^+-free growth medium ($K^+ < 0.01$ m*M*). At intervals, aliquots were removed, centrifuged, briefly resuspended in isotonic choline chloride, and immediately washed free of extracellular fluid as described for influx studies. Intracellular cation contents were then determined by atomic absorption or emission spectroscopy.

K^+ efflux followed single-exponential kinetics (Fig. 11.4), the half-time for K^+ loss being 55 min. As in influx studies, furosemide had no detectable effect.

7. DMSO INDUCTION

The cells respond to DMSO in a highly dose-dependent fashion, 1% (v/v) producing essentially no effect, 2% being rapidly lethal. 1.5% DMSO has proved to be optimal for induction of our line of HL-60. After the addition of DMSO, the cells slowly begin to take on the characteristics of mature granulocytes. They undergo two rounds of cell division at an unaltered rate and

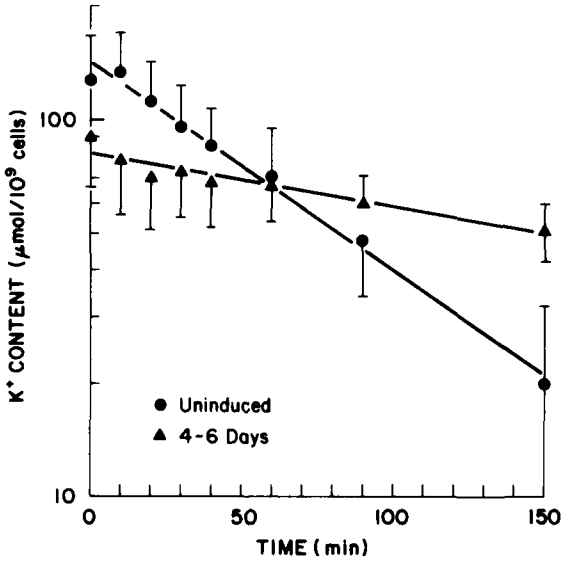

Figure 11.4. Semilogarithmic plot of K^+ efflux from HL-60 cells after 0 and 6 days induction with 1.5% DMSO. Efflux was at 37°C into K^+-free buffer. Data points represent the mean of four experiments for the induced cells, eight experiments for the controls. Lines represent a least squares fit to the points. Correlation coefficient was 0.99 for control, 0.89 for induced. The mean initial K^+ content in these experiments was 0.128 ± 0.039 mmol/10^9 cells for the uninduced cells (●), and 0.091 ± 0.025 mmol/10^9 cells for the induced cells (▲). Rates are presented in Table 11.4.

then halt further division without any impairment in viability. Cell volume is unaltered at 24 h induction, but the cells shrink over the second and third day to a volume of 500 μm^3. By the third day, morphological features of the granulocyte begin to appear, and by the sixth day expression is maximal. The cytoplasm of this small cell is now packed with specifically staining lysosomal granules; the nucleus is small, dense, and lobulated; and nucleoli are absent (Fig. 11.2B). Fully mature segmented polymorphonuclear cells, however, are only rarely produced. Throughout this process of differentiation, in the face of massive volume shifts, the cells maintain a high intracellular K^+ concentration and a low intracellular Na^+ concentration, similar to the concentrations in the uninduced cell (Table 11.5).

8. K^+ TRANSPORT PROPERTIES OF THE MATURE HL-60 CELL

Because of the striking homeostasis found in intracellular cation concentrations, changes in individual transport systems were investigated further. Potassium transport was found to be dramatically reduced in the 6-day in-

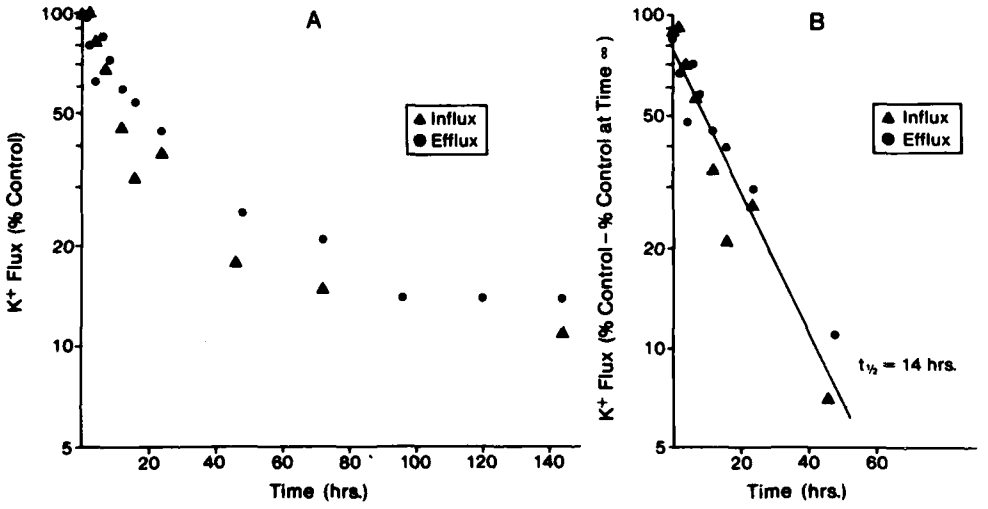

Figure 11.5. Changes in K^+ flux following the addition of DMSO to a culture of HL-60 cells. (*A*) The initial steady-state ouabain-sensitive K^+ influx at 10 m*M* $K\delta$ (▲) and the initial rate of unidirectional K^+ efflux (●), both at 37°C, are given for cells exposed to DMSO for 0 to 144 h. Rates are expressed as percent of the uninduced control and are plotted on a semilogarithmic scale. Influx data were derived from two independent sets of experiments, each covering all time points, and means were plotted. Efflux data were derived from eight independent sets of experiments, each covering the range of time points, and means were plotted. (*B*) Data from (*A*) have been replotted as percent of control flux minus percent of control flux at time infinity. A regression line fitted to the points (correlation coefficient −.95) had a slope of −0.047 h, given a $t_{1/2}$ of 14 h.

TABLE 11.5. INTRACELLULAR CATION CONCENTRATIONS OF HL-60 DURING DMSO-INDUCED DIFFERENTIATION

	Uninduced Cells[a]	Induced Cells[b]
Potassium (mmol/l·cells)	145 ± 25	154 ± 27
Sodium (mmol/l·cells)	30 ± 16	38 ± 8

[a] Uninduced cell values, mean ± 1 S.D., pooled from 11 experiments.

[b] Induced cell values, mean ± S.D., pooled from 37 cultures in 11 experiments, each induced from 0.5 to 6 days.

duced HL-60 cell compared to the uninduced control. The V_{max} of the ouabain-sensitive component of influx was one-ninth that of the control without any change in ouabain sensitivity or K^+ affinity (Fig. 11.3, Table 11.4). The rate constant for K^+ efflux was one-fourth that of the uninduced cell (Fig. 11.4), corresponding to a sixfold reduction in K^+ efflux (Table 11.4). These rates are quite comparable to those measured in peripheral blood neutrophils by Simchowitz et al. (39). Therefore another marker of maturing neutrophil function in HL-60 cells following DMSO induction is the development of a membrane with K^+ transport characteristics similar to those of the normal, mature neutrophil.

9. CHANGES IN K^+ TRANSPORT FOLLOWING INDUCTION OF HL-60

Immediately following the addition of DMSO to a culture of HL-60 cells, transmembrane K^+ fluxes begin to decrease exponentially in a coordinated fashion. In the results presented in Fig. 11.5, the V_{max} of the ouabain-sensitive system and of K^+ efflux fell together with a half-time of 14 h. These changes are among the most rapid occurring after DMSO addition.

10. SPECIFICITY OF K^+ TRANSPORT CHANGES

DMSO, however, does not alter K^+ transport in all cells. $LMTK^-$, a mouse fibroblast line with well characterized K^+ transport activities (14, 15, 22) does not undergo differentiation following DMSO exposure and does not show a reduction in transmembrane K^+ flux (Table 11.6). Another indication of specificity is that all membrane transport systems of HL-60 cells do not change in concert after induction. Glucose and Na^+-independent α-ami-

TABLE 11.6. EFFECTS OF DMSO ON K^+ TRANSPORT IN HL-60 AND LMTK$^-$

	Three-Day Induced Cells[a]	
	HL-60	LMTK$^-$
Rate constant for K^+ efflux (% uninduced control)	21%	117%
Rate of ouabain-sensitive K^+ influx (% uninduced control)	41%	127%

[a] Cells were grown in the presence of 1.5% (v/v) DMSO for 3 days. Efflux measurements were performed as described in the text. The initial rate of influx was determined at 1 m*M* K_o^+. 10^{-3} *M* ouabain was used to inhibit LMTK$^-$; 10^{-4} *M* for HL-60. Results are pooled for two representative experiments.

noisobutyric acid (AIB) transport remain unchanged after DMSO exposure, although Na^+-dependent AIB uptake falls (R. W. Mercer, personal communication). The change in Na^+-dependent AIB transport may be independent or may be a consequence of changes in cation transport (17, 26).

11. MECHANISM OF K^+ TRANSPORT CHANGES

Perhaps the most surprising finding in this study is the absence of a change in intracellular cation concentrations following DMSO induction, in spite of marked changes in unidirectional ion transport rates and net water movement. This implies pump-leak communication of some form more complex than substrate inhibition or activation. Further, it is highly unlikely that a nonspecific change in the state of the membrane could quantitatively alter transport through two such diverse systems as the Na^+/K^+ pump and the passive membrane leak to the same degree by chance alone. The simplest hypothesis is that one system is altered primarily by the inducer, the other adjusting to maintain homeostasis. A consequence of the detected constancy of the intracellular cation milieu is that, if a change in K^+ metabolism serves as a signal for differentiation, it cannot do so by means of the steady-state chemical concentration of potassium.

12. DISCUSSION

The rapid decrease in K^+ fluxes following DMSO addition to HL-60 cells suggests that they may play a causative role in the sequence of further

events leading to granulocytic differentiation. For one event (e.g., A) to be considered causative of another (e.g., B), the following relationships should be demonstrated: (1) event A always precedes event B; (2) events A and B are obligatorily linked: induction of A always leads to B, and blockage of A prevents B. The failure to observe any one of these relationships indicates that event A does not cause event B; observing them, however, does not *prove* a causative role, since events A and B may be independent consequences of a third and unknown event.

Several attempts have been made in the past to demonstrate causative roles for events that occur during HL-60 differentiation. Three of these (increased arachadonic acid and polyamine metabolism and decreasd membrane fluidity) fail the test of prior occurrence and obligate covariance (3, 8, 19, 20, 25). In Friend erythroleukemia cells, however, a decrease in Na^+,K^+-ATPase activity fulfills both criteria listed and is thus a strong candidate for a causative event in differentiation (2, 26).

In HL-60 the rapid decreases in K^+ fluxes (ouabain-sensitive influx, presumably reflecting Na^+,K^+-ATPase activity, and K^+ efflux) fulfill the criterion of prior occurrence relative to other differentiation events. It has not yet been possible to investigate obligatory coupling, however, since ouabain (which induces differentiation in Friend cells) kills HL-60 cells at extremely low concentrations (10^{-7} to 10^{-6} *M*). Even in Friend cells, the successful induction of differentiation by ouabain has generally required the use of ouabain-resistant mutants (2, 26). We have recently isolated ouabain-resistant HL-60 cells and will use them in further attempts to induce granulocytic differentiation with sublethal doses of ouabain. Until such experiments are done, a causative role of K^+ flux changes in HL-60 differentiation must be considered an interesting possibility.

REFERENCES

1. Baker, P. F. and Willis, J. S. (1972) *J. Physiol. (Lond.)*, **224**, 441–462.
2. Bernstein, A. D., Hunt, D. M., Crichley, V., Mak, T. W. (1976) *Cell*, **9**, 375–381.
3. Bonser, R. W., Siegel, M. I., McConnell, R. T., Cuatrecasas, P. (1981) *Biochem. Biophys. Res. Commun.*, **98**, 614–620.
4. Breitman, T. R., Selonick, S. E., Collins, S. J. (1980) *Proc. Natl. Acad. Sci. USA*, **77**, 2936–2940.
5. Collins, S. J., Gallo, R. C., Gallagher, R. E. (1977) *Nature*, **270**, 347–349.
6. Collins, S. J., Ruscetti, F. W., Gallagher, R. E., Gallo, R. C. (1978) *Proc. Natl. Acad. Sci. USA*, **75**, 2458–2462.
7. Collins, S. J., Ruscetti, F. W., Gallagher, R. E., Gallo, R. C. (1979) *J. Exp. Med.*, **149**, 969–974.
8. Cooper, R. A., Ip, S. H. C., Cassileth, P. A., Kuo, A. L. (1981) *Cancer Res.* **41**, 1847–1852.
9. Cooper, R. A., Braunwald, A. D., Kuo, A. L. (1982) *Proc. Natl. Acad. Sci. USA*, **79**, 2865–2869.
10. Fibach, E., Peled, T., Rachmilewitz, E. A. (1982) *J. Cell. Physiol.* **113**, 152–158.

11. Friend, C., Scher, W., Holland, J. G., Sato, T. (1971) *Proc. Natl. Acad. Sci. USA*, **68,** 378–382.
12. Gahmberg, C. G., Nilsson, K., Andersson, L. C. (1979) *Proc. Natl. Acad. Sci. USA*, **76,** 4087–4091.
13. Gallagher, R., Collins, S., Trujillo, J., McCredie, K., Ahearn, M., Tsai, S., Metzgar, R., Aulakh, G., Ting, R., Ruscetti, F., Gallo, R. (1979) *Blood*, **54,** 713–733.
14. Gargus, J. J., Miller, I. L., Slayman, C. W., Adelberg, E. A. (1978) *Proc. Natl. Acad. Sci. USA*, **75,** 5589–5593.
15. Gargus, J. J. and Slayman, C. W. (1980) *J. Membrane Biol.*, **52,** 245–256.
16. Glynn, I. M. and Karlish, S. J. D. (1975) *Ann. Rev. Physiol.*, **37,** 13–55.
17. Graves, J. S. and Wheeler, D. D. (1982) *Am. J. Physiol.*, **243,** C124–C132.
18. Huberman, E. and Callaham, M. F. (1979) *Proc. Natl. Acad. Sci. USA*, **76:**1293–1297.
19. Huberman, E., Weeks, C., Herrmann, A., Callaham, M., Slaga, T. (1981) *Proc. Natl. Acad. Sci. USA*, **78,** 1062–1066.
20. Ip, S. H. C. and Cooper, R. A. (1980) *Blood*, **56,** 227–232.
21. Koeffler, H. P. and Golde, D. W. (1980) *Cancer Res.*, **40,** 1858–1862.
22. Lamb, J. F. and MacKinnon, M. G. A. (1971) *J. Physiol. (Lond.)*, **213,** 665–682.
23. Lamb, J. F. and McCall, D. (1972) *J. Physiol. (Lond.)*, **225,** 559–617.
24. Lopez-Rivas, A., Adelberg, E. A., Rozengurt, E. (1982) *Proc. Natl. Acad. Sci. USA*, **79,** 6275–6279.
25. Luk, G. D., Civin, C. I., Weissman, R. M., Baylin, S. B. (1982) *Science*, **216,** 75–77.
26. Mager, D. and Bernstein, A. (1978) *J. Cell. Physiol.*, **94,** 275–286.
27. Mankovitz, R., Buchwald, M., Baker, R. M. (1974) *Cell*, **3,** 221–226.
28. Marks, P. A. and Rifkind, R. A. (1978) *Ann. Rev. Biochem.*, **47,** 419–448.
29. Marquardt, D. W. (1963) *J. Soc. Ind. Appl. Math*, **11,** 431–441.
30. Mendelsohn, N., Michl, J., Gilbert, H. S., Acs, G., Christman, J. K. (1980) *Cancer Res.*, **40,** 3206–3210.
31. Newburger, P. E., Chovaniec, M. E., Greenberger, J. S., Cohen, H. J. (1979) *J. Cell Biol.*, **82,** 315–322.
32. Reuben, R. C., Rifkind, R. A., Marks, P. A. (1980) *Biochim. Biophys. Acta*, **605,** 325–346.
33. Roberts, P. J., Cross, A. R., Jones, O. T. G., Segal, A. W. (1982) *J. Cell Biol.*, **95,** 720–726.
34. Roberts, P. J., and Pegram, S. M. (1980) in Dierch, M. P., Fust, G., and Turner, M. W., Eds., *The Triggering of Phagocyte Cells*, Medicina Publishing House, Budapest, pp. 281–285.
35. Rozengurt, E. and Heppel, L. A. (1975) *Proc. Natl. Acad. Sci. USA*, **72,** 4492–4495.
36. Rozengurt, E. and Mendoza, S. (1980) *Ann. N.Y. Acad. Sci.*, **339,** 175–189.
37. Rovera, G., O'Brien, T. G., Diamond, L. (1979) *Science*, **204,** 868–870.
38. Rovera, G., Santoli, D., Damsky, C. (1979) *Proc. Natl. Acad. Sci. USA*, **76,** 2779–2783.
39. Simchowitz, L., Spilberg, I., DeWeer, P. (1982) *J. Gen. Physiol.*, **79,** 452–479.
40. Stanners, C. P., Eliceiri, G. L., Green, H. (1971) *Nature New Biol.*, **230,** 52–54.
41. Stendahl, O., Dahlgren, C., Hed, J. (1982) *J. Cell. Physiol.*, **112,** 217–221.
42. Stendahl, O., Dahlgren, C., Hed, J. (1982) *Adv. Exp. Med.*, **141,** 531–537.
43. Tarella, C., Ferrero, D., Gallo, E., Pagliardi, G. L., Ruscetti, F. W. (1982) *Cancer Res.*, **42,** 445–449.
44. Vorbrodt, A., Meo, P., Rovera, G. (1979) *J. Cell Biol.*, **83,** 300–307.
45. Yamada, M., Mori, M., Sugimura, R. (1981) *Biochem. Biophys. Res. Commun.*, **98,** 219–226.

CHAPTER 12

ION FLUXES AND DIFFERENTIATION IN TRANSFORMED CELL LINES

PHILIP M. ROSOFF
LEWIS C. CANTLEY
Department of Biochemistry and Molecular Biology
Harvard University
Cambridge, Massachusetts

Recent research from several laboratories has suggested that changes in ion fluxes across the plasma membrane may act as signals for differentiation and growth regulation (3, 4, 9, 12, 14, 32). A variety of mitogens have been shown to stimulate rapid changes in transmembrane Na^+, H^+, Ca^{2+}, and K^+ fluxes in a number of cultured cell lines. The mechanisms by which these fluxes are stimulated are somewhat unclear and may differ from system to system. For example, quiescent 3T3 fibroblasts exposed to a variety of growth factors show an increase in $[Na^+]_i$ as a result of activation of a membrane electroneutral Na^+/H^+ exchange system.* The rise in $[Na^+]_i$ stimulates the Na^+,K^+-ATPase as indicated by an increase in the ouabain-sensitive $^{86}Rb^+$ uptake. This Na^+/H^+ exchange is sensitive to the diuretic amiloride which can block 3T3 proliferation when present in micro-to-millimolar concentrations (32, 34). This amiloride-sensitive transport system has also been implicated in the growth-factor-stimulated proliferation of mouse soleus muscle (1), frog muscle (25), dog kidney cells (29), neuroblastoma cells (6, 24), Chinese hamster fibroblasts (28), human fibroblasts (22, 31), and probably rat hepatocytes (16). In none of these systems however, has it been possible to show that activation of Na^+/H^+ exchange is sufficient to enhance proliferation or induce differentiation.

A limited number of transformed cell lines are capable of undergoing differentiation in culture. These cell lines provide an opportunity for investigating the role of cation fluxes not only in growth regulation but also in signaling terminal differentiation. In some cell culture systems, ionophores that transport Na^+, H^+, or Ca^{2+} ions can themselves accelerate the differentiation process (18). However, with the exception of certain oocytes in which Ca^{2+} ionophores alone can induce maturation, it has not been conclusively demonstrated that changes in cation fluxes alone are sufficient to signal differentiation.

We have been investigating the role of transmembrane cation fluxes in two established cell lines capable of being stimulated to undergo differentiation in culture: Friend virus-transformed murine erythroleukemia cells (MEL cells) and the chemically transformed pre-B lymphocyte cell line 70Z/3. In this paper we summarize prior studies using these cells and present more recently obtained data.

1. FRIEND ERYTHROLEUKEMIA CELLS

Friend murine erythroleukemia cells (MEL) were initially isolated from the spleens of mice infected with Friend virus, a defective RNA tumor virus. These cells grow continuously in suspension culture. Upon exposure to

* Abbreviations used: LPS, lipopolysaccharide; DMSO, dimethyl sulfoxide; EGTA, ethylene glycol bis(β-aminoethyl ether)-*N,N,N',N'*-tetraacetic acid; $[Na^+]_i$, intracellular Na^+ concentration; MEL, murine erythroleukemia cells; FCCP, carbonyl cyanine, *p*-trifluoromethoxyphenyl hydrazone.

dimethyl sulfoxide (DMSO) or a variety of other agents, these cells undergo terminal erythroid differentiation with loss of cell nuclei and production of hemoglobin (39). Mager and Bernstein previously demonstrated that agents that induce differentiation in MEL cells inhibit the activity of the plasma membrane Na^+,K^+-ATPase thus leading to a decrease in K^+ uptake (21). Indeed, ouabain, a specific inhibitor of this transport mechanism, was able to induce terminal erythropoiesis in a MEL cell line selected for partial ouabain resistance (3). These early observations implied an important role for the Na^+/K^+ pump in differentiation of MEL cells.

Recently, we have observed changes in both Ca^{2+} flux (18) and mitochondrial membrane potential accompanying DMSO induction (19). We have suggested that all of these effects may be secondary to the initial decrease in Na^+/K^+ pump activity. Several observations support this conclusion: (1) treatment of MEL cells with ouabain to inhibit the Na^+,K^+-ATPase raises cellular Na^+ levels and enhances $^{45}Ca^{2+}$ influx into the cells (36); (2) amiloride, an inhibitor of Na^+-H^+ and Na^+–Ca^{2+} exchange prevents the DMSO-stimulated Ca^{2+} influx; and (3) the DMSO-induced decrease in cyanine dye uptake by mitochondria can be blocked by amiloride or EGTA (19). The decrease in dye uptake appears to result from the increased Ca^{2+} flux, which in turn is secondary to the inhibition of the Na^+/K^+ pump. These data suggest very strongly that the initial sequence of events in DMSO-induced MEL cell differentiation includes alterations in the flux rates of both Na^+ and Ca^{2+}. These data do not rule out the possibility, however, that DMSO could be affecting other cation transport systems by mechanisms separate from the effect on the Na^+,K^+-ATPase. The Ca^{2+} flux changes induced by DMSO appear to be essential for differentiation. EGTA blocks DMSO induction at chelator concentrations that still permit cell growth (4). Amiloride also blocks differentiation at concentrations that inhibit the DMSO-stimulated Ca^{2+} influx (18).

Studies with specific ionophores further suggest that cation flux changes are important signals for differentiation in MEL cells. To date, we have been unable to induce terminal erythropoiesis in MEL cells with ionophores alone. However, commitment can be accelerated when these agents are used along with DMSO (4). The kinetics of MEL cell commitment have been well studied by Levenson and Housman (17). A lag period of approximately 12 h occurs between addition of the inducing agent and the appearance of significant percentages of cells capable of erythropoiesis independent of the inducer. Commitment occurs in a stochastic manner after the lag period. The 12-h lag may be eliminated by addition of the Ca^{2+} ionophore A23187 1 h prior to adding DMSO (4); this drug alone does not produce commitment and proves toxic with prolonged treatment. This result suggested that a change in Ca^{2+} flux was a rate-limiting step in MEL cell commitment. However, while this Ca^{2+} influx may be essential for commitment to occur, it is insufficient by itself to induce differentiation. Table 12.1 summarizes these results.

Na^+ ionophores also affect the lag time: ouabain and the carboxylic Na^+/

TABLE 12.1. EFFECTS OF VARIOUS AGENTS ON KINETICS OF FRIEND CELL COMMITMENT TO ERYTHROPOIESIS

Drug[a]	Percent Cells Committed[b] 18 h	50 h	Reference
Control	<5	<5	4, 18, 19, 36
DMSO	<5	60	18
A23187 (1 h)	<5	<5	4
FCCP (1 h)	<5	<5	19
Monensin (4 h)	<5	<5	36
Ouabain (4 h)	<5	<5	36
Ouabain + monensin (4 h)	<5	<5	36
DMSO + A23187 (1 h)	20	60–65	4, 19
DMSO + FCCP (1 h)	18	60–65	19
DMSO + monensin (4 h)	9	60	36
DMSO + ouabain (4 h)	8	59	36
DMSO + ouabain (4 h) + monensin (4 h)	24	70	36
Butyric acid	7	41	20
Butyric acid + A23187 (1 h)	20	60	20
Butyric acid + FCCP (1 h)	18	~55	20
Hypoxanthine	5	45	20
Hypoxanthine + A23187 (1 h)	20	65	20
Hypoxanthine + FCCP (1 h)	21	55	20

[a] All drugs were present for the full 18- or 50-h incubation period unless otherwise indicated in parentheses. Drug concentrations were DMSO, 1.5% (v/v); A23187 1 μg/ml; FCCP, 10 μg/ml; ouabain 150 μ*M*; monensin 5 μg/ml; butyric acid, 1 m*M*; hypoxanthine, 0.5 mg/ml.

[b] Commitment to terminal erythropoiesis was assayed by the plasma clot assay as described by Levenson and Housman (17).

H^+ ionophore monensin together will eliminate the lag when added prior to DMSO. These results would be expected in light of the data that demonstrated that both of these drugs enhance Na^+ and Ca^{2+} influx into MEL cells (36). Interestingly, the time required for inducer to reduce the activity of the Na^+/K^+ pump (measured by ouabain-sensitive $^{86}Rb^+$ uptake) is approximately equal to the lag time of 12 h. Thus the data are consistent with our hypothesis that the rate-limiting event in commitment is a decrease in the activity of the Na^+,K^+-ATPase. The subsequent increase in cellular Na^+ in turn leads to an enhanced Ca^{2+} flux.

Finally, because an inhibition of the Na^+/K^+ pump appears to play a

primary and integral role in differentiating MEL cells, we have examined the mechanism by which DMSO acts on this pump. Yeh, et al (40) demonstrated that the 100,000-dalton catalytic subunit of the Na^+/K^+ pump is phosphorylated by a highly specific, membrane-bound protein kinase in both purified plasma membranes and living MEL cells. At room temperature this kinase catalyzes the addition of approximately three phosphate molecules per 100,000 dalton peptide per 10 min (5). The kinase does not appear to be regulated by Ca^{2+} or cAMP and is not inhibited by either heparin or EGTA. DMSO treatment of MEL cells leads to a decrease in phosphorylation of the pump in parallel with the inhibition in pump activity. The number of copies of the pump is unchanged during the first 20 h after DMSO treatment (41). These data suggest that DMSO acts to change the activity of the Na^+,K^+-ATPase by altering its level of phosphorylation.

2. 70Z/3 CELLS

Agents that stimulate lymphocyte proliferation also cause rapid changes in ion fluxes. Using the T lymphocyte mitogen concanavalin A (con A), Averdunk showed an increase in the plasma membrane fluxes for Na^+, K^+, Mg^{2+}, and Ca^{2+} in mouse thymocytes (2). Con A also increased the permeability of the plasma membrane for Na^+ in human peripheral blood lymphocytes (7, 8, 9) and pig mesenteric lymphocytes (10, 11, 35). In mouse thymocytes, con A stimulation causes a hyperpolarization of the plasma membrane resting potential, which apparently results from the activation of a quinine-sensitive, Ca^{2+}-dependent K^+ channel (10). This hyperpolarization can be mimicked by the Ca^{2+} ionophore A23187. Con A also causes a rise in cytoplasmic Ca^{2+}, activation of a K^+ channel and plasma membrane hyperpolarization when added to pig nodal lymphocytes (11, 13, 23, 38).

A major problem with all of these studies has been the lack of use of cloned, stable, homogenous cell lines. Most of these investigators have utilized normal, fresh, heterogeneous, fully differentiated thymocytes, nodal lymphocytes, or peripheral blood lymphocytes. It has not always been clear what populations of cells undergo changes in ion fluxes and what fraction was being stimulated to proliferate, or whether they were identical. In such systems it is difficult to prove that ion flux changes have an essential role. In addition, these studies have used terminally differentiated cells and thus offer little insight into the role of ion fluxes on the differentiation process. It is important to distinguish between undifferentiated and fully differentiated cells. The latter may only be stimulated to proliferate, whereas the former have the capacity for both growth and forward maturation to a more differentiated phenotype.

70Z/3 is a BDF_1, murine lymphoid tumor line that has been adapted to liquid tissue culture. It was originally isolated from the spleens of mice treated with the carcinogen methyl nitrosourea. It has the phenotype of a

pre-B lymphocyte: the immunoglobulin genes have rearranged and the heavy chain of IgM is synthesized in its cytoplasmic form, but light chain is not produced nor does IgM appear on the cell surface (27). When treated with the polyclonal B cell mitogen, lipopolysaccharide (LPS), or supernatants from mitogen-stimulated, cloned T-helper cell lines, light chain and mature (surface) μ heavy chain are synthesized and inserted into the plasma membrane as IgM (26, 27). This process apparently represents differentiation to a more mature B cell (15). DMSO, butyric acid, and retinoic acid, agents that induce differentiation in other transformed cells lines, have no inducing effects on 70Z/3 cells (26).

70Z/3 cells require continuous exposure to LPS for 24 h to obtain maximum expression of surface IgM. LPS treatment for less than 12 h results in an insignificant percentage of surface Ig-positive cells when the assay is performed 24 h after the initial addition of LPS (30). All of our experiments were performed with an LPS concentration (*E. coli* LPS; Sigma) of 10 μg/ml, as this has been shown to be more than sufficient for maximal induction (26); raising the LPS concentration above 10 μg/ml had no effect on the kinetics of induction. These results are very similar to those seen with DMSO treatment of MEL cells in which there is a 12-h lag period after adding the DMSO before significant number of committed cells appear.

3. INTRACELLULAR Na^+ AND 70Z/3 DIFFERENTIATION

As discussed previously, agents that raise intracellular Na^+ levels also accelerate commitment of MEL cells to terminal erythropoiesis. We therefore wished to determine whether changes in $[Na^+]_i$ played a role in LPS induction of 70Z/3 cells. Ouabain raises $[Na^+]_i$ by specifically inhibiting the plasma membrane Na^+/K^+ pump thereby leading to a decrease in the Na^+ efflux rate and an influx of Na^+ along a concentration gradient. Monensin, a carboxylic ionophore, specifically exchanges Na^+ for H^+ to increase $[Na^+]_i$.

Incubation of 70Z/3 cells with low doses of either monensin or ouabain caused 20–30% of the cells to express surface IgM 24 h later (Table 12.2). When the exposure time was limited to 4 h, cell viability was not affected. When the two drugs were used simultaneously, a synergistic effect was seen. These agents also enhanced the ability of LPS to induce surface IgM expression. Although these data imply that ouabain and monensin mediate their effects on differentiation within the 4-h exposure period, these drugs dissociate slowly from cells and may be affecting cellular Na^+ long after their removal from the culture medium. Failure to induce a higher percentage of cells with ionophore alone may be due to the relative mitotic asynchrony of 70Z/3 cells in culture. The results of these experiments argued that an increase in $[Na^+]_i$ is sufficient for inducing 70Z/3 cells to differentiate (30).

We also showed that LPS increases the cellular Na^+ concentration (30).

TABLE 12.2. 70Z/3 DIFFERENTIATION INDUCED BY OUABAIN AND MONENSIN

Drug[a]	Percent of Cells Positive for Surface IgM at 24 h[b]
Control	1
LPS (4 h)	3–6
LPS (8 h)	8
LPS (24 h)	71–80
Monensin (4 h)	27
Ouabain (4 h)	22
Ouabain + LPS (4 h)	35
Monensin + LPS (4 h)	51
Ouabain + monensin (4 h)	75

[a] Drug concentrations were LPS, 10 μg/ml; monensin 2.5 μg/ml; ouabain 400 μ*M*. When a drug was removed, cells were washed three times in fresh medium (RPMI 1640 made 15% with fetal calf serum) and then resuspended.

[b] Surface IgM expression was assayed 24 h after addition of drug(s) by staining with a fluorescein-conjugated goat antimouse IgM antibody and counting the number of fluorescent cells in a fluorescence microscope (30). A minimum of 500 cells per sample were counted; percentages represent means of three experiments.

The $[Na^+]_i$ increased from approximately 28 mmol/liter cell water to 40 mmol/liter during the 2 h following LPS addition. This increase was blocked by 1 m*M* amiloride. Thus the LPS stimulation of surface IgM expression could also result from an elevation of cellular Na^+.

To further examine the hypothesis that LPS was acting to induce 70Z/3 cell differentiation by increasing Na^+ uptake, we investigated the ability of amiloride to block LPS-induced differentiation. An amiloride concentration of 66 μ*M* was chosen for use in the following experiments; this dose was found to be nontoxic over the 24-h induction period. 70Z/3 cells were exposed to 66 μ*M* amiloride for varying periods of time up to 24 h, with LPS present for the whole induction period, after which we tested for expression of surface IgM. Amiloride was ineffective unless added within 8 h after the LPS addition (data not presented). Nearly 100% protection was observed when amiloride was present for the full 24 h (Table 12.3). The fact that monensin overcomes the amiloride block of 70Z/3 cell differentiation (Table 12.3) further indicates that amiloride is acting by inhibiting a Na^+/H^+ exchange system.

We also investigated the concentration dependence of amiloride's effects on Na^+ uptake. When 70Z/3 cells were cultured with 66 μ*M* amiloride for 16

TABLE 12.3. 70Z/3 DIFFERENTIATION BLOCKED BY AMILORIDE

Drug[a]	Percent of Cells Positive for Surface IgM at 24 h[b]
Control	1–2
LPS (24 h)	80
LPS + amiloride (24 h)	2.5
LPS + amiloride + monensin[c]	83

[a] Drug concentrations were LPS, 10 μg/ml; amiloride, 66 μM; monensin, 2.5 μg/ml.

[b] Surface IgM expressed assayed 24 h after addition of drug(s) by staining with fluorescein-conjugated goat antimouse IgM (30). Cells were counted for surface fluorescein in a Zeiss fluorescence microscope. Percentages represent means of three experiments.

[c] Amiloride and LPS added at $t = 0$ h with monensin added at hour 4 of the 24-h incubation period to give adequate time for amiloride to be taken up by the cells (see text and ref. 36).

h at 37°C, the ability of LPS to raise $[Na^+]_i$ was almost completely blocked. However, when amiloride was not preincubated, but added with the LPS, inhibition was not observed until the amiloride concentration reached 400 μM, with a maximum effect at approximately 1.75 mM ($K_I \sim 0.8$ mM) in the presence of 145 mM extracellular Na^+. These results indicate that amiloride may inhibit Na^+ influx from inside the cell.

Amiloride is slowly concentrated into dividing cells in culture: in MEL cells incubated with 40 μM amiloride, the cellular concentration is 1 mM after 4 h at 37°C (36). In 70Z/3 cells a similar time course for uptake is seen (Fig. 12.1). A reasonable explanation for the ability of amiloride to inhibit LPS-induced Na^+ transport almost immediately at high concentrations and in a time-dependent way at low concentrations is that it is capable of blocking the Na^+ influx from both sides of the plasma membrane.

The foregoing experiments indicate that LPS raises the cellular Na^+ by activating entry through an amiloride-sensitive uptake system rather than by inhibiting efflux. To examine this further, we determined the activity of the Na^+/K^+ pump at various times after addition of LPS to 70Z/3 cells. The activity of the pump, as measured by ouabain-sensitive $^{86}Rb^+$ uptake, was increased by approximately 50% (data not shown). This result confirms that LPS is activating a ouabain-resistant Na^+ uptake system; the increase in $[Na^+]_i$ resulting from LPS treatment apparently causes substrate activation of the Na^+/K^+ pump. We also investigated the net rate of Na^+ uptake into 70Z/3 cells in the presence of ouabain to inhibit Na^+ efflux. LPS causes a 20–30% increase in the rate of uptake (Fig. 12.2). 1 mM amiloride was capable of completely blocking this LPS effect.

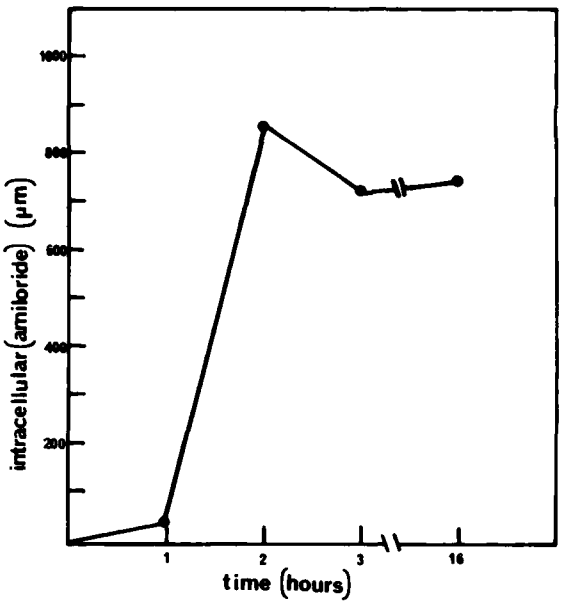

Figure 12.1. Uptake of amiloride by 70Z/3 cells. 70Z/3 cells were incubated at 37°C, in RPMI 1640 medium made 15% in fetal calf serum and 66 μM with amiloride. At the indicated times 1×10^6 cells were removed, washed three times with ice-cold phosphate-buffered saline (PBS). Fluorescence intensity spectra were measured in an Aminco spectrofluorometer with excitation at 300–400 nm and emission determined at 410 nm. These were compared with a standard calibration curve for a range of amiloride concentrations in the SDS/PBS buffer to obtain the intracellular [amiloride].

As mentioned at the beginning of the chapter, several investigators have implicated an amiloride–sensitive Na^+/H^+ antiport as responsible for Na^+ influx following growth-factor stimulation of quiescent cells. We have data suggesting a similar mechanism for the LPS-induced rise in $[Na^+]_i$ in 70Z/3 cells. Using the pH-sensitive fluorescent dye 6-carboxy-fluorescein (37), we have been able to demonstrate a small, but significant increase in pH_i following addition of LPS to 70Z/3 cells at 37°C. This cytoplasmic alkalinization is detectable after 2-min exposure to the mitogen. A concentration of 1 mM amiloride appears to be capable of blocking the rise of pH_i. These data would suggest that LPS activates an amiloride–sensitive Na^+/H^+ exchange mechanism thereby leading to both an increase in $[Na^+]_i$ and pH_i (42).

4. CONCLUSIONS

In both the chemically transformed 70Z/3 pre-B lymphocyte cell line and the Friend virus murine erythroleukemia cells, agents that induce differentiation do so by increasing the cellular Na^+ level. In MEL cells this is accomplished by an inhibition of the Na^+/K^+ pump leading to a decreased rate of Na^+ efflux. In 70Z/3 cells LPS activates an amiloride-sensitive Na^+ channel,

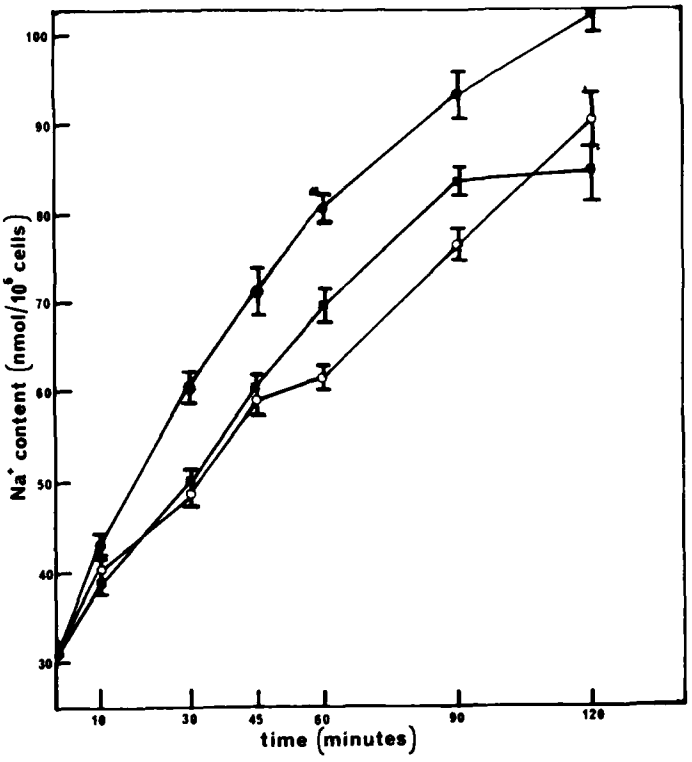

Figure 12.2. LPS induces Na^+ uptake by 70Z/3 cells by an amiloride-sensitive, ouabain-resistant mechanism. 70Z/3 cells were suspended at 2×10^6 cells per milliliter in RPMI 1640 medium made 15% in FCS and incubated at 37°C after equilibration with trace $^{22}NaCl$ for 15 min. Amiloride (1 m*M*) was added 15 min before the $^{22}Na^+$; LPS (10 μg/ml) and ouabain (1 m*M*) were added at $t = 0$. At the indicated times 0.5-ml aliquots ($= 1 \times 10^6$ cells) were removed and centrifuged through 1 : 1 dinonyl phthalate:silicone oil (v/v) and ice-cold Ringer's solution, and radioactivity was determined in the pellet.[30,36] Results are expressed as nanomoles of $Na^+/10^6$ cells. Data points represent means ± standard deviation on quadruplicate experiments. ●—● LPS + ouabain; ■—■ ouabain alone; ○—○ LPS + ouabain + amiloride.

and this channel may be a Na^+/H^+ antiport. In MEL cells Na^+ and Ca^{2+} ionophores accelerate DMSO-induced differentiation but by themselves do not induce commitment. However, in 70Z/3 cells both monensin and ouabain are capable of independently and synergistically inducing surface IgM expression. In both cell lines, an increase in $[Na^+]_i$ appears to be a critical, rate-limiting step for differentiation to proceed.

ACKNOWLEDGMENTS

This research was supported by a National Institutes of Health Grant GM28538. Lewis C. Cantley is an Established Investigator of the American Heart Association. Philip M. Rosoff was supported by Public Health Service Training Grant CA09172-08 awarded to the Dana-Farber Cancer Institute.

Division of Pediatric Oncology, Department of Pediatrics, Harvard Medical School, Boston, Massachusetts and a fellowship from the David Abraham Foundation. The authors wish to thank I. Macara, L. A. Yeh, L. Ling, and J. Schulz for many helpful discussions and critical comments.

REFERENCES

1. Aickin, C. and R. C. Thomas (1977) *J. Physiol. (Lond.)*, **273,** 295–316.
2. Averdunk, R. (1976) *Biochem. Biophys. Res. Comm.* **70,** 101–109.
3. Bernstein, A., Hunt, V., Crichley, V., and Mak, T. W. (1976) *Cell*, **9,** 375–391.
4. Bridges, K., Levenson, R., Housman, D., and Cantley, L. (1981) *J. Cell Biol.*, **90,** 542–544.
5. Cantley, L., Yeh, L.-A., Ling, L., Schulz, J., and English, L. (1983) in Palmieri, F., Ed., *Structure and Function of Membrane Proteins*, Elsevier-North Holland Biochemical Press, Amsterdam.
6. Deutsch, C., Erecinska, M., Werrlein, R., and Silver, I. A. (1979) *Proc. Natl. Acad. Sci. USA*, **76,** 2175–2179.
7. Deutsch, C. and M. A. Price (1982) *Biochim. Biophys. Acta*, **687,** 211–218.
8. Deutsch, C. and M. Price (1982) *J. Cell Phys.*, **113,** 73–79.
9. Deutsch, C., Price, M. A., and C. Johansson (1981) *Exp. Cell Res.*, **136,** 359–369.
10. Felber, S. M. and Brand, M. D. (1983) *Biochem. J.*, **210,** 885–891.
11. Felber, S. M. and Brand, M. D. (1983) *Biochem. J.*, **210,** 893–897.
12. Hesketh, T. R., Smith, G. A., Houslay, G. B., Warren, G. B. and Metcalfe, J. C. (1977) *Nature*, **267,** 490–494.
13. Hesketh, T. R., Smith, G. A., Moore, J. P., Taylor, M. V., and Metcalfe, J. C. (1983) *J. Biol. Chem.*, **258,** 4875–4882.
14. Jaffe, L. F. (1980) *Ann. New York Acad. Sci.*, **399,** 86–101.
15. Kincaide, P. W. (1981) *Adv. Immunol.*, **31,** 177–245.
16. Koch, K. S. and Leppert, H. L. (1979) *Cell*, **18,** 153–163.
17. Levenson, R. and Housman, D. (1979) *Cell*, **17,** 485–490.
18. Levenson, R. L., Housman, D., and Cantley, L. (1980) *Proc. Natl. Acad. Sci. USA*, **77,** 5948–5952.
19. Levenson, R., Macara, I. G., Smith, R. L., Cantley, L., and Housman, D. (1982) *Cell*, **28,** 855–863.
20. Levenson, R., Macara, I., Cantley, L., and Housman, D. (1983) *J. Cell Biochem.*, **21,** 1–8.
21. Mager, D. and Bernstein, A. (1978) *J. Cell. Physiol.*, **94,** 275–286.
22. Mendoza, S. A., Wigglesworth, N. M., Pohjanpelto, P., and Rozengurt, E. (1980) *J. Cell. Physiol.*, **103,** 17–27.
23. Metcalfe, J. C., Pozzan, T., Smith, G. A., and Hesketh, T. R. (1980) *Biochem. Soc. Symp.*, **45,** 1–26.
24. Moolenaar, W., Boonstra, J., Van der Saag, P., and DeLaat, S. (1981) *J. Biol. Chem.*, **256,** 12883–12887.
25. Moore, R. D. (1981) *J. Biophys.*, **33,** 203–210.
26. Paige, C. J., Kincade, P. W., and Ralph, P. (1978) *J. Immunol.*, **121,** 641–647.
27. Paige, C. J., Schreier, M. H., and Sidman, C. L. (1982) *Proc. Natl. Acad. Sci. USA*, **79,** 4756–4760.

28. Pouysségur, J., Jacques, Y., and Lazdunski, M. (1980) *Nature*, **286,** 162–164.
29. Rindler, M., Jaub, M., and Sauer, M. (1979) *J. Biol. Chem.*, **254,** 11431–11439.
30. Rosoff, P. M. and Cantley, L. C. (1983) *Proc. Natl. Acad. Sci. USA*, **80:**7547–7550.
31. Rothenburg, P., Glaser, L., Schlesinger, P., and Cassel, D. (1983) *J. Biol. Chem.*, **258,** 4883–4889.
32. Rozengurt, S. (1981) *Adv. Enzyme Reg.*, (Weber, G., Ed.) **19,** 61–85.
33. Rozengurt, E., Gelehrier, D., Legg, A., and Pettican, D. (1981) *Cell*, **23,** 781–788.
34. Schuldiner, S. and Rozengurt, E. (1982) *Proc. Natl. Acad. Sci. USA*, **79,** 7778–7782.
35. Segal, G. B., Simon, W., and Lightman, M. A. (1979) *J. Clin. Invest.*, **64,** 834–841.
36. Smith, R. L., Macara, I. G., Levenson, R., Housman, D., and Cantley, L. (1982) *J. Biol. Chem.*, **257,** 773–780.
37. Thomas, J. A., Buchsbaum, R. N., Zimniak, A., and Racker, E. (1979) *Biochem.*, **18,** 2210–2218.
38. Tsein, R. Y., Pozzan, T., and Rink, T. J. (1982) *Nature*, **295,** 68–71.
39. Volloch, V. and Housman, D. (1982) *J. Cell Biol.*, **93,** 390–394.
40. Yeh, L. A., Ling, L., English, L., and Cantley, L. (1983) *J. Biol. Chem.*, **258,** 6567–6574.
41. Yeh, L. A., Macara, I. G., and Cantley, L. C., manuscript in preparation.
42. Rosoff, P. M., Stein, L. F., and Cantley, L. C. (1984), *J. Biol. Chem.* **259,** 7056–7060.

CHAPTER 13

GLUCOSE AND CATION TRANSPORT DURING *in Vitro* ADIPOCYTE DIFFERENTIATION

MARILYN D. RESH
GUIDO GUIDOTTI
Department of Biochemistry and Molecular Biology
Harvard University
Cambridge, Massachusetts

Cells of the 3T3-L1 line isolated by Green (1) have the ability to undergo *in vitro* differentiation from a fibroblastlike appearance into adipocytes and to acquire the biochemical characteristics of mature fat cells (2).

This circumstance allowed us to compare the rates of transport of glucose (deoxyglucose) and of Na^+/K^+ (Rb^+) between cells in different stages of development. The results are shown in Fig. 13.1 for deoxyglucose transport and in Fig. 13.2 for Rb^+ transport (3).

The unfilled bars in Fig. 13.1*A* and *B* show that the rate of deoxyglucose transport drops dramatically as cells become confluent (day 0) and then continues to drop as the cells are maintained in the confluent state (up to day 7). In the induced cells, the rate of glucose transport at day 7 is even lower than in the noninduced cells. The filled bars represent the insulin-stimulated deoxyglucose transport rate. According to the results of Karnieli et al. (4) and Kono et al. (5) these rates are an approximation of the total glucose transport capacity of the cell. It is striking that although the total (insulin-

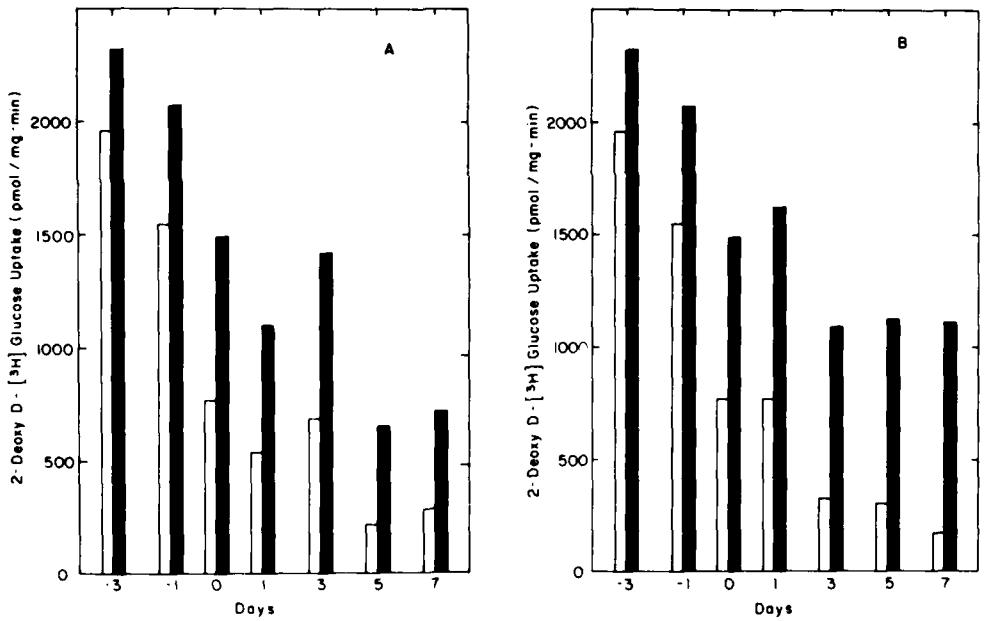

Figure 13.1. Rate of transport of deoxyglucose by 3T3-L1 cells at different stages of growth and differentiation. 3T3-L1 cells were plated at low density (day −7), and transport activity was monitored as described. Cells were approximately 70% confluent on day −3, 90–95% confluent on day −1, and confluent on day 0. Uninduced cells were maintained in standard medium containing 10% fetal bovine serum; induced cells were treated identically, except for treatment with MIX/DEX on days 1 and 2. Cells were fed on days −5, −2, 1, 3, and 5; all transport assays were performed at least 12 h after refeeding with fresh media. (*A*), uninduced 3T3-L1 cells; (*B*) induced 3T3-L1 cells. The data for days −3, −1, and 0 are the same for (*A*) and (*B*) and are presented in duplicate to facilitate comparison. The transport data are the average of triplicate determinations; the mean standard deviation was 10–15% during days −3 to −1 and less than 10% during Days 0 to 7. Unfilled bars, basal rate of uptake; filled bars, uptake rate in the presence of 1.6 μM insulin.

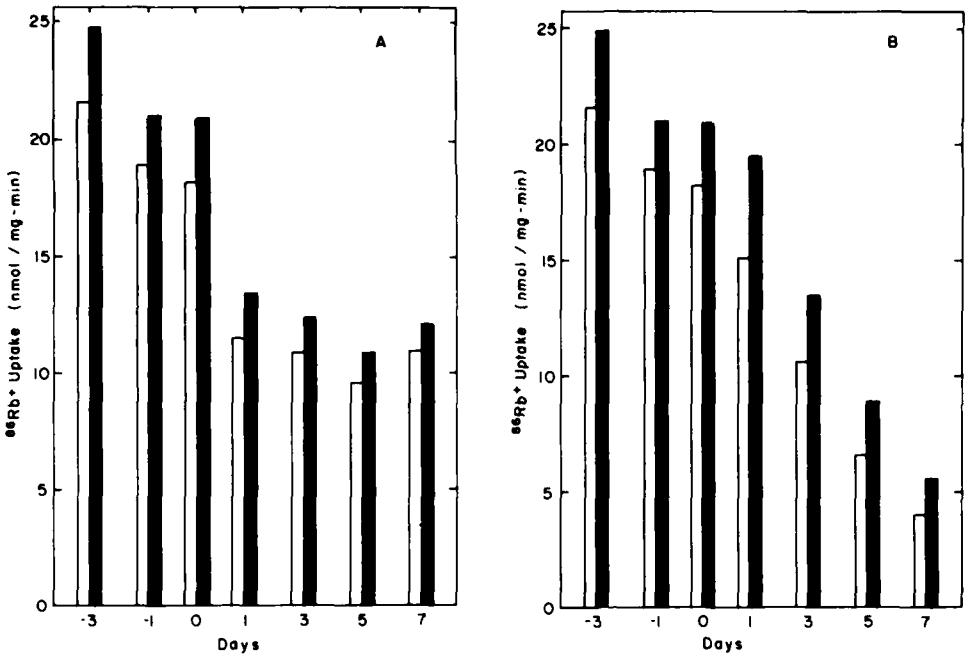

Figure 13.2. Rate of transport of Rb^+ by 3T3-L1 cells at different stages of growth and differentiation. The experiment was the same as that depicted in Fig. 13.1. Values presented are the average of triplicate determinations; the mean standard deviation was approximately 10% during days −3 to −1, and less than 5% during days 0 to 7. (*A*) uninduced 3T3-L1 cells; (*B*) induced 3T3-L1 cells. Data for days −3, −1, and 0 are the same in (*A*) and (*B*). Unfilled bars, basal rate; filled bars, rate in the presence of 1.6 μM insulin.

stimulated) deoxyglucose transport capacity also decreases as the cells reach confluence, the decrease subsequent to confluence is more pronounced for uninduced cells than for induced cells. Consequently, at day 7 after induction, the following situation exists: induced cells have a larger total glucose transport capacity than uninduced cells, but in the basal state a smaller number of transporters are in the plasma membrane of the induced cells as compared to the uninduced cells.

Figure 13.2 shows the effects of growth and differentiation on Rb^+ transport by the 3T3-L1 cells. In both uninduced and induced cells the rate of Rb^+ transport is lower in cells that are maintained at confluence than in growing cells; however, the decrease is greater for induced cells than for noninduced cells.

In contrast to the difference in the rate of Rb^+ transport between induced and uninduced cells at day 7, the number of phosphorylation sites (Na^+/K^+ pumps) is the same in the induced and the uninduced cells (3). The simplest conclusion is that the Na^+,K^+-ATPase in the adipocytes is inhibited in some fashion as compared to the enzyme in fibroblasts.

This conclusion is supported by evaluation of the number and activity of the Na^+,K^+-ATPase in the rat adipocyte plasma membrane (Table 13.1).

TABLE 13.1. RAT ADIPOCYTE Na^+,K^+-ATPase

	Cells	Plasma Membrane
Na^+ pump sites[a]	6×10^5/cell	6×10^{12}/mg
Na^+,K^+-ATPase activity[b]	1×10^9/cell/min	8.4×10^{16}/mg/min
Turnover number for ATP[c]	1.7×10^3/site/min	1.4×10^4/site/min
Efficiency[d]	12%	100%

[a] The number of Na^+ pump sites was determined from the data in ref. 6 and was calculated for cells assuming 100×10^{-9} mg of membrane protein per cell.
[b] Activity was determined from the data in ref. 6 for membranes and was calculated for cells using the V_{max} of Rb^+ transport determined in ref. 7 and assuming 2 Rb^+ (K^+) transported per ATP hydrolyzed.
[c] Turnover number = Na^+,K^+-ATPase activity/Na^+ pump sites.
[d] Efficiency is expressed as percent maximal turnover number.

The data indicate that there are 600,000 pump sites per cell and that their activity is 12% of the maximal activity possible. Thus the adipocyte, as in the muscle cell (8), has a reservoir of pump site activity which can be brought into action.

Since insulin has been shown to increase the activity of the Na^+,K^+-ATPase in the adipocyte (7) and in the muscle cell (9), we wondered whether this activation was caused by an increase in activity of the Na^+/K^+ pumps already in the membrane (see Table 13.1) or by recruitment of additional pumps from a nonplasma membrane pool [as in the situation with the glucose transporter (4, 5)].

The latter possibility was especially appealing because there is a great similarity in the way insulin causes activation of glucose transport and of Rb^+ transport in the adipocyte. In particular, the stimulations of deoxyglucose and Rb^+ uptake have the same dependence on insulin concentration (3), the same lag time and temperature dependence of the lag time (10), parallel responses to substances that mimick the insulin effect, and the same tissue distribution (11).

Nevertheless, there is no change in the number of Na^+,K^+-ATPase molecules in the plasma membrane as a consequence of insulin stimulation, or is there a measurable pool of enzyme in membranes other than the plasma membrane (6).

One must conclude, therefore, that insulin activation of the Na^+,K^+-ATPase in the adipocyte must take place by a change in activity of the enzyme already in the plasma membrane. Since the enzyme is only operating at 12% of its maximal activity before insulin stimulation, a doubling of the activity by insulin would result in an increase to 24% of the maximal enzymatic activity. The mechanism of this activation is not clear at this time.

REFERENCES

1. Green, H. and Kehinde, O. (1976) *Cell*, **7**, 105–113.
2. Green, H. (1978) in Ahmad, F., Schultz, J., Russel, T. R., and Werner, R., Eds., *Tenth Miami Winter Symposium on Differentiation and Development*, Academic, New York, pp. 13–33.
3. Resh, M. D. (1982) *J. Biol. Chem.*, **257**, 6978–6986.
4. Karnieli, E., Zarnowski, M. J., Hissin, P. J., Simpson, I. A., Salans, L. B., and Cushman, S. W. (1981) *J. Biol. Chem.*, **256**, 4772–4777.
5. Kono, T., Robinson, F. W., Blevins, T. L., and Evans, O. (1982) *J. Biol. Chem.*, **257**, 10942–10947.
6. Resh, M. D. (1982) *J. Biol. Chem.*, **257**, 11946–11952.
7. Resh, M. D., Nemenoff, R. A., and Guidotti, G. (1980) *J. Biol. Chem.*, **255**, 10938–10945.
8. Clausen, T. and Hansen, O. (1974) *Biochim. Biophys. Acta*, **345**, 387–404.
9. Clausen, T. and Kohn, P. G. (1977) *J. Physiol.*, **265**, 19–42.
10. Resh, M. D. (1983) *Biochemistry*, **22**, 2781–2784.
11. Resh, M. D. (1982) Ph.D. Thesis, Harvard University, Cambridge, Massachusetts.

CHAPTER 14

DEVELOPMENTAL ASPECTS OF SODIUM-DEPENDENT TRANSPORT PROCESSES OF PREIMPLANTATION RABBIT EMBRYOS

DALE J. BENOS
JOHN D. BIGGERS
Department of Physiology and Biophysics
Laboratory of Human Reproduction and Reproductive Biology
Harvard Medical School
Boston, Massachusetts

ROBERT S. BALABAN
Laboratory of Kidney and Electrolyte Metabolism
National Institutes of Health
Bethesda, Maryland

JOHN W. MILLS
Department of Anatomy
Dartmouth Medical School
Hanover, New Hampshire

ERIC W. OVERSTRÖM
Department of Anatomy and Cellular Biology
Tufts University Schools of Medicine
Boston, Massachusetts

Implantation is a process that involves initially the interaction of two epithelia: the maternal endometrium and the trophectoderm of the blastocyst. The establishment of contact between these epithelia is called adhesion. Prior to adhesion, the blastocyst lies free in the uterine fluid and exchanges occur between this fluid and the embryo. Apposition of these epithelia is brought about in part by expansion of the blastocyst and removal of the uterine fluid. Once the uterine fluid compartment is eliminated, the embryo exchanges material directly with maternal tissue. Thus the pathways of exchange between the blastocyst and mother change radically as a result of adhesion. For some time, our laboratory has been studying the physiological processes involved in solute and fluid transport by the epithelium of the mammalian blastocyst, and in this chapter we summarize some of our more recent findings.

Because the blastocyst is a developing system, it is subject to two types of change. One type is reversible and is concerned with maintenance of homeostatic functions. An example of this type of change is the nature of the coupling of metabolism with the magnitude of the transport processes involved in its growth. The second type of change is irreversible. These changes are features of a developing system responding to the sequential reading of its genome. An example of this may be the biphasic increase in the number of ouabain-binding sites (Na^+,K^+-ATPase) in the rabbit between days 4 and 7 after fertilization (5).

An analysis of blastocyst function, however, is much more complicated than describing these reversible and irreversible changes in the most convenient animal model system, for at least two reasons. First, two very different types of blastocyst have appeared during mammalian evolution. One is the maximally-expanding blastocyst, typified by the rabbit, whose volume increases by several orders of magnitude during the preadhesion period. The other is the minimally expanding blastocyst, typified by the mouse, whose volume increases by less than one order of magnitude. The limited information on the human blastocyst suggests it expands minimally. Second, although the blastocyst develops primarily under the control of the genetic information inherited, it may also need maternal signals at critical stages. The classical illustration of this possibility is the phenomenon of delayed implantation or embryonic diapause. In the mouse or rat, for example, the blastocyst will remain developmentally arrested until it receives an estrogenic signal. Similarly, it is known that specific proteins may appear in the uterine fluids around the time of implantation. The most well-known example is uteroglobin (often called blastokinin) in the rabbit (see ref. 3 for a review).

This chapter initially summarizes some important work on the transport of ions and nutrients across the wall of the blastocyst. We focus on our recent experiments addressing the problem of the molecular basis of solute transport in preimplantation rabbit blastocysts. Our discussion is divided into three main headings: (1) a description of the time-dependent changes in

Na^+-dependent solute transport mechanisms; (2) the relationship between oxidative metabolism and active Na^+ transport; and (3) an analysis of protein synthetic patterns at different stages of preimplantation development.

1. DEVELOPMENTAL CHANGES IN Na^+-DEPENDENT TRANSPORT SYSTEMS

Up to the morula stage the individual cells (blastomeres) of the embryo are only in loose contact with one another and are held in close proximity by an acellular glycoprotein matrix, the zona pellucida. Each cell is completely surrounded by uterine fluid, that is, no extracellular fluid is present. Eventually (3–3.5 days postfertilization in the rabbit) the morula undergoes a transformation characterized by a loss of visual identity of the boundaries of the outer cells. This process is called compaction (27). Morphological studies of compaction have established that the cells occupying the periphery of the morula form tight junctions (14, 19, 23, 24, 34). As a result, the embryo becomes enclosed by a simple squamous epithelium, the trophectoderm, which establishes an outer permeability seal that separates the inner regions of the embryo from its uterine microenvironment (see Fig. 14.1 for a schematic representation of the blastocyst).

There is considerable evidence in the literature that blastocoele fluid has a unique composition (see ref. 28 for a review). Borland, Biggers, and Lechene (12,13) have used electron-probe microanalysis to study the elemental composition of rabbit blastocoele fluid at different developmental stages. They found that the blastocoelic $[Na^+]$, $[K^+]$, and $[Ca^{2+}]$ averaged 140 m*M*, 9.6 m*M* and 1.3 m*M*, respectively, in the six-day postcoitum (p.c.) blastocyst. Unfortunately, it is experimentally difficult to obtain even picoliter uterine fluid samples for analysis because of the paucity of fluid in the uterus around the time of implantation. However, an earlier ion-selective microelectrode study by Petzoldt (32) found concentrations of 70 m*M*, 17 m*M*, and 5 m*M* for Na^+, K^+, Ca^{2+}, respectively, in the uterine fluid of pregnant rabbits six days p.c. Thus a high $[Na^+]$ is maintained in the blastocoele fluid (140 m*M* versus 70 m*M*) relative to uterine fluid. Conversely, much lower $[K^+]$ and $[Ca^{2+}]$ are present in blastocoele fluid as compared to the surrounding uterine fluid environment.

Functionally, the paradigm for understanding the transepithelial movement of ions, particularly Na^+, is the Koefoed–Johnson–Ussing model (Fig. 14.1). Na^+ enters the cell from the uterine or apical membrane side down its electrochemical potential energy gradient, and is then actively transported out of the cells into the blastocoelic cavity by a Na^+ pump. This pump is comprised of the ubiquitous enzyme Na^+,K^+-activated adenosine triphosphatase (ATPase) and is sensitive to inhibition by the drug ouabain. Although intracellular Na^+ activities have not been measured in mammalian blastocyst tissues, we know that tranepithelial Na^+ transport is active be-

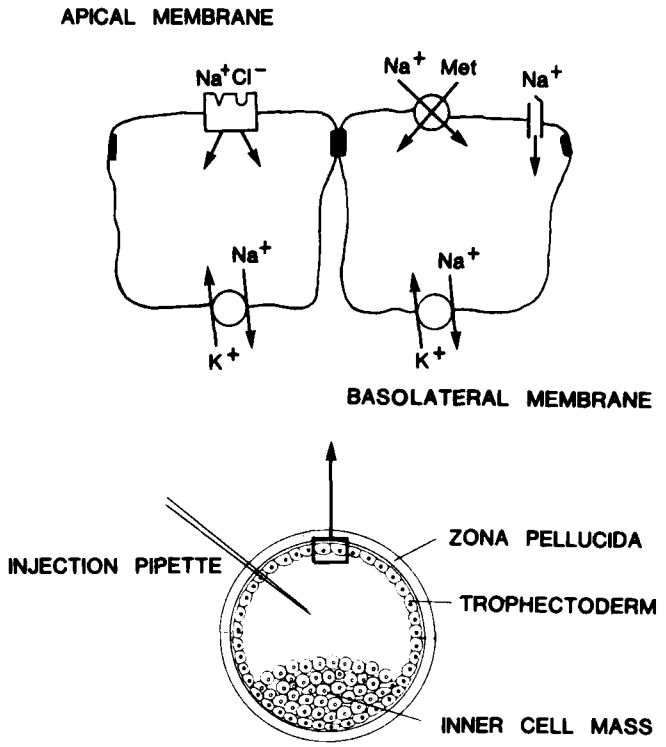

Figure 14.1. Summary of the properties of late (day 6–7 p.c.) preimplantation rabbit blastocyst trophectodermal epithelium with respect to Na , Cl , and methionine transport. Also illustrated is a diagramatic representation of the rabbit blastocyst in cross-section. The apical membrane faces the uterine microenvironment.

cause of the following observations: (1) net movement of Na^+ into the blastocoele occurs against a gradient of electrochemical potential energy; and (2) both unidirectional and net transepithelial Na^+ influx is abolished either by ouabain or cyanide (8).

Previous results from our laboratory have shown that the rabbit blastocyst undergoes enormous developmental changes pertinent to solute transport during its preimplantation period. These changes include:

1. The number of ouabain-binding sites Na^+,K^+-ATPase of the rabbit blastocyst increases with development in a biphasic fashion during this period (Fig. 14.2*a*).
2. The demonstration that the rabbit trophectoderm, in addition to changes in its fluid transporting function, alters its solute-transporting characteristics during preimplantation development in the following ways:

   a. The acquisition of an amiloride-sensitive component to transepithelial Na^+ influx between days 6 and 7 p.c.

b. The acquisition of a phloretin-sensitive component to transepithelial urea influx between days 6 and 7 p.c.

c. The acquisition of a furosemide-sensitive, NaCl cotransport system between days 5 and 6 p.c.

d. The loss of a Na^+-dependent methionine uptake system between days 6 and 7 p.c.

e. The conversion of the trophectoderm from a very low electrical resistance epithelium to a high-resistance epithelium between 4 and 6 days p.c.

1.1. Ouabain-Binding Studies

The total number of ouabain-binding sites as well as the ouabain-sensitive component of the Na^+ influx has been determined for different-aged, preimplantation rabbit blastocysts (5). The number of molecules bound increases about 50 times between days 4 and 5; little change occurs between days 5 and 6, and then the number increases about five times by day 7. The surface area of the blastocyst does not increase in a similar biphasic way, so that when the results are expressed as the number of ouabain molecules bound per unit area there is a significant drop between days 5 and 6. These results suggest that there are two phases of appearance of Na^+,K^+-ATPase, one between days 4 and 5 p.c. and another after day 6. Because the trophoblast cells continue to divide between days 5 and 6, the density of Na^+,K^+-ATPase molecules per unit area diminishes during this time. The ouabain-inhibited Na^+ influx remains essentially constant at 0.20 μmol/cm^2 h on day 5 and day 6 p.c. (Table 14.1). Therefore, the increase in active Na^+ transport observed during the 4–6-day p.c. period results from an increase in the absolute number of pump sites and not from an increase in the capacity of each site to transport more Na^+ per unit time, assuming that all ouabain-

TABLE 14.1. FLUID ACCUMULATION, NET AND OUABAIN-SENSITIVE Na^+ INFLUXES, AND OUABAIN-BINDING SITES IN SIX-DAY PREIMPLANTATION RABBIT BLASTOCYSTS

Days Post-Coitum	Fluid Accumulation Rate[a] (μl/cm^2 h)	Net Na^+ Accumulation Rate[a] (μmol/cm^2 h)	Ouabain-Sensitive Na^+ Influx[b] (μmol/cm^2 h)	Ouabain-Binding Sites[a] (billion/cm^2)	Turnover Number (ion/sec per site)
4	7.57	0.098	—	27.2	—
5	26.05	0.342	0.20	229	146
6	32.26	0.452	0.19	91.3	348
7	70.98	0.820	0.09	170	91

[a] From Borland et al. (12).
[b] From Benos (5).

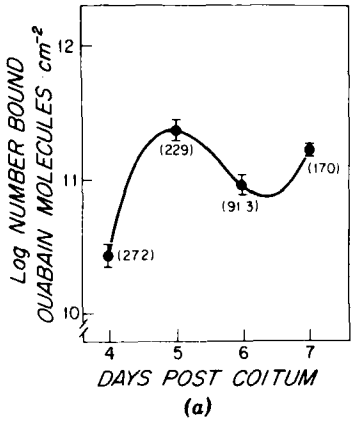

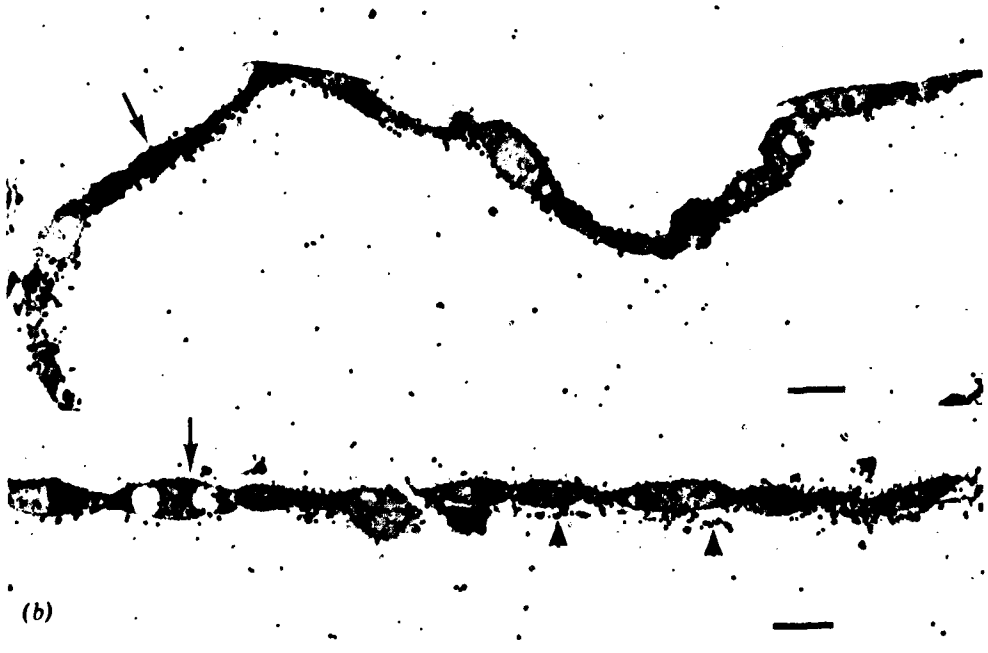

Figure 14.2. Log number of ouabain molecules bound per unit surface area of rabbit blastocyst as a function of age. The numbers in parentheses refer to the average number of ouabain molecules in billions, while the vertical lines represent ± S.D. The data were fitted by orthogonal polynomial regression analysis. The minimum order of polynomial to which these data were fit is three. At least five blastocysts per point were used. These data were taken from Benos (5). (*b*) Autoradiograph of 6-day p.c. rabbit blastocyst after exposure to [^{3}H]ouabain. The tissue was exposed for 90 min to 0.5 μM ouabain containing 0.2 μCi of [^{3}H]ouabain, followed by extensive washing, as described in Benos (5). Both figures show that ouabain is distributed all along the basolateral surfaces with a higher density of grains between adjacent cells. The bottom figure shows "possible" binding to endodermal cells (arrowheads). The long arrows indicate microvilli on the apical surface. The solid bars in the figures indicate 10 μm. Samples were frozen, freeze-dried, coated with NTB-2 emulsion, exposed, and photographed according to published procedures (20).

binding sites are involved in transepithelial Na^+ transport. By day 7 p.c., however, the magnitude of the ouabain-sensitive transepithelial Na^+ influx falls to 0.09 μmol/cm^2 h, a value only marginally significantly different from zero ($P = 0.1$). This decrease in ouabain-sensitive Na^+ influx is paradoxical in light of the measured increase in ouabain-binding sites at this stage of development.

These studies, however, were unable to differentiate whether all Na^+,K^+-ATPase molecules are located on the blastocoelic side of the trophectoderm. We have recently determined by autoradiography the morphological location of [^{3}H]ouabain-binding sites at different stages of preimplantation development in the rabbit. At all stages, ouabain is bound only on the blastocoelic side of the epithelium (Fig. 14.2*b*); no ouabain binding to apical membranes has ever been seen. Interestingly, many ouabain-binding sites are located on the thin endodermal cells which begin to proliferate around the inside of the blastocoele on day 6 p.c. and almost completely cover the inner aspect of the trophectoderm on day 7 p.c. These endodermal ouabain-binding sites may be responsible for the increase in the number of [^{3}H] ouabain-binding sites observed between days 6 and 7. The observation of little or no ouabain sensitivity to J^i_{Na} on day 7 p.c. in spite of a large increase in the total number of binding sites may possibly be explained by the binding of ouabain to these endodermal cells, which presumably are not involved in transepithelial Na^+ transport.

1.2. Amiloride-Sensitive Na^+ Transport

Recent work in our laboratory has shown that the rabbit blastocyst acquires an amiloride-sensitive component to Na^+ influx between 6 and 7 days after fertilization (5, 33; Fig. 14.3). We have conducted some experiments designed to address the question "Is the appearance of the amiloride-sensitive Na^+ entry process a result of genetic preprogramming, or are exogenous maternal 'factors' involved?" We collected embryos on day 5 p.c., cultured them for 48 h at which time measurements of $^{22}Na^+$ influx in the absence and presence of 0.1 m*M* amiloride were performed. The results are presented in Table 14.2. It is apparent that the cultured blastocysts do not have any amiloride sensitivity, suggesting that some component (or components) of the uterine secretions may be necessary for ultimate expression of this particular transport system. These experiments, however, are very preliminary and thus not conclusive. For one thing, we have not yet optimized our culture conditions since the *in vitro* blastocysts were considerably smaller compared to their *in vivo* counterparts. The rabbit zygote has been successfully cultured *in vitro* up to the blastocyst stage in chemically defined medium (17, 25, 37). Although able to blastulate, these embryos fail to expand and grow. Growth rates have been improved with certain modifications of F10 medium (18), but it has not yet been possible to obtain continued growth

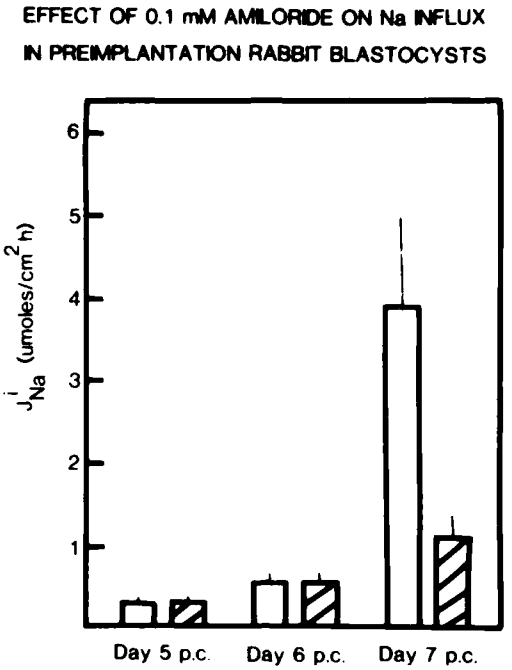

Figure 14.3. Transepithelial $^{22}Na^+$ influx into different-aged preimplantation rabbit blastocysts in the absence and presence (hatched bars) of 0.1 m*M* external amiloride. Probabilities that the difference between mean influx rates plus and minus amiloride was significant are $p > .5$, $p > .5$, and $p < .025$ for day 5, 6, and 7 p.c. embryos, respectively. (From Benos, ref. 5.)

comparable to that observed in *in vivo* blastocysts. The nutrient requirements for successful development are complex; these include amino acids, vitamins, proper osmolality and atmospheric pressure, and a source of protein. Krishnam and Daniel (26) found that a uterine protein component (uteroglobin/blastokinin) was necessary for expansion of blastocysts cultured *in vitro*

TABLE 14.2. THE EFFECT OF AMILORIDE ON $^{22}Na+$ INFLUX INTO FRESHLY COLLECTED OR CULTURED SEVEN-DAY P.C. BLASTOCYSTS[a]

	Freshly Collected Day-7 p.c. Blastocysts	Blastocysts Cultured *in vitro* from Day 5 p.c.
Control	3.90 ± 1.10 (n = 9)	3.72 ± 0.99 (n = 8)
Amiloride (0.1 m*M*)	1.10 ± 0.20 (n = 11)	3.75 ± 1.17 (n = 8)

[a] Units are expressed in micromoles of Na^+ per square centimeter per hour.

from morulae. Maurer and Beier (30), however, found that uteroglobin obtained from six-day pregnancy uteri did not improve blastocyst expansion rates over that observed in BSA-supplemented medium.

In collaboration with Ms. Loretta Nielsen, we have developed procedures for the extraction, separation, and radioimmunoassay of steroid hormones from plasma samples of the rabbit, and have developed techniques for the measurement of steroid receptors in blastocyst tissue. We are currently studying the possible involvement of aldosterone, cortisol, and corticosterone, as well as the uterine secretory protein uteroglobin, in blastocyst fluid expansion and Na^+ transport. These steroid hormones have been implicated as hormonal signals for the synthesis and expression of enhanced amiloride-sensitive Na^+ influx in rat colon (36), neonatal pig colon (21), and cultured amphibian kidney cells (35).

We have found that when rabbit blastocysts are collected from the mother on day 5 p.c. and maintained *in vitro*, the amiloride sensitivity of Na^+ influx fails to develop (Table 14.2). This observation, coupled to the fact that the embryo does not expand, leads us to the hypothesis that certain components derived from the mother are necessary for the proper functioning (and/or expression) of the physiological mechanisms involved in blastocyst fluid accumulation.

We now turn to two other types of experiments designed to investigate further the role of Na^+ in the transport processes that develop in the rabbit trophectoderm.

1.3. NaCl Cotransport

On the basis of the short-circuit and tracer flux measurements of Cross (16) it is possible that the 6-day p.c. rabbit embryo may transport Na^+ and Cl^- into the blastocoele cavity in a coupled fashion. We have performed experiments designed to test this hypothesis. The unidirectional, transepithelial influx of $^{36}Cl^-$ (J^i_{Cl}) and $^{22}Na^+$ (J^i_{Na}) in 6-day-old blastocysts was measured in the presence and absence of 1 m*M* furosemide. The results are shown in Fig. 14.4. These results show that J^i_{Na} is reduced relative to control when the blastocysts are incubated in a Cl^--free medium or when 1 m*M* furosemide is present. Likewise, J^i_{Cl} is reduced by incubating embryos in Na^+-free medium or in the presence of 1 m*M* furosemide. The addition of DIDS (4,4′-diisothiocyanostilbene 2,2′-disulphonic acid), which is a potent inhibitor of coupled anion exchange systems, had no effect on J^i_{Cl}. Removal of external bicarbonate, or addition of 1 m*M* acetazolamide or amiloride produced no change in either J^i_{Na} or J^i_{Cl} (data not shown).

Important quantitative conclusions from these results are that the reduction in J^i_{Cl} and J^i_{Na} in Na^+- and Cl^--free media, respectively, is not significantly different, and the magnitude of the reduction of J^i_{Cl} and J^i_{Na} in the presence of furosemide is also not different. These observations are consis-

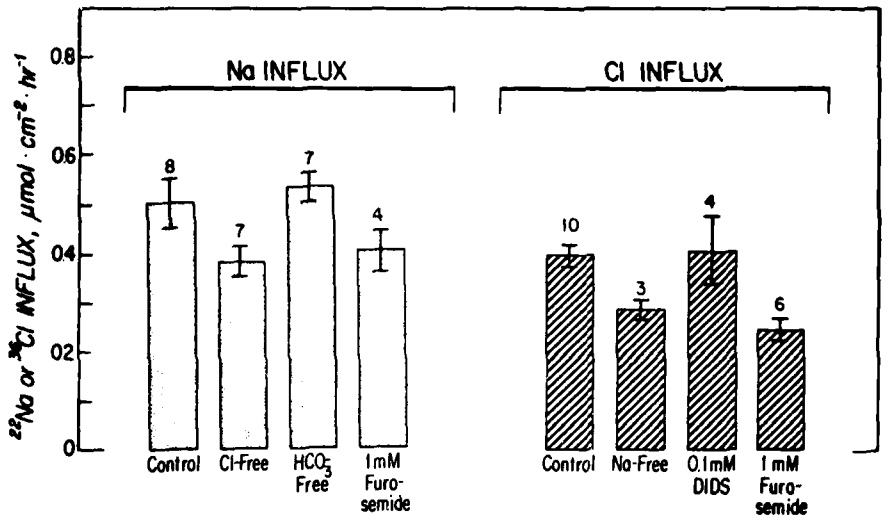

Figure 14.4. The effect of various experimental manipulations on either $^{22}Na^+$ or $^{36}Cl^-$ influxes in 6-day p.c. rabbit embryos. Vertical lines represent 1 S.E. of the mean, and the numbers directly above the error bars indicate the number of blastocysts used per group. (Data from Benos and Biggers, Ref. 7.)

tent with the idea that a portion of both the Na^+ and Cl^- influxes into 6-day p.c. blastocysts are coupled.

In some epithelial systems like rabbit ileum (31) and gallbladder (22), elevated levels of cyclic AMP (cAMP) inhibit NaCl cotransport. We have repeated these experiments in the rabbit blastocyst and show that 1 m*M* cAMP or furosemide inhibit J^i_{Na} and J^i_{Cl} to the same extent, and the addition of these two agents together produces no further inhibitory effect (Table 14.3). Removal of external K^+ does not alter J^i_{Na} or J^i_{Cl}, or does this treatment alter the furosemide sensitivity of either flux.

From the foregoing experiments we conclude that there is a significant NaCl-coupled cotransport system present in the uterine-facing membrane of the 6-day-old rabbit blastocyst, which comprises 25–35% of the total transepithelial fluxes of these ions. This transport system can be inhibited by either cAMP or furosemide. There is no evidence for the presence of either a $Cl^- : Cl^-$ or $Cl^- : HCO_3^-$ exchange system.

This NaCl cotransport system, like the amiloride-sensitive Na^+ transport system, appears during the development of the rabbit blastocyst (Fig. 14.5). The unidirectional J^i_{Cl} was measured in rabbit blastocysts 5, 6, and 6.5 days old in control medium and in the presence of 1 m*M* furosemide. The total J^i_{Cl} does not change significantly in control medium but its sensitivity to furosemide increases with development. Our results suggest that this NaCl cotransport system only develops after the fifth day of development.

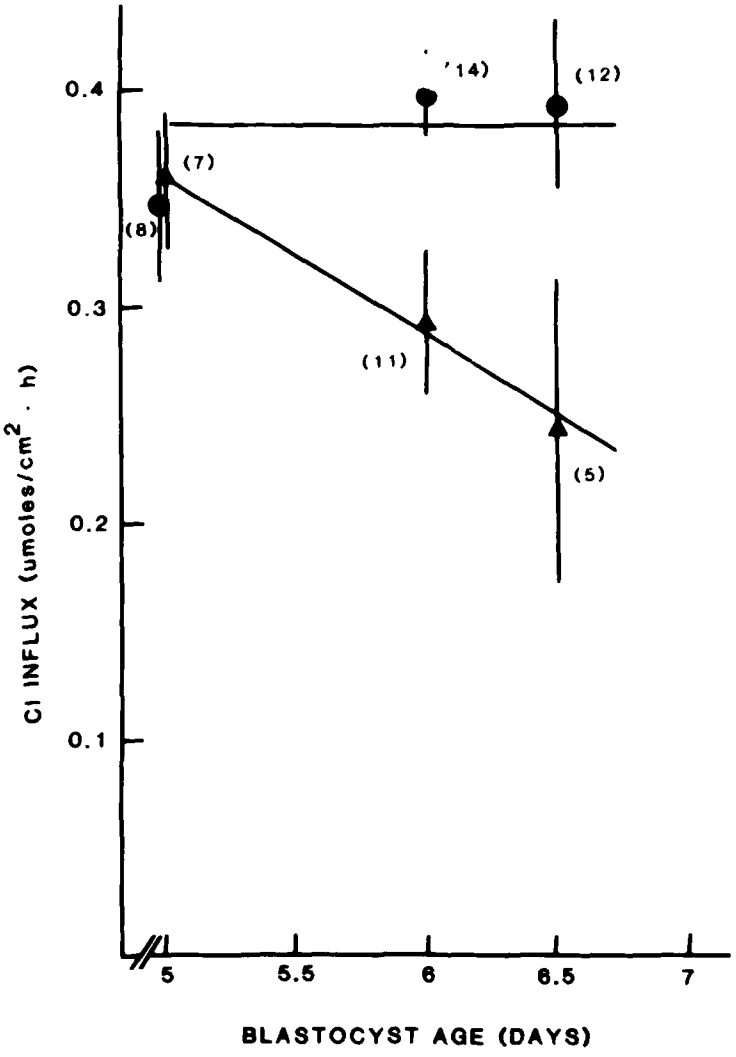

Figure 14.5. The effect of 1 m*M* furosemide (▲) on transepithelial $^{36}Cl^-$ influx in different-aged preimplantation rabbit embryos. Solid circles represent mean values of Cl influx in non-furosemide-treated blastocysts. Vertical lines indicate one S.E. of the mean of (*N*) experiments. (Data from Benos and Biggers, ref. 7.)

1.4. Na^+-Dependent Amino Acid Uptake by the Rabbit Blastocyst

Christensen (15) first reported that in Ehrlich ascites cells and red blood cells, the neutral amino acid methionine is transported by two mechanisms, one Na^+ independent, and one Na^+ dependent. We have examined the uptake of [^{3}H]methionine by 6-day rabbit blastocysts in the presence and absence of Na^+. Intact blastocysts were exposed to different concentrations of

TABLE 14.3. THE EFFECT OF FUROSEMIDE AND DIBUTYRYL CYCLIC AMP ON J^i_{Na} AND J^i_{Cl} IN SIX-DAY P.C. RABBIT BLASTOCYSTS[a]

Treatment	J^i_{Na} (μmol/cm^2 h)	J^i_{Cl} (μmol/cm^2 h)
Control (KRBG)	0.38 ± 0.04 (N = 8)	0.40 ± 0.02 (N = 10)
+1 m*M* Furosemide	0.30 ± 0.01 (N = 8)	0.29 ± 0.02 (N = 7)
+1 m*M* Dibutyryl cAMP	0.31 ± 0.02 (N = 9)	0.31 ± 0.03 (N = 13)
1 m*M* Furosemide + 1 *mM* Dibutyryl cAMP	0.31 ± 0.02 (N = 10)	0.30 ± 0.04 (N = 14)
Pooled error mean square:	0.006, d.f. = 31	0.031, d.f. = 40

[a] Data from Benos and Biggers (9).

methionine for 20 min and the radioactivity of the washed tissue determined. The surface area of the blastocyst was determined from video images before incubation, so that the uptake is expressed as nanomoles per square centimeter per hour.

The uptake of [^{3}H]methionine increases in control media with [Met], and is particularly marked over the lower concentrations. Thus raising [Met] to 10 m*M* increases the uptake to about 5 nmol/cm^2 h, while a further increase of 10 m*M* only increases the uptake by a further 2.25 nmol/cm^2 h. The uptake of [^{3}H]methionine also increases in Na^+-free media with [Met], but in contrast to the results with control media, the increase is more marked over the higher concentrations. Thus raising the [Met] in Na^+-free medium to 10 m*M* raises the uptake to 1.75 nmol/cm^2 h, while a further 10 m*M* increase of methionine increases the uptake by 2.25 nmol/cm^2 h. The two concentration-response curves are very significantly different, showing that methionine is taken up by the 6-day rabbit blastocyst using both Na^+-independent and Na^+-dependent processes.

Regression analysis shows that the relation between the natural logarithm of the uptake of [^{3}H]methionine and [Met] in Na^+-free media does not depart significantly from linearity. This fact provides good evidence that the Na^+-independent uptake of methionine does not occur by simple diffusion. Whether the uptake is determined by Christensen's L system has yet to be determined from studies with other amino acids.

The difference between the two concentration-response curves represents the Na^+-dependent uptake (Fig. 14.6b). The Na^+-dependent uptake

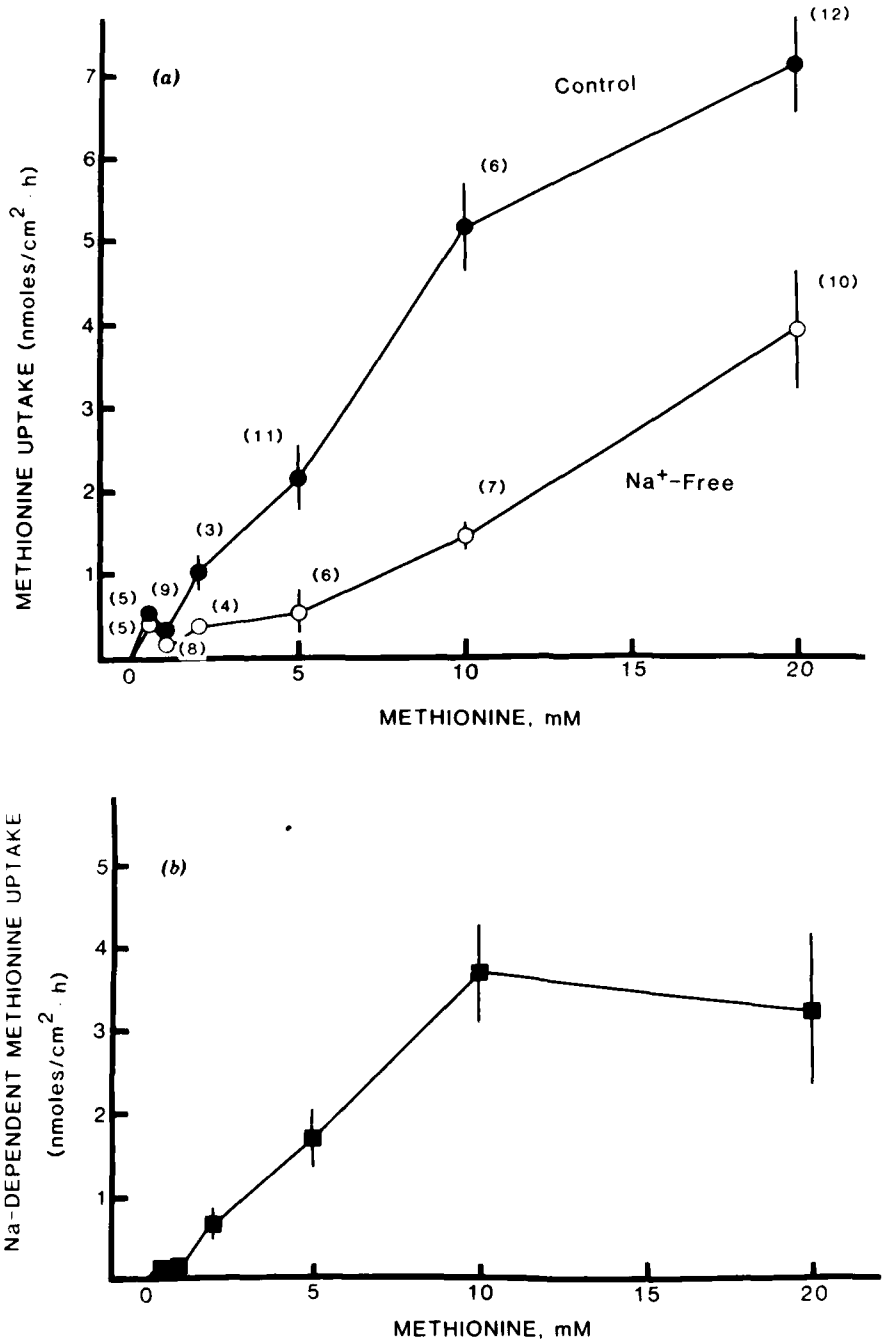

Figure 14.6. (a) Tissue uptake of [^{3}H]methionine into 6-day p.c. rabbit trophectoderm measured in the presence (solid circles) or absence (open circles) of external sodium (Figure 6a). All measurements were conducted on single embryos, and the tissue [^{3}H]methionine counts were corrected for extracellular space trapping using [^{14}C]polyethylene glycol as a marker. The points represent the mean value of (*N*) determinations, and the vertical lines indicate one S.E. of the mean. (*b*) The Na^+-dependent methionine uptake (the difference between the two curves shown in Fig. 14.a) is plotted versus the external methionine concentration.

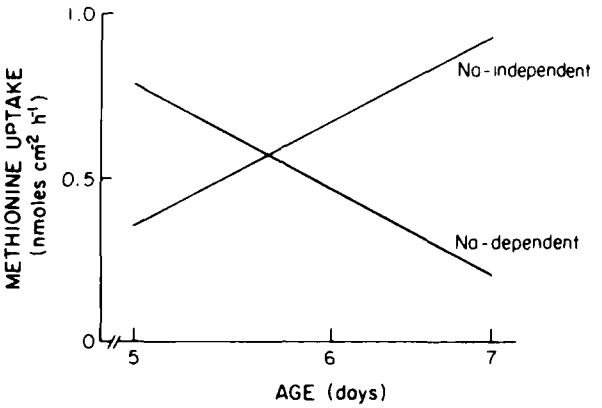

Figure 14.7. Tissue uptake of [^{3}H]methionine by way of Na^+-dependent and Na^+-independent routes versus blastocyst age. Lines were determined from regression analysis of the data of Benos (4). Final methionine concentration in all media was 0.12 m*M*. An equimolar quantity of choline chloride was used to substitute for NaCl in these experiments.

increases with [Met] up to a concentration of 10 m*M* and then levels off. This fact suggests that the system becomes saturated. Unfortunately, the data are insufficient to determine whether it obeys Michaelis–Menten kinetics. Whether this component of total uptake is by way of Christensen's A system has yet to be determined using comparisons with the behavior of other amino acids.

Benos (4) compared the uptake of [^{3}H]methionine by 5-, 6- and 7-day rabbit blastocysts in control- and Na^+-free media. We have reevaluated these results using regression analyses (Fig. 14.7). The total uptake does not change significantly in control media over the interval of 5–7 days and has a mean value of 1.16 nmol/cm^2 h. In Na^+-free media, however, the uptake increased significantly from 0.32–0.82 nmol/cm^2 h over the same period. Thus the Na^+-independent component increases, while the Na^+-dependent component of methionine uptake decreases between the fifth and seventh day of development (Fig. 14.7).

We have also measured the Na^+ dependence of uptake of other amino acids, including glycine, aminoisobutyric acid, and leucine. Of these, only glycine uptake displays Na^+-independence. Removal of external Na^+ reduces leucine uptake by 80% and 42% in 6- and 6.5-day embryos, respectively (at 0.9 m*M* external leucine). We have not yet determined whether leucine uptake depends on external Na^+ in 5-day p.c. blastocysts.

2. METABOLISM AND TRANSPORT

A linear relationship between the rate of oxygen consumption and active Na^+ transport has been observed in many transporting epithelia (29). Transepithelial fluid transport across the rabbit trophectoderm is, at least in part,

mediated by the Na^+,K^+-ATPase (11). As there is a large, ouabain-sensitive component to Na^+ influxes (5), the relative metabolic cost of active Na^+ transport can be determined by measuring the oxygen consumption (Q_{O_2}) of blastocysts before and after injection with ouabain. A decrease in active transport produced by ouabain would result in a decrease in the rate of ATP hydrolysis, which in turn would manifest itself as a decrease in the rate of blastocyst Q_{O_2}. Benos and Balaban (6) have shown that approximately 70% of the total oxygen consumption of 4–6 day p.c. rabbit blastocysts is inhibited by ouabain, whereas only 16% of Q_{O_2} of 7-day p.c. embryos is ouabain sensitive. The absolute magnitude of the Q_{O_2} of 6–7-day-old rabbit blastocysts averaged 88 ± 7 nmol O_2/cm^2 h, and was higher for 4- and 5-day p.c. embryos (132 ± 10 nmol O_2/cm^2 h).

We wanted to determine how much of this ouabain-sensitive Q_{O_2} was directly associated with active transepithelial Na^+ transport in this tissue, as well as to determine the stoichiometry of active Na^+ transport and ATP production. These determinations were done by measuring the increase in total ATP production (from Q_{O_2} and lactate production) after transepithelial Na^+ transport had been stimulated by the addition of amphotericin B to the blastocyst incubation medium (7). Amphotericin B stimulates Na^+ transport by increasing the Na^+ permeability of the rate-limiting uterine-facing cell membrane of the trophectoderm, allowing more Na^+ to gain access to the Na^+ pump. The results of these experiments are summarized in Table 14.4. Amphotericin B stimulated ouabain-sensitive Na^+ transport by a factor of 7 while causing a 32% increase in total ATP production. From these data, the calculated Na^+/ATP stoichiometry is 3. This value is in excellent agreement with the measured Na^+,K^+-ATPase stoichiometry of Na^+,ATPase on other cellular and epithelial tissues (29). This analysis has not been done for 4-, 5- or 7-day-old rabbit blastocysts.

To maintain a rate of net transepithelial Na^+ transport of 0.19 μmol/cm^2 h (Table 14.2), some 0.063 μmol ATP/cm^2 h must be consumed by the day-6

TABLE 14.4. THE EFFECT OF AMPHOTERICIN B ON OUABAIN-SENSITIVE TRANSEPITHELIAL Na^+ INFLUX AND TOTAL ATP PRODUCTION IN SIX-DAY RABBIT BLASTOCYSTS[a]

	Control	+ Amphotericin B (5 μg/ml)	Δ
Ouabain-sensitive J^L_{Na}	0.19	1.27	1.08
Total ATP production (Oxidative and glycolytic)	1.10	1.45	0.36

[a] Units are expressed as micromoles per square centimeter per hour. The data were taken from Benos and Balaban (7).

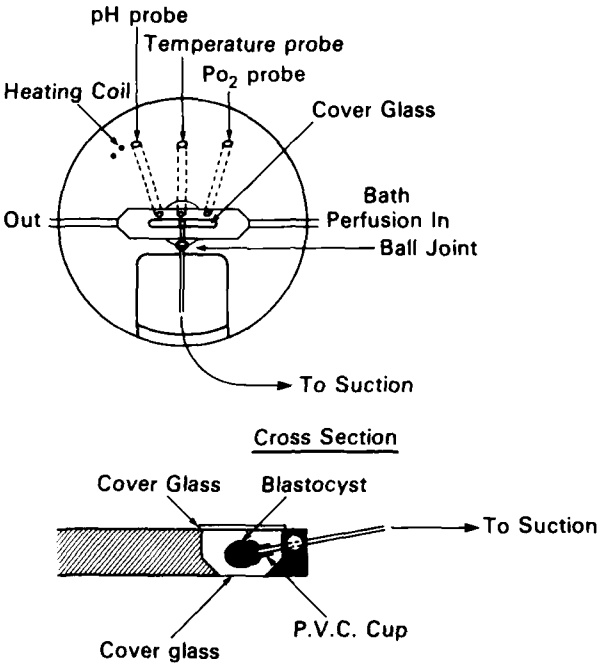

Figure 14.8. Specially designed, temperature-regulated blastocyst holding chamber for simultaneous superfusion, fluorescence, and differential interference microscopy of living mammalian embryos. The P.V.C. suction cup is replaceable and can be changed to accomodate embryos of any size.

p.c. embryo. Thus, under *in vitro* conditions (with glucose as the sole exogenous substrate), ouabain-sensitive Na^+ transport utilizes only 6–11% of the total ATP output of this tissue, not 70% as suggested by the inhibition of Q_{O_2} by ouabain. Clearly, some process or processes other than active transepithelial Na^+ transport must be inhibited by ouabain. The lower inhibition of Q_{O_2} by ouabain in the 7-day p.c. embryo may be indicative of an "uncoupling" of the ouabain sensitivity of these other processes, a cessation of ouabain-sensitive transepithelial Na^+ transport, and/or a shift in the utilization of the energy derived from oxidative metabolism from one of transport to the support of other functions of the trophectoderm and inner cell mass that begin at day 7 p.c., the day of implantation. Studies are presently underway to evaluate all of these possibilities.

We have also begun studies of living blastocyst tissue using combined differential interference-contrast and fluorescence microscopy for analysis of cellular metabolic parameters. Bereiten-Hahn (10) has described the use of dimethylaminostyrylmethyl-pyridiniumiodine (DASPMI) as a specific fluorescent probe for mitochondrial staining *in situ*. Since blastocyst tissue has a high rate of oxygen consumption, and its metabolism is almost entirely based on oxidative processes, we wanted to visualize the distribution of mitochondria within the embryo itself, especially comparing trophectoderm

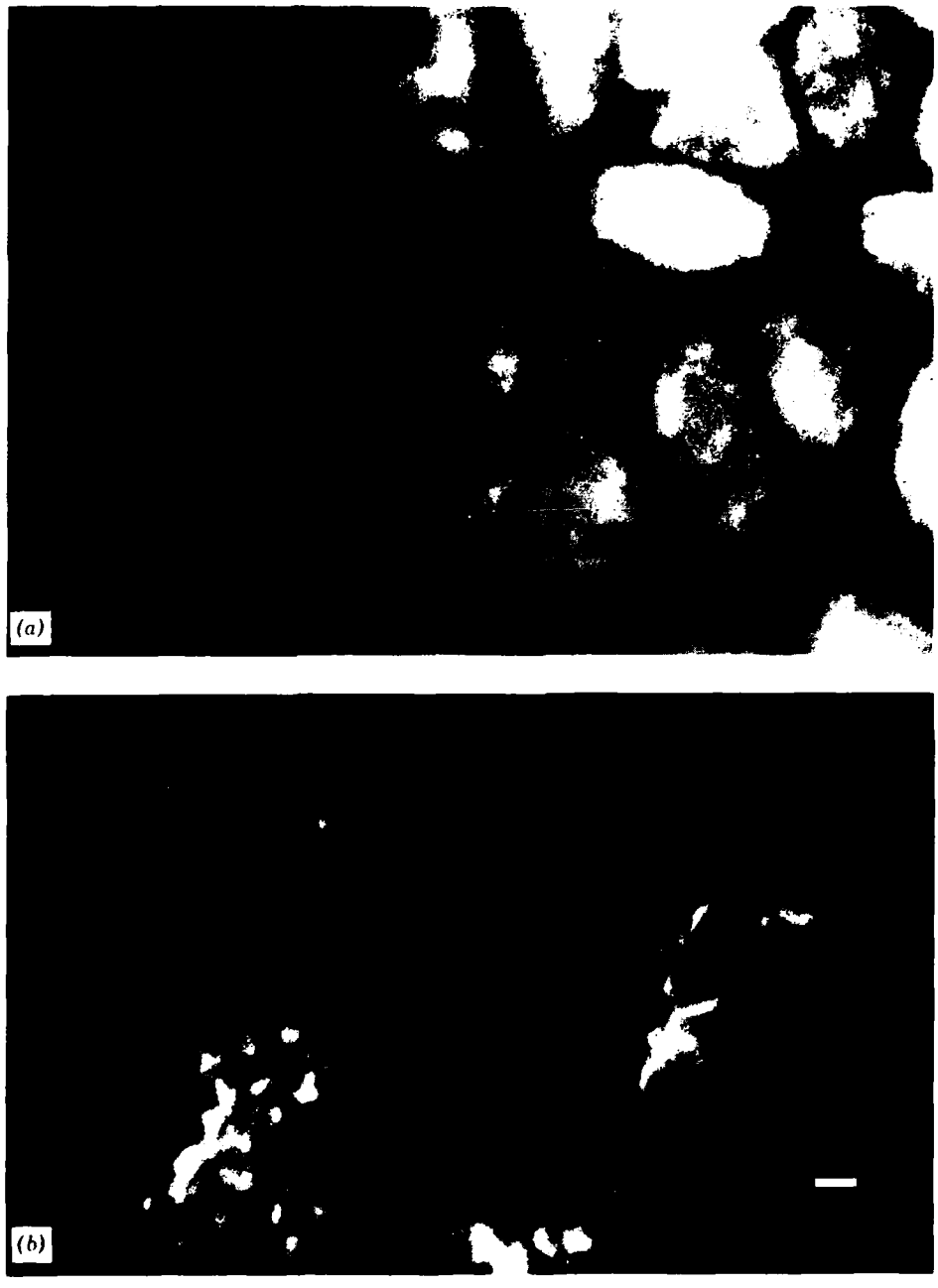

Figure 14.9. Fluorescence micrographs of DASPMI-stained 6-day p.c. rabbit (*a*) trophectoderm and (*b*) inner cell mass. Fluorescence examination was performed using a filter combination giving 404.7 nm excitation wavelength and emission above 510 nm. Bar in figures indicates 2.5 μm.

to inner cell mass. Blastocysts were incubated for 30 min in the dark with 5 μM DASPMI in Ringer's solution. The embryos were transferred to a chamber designed for simultaneous monitoring of metabolic processes and microscopy (Figure 14.8). Figure 14.9 is a fluorescent photomicrograph of a DASPMI-stained, 6-day p.c. rabbit blastocyst. All cells of the trophectoderm (Fig. 14.9*a*) display intense fluorescence, while only a few cells of the inner cell mass contain mitochondria (Fig. 14.9*b*). These results suggest that the blastomeres of the trophectodermal epithelium are largely aerobic, whereas the majority of the presumptive fetal cells are glycolytic. Precise quantification of this hypothesis is presently being undertaken using differential interference/fluorescence microscopy combined with *in vivo* measurements of mitochondrial NAD redox levels (2).

3. PROTEIN SYNTHESIS, CELL POLARITY, AND DEVELOPMENT

A major goal of our laboratory is to gain insight into the biochemical and molecular mechanisms underlying these dramatic changes in epithelial transport activity in the expanding rabbit blastocyst. To this end, we have initiated studies in which we are quantitatively examining the developmental rates of synthesis of major blastocyst proteins using two-dimensional polyacrylamide gel electrophoresis and fluorography (see ref. 37 for the methodological details). During the conduct of these experiments we have developed a technique, based on orthogonal multiple regression analysis (1), that permits quantitative comparisons of synthetic patterns between groups or clusters of individual proteins.

Blastocysts, recovered from the uteri of rabbits on days 4, 5, 6, and 7 after mating, were incubated at 37°C in a humidified atmosphere of 5% CO_2 in air in the presence of 180–200 μCi/ml [^{35}S]methionine (specific activity 1200 Ci/mmol) for 3 h in Ham's F-10 medium. After the incubation period blastocysts were washed, the zona pellucida removed, the tissue solubilized in lysis buffer and subjected to two-dimensional gel electrophoresis. Six to twenty blastocysts were used per experimental point, and each experiment was repeated five times. To serve as known protein markers, preparations of purified Na^+,K^+-ATPase and actin were added to the blastocyst tissue lysate. Protein spots were first visualized using a silver stain procedure (30a) followed by fluorography. The spots corresponding to these proteins plus 17 other major proteins were cut out, solubilized, and the incorporated radioactivity determined by liquid scintillation spectroscopy. The amount of ^{35}S label (dpm) incorporated in each protein spot was expressed as percent of total acid precipitable (TCA) radioactivity per blastocyst.

Figure 14.10 shows a two-dimensional gel of radiolabeled 6-day rabbit blastocyst proteins. Twenty individual proteins, referenced by letter, were analyzed for synthetic rate during preimplantation development as described

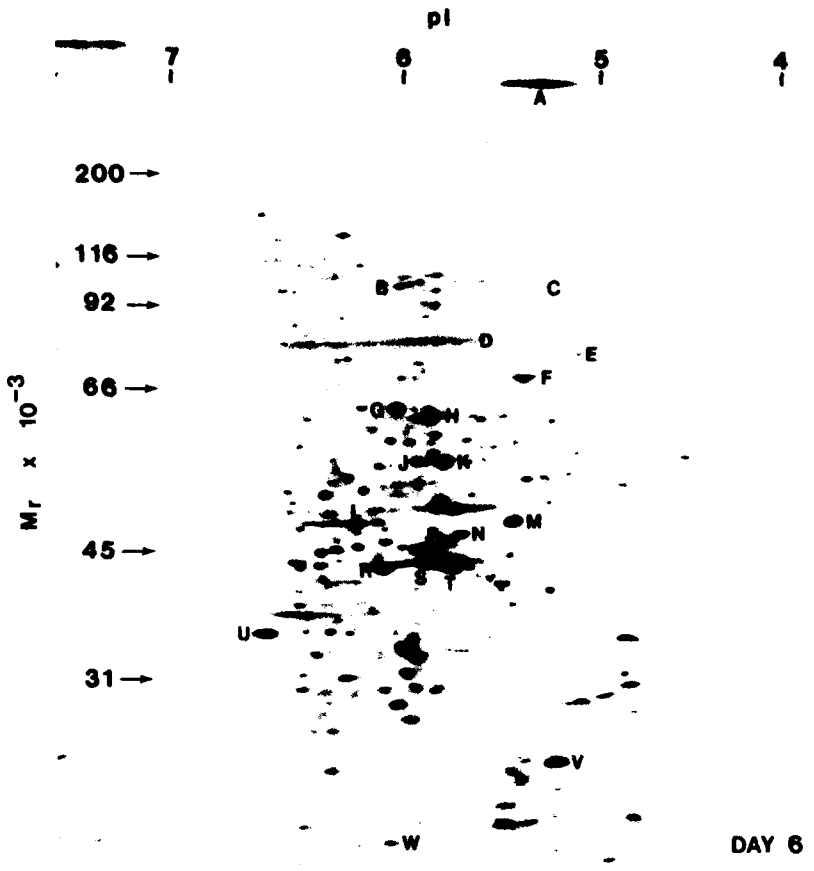

Figure 14.10. Two-dimensional gel of [^{35}S]-radiolabeled 6-day p.c. rabbit blastocyst proteins. Protein spots, stained with silver, are referenced by letter.

before. Specifically, as determined by coelectrophoresis or immunoblotting techniques, protein B is Na^+, K^+-ATPase, and proteins labeled S and T are γ and β actin, respectively. Figure 14.11 illustrates the time course of [^{35}S]methionine incorporation into 6-day p.c. blastocyst tissue. The rate of specific, TCA-precipitable ^{35}S incorporation was essentially linear over the 3-h incubation period and averaged 360,000 dpm per blastocyst per hour.

The incorporation rate of [^{35}S]methionine into total blastocyst tissue protein at 4, 5, 6, and 7 days after fertilization is shown in Figure 14.12. Incorporation increases approximately eight-fold between days 4 and 5 p.c., 2.5-fold between days 5 and 6, and then decreases four-fold by day 7. This same general pattern is seen when examining individual protein spots (Fig. 14.13). The developmental significance of the reported decrease in [^{35}S]methionine incorporation rate by 7-day p.c. blastocysts is unclear. Significant shifts in the metabolic activities of the predominant trophoblast cells in preparation for implantation, that is, changes in protein turnover and/or degradation,

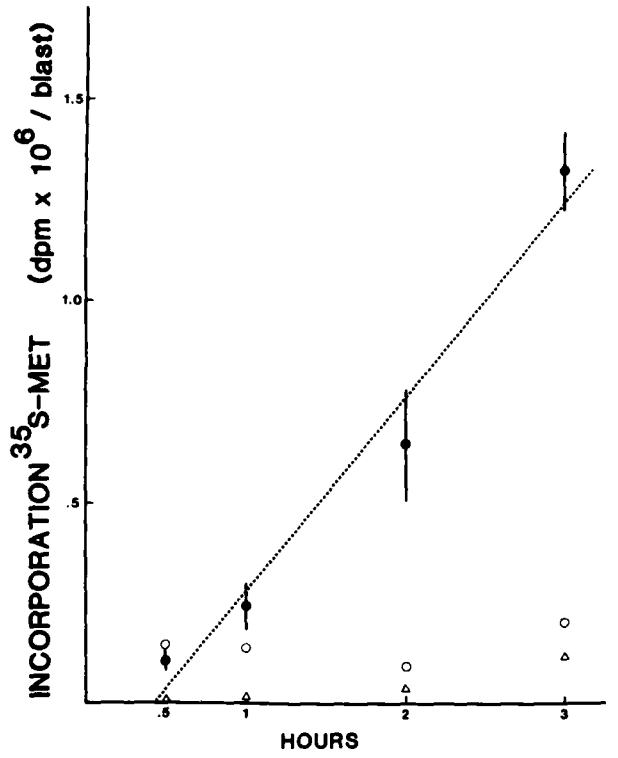

Figure 14.11. Time course incorporation of [^{35}S]methionine into total protein pool of 6-day p.c. rabbit embryos. TCA precipitable radioactivity (●) was linear over 3-h incubation period (correlation coefficient = .98). Non-TCA-precipitable [^{35}S] radioactivity associated with blastocyst tissue (○) and total dpm's associated with the zona pellucida (△) represent nonspecific uptake. This component of uptake saturated within 30 min and thereafter remained constant.

may account for this observation. Studies are underway to investigate these possibilities.

Statistical analysis shows that the protein synthetic rate versus developmental age data for all of the individual proteins examined can be fit to a quadratic equation using orthogonal regression analysis (see Figs. 14.12 and 14.13). A comparison of the linear regression coefficients of the different proteins indicates the relative degree of protein synthetic rate, that is, the higher the linear regression coefficient, the greater the increase in rate of synthesis between days 4 and 7 p.c. Figure 14.14 ranks the linear regression coefficient for all of the 20 proteins examined in relation to one another. Further statistical comparisons between each protein suggest that certain proteins can be grouped according to the similarity of their pattern of changing rates of protein synthesis. In Fig. 14.14, of the 20 proteins examined, proteins A and W have the greatest increase in synthetic rate, whereas proteins H, G, and R the lowest. Of particular importance is the observation that the synthetic rate of Na^+,K^+-ATPase, protein B, increases 90-fold be-

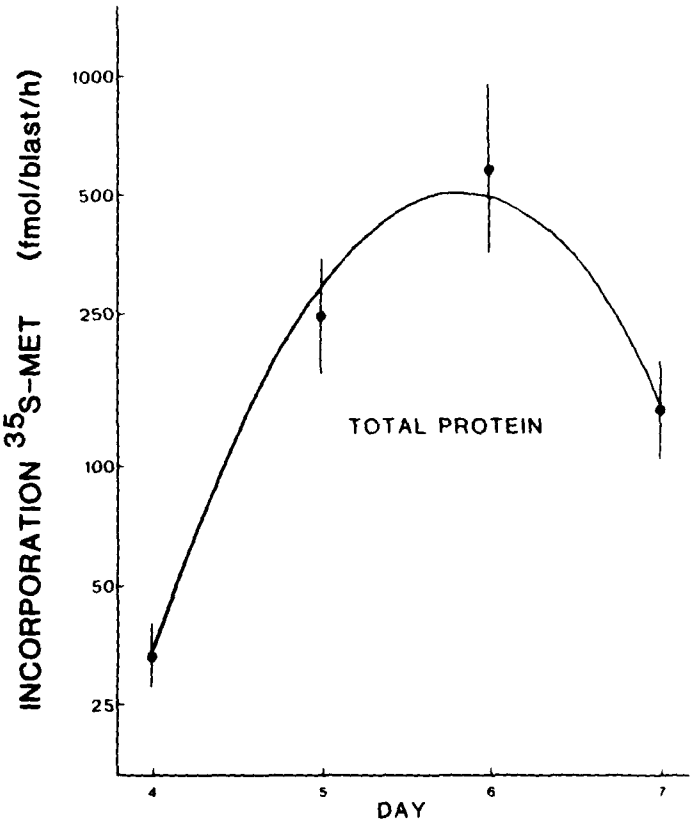

Figure 14.12. The rate of incorporation of [^{35}S]methionine into total blastocyst tissue protein at 4, 5, 6 and 7 days p.c. (expressed as femtomoles per blastocyst per hour, log scale).

tween day 4 and day 6 of development. This large increase in Na^+,K^+-ATPase synthesis parallels the period of maximal blastocyst expansion and blastocoele fluid accumulation. Also note that proteins S and T, the structural proteins γ and β actin, are grouped together, whereas protein B, the Na^+,K^+-ATPase, is categorized in another group. We suggest that these differential patterns of protein synthesis may be indicative of the simultaneous reading of the genome for coding of a group of particular proteins for a specified function, for example, membrane transport proteins and structural proteins.

Since our primary objective is to correlate developmental changes of epithelial transport activity with alterations in plasma membrane protein composition, we decided to take advantage of the geometry of the blastocyst system and differentially label apical or basolateral membrane proteins with ^{125}I using the glucose–glucose oxidase–lactoperoxidase reagent system. Blastocysts were either radiolabeled on their apical surface by incubation in a solution containing 100 μCi Na ^{125}I, 20 IU lactoperoxidase, 2 IU glucose

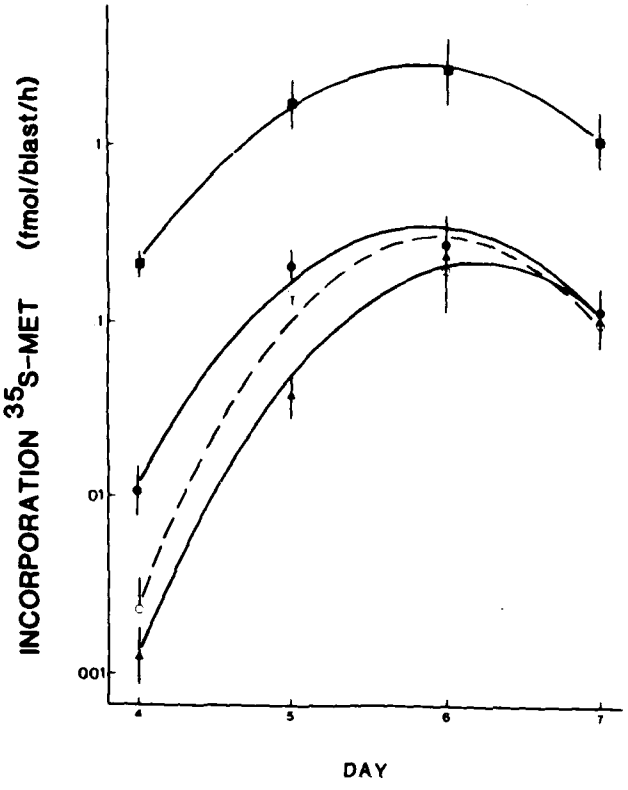

Figure 14.13. Comparison of [^{35}S]methionine incorporation rates into four major blastocyst proteins versus developmental age. Legend: (■) protein T (β actin); (●) protein S (γ actin); (○) protein B (Na^+,K^+-ATPase); (▲) protein A (350,000 dalton unknown protein).

oxidase per milliliter of phosphate-buffered saline plus 5 m*M* glucose, or microinjected with these reagents, thereby labeling protein constituents of the basolateral plasma membranes. After extensive washing with ice-cold saline containing 0.1 m*M* NaI and 0.5 m*M* phenylmethylsulfonyl fluoride, the blastocyst tissues were homogenized and their proteins solubilized and subjected to one- and two-dimensional gel electrophoresis and subsequent autoradiographic analysis. Labeled apical membrane components were characterized by three major bands with apparent molecular weights between 45,000 and 85,000 daltons. In contrast, iodinated basolateral membranes displayed a more varied pattern of labeled proteins with several major components resolved between 25,000 and 130,000 daltons. Two-dimensional separation of iodinated blastocyst membrane proteins revealed 10–20 polypeptides which were characteristic of their apical or basolateral domain (Fig. 14.15). We are at present comparing apical and basolateral membrane protein composition in different-aged embryos in an attempt to define qualitative and quantitative changes in the developmental expression of trophectodermal membrane constituents.

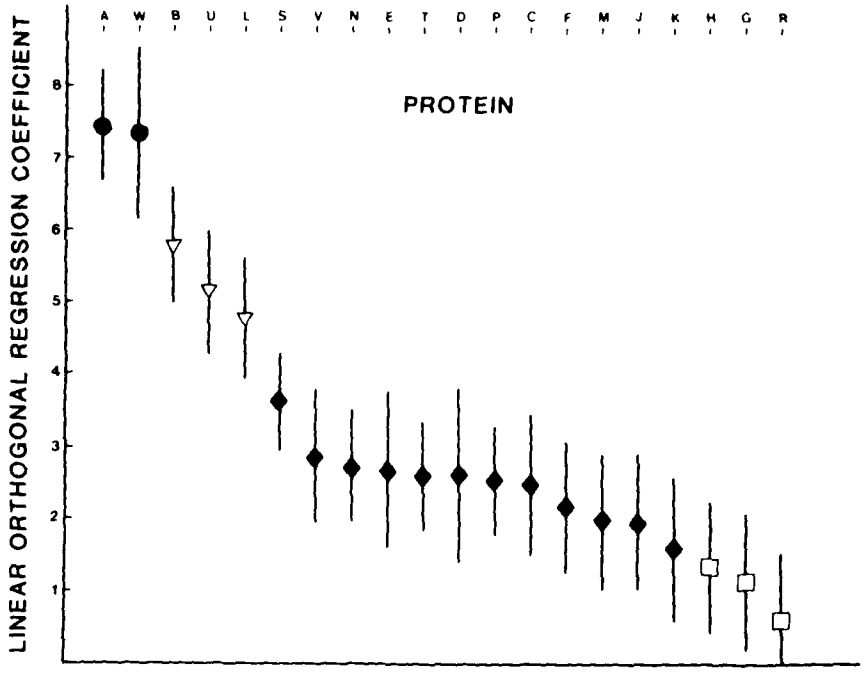

Figure 14.14. Orthogonal linear regression coefficients determined from best-fit curves of developmental protein synthesis patterns of the type shown in Figure 14.13, for each of the 20 actively synthesized proteins. See text for details.

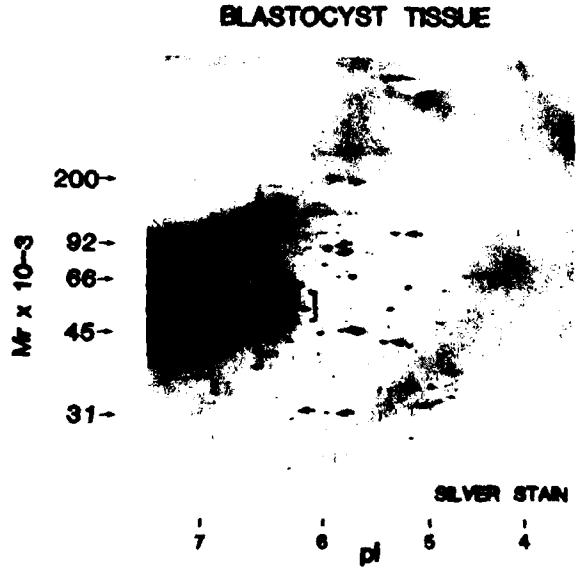

Figure 14.15. Two-dimensional, silver-stained gel of 6-day p.c. rabbit blastocyst proteins. Before protein solubilization, apical or basolateral plasma membranes were enzymatically iodinated (^{125}I) using the glucose–glucose oxidase–lactoperoxidase system. Arrows pointing right indicate apical membrane proteins; arrows pointing left indicate basolateral membrane proteins. Membrane localization of these proteins was assessed from simultaneously run autoradiographs.

4. SUMMARY

It is well established that the trophectoderm of the preimplantation rabbit blastocyst can actively transport solutes that, in turn, are believed to mediate the accumulation of blastocoelic fluid. Consequently, the rabbit blastocyst serves as an ideal model to investigate epithelial transport mechanisms during embryonic development. The trophectoderm is considered to be an electrically "tight" epithelium, as values for the transepithelial electrical resistance and potential difference are high for both day-6 and day-7 p.c. blastocysts. However, during development the trophectoderm displays marked changes in epithelial transport properties, particularly between day 6 and day 7 p.c. These changes (see Fig. 14.1) are characterized by (1) the loss of a Na^+-dependent methionine transport mechanism, (2) the development of an amiloride-sensitive component to Na^+ influx, (3) a decrease in ouabain-sensitive oxygen consumption with a concomitant increase in ouabain binding, and (4) the acquisition of a furosemide-sensitive NaCl cotransport system. During this period the rate of fluid accumulation doubles, resulting in a five-fold increase in blastocoele volume. We have also presented results showing that individual proteins of expanding blastocysts can be grouped with respect to their synthetic rates and that plasma membrane proteins can be uniquely characterized by their apical and basolateral domains. We suggest that the dramatic changes in epithelial transport mechanisms observed during preimplantation development of the rabbit blastocyst are a consequence of the changing developmental expression of trophectodermal membrane constituents. The blastocyst tissue is thus a useful model not only for understanding epithelial transport function in general, but also for understanding the physiological events associated with normal embryonic development.

ACKNOWLEDGMENTS

The excellent technical assistance of Ms. Marie Angela Blazonis is gratefully acknowledged. We thank Ms. Tamara Hardenbergh for typing. This work was supported by Grant HD 12353 from the National Institutes of Health and by funds from the Andrew W. Mellon Foundation.

REFERENCES

1. Armitage, P. (1971) *Statistical Methods in Medical Research*, Blackwell Scientific Publications, Oxford.
2. Balaban, R. S., Dennis, V. W. and Mandel, L. J. (1981) *Am. J. Physiol.*, **240**, F337–F342.
3. Beier, H. M. (1979) Endometrial secretion proteins—biochemistry and biological significance, in Beller, F. K. and Schumacher, G. F. B., Eds., *The Biology of the Fluids of the Female Genital Tract*, Elsevier, New York, pp. 89–114.

4. Benos, D. J. (1981a) *J. Physiol. (Lond.)*, **316**, 191–202.
5. Benos, D. J. (1981b) *Dev. Biol.*, **83**, 69–78.
6. Benos, D. J. and Balaban, R. S. (1980) *Biol. Reprod.*, **23**, 941–947.
7. Benos, D. J. and Balaban, R. S. (1983) *Am. J. Physiol.*, **245**, C40–C45.
8. Benos, D. J. and Biggers, J. D. (1981) Blastocyst fluid formation, in Mastroianni, L., Jr. and Biggers, J. D., Eds., *Fertilization and Embryonic Development in Vitro*, Plenum, New York, pp. 283–297.
9. Benos, D. J. and Biggers, J. D. (1983) *J. Physiol. (Lond.)*, **342**, 23–33.
10. Bereiter-Hahn, J. (1976) *Biochim. Biophys. Acta*, **423**, 1–14.
11. Biggers, J. D., Borland, R. M., and Lechene, C. P. (1978) *J. Physiol. (Lond.)*, **280**, 319–330.
12. Borland, R. M., Biggers, J. D., and Lechene, C. P. (1976) *Dev. Biol.*, **50**, 201–211.
13. Borland, R. M., Biggers, J. D., and Lechene, C. P. (1977) *J. Reprod. Fertil.*, **51**, 131–135.
14. Calarco, P. G. and Brown, E. A. (1969) *J. Exp. Zool.*, **171**, 253–284.
15. Christensen, H. N., Liang, M., and Archer, E. G. (1967) *J. Biol. Chem.*, **242**, 5237–5246.
16. Cross, M. H. (1973) *Biol. Reprod.*, **8**, 566–575.
17. Daniel, J. C. (1963) *Am. Zool.*, **3**, 526–527.
18. Daniel, J. C. (1965) *J. Embryol. Morphol.*, **13**, 83–95.
19. Ducibella, T., Albertini, D. F., Anderson, E., and Biggers, J. D. (1975) *Dev. Biol.*, **45**, 231–250.
20. Ernst, S. A. and Mills, J. W. (1977) *J. Cell Biol.*, **75**, 74–94.
21. Ferguson, D. R., James, P. S., Paterson, J. V. P., Saunders, J. S., and Smith, M. W. (1979) *J. Physiol. (Lond.)* **292**, 495–504.
22. Frizzell, R. A., Field, M., and Schultz, S. G. (1979) *Am. J. Physiol.*, **236**, F1–F8.
23. Hastings, R. A. and Enders, A. C. (1975) *Anat. Rec.*, **181**, 17–34.
24. Izquierdo, L., Fernandez, S., and Lopez, T. (1976) *Arch. Biol. Med. Exp.*, **10**, 130–134.
25. Kane, M. T. and Foote, R. H. (1970) *Proc. Soc. Exp. Biol. Med.*, **133**, 921–925.
26. Krishnam, R. S. and Daniels, J. C. (1967) *Science*, **158**, 490–492.
27. Lewis, W. H. and Gregory, P. W. (1929) *Science*, **69**, 226–229.
28. Lutwak-Mann, C. (1971) The rabbit blastocyst and its environment: physiological and biochemical aspect, in, Blandau, R. J., Ed., *The Biology of the Blastocyst*, University of Chicago Press, Chicago, pp. 243–260.
29. Mandel, L. J. and Balaban, R. S. (1981) *Am. J. Physiol.*, **240**, F357–F371.
30. Maurer, R. R., and Beier, H. M. (1976) *J. Reprod. Fertil.*, **48**, 33–41.
30a. Morrissey, J. H. (1981) *Annal. Biochem.* **117**, 307–310.
31. Nellens, H. N., Frizzell, R. A., and Schultz, S. G. (1973) *Am. J. Physiol.*, **225**, 467–475.
32. Petzoldt, U. (1971) *Zool. Jb. Physiol. Bd.*, **75**, 547–593.
33. Powers, R. D., Borland, R. M., and Biggers, J. D. (1977) *Nature*, **270**, 603–604.
34. Schlafke, S. and Enders, A. C. (1967) *J. Anat. (Lond.)*, **102**, 13–32.
35. Watlington, C. O., Perkins, F. M., Munson, P. J., and Handler, J. S. (1982) *Am. J. Physiol.*, **242**, F610–F619.
36. Will, P. C., Lebowitz, J. L., and Hopfer, U. (1980) *Am. J. Physiol.*, **238**, F261–F268.
37. Van Blerkom, J. (1978) Methods for the high-resolution analysis of protein synthesis: applications to studies of early mammalian development, in, Daniel, J. C., Jr, Ed., *Methods in Mammalian Reproduction*, Academic, New York, pp. 67–109.
38. Van Blerkom, J., Manes, C., and Daniel, J. C. (1973) *Dev. Biol.*, **35**, 262–282.

CHAPTER 15

THE DEVELOPMENTAL REGULATION OF TTX-SENSITIVE SODIUM CHANNELS IN RAT SKELETAL MUSCLE *IN VIVO* AND *IN VITRO*

SCOTT J. SHERMAN
WILLIAM A. CATTERALL
Department of Pharmacology
University of Washington School of Medicine
Seattle, Washington

The development of skeletal muscle has been studied extensively, in part, because it provides an excellent example of a target tissue with neuronal regulation. A wide variety of muscle cell properties is regulated by innervation, including the principal proteins involved in impulse transmission: the acetylcholine receptor, acetylcholinesterase, and voltage-sensitive sodium channel (for reviews see refs. 7, 12, 29). In mammalian muscle each of these cell surface proteins has a functionally active embryonic counterpart which is present in fetal muscle prior to innervation and reappears upon denervation of adult muscle (7, 12, 29, 42). In rat skeletal muscle the embryonic and adult forms of the voltage-sensitive sodium channel can be distinguished by their affinity for the potent neurotoxins tetrodotoxin (TTX) and saxitoxin (STX). These toxins have a high affinity for a common receptor site on the voltage-sensitive sodium channel of adult muscle at which they bind and block ionic flux at nanomolar concentrations (25, 31). This adult form has been termed the TTX-sensitive sodium channel.

Uninnervated fetal (2, 18, 33, 37) and denervated adult (26, 30) muscle possess a second type of voltage-sensitive sodium channel which requires a 200-fold higher concentration of TTX to block ionic flux and action potentials. This embryonic form of the channel has been termed the TTX-insensitive sodium channel. Although the presence of the TTX-insensitive channel is clearly related to the absence of innervation, the regulatory influence of the motor neuron on the development of TTX-sensitive channels has not been well defined. Previous studies indicate that denervation of adult muscle causes, at most, a partial reduction of the sarcolemmal density of TTX-sensitive sodium channels (1, 14, 32). The studies presented in this chapter were designed to define more clearly the factors that influence the development of the TTX-sensitive sodium channel in skeletal muscle.

1. DEVELOPMENT OF TTX-SENSITIVE Na^+ CHANNELS IN VIVO

The development *in vivo* of TTX-sensitive channels was studied using the rat triceps surae muscle. The sarcolemmal density of TTX-sensitive channels was quantitated as a function of postnatal age by measuring the specific binding of [^{3}H]STX (1, 36). This technique has been shown by a number of investigators to give a reliable estimate of the total number of TTX-sensitive Na^+ channels (25, 31). The muscle was homogenized and incubated with [^{3}H]STX for 30 min at 0°C. The muscle membranes were then collected on glass fiber filters and washed to remove unbound [^{3}H]STX. Nonspecific binding was determined by including excess TTX in the incubation medium. Figure 15.1*a* shows the total and nonspecific binding of [^{3}H]STX to adult triceps surae at a range of [^{3}H]STX concentrations. Nonspecific binding is unaffected by TTX and increases linearly with [^{3}H]STX concentration (31). The specific binding is the difference between the total and nonspecific bind-

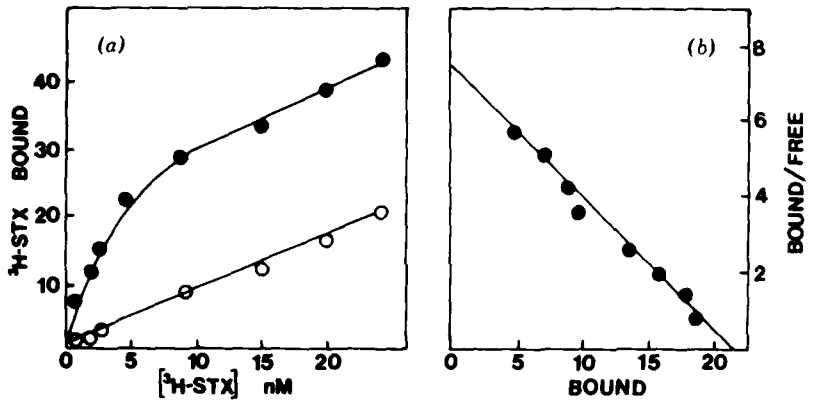

Figure 15.1. Binding of [^{3}H]STX to TTX-sensitive sodium channels in adult triceps surae. (*a*) Muscle homogenates were incubated with increasing concentrations of [^{3}H]STX (●) or [^{3}H]STX plus 2 μM TTX (○) at 0°C, and bound [^{3}H]STX was measured by rapid filtration. (*b*) Specific binding was calculated from the data in (*a*) and is presented as a Scatchard plot. The units shown on the abcissa are femtomoles per milligram wet weight per nanomolar concentration. Least squares analysis gave values of: K_D = 2.9 nM and B_{max} = 21 fmol/mg wet wt.

ing and is plotted according to Scatchard in Fig. 15.1*b*. The data are best fit by straight line, indicating the presence of a single class of saturable, high affinity (K_D = 2.9 nM) receptor sites. The total binding capacity (B_{max}) is 21.7 fmol/mg wet weight. Similar experiments using adult rat diaphragm as the muscle source gave values of K_D = 3.3 nM and B_{max} = 24 fmol/mg wet weight. These values are in good agreement with values previously reported for rat leg muscle (1) and, also, with values measured in whole diaphragm (32) and small pieces of muscle (14), indicating homogenization did not adversely affect the STX receptor.

To study the development of the TTX-sensitive channel, an estimate of B_{max}, as a function of postnatal age, was obtained by assaying binding at 15 nM [^{3}H]STX in the absence and presence of 2 μM TTX. At this concentration 83% of the receptors will have bound [^{3}H]STX. Higher concentrations, although they saturate a greater percentage of the sites, give a less favorable ratio of specific to nonspecific binding. Figure 15.2 illustrates the time course of the appearance of high-affinity [^{3}H]STX binding sites for both diaphragm and triceps surae. For triceps surae, binding was approximately 10% of the adult value at day 3, the earliest age assayed, and increased in a roughly linear fashion until the adult value of 21 fmol/mg wet wt. was reached at day 21. For diaphragm, a similar linear development was observed, occurring approximately 3 days earlier than in triceps surae. Although a detailed study of K_D as a function of age was not performed, binding was measured at 25 nM [^{3}H]STX as well as 15 nM in some experiments, and the results indicated that 15 nM gave at least 83% saturation of the STX receptor sites throughout the developmental time course. The changes observed therefore represent changes in B_{max} for [^{3}H]STX binding.

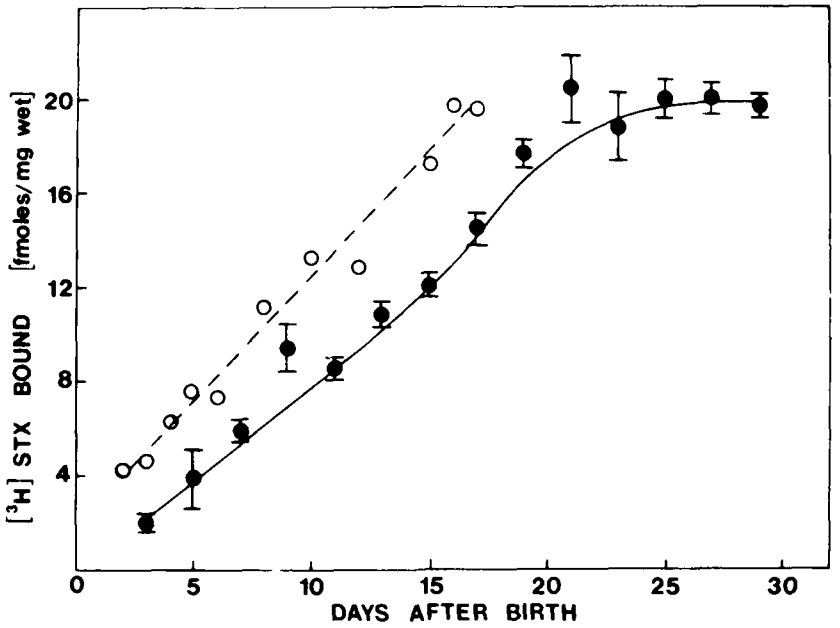

Figure 15.2. Development of TTX-sensitive sodium channels *in vivo*. The specific binding of [^{3}H]STX at 15 n*M* to homogenates of triceps surae (●) and diaphragm (○) was determined as a function of postnatal age. The error bars denote ± s.e.m. for data from at least three separate groups of animals.

The motor neuron has a profound regulatory effect not only on the voltage-sensitive sodium channel but also on the acetylcholine receptor (AChR) and acetylcholinesterase (7, 42). Thus it is of interest to compare the time course for changes in these three proteins that are essential for neuromuscular transmission. During development of rat diaphragm, AChR's are located along the entire length of the muscle fibers. As development proceeds, extrajunctional AChR's are progressively lost until finally AChR's are located only in the region of the neuromuscular junction (7). Figure 15.3 compares the developmental increase in TTX-sensitive sodium channels to the decrease in extrajunctional AChR's. The solid circles are the same data shown in Fig. 15.2 for diaphragm. The open circles represent the data of Steinbach et al. (39), who used several methods to estimate the percentage of AChR's that were extrajunctional in developing rat diaphragm. Their data have been averaged and are represented by a single point ± s.e.m. for each age. As shown, these two processes have a remarkably similar time course. Both have occurred to a small extent by birth and continue in a roughly linear fashion for the next 3 weeks, when adult levels are achieved. The end-plate specific form of acetylcholinesterase appears in rat skeletal muscles over a generally similar time course (42). It seems likely that the concordant development of the adult forms of these proteins reflects an important functional maturation in neuromuscular transmission.

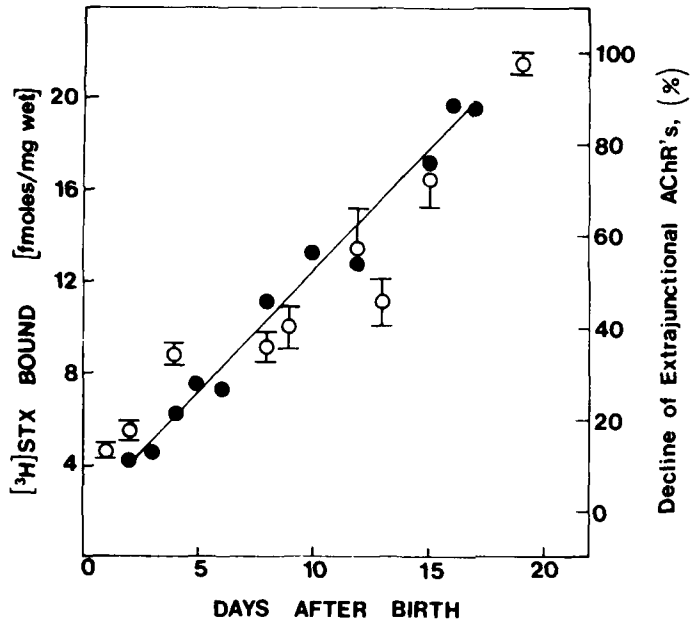

Figure 15.3. Comparison of the development of TTX-sensitive sodium channels and loss of extrajunctional acetylcholine receptors. The specific binding of [^{3}H]STX to diaphragm (●) is redrawn from Fig. 15.2. The percentage decrease of extrajunctional acetylcholine receptors (○) is derived from the data of Steinbach et al.[39] Error bars represent ± s.e.m.

Since the motor neuron has such a profound regulatory influence on a wide variety of muscle properties, including the presence of TTX-insensitive sodium channels (2, 18, 26, 30, 33, 37) the effect of denervation on the development of TTX-sensitive channels is of great interest. Previous studies of the effects of denervation of adult skeletal muscle on the density of TTX-sensitive sodium channels are not in close agreement. Recent voltage clamp studies indicate that after denervation at least 75% of the sodium current is carried by the TTX-sensitive sodium channel (26). Hansen Bay and Strichartz (14) found that denervation of the extensor digitorum longus of rat caused a 20% decrease in [^{3}H]STX binding per milligram wet weight, but this decrease was not considered statistically significant. Ritchie and Rogart (32) found a 32% decrease in [^{3}H]STX binding to intact rat diaphragm but attributed this to postdenervation swelling of the muscle fibers, and they concluded that there was no change in the sarcolemmal density of the TTX-sensitive sodium channels. On the other hand, Barchi and Weigele (1) found that denervation produced a 43% decrease in the binding of [^{3}H]STX to sarcolemmal membranes isolated from rat gastrocnemius and tibialis. In no case was a significant change in the K_D for [^{3}H]STX binding reported. This latter study suggests that denervation produces a true change in the sarcolemmal density of TTX-sensitive Na^+ channels. Thus, to define more clearly the role of innervation in the regulation of these channels, we have investi-

gated the effects of denervation on the density of [^{3}H]STX binding sites in rat triceps surae at several points during the developmental time course defined in Fig. 15.2. Figure 15.4 shows the results of experiments in which the triceps surae was denervated unilaterally at postnatal day 17. After a short lag period, the site density in denervated muscle begins a gradual decline that continues for the next 6 days until a plateau is reached at 9.2 fmol/mg wet wt or 47% of the adult value. The values for the contralateral control muscles are in close agreement with the data for normal development as illustrated in Fig. 15.4.

The results of similar experiments in which the triceps surae was denervated at day 11 are shown in Fig. 15.5. The STX receptor site density of the denervated muscles exhibits a gradual increase from 8.4 to 10.4 fmol/mg wet wt over the ensuing 10 days. The contralateral control muscles remained within the range of normal development. Thus, denervation at day 11 blocks essentially all further TTX-sensitive channel development leading to a plateau of 53% of the adult level. The changes in STX binding induced by denervation could reflect a markedly decreased affinity for STX rather than a reduction in the total site density. To exclude this possibility, the K_D and B_{max} values for STX binding to muscles denervated at day 11 and contralateral control muscles were determined at day 23 by Scatchard analysis (Fig. 15.6). The K_D values were found to be 2.9 nM in each case, whereas B_{max}

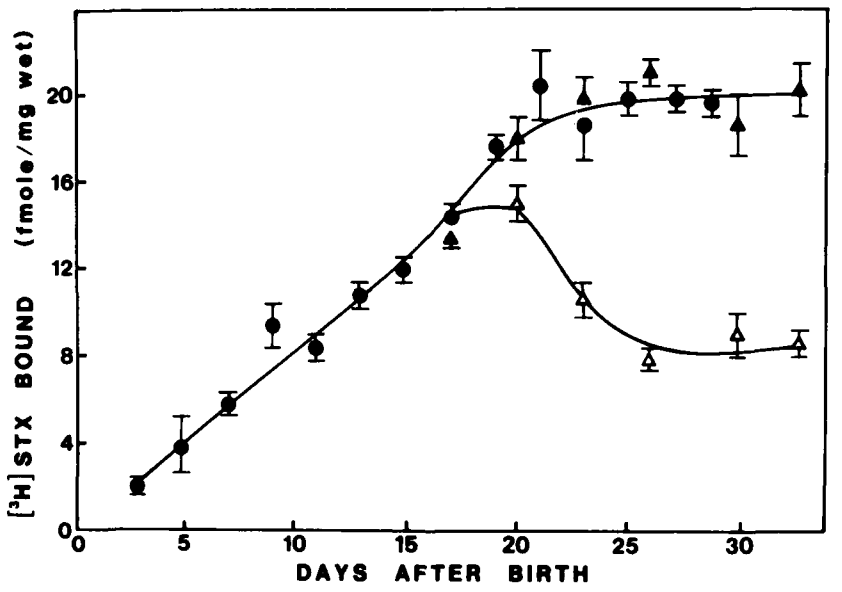

Figure 15.4. Effect of denervation at day 17 in the development of TTX-sensitive sodium channels. The triceps surae of 17-day-old animals were denervated unilaterally by section of the sciatic nerve. The muscles were removed at various times after denervation, and the specific binding of [^{3}H]STX at 15 nM was determined (△). The contralateral triceps surae served as the control (▲ and is compared with the normal developmental time course redrawn from Fig 15.2 (●). Error bars represent ± s.e.m. of four experiments.

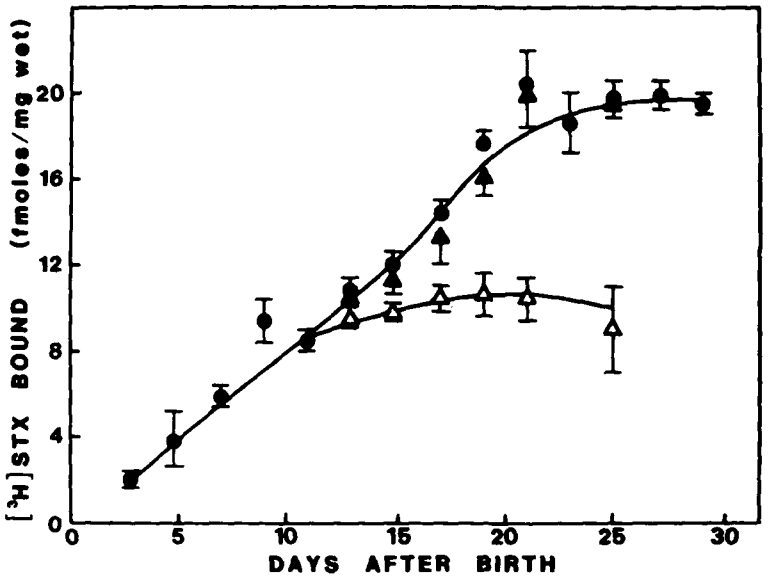

Figure 15.5. Effect of denervation at day 11 on the development of TTX-sensitive sodium channels. The triceps surae of day 11 animals were denervated. The muscles were removed at various times after denervation, and the specific binding of [^{3}H]STX at 15 n*M* was determined (△). The contralateral triceps surae served as control (▲) and is compared to the normal developmental time course (●) which is redrawn from Fig. 15.2. The error bars represent ± s.e.m. from three experiments.

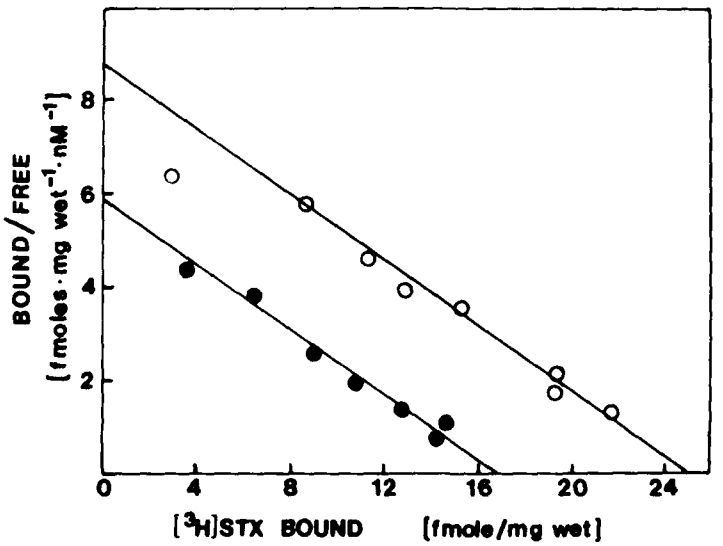

Figure 15.6. Effect of denervation on day 11 of the affinity of [^{3}H]STX for its receptor. Triceps surae muscles were denervated unilaterally on postnatal day 11 and removed 11 days later. The contralateral triceps surae served as controls. Specific binding of [^{3}H]STX was determined at concentrations ranging from 1 to 30 n*M* and is presented as a Scatchard plot. Denervated muscles (●) gave values of K_D = 2.9 n*M* and B_{max} = 16.8 fmol/mg wet wt. Control muscles (○) gave values of K_D = 2.9 n*M* and B_{max} = 25 fmol/mg wet wt.

decreased from 25 to 16.5 fmol/ mg wet wt. This indicates that denervation causes a true reduction in the number of TTX-sensitive channels.

In contrast to denervation at day 11 and 17, denervation at day 5 had a biphasic effect. From day 5 through day 9, STX receptor density increased at a similar rate in both control and denervated muscles (Fig. 15.7). From day 9 through day 13, STX receptor density actually increased more rapidly in denervated muscles than in controls. This increased rate of development led to a statistically significant increase in receptor levels on days 11 through 15 in denervated muscle as compared with control muscles ($p < .01$, Student's t-test). Throughout the entire developmental time course, the STX receptor densities for contralateral control muscles were within the range of values observed for normal animals. Thus our results show that continuing innervation is not required for the first phase of development of TTX-sensitive channels from day 5 to 13 after birth and actually slows the appearance of TTX-sensitive channels on days 9 through 13.

In muscles denervated at day 5, however, the development of STX receptor sites stops abruptly on day 13 (Fig. 15.7) and begins a gradual decline. By day 17, the STX receptor site density has dropped below that of controls and eventually reaches a plateau value of 11.1 fmol/mg wet wt, or 57% of the final adult value. Thus, as observed in muscles denervated at days 11 or 17, continuing innervation is required for maintenance of a STX receptor site

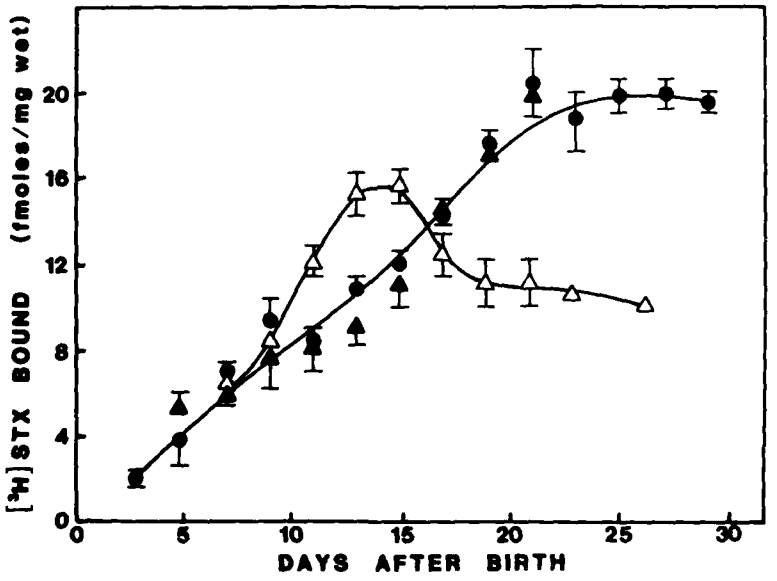

Figure 15.7. Effect of denervation at day 5 on the development of TTX-sensitive sodium channels. The triceps surae of 5-day animals were denervated unilaterally. The denervated muscles were removed at various times after denervation, and the specific binding [³H]STX was determined at 15 n*M* (△). The contralateral triceps surae served as control (▲) and is compared with the normal developmental time course (●) redrawn from Fig. 15.2. The error bars represent ± s.e.m. of three experiments.

density above approximately 11 fmol/mg wet wt. Denervation at day 5, 11, or 17 results in TTX-sensitive channel development to approximately the same final plateau level of 47–57% of the adult value.

These results define a biphasic regulation of appearance of TTX-sensitive channels by innervation. Continuing innervation is not required for development of high-affinity STX receptor sites from days 5–11 after birth and actually slows the increase in site density on days 9–11. The initial innervation-independent phase of development results in the appearance of 47–57% of the adult complement of TTX-sensitive channels. This critical density of TTX-sensitive channels is reached after denervation at 5, 11, or 17 days. After day 11, continuing innervation is required for the development and maintenance of a STX receptor site density greater than 11 fmol/mg wet wt. This second innervation-dependent phase of development results in the achievement of the adult complement of TTX-sensitive channels by postnatal day 25. It is probable that the loss of up to 40% of STX receptor sites upon denervation of adult muscle (1, 14, 32) also represents a reversal of the second, innervation-dependent phase of development. Since the complete time course of the effect of denervation was not determined in the previous studies of adult muscle (1, 14, 32), the values reported may not reflect the final extent of the receptor site decrease.

2. TTX-SENSITIVE AND INSENSITIVE SODIUM CHANNELS IN CULTURED RAT MUSCLE CELLS

Myocytes obtained from enzymatically dissociated fetal muscle and maintained under tissue culture conditions have been studied extensively since they undergo many of the same maturational changes that occur *in vivo*. As observed during normal myogenesis, cultured myocytes fuse together to form multinucleate myotubes (43), they express the muscle-specific proteins necessary for contraction (34), and they form functional synapses with cholinergic neurons (8). Since a wide variety of experimental manipulations that are not feasible in the whole animal can be easily performed *in vitro*, these cultured muscle cells may provide a useful model system for the study of the development and regulation of voltage-sensitive Na^+ channels. Of course, it is first necessary to characterize fully the voltage-sensitive Na^+ channels present *in vitro*.

In previous electrophysiological and ion flux studies of cultured rat muscle cells (2, 18, 20, 33, 37), only TTX-insensitive Na^+ channels were detected. Since we found an innervation-independent phase of development, it was of interest to examine cultured rat muscle cells more closely for the presence of TTX-sensitive channels. Our more recent studies demonstrate the coexistence of TTX-sensitive and TTX-insensitive Na^+ channels in primary cultures of fetal rat muscle and compare their neurotoxin-binding characteristics and developmental regulation (35).

To detect a small number of TTX-sensitive Na^+ channels directly, specific binding of [^{3}H]STX in homogenates of cultured fetal muscle cells was measured using the same methods described earlier for muscle from postnatal rats. Since technical difficulties prevent the accurate measurement of the wet weight of cultured cells, the density of binding sites present *in vitro* is expressed and compared to whole muscle on the basis of femtomoles per milligram of total cellular protein. Figure 15.8*a* shows the total and nonspecific binding of [^{3}H]STX to a homogenate of fetal rat muscle cells maintained in culture for 11 days. In Fig. 15.8*b*, the specific binding has been calculated from the data in Fig. 15.1*a* and is presented as a Scatchard plot. The data are best fit by a straight line which indicates that there is a single class of saturable sites with K_D = 9.6 n*M* at 36°C. At 0°C, the K_D for STX is 3 n*M* (data not shown). In the experiment of Fig. 15.8, the total number of these high-affinity sites was 72.4 fmol/mg protein. The average of six separate experiments gave a value for the total number of STX receptors of 69.3 ± 11.3 fmol/mg protein. The affinity of TTX for these receptor sites can be determined by measuring the displacement of specifically bound [^{3}H]STX by increasing concentrations of TTX. The K_D for TTX measured by this competitive inhibition of [^{3}H]STX binding was found to be 39.2 n*M* (data not shown, see ref. 35).

These results indicate that high-affinity STX receptors, similar to those found in adult skeletal muscle, are present in substantial numbers in uninnervated cultured fetal muscle cells. The K_D values for [^{3}H]STX and TTX binding are in good agreement with values reported for adult muscle (1, 14, 32),

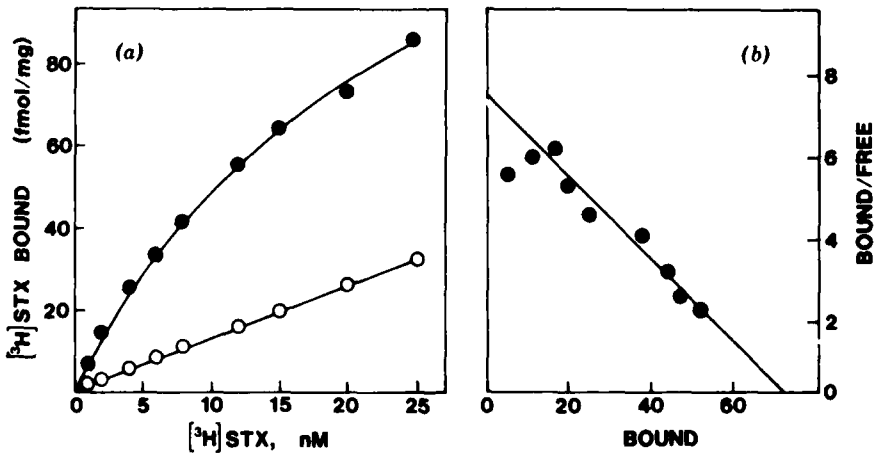

Figure 15.8. Binding of [^{3}H]STX to TTX-sensitive sodium channels in homogenates of cultured fetal rat muscle. (*a*) Muscle homogenates were incubated with increasing concentrations of [^{3}H]STX (●) or [^{3}H]STX plus 2 μM TTX (○) and the bound [^{3}H]STX determined by rapid filtration. (*b*) Specific binding was calculated from the data in (*a*) and is presented as a Scatchard plot. The units shown on the abscissa are femtomoles per milligram protein. The units shown on the ordinate are femtomoles per milligram per nanomolar concentration. Least squares analysis gave values of: K_D = 9.6 n*M* and B_{max} = 72 fmol/mg protein.

and the density of high-affinity STX receptors on cultured muscle cells represents 58 ± 9.2% of the adult density when compared on the basis of femtomoles [^{3}H]STX bound per milligram protein. Although cultured fetal and normal adult muscle may differ with respect to the ratio of sarcolemmal surface area to total fiber protein, it seems clear that the number of high-affinity STX receptors in cultured fetal rat muscle cells represents a substantial fraction of the adult density.

In other experiments, in which [^{3}H]STX binding to intact monolayers of cultured muscle cells was measured, Scatchard analysis gave values of 48.6 ± 11.6 fmol/mg protein. The ratio of specific to nonspecific binding was lower in these experiments, and the results from intact cells are therefore less accurate than the results from binding experiments performed with muscle cell homogenates. Nevertheless, these results indicate that most, if not all, of the high-affinity STX receptors are present on the surface of the muscle cells as in adult muscle.

Since the TTX-insensitive sodium channels in these rat muscle cells have a K_I for STX of 0.25 μM (35), only 2% of these sites will be occupied at the highest concentrations of STX used in our binding experiments. At concentrations of [^{3}H]STX high enough to occupy a substantial fraction of these sites, the nonspecific component of toxin binding becomes so large that specific binding to these low-affinity sites is obscured. Therefore, TTX-insensitive sodium channels in these muscle cells are best studied by ion flux procedures.

Muscle fibers newly formed *in vitro* contract spontaneously. Sodium channels are required for this spontaneous activity since it is inhibited by TTX. To examine the physiological role of TTX-sensitive and -insensitive sodium channels in this contractile activity, we have studied the effect of increasing concentrations of TTX on spontaneous muscle cell contraction. In the dense cultures of muscle cells that are optimal for our biochemical experiments, the myotubes in a single microscopic field usually contract synchronously. The effect of TTX is an all-or-none inhibition of the contraction of the group of cells rather than a progressive reduction in contractile rate. Therefore we measured the fraction of multiwell cultures that contracted spontaneously in the presence of increasing TTX concentrations (Fig. 15.9). Spontaneous contraction was inhibited with a K_I = 26 nM. This inhibition was reversible; after extensive washes contractile activity returned to control values. The inset in Fig. 15.9 shows an Eadie–Hofstee plot of these data. The points are best fit by a straight line, indicating that a single class of sites is responsible for the inhibition of contraction. The K_I of TTX for inhibition of spontaneous contractile activity agrees well with its K_D derived from [^{3}H]STX displacement. This is consistent with the conclusion that TTX-sensitive Na^+ channels are required for spontaneous contractile activity and indicates that the high-affinity [^{3}H]STX-binding sites present in these cells are associated with physiologically active Na^+ channels.

The voltage-sensitive Na^+ channels present in monolayers of cultured

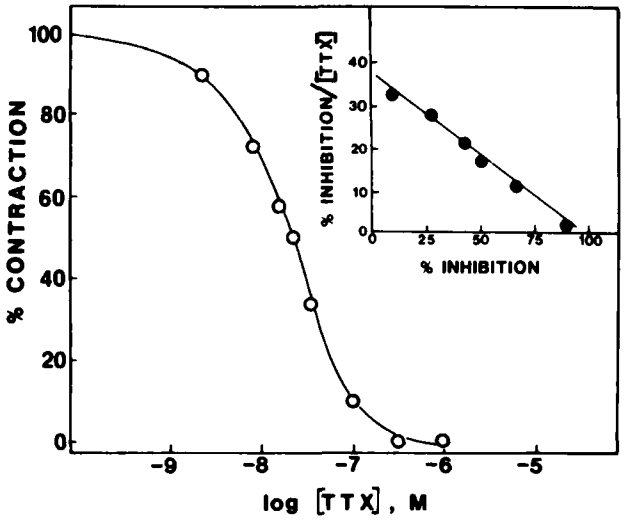

Figure 15.9. Inhibition of spontaneous contractile activity determined in the presence of increasing concentrations of TTX as described in the text. In the inset the data are redrawn as an Eadie–Hofstee plot. The K_I calculated from these data is 26 n*M*.

cells may be effectively studied using ion flux techniques (2, 20, 33, 37). The influx of $^{22}Na^+$ that is mediated by voltage-sensitive Na^+ channels can be readily quantitated when these channels have been persistently activated by neurotoxins. When the rate of $^{22}Na^+$ influx is measured under conditions of constant membrane potential, the values obtained accurately reflect the density of voltage-sensitive Na^+ channels present (20).

At least three distinct neurotoxin receptor sites are present on both TTX-sensitive and -insensitive channels (4). STX and TTX block ionic flux by binding to neurotoxin receptor site 1. As described earlier, the large differences in the affinity of these toxins for receptor site 1 are useful in differentiating the adult (TTX-sensitive) and embryonic (TTX-insensitive) forms of the voltage-sensitive Na^+ channel. The alkaloids veratridine and batrachotoxin bind at neurotoxin receptor site 2 and exert similar effects on both TTX-sensitive and -insensitive Na^+ channels (20). These toxins both shift the voltage dependence of activation and block inactivation and thereby cause persistent activation of Na^+ channels at the resting membrane potential (4). Polypeptide toxins isolated from scorpion venoms or sea anemone nematocysts bind at neurotoxin receptor site 3, inhibit sodium channel inactivation, and enhance the persistent activation of sodium channels produced by alkaloid toxins (4). TTX-sensitive sodium channels in nerve cells bind scorpion toxin with high affinity and sea anemone toxin with relatively low affinity (4, 5). In contrast, TTX-insensitive sodium channels in cultured rat muscle cells have higher affinity for sea anemone toxin II than for scorpion toxin (20, 21). Thus, in comparison to sodium channels in nerve, the toxin-binding affinity of TTX-insensitive sodium channels in cultured rat muscle

cells appears different at neurotoxin receptor site 3 as well neurotoxin receptor site 1.

Figure 15.10*a* shows the effect of increasing concentrations of TTX on $^{22}Na^+$ influx stimulated by incubation with 200 μM veratridine plus 30 nM scorpion toxin. It is evident that inhibition occurs over about four orders of magnitude of TTX concentrations, suggesting a heterogeneous population of TTX receptors. Nearly 40% inhibition is produced by 10^{-7} M TTX, a concentration that should inhibit only 5% of influx due to the TTX-insensitive Na^+ channel (20, 35). Thus, under these conditions, TTX-sensitive sodium channels are persistently activated. In Fig. 15.10*b*, these data are replotted as an Eadie–Hofstee plot. The curvilinear plot indicates the presence of both TTX-sensitive and -insensitive $^{22}Na^+$ influx. A computer-derived, least sum of squares fit of these data to a two-site model defines a high-affinity site with a K_I of 21 nM accounting for 40.8% of the $^{22}Na^+$ influx and a low-affinity site with a K_I of 1.8 μM accounting for 59.2% of the $^{22}Na^+$ influx. The K_I of the high-affinity site is consistent with the K_D of TTX derived from [^{3}H]STX displacement experiments (39.2 nM) and with the K_I for inhibition of spontaneous contractile activity (26 nM, Fig. 15.9).

Our experiments clearly show that uninnervated rat muscle cells cultured *in vitro* have a substantial number of the TTX-sensitive sodium channels characteristic of adult muscle. The STX receptor sites present in these cells bind STX and TTX with K_D values (9.6 nM and 39 nM at 36°C) that are very similar to those of adult rat muscle (1, 4, 14, 31, 32). The binding capacity expressed in femtomoles per milligram of protein is 58% of that of adult muscle. These high-affinity STX receptors are associated with functional sodium channels since binding of TTX at this site is sufficient to block spontaneous contraction of the cultured muscle cells (K_I = 26 nM). The TTX-sensitive sodium channels can be effectively activated by incubation of the cells with veratridine plus scorpion toxin. Under these conditions, they contribute 40.8% of the neurotoxin-activated $^{22}Na^+$ influx and are blocked by TTX with a K_I of 21 nM.

Since primary cultures of fetal muscle cells contain both TTX-sensitive and -insensitive sodium channels, they provide an excellent system in which to compare the sensitivities of the two classes of channels to various neurotoxins. At each activating neurotoxin concentration, Na^+ influx was measured in the presence and absence of 10^{-7} M TTX. This concentration should inhibit 85% of the TTX-sensitive influx but only 5% of the TTX-insensitive influx. Thus TTX-sensitive influx is defined as the difference between total influx and influx in the presence of 10^{-7} M TTX. TTX-insensitive influx is defined as the difference between influx in the presence of 10^{-7} M TTX and background influx measured in the absence of activating neurotoxins. The effect of veratridine on TTX-sensitive and -insensitive $^{22}Na^+$ influx was determined in this manner over a concentration range of 10–300 μM. The TTX-sensitive $^{22}Na^+$ flux was approximately 45% of the TTX-insensitive influx, or approximately 30% of the total influx at all concentrations tested.

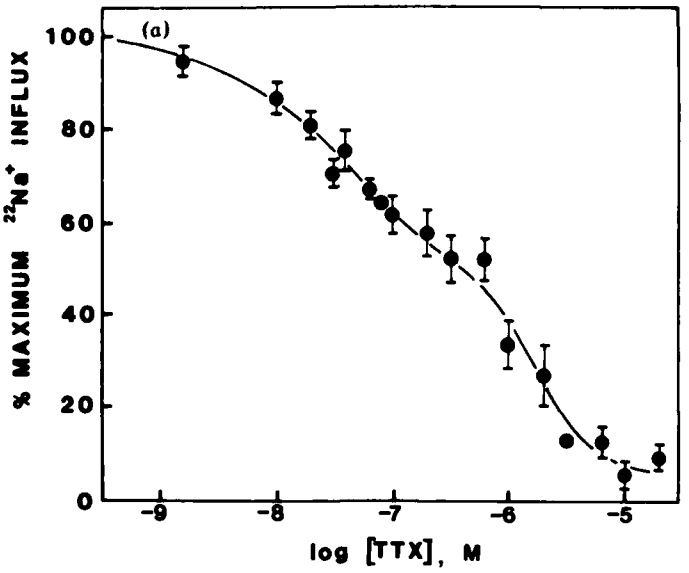

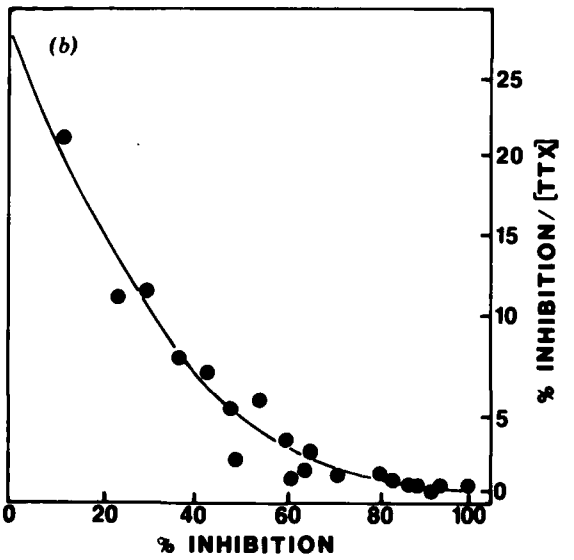

Figure 15.10. Inhibition of scorpion toxin and veratridine-activated $^{22}Na^+$ influx by TTX. (*a*) Cultured rat muscle cells were first incubated with 30 n*M* scorpion toxin plus TTX at the indicated concentrations. The initial rate of $^{22}Na^+$ influx was then measured in the presence of 200 μM veratridine plus the indicated concentrations of TTX. Error bars represent the s.e.m. of at least three determinations. (*b*) The data from (*a*) are presented as an Eadie–Hofstee plot. The best fit to a two-site model gave K_I values of 21 n*M* and 1.7 μM, accounting for 40.8 and 59.2% of the $^{22}Na^+$ influx, respectively.

The $K_{0.5}$ for veratridine activation of TTX-sensitive and -insensitive channels was 51 μM and 72 μM, respectively.

The alkaloid neurotoxins such as veratridine and batrachotoxin are able to cause persistent activation of the Na^+ channel and thus enhance Na^+ influx (4, 25). In contrast, the polypeptide toxins, scorpion toxin and sea anemone toxin II, block sodium channel inactivation but do not cause persistent activation (4). The polypeptide toxins do, however, enhance the persistent activation caused by the alkaloid neurotoxins through the allosteric coupling of the polypeptide and alkaloid neurotoxin binding sites (4). In neuroblastoma cell lines (3) and in synaptosomes (19, 41) the polypeptide neurotoxins decrease the $K_{0.5}$ of the full agonist batrachotoxin and both reduce $K_{0.5}$ and increase the fraction of sodium channels activated by the partial agonist veratridine. To test the affinity of the polypeptide toxins for the TTX-sensitive and -insensitive sodium channels in cultured muscle, we have investigated their ability to enhance the $^{22}Na^+$ influx caused by veratridine. Figure 15.11 shows the effect of increasing concentrations of scorpion toxin on $^{22}Na^+$ influx produced by 50 μM veratridine. Both TTX-sensitive and -insensitive $^{22}Na^+$ influx are substantially enhanced (2.7 and 5.0-fold, respectively) by scorpion toxin. The $K_{0.5}$ for this effect, however, is substan-

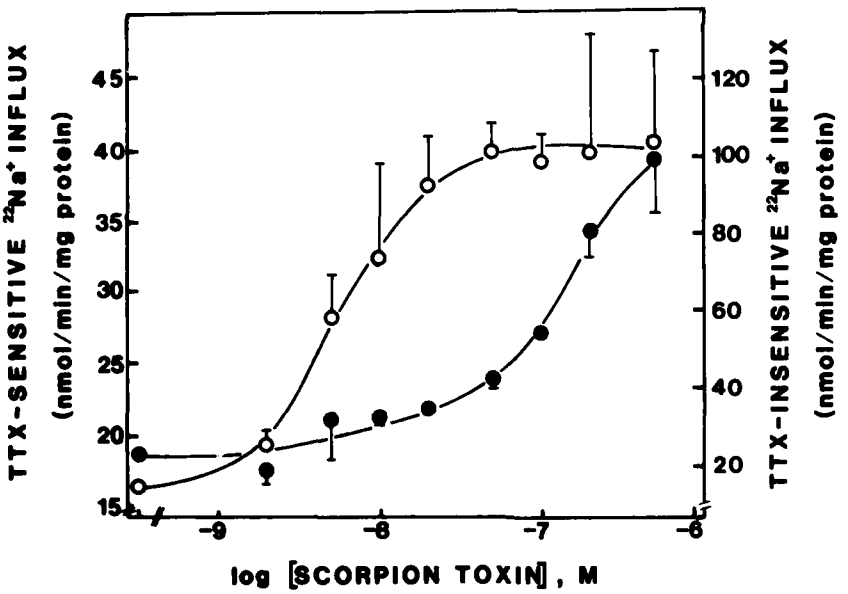

Figure 15.11. Effect of scorpion toxin on veratridine-induced $^{22}Na^+$ influx. Cultured muscle cells were first incubated with increasing concentrations of scorpion toxin. The initial rate of $^{22}Na^+$ influx was then determined in the presence of 50 μM veratridine plus the indicated concentration of scorpion toxin. TTX-sensitive and -insensitive components were determined by performing experiments with and without 10^{-7} TTX as described in the text. Note that different ordinate scales are used for TTX-sensitive and -insensitive influx. Error bars represent the s.e.m. of at least three separate experiments. The $K_{0.5}$ values for enhancement of TTX-sensitive (○) and TTX-insensitive (●) Na^+ influx are 6 nM and 150 nM, respectively.

tially different for the two types of Na^+ channels. The $K_{0.5}$ for the TTX-sensitive channel is 6 n*M*, whereas the TTX-insensitive channel has a $K_{0.5}$ of 150 n*M*. Thus, like the TTX-sensitive sodium channel of nerve, the TTX-sensitive sodium channel of cultured rat muscle cells has high affinity for scorpion toxin relative to TTX-insensitive sodium channels.

The effect of sea anemone toxin II on veratridine activation of sodium channels was also investigated. TTX-insensitive $^{22}Na^+$ flux stimulated by 50 μM veratridine is increased nearly 2.4-fold by 500 n*M* sea anemone toxin II (from 74.8 ± 8.3 to 207 ± 11 nmol/min mg protein). TTX-sensitive flux, however, is apparently unaffected. Veratridine alone at 50 μM gave a value of 22.7 ± 1.1 nmol/min mg protein while 50 μM veratridine plus 500 n*M* sea anemone toxin II produced a value of 21.9 ± 9.7 fmol/min mg protein. Because of the large activation of the TTX-insensitive channel by sea anemone toxin II, it is difficult to obtain an accurate estimate of the TTX-sensitive component. In view of the large error associated with these measurements it is not possible to conclude that sea anemone toxin II is completely without effect at the TTX-sensitive Na^+ channel. Nevertheless, it is clear that sea anemone toxin II is a much poorer activator of the TTX-sensitive channel than at the TTX-insensitive channel. Thus the TTX-sensitive sodium channel of cultured muscle is similar to the TTX-sensitive channel found in neural tissue with regard to the potency of polypeptide neurotoxins acting at receptor site 3. The differential toxin sensitivities at receptor site 3 probably explain the failure of other studies (2, 10, 33, 37) to detect TTX-sensitive Na^+ flux in cultured rat muscle. In these studies the voltage-sensitive Na^+ channels were activated by anemone toxin II plus an alkaloid-neurotoxin. This combination of neurotoxins will fully activate the TTX-insensitive channels and thereby obscure the relatively smaller TTX-sensitive Na^+ influx.

3. DEVELOPMENTAL REGULATION OF TTX-SENSITIVE SODIUM CHANNELS *IN VITRO*

The TTX-sensitive and -insensitive sodium channels differ not only in the neurotoxin sensitivities just described but also in their *in vivo* regulation by motor neuron innervation. Since the *in vitro* development of Na^+ channels in primary muscle cultures occurs in the absence of innervation, it was of interest to determine the time courses of development of TTX-sensitive and -insensitive Na^+ channels and compare them with the results from *in vivo* experiments. The development of TTX-sensitive Na^+ channels was assessed by measuring the total number of [^{3}H]STX-binding sites as the muscle cells matured in cell culture. The development of the TTX-insensitive Na^+ channel was assessed by measuring the amount of $^{22}Na^+$ influx elicited by maximal neurotoxin stimulation with sea anemone toxin II and batrachotoxin as a function of time in culture.

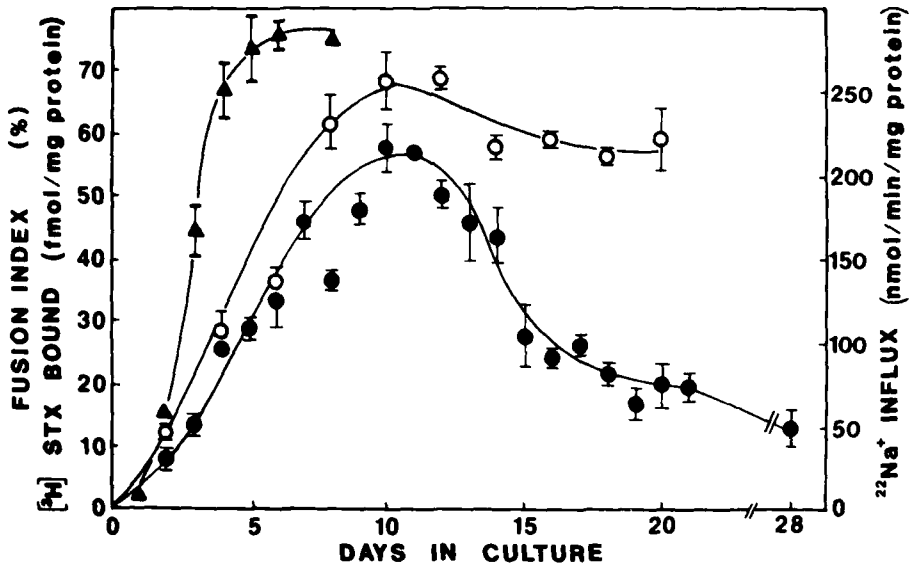

Figure 15.12. Developmental time course of TTX-sensitive and -insensitive sodium channels. TTX-insensitive influx (○) was measured as a function of time maintained in culture by activating Na^+ channels with 2.4 μM batrachotoxin and 1 μM sea anemone toxin II in the presence of 10^{-7} M TTX. Specific binding of [^{3}H]STX (●) was measured in cell homogenates with 15 nM[^{3}H]STX at 0°C. The fusion index (▲) was determined as described in the text. Error bars represent the s.e.m. of at least three experiments.

As shown in Fig. 15.12 the development of [^{3}H]STX-binding sites is biphasic. The density of binding sites increases from an undetectable level on the first day in culture to a maximum level of 59 fmol/mg protein at day 10. During days 10–16 there is a decline in the binding-site density until a plateau level of 21 fmol/mg protein is reached. The [^{3}H]STX-binding sites do not completely disappear, since at day 28 there are still 12 fmol STX-binding sites per milligram of protein present.

In contrast to the biphasic time course of development of the high-affinity [^{3}H]STX-binding sites, the $^{22}Na^+$ influx data (Fig. 15.12) indicate that the TTX-insensitive sodium channels appear in parallel with TTX-sensitive channels until day 10, but then remain at a plateau level that is 85% of the maximum value until day 20, while the level of [^{3}H]STX-binding sites is reduced. To be certain that the different time course of development of the TTX-sensitive and -insensitive sodium channels was not due to the different methods of measurement used, we also examined the level of TTX-sensitive $^{22}Na^+$ influx in one set of cultures after incubation with 200 μM veratridine plus 30 nM scorpion toxin. At day 11, TTX-sensitive $^{22}Na^+$ influx was 42.7 nmol/min mg and declined to 15.8 nmol/min mg at day 15. These results suggest that the TTX-sensitive and -insensitive sodium channels are regulated by means of separate pathways in muscle cells developing *in vitro* in the absence of innervation, as well as *in vivo*.

In Fig. 15.12, we have also presented the time course of fusion of mononucleate myocytes into multinucleate myotubes. The fusion index, which is equal to the percent of nuclei in myotubes, increases from 0 to 72% during days 0–4 of growth *in vitro*. Fusion is essentially complete by day 4 when the values of [^{3}H]STX binding and TTX-insensitive Na^+ influx are less than 30% of their maximum levels. These data indicate that both types of sodium channels appear after fusion of myoblasts into myotubes during normal muscle development. During postnatal development *in vivo*, TTX-insensitive sodium channels are lost (15) and TTX-sensitive sodium channels appear (Fig. 15.2). Since denervation of adult muscle causes the reappearance of TTX-insensitive sodium channels (26, 30), it is likely that the level of these channels is regulated by the motor neuron. The regulation of TTX-sensitive sodium channels by innervation is more complex, as discussed in the first section of this chapter. The pattern of development of TTX-sensitive and -insensitive sodium channels in cell culture parallels their development *in vivo*. As expected for denervated skeletal muscle, TTX-insensitive sodium channels appear within a few days *in vitro* and are maintained at a plateau level throughtout the life of the cultures (Fig. 15.12). In contrast, TTX-sensitive sodium channels initially increase along the same time course but subsequently decline to a low level (Fig. 15.12). This time course is very similar to that of development of TTX-sensitive sodium channels in denervated muscle *in vivo*.

Figure 15.13 compares the appearance of TTX-sensitive sodium channels in muscle cells denervated at day 0 *in vitro* or day 5 *in vivo*. The results from the experiment shown in Fig. 15.7 have been expressed in terms of femtomoles of [^{3}H]STX bound per milligram of protein to allow direct comparison to the *in vitro* results shown in Fig. 15.12. Since the cultured muscle cells are prepared from fetal rats during the last day of gestation, the time maintained *in vitro* corresponds to the *postpartum* age *in vivo*. When compared in this manner, the results show that *in vivo* and *in vitro* development follow a parallel time course until day 10. At this time, the *in vitro* density of TTX-sensitive channels reaches a peak and then declines to a new plateau level. STX receptor density of skeletal muscle denervated *in vivo* continues increasing to achieve a much greater peak value at days 11–13. Subsequently, as *in vitro*, the density of high-affinity STX receptors *in vivo* declines to a final plateau value. In both cases, receptor development continues for 8–10 days after denervation and then declines over the next 4–6 days to reach a final plateau value. Since the results presented in the first section of this chapter indicate that continuing innervation is required for the development of TTX-sensitive sodium channels after postnatal day 11, it seems likely that the reduction in the level of TTX-sensitive Na^+ channels maintained for more than 10 days *in vitro* is also due to lack of innervation. Thus the development of TTX-sensitive channels observed *in vitro* correlates with the first innervation-independent phase of development *in vivo*. Since the *in vitro* cell culture system follows the pattern of development observed *in*

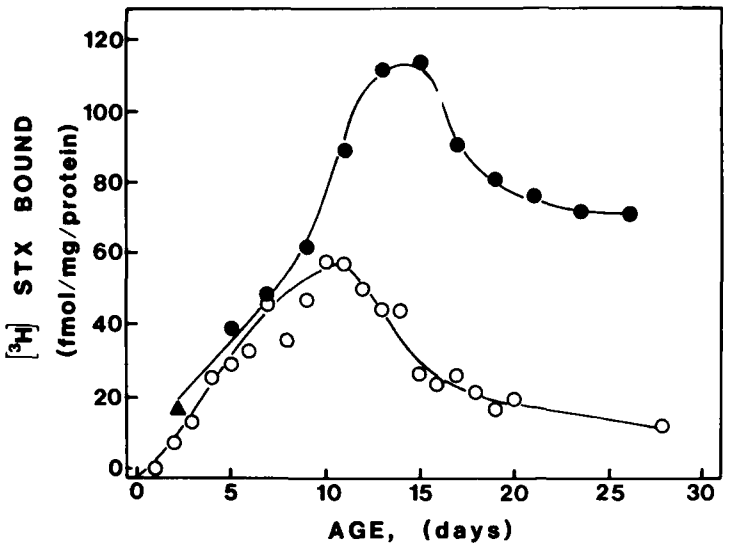

Figure 15.13. Comparison of STX receptor development *in vivo* and *in vitro*. Data for STX receptor development *in vitro* (○) are redrawn from Fig. 15.12. Data for *in vivo* development (see Fig. 15.7) show the time course for STX receptor development in triceps surae of rats in which this muscle was denervated at day 5 (●). The value for STX receptor density *in vivo* at day 3 (▲) is for innervated triceps surae.

vivo, it is likely that this experimental system will provide a good model for examining the mechanism of neuronal regulation of TTX-sensitive sodium channels in mammaliam muscle.

As described earlier, innervation plays an important role in the developmental regulation of the TTX-sensitive sodium channel. These effects of innervation may be mediated by neurally imposed electrical activity or by neurally released chemical factors (12). It is difficult to assess the relative importance of these two mechanisms in experiments performed *in vivo*. We have therefore investigated the role of electrical activity and cytosolic Ca^{2+}, *in vitro*, in uninnervated cultures of fetal muscle cells. As shown in Fig. 15.8 these cells display a spontaneous electrical and contractile activity that is mediated, at least in part, by the TTX-sensitive sodium channel. We have investigated the regulatory role of this electrical activity by determining its effect on the *in vitro* development of [^{3}H]STX-binding sites.

Figure 15.14 shows the effect of blocking spontaneous contractile activity on the time course of development of TTX-sensitive sodium channels. After 4 days in culture, cells were grown in the presence of 1 μM TTX, 40 μM bupivacaine, or 50 mM KCl. TTX and the local anesthetic bupivacaine eliminate electrical activity directly by blocking ionic flux through the voltage-sensitive sodium channel, whereas maintenance in 50 mM KCl abolishes spontaneous electrical activity indirectly by chronically depolarizing the cells and inactivating the sodium channels. Each of these treatments produced a significant increase in the number of TTX-sensitive sodium chan-

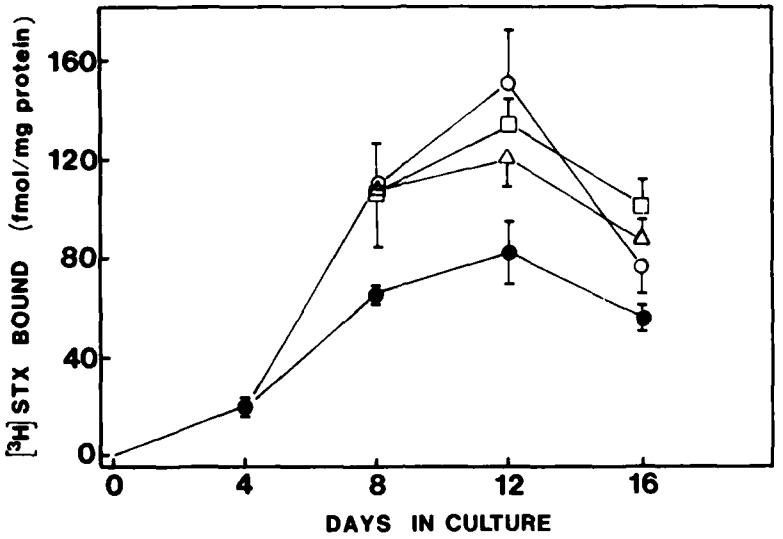

Figure 15.14. Pharmacological blockade of spontaneous contractile activity increases the density of TTX-sensitive sodium channels. After 4 days in culture, muscle cells were maintained for the indicated period of time in growth medium containing 40 μM bupivacaine (○), 1 μM TTX (□), 50 mM KCl (△), or no additions (●). The specific binding of [^{3}H]STX at 15 nM to muscle cell homogenates was then determined. Error bars represent ± s.e.m.

nels measured at days 8, 12, and 16 (Fig. 15.14). The treated cells still show a decline in channel number after day 12 that parallels the decrease observed in the controls. Thus the regulatory effect produced by blocking spontaneous electrical activity is apparently superimposed upon whatever regulatory process is responsible for the biphasic nature of the developmental time course observed in the control cultures. In addition to the foregoing methods of eliminating spontaneous electrical activity, we also examined the effects of treating cells with veratridine (10 μM) which blocks action potential production by causing chronic depolarization due to increased influx of extracellular Na^+ (4). At day 12, veratridine-treated cells had 2.1-fold more TTX-sensitive channels than controls ($p < .005$, Student's t-test).

Since the increase in sodium channel number is caused by indirect blockade of electrical activity as well as by agents that act directly on the voltage-sensitive sodium channel at different receptor sites (4, 25), it seems unlikely that this effect simply results from receptor-ligand interaction. Rather, the common mechanism must be related to the loss of spontaneous electrical activity. Block of spontaneous electrical activity in skeletal muscle prevents the phasic increase in cytosolic Ca^{2+} that accompanies each contraction. To evaluate the role of Ca^{2+} in regulation of sodium channel density, we examined the effect of the Ca^{2+} ionophore A23187. This ionophore specifically increases the permeability of both sarcolemmal and sarcoplasmic reticulum membranes to Ca^{2+} (13, 17) and causes both an increase in cytosolic Ca^{2+} and a tonic contracture of intact muscle (13, 38). Figure 15.15 shows that

growth of cells in the presence of 1 μM A23187 nearly abolishes the further development of TTX-sensitive sodium channels from day 4 to day 10 *in vitro*. Growth of cells in 40 μM bupivacaine leads to a five-fold increase in the number of TTX-sensitive sodium channels as compared to growth under conditions of high cytosolic Ca^{2+} (1 μM A23187). The sodium channel density of cells grown in the presence of bupivacaine plus A23187 is not significantly different from that of cells grown in A23187 alone (Fig. 15.15). This result is expected since the tonically increased Ca^{2+} influx mediated by the A23187 should override the loss of phasic Ca^{2+} influx produced by blockade of electrical activity. These results are consistent with the hypothesis that cytosolic Ca^{2+} levels modulate the levels of TTX-sensitive sodium channels in response to changes in electrical activity.

The data presented in Fig. 15.15 indicate that manipulations which affect the spontaneous electrical activity of cultured myotubes have significant regulatory effects on the density of voltage-sensitive sodium channels. It is possible to obtain an index of the extent to which a pharmacological agent blocks voltage-sensitive sodium channels by visually observing and tabulating the degree of spontaneous contractile activity that is present. If growth of cells in the presence of bupivacaine leads to an increased level of sodium channel by virtue of its specific effect on voltage-sensitive sodium channels, then the dose-response curves for inhibition of spontaneous contractile activity and increase of STX receptor density should overlap. Our results

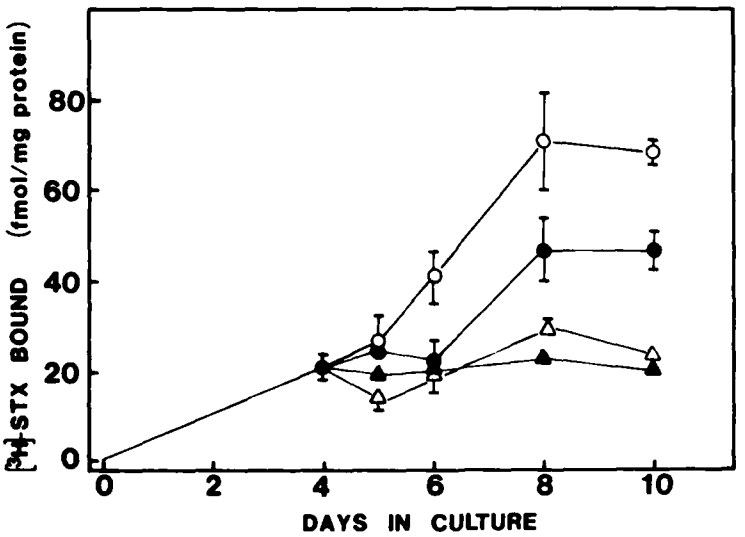

Figure 15.15. Effect of A23187 on the development of TTX-sensitive Na^+ channels. After 4 days in culture, myotubes were maintained for the indicated period of time in growth medium containing 1 μM A23187 (▲), 40 μM bupivacaine (○), 1 μM A23187 + 40 μM bupivacaine (△), or with no additions (●). The density of TTX-sensitive sodium channels was determined by measuring the specific binding of [^{3}H]STX at 15 nM. Each point represents the mean of at least three separate experiments. Error bars denote the s.e.m.

indicate that this is indeed the case. When the dose response of blockade of spontaneous contractile activity and increase in STX receptor density are expressed as the percentage of the maximal effect, the values for both of these parameters fall on a single curve with a $K_{0.5}$ of 3.3 μM. This value is in good agreement with the results of studies in which the K_D for bupivacaine was found to be 2.6 μM (27) in neurotoxin-binding experiments. This result is consistent with the conclusion that bupivacaine acts by blocking spontaneous electrical activity rather than by a nonspecific membrane effect.

A similar dose-response study was carried out in cells grown in increasing concentrations of A23187. The results indicate that A23187 induces a dose-dependent reduction in both STX receptor density and spontaneous contractile activity with a $K_{0.5}$ of 0.5 μM. At 2 μM A23187, the level of TTX-sensitive sodium channels was decreased to 24% of the control value. At this concentration of A23187 no toxic effects were apparent upon visual inspection of the cells. The inhibition of spontaneous contractile activity probably results from membrane depolarization due to increased Ca^{2+} flux (40). Our results indicate that this increased Ca^{2+} flux also reduces the number of TTX-sensitive sodium channels.

In these experiments the number of STX receptors was estimated by measuring binding in the presence of 15 nM [^{3}H]STX. We have previously shown this concentration to be sufficient to occupy greater than 85% of the receptors present (35). Nevertheless, it is possible that the regulatory effects on STX binding reflect changes in the affinity of the receptor for its ligand as well as changes in the number of sarcolemmal TTX-sensitive channels. To exclude this possibility, we have performed Scatchard analysis of [^{3}H]STX binding to control cells and cells treated with bupivacaine or A23187. Growth of cells for 6 days in the presence of 40 μM bupivacaine or 1 μM A23187 had no significant effect on the affinity of [^{3}H]STX for its receptor. The total receptor density, however, is increased 70% by treatment with bupivacaine and reduced 33% by A23187 treatment, indicating that these agents cause a true change in the sarcolemmal density of TTX-sensitive channels.

These results indicate that electrical activity can regulate the density of TTX-sensitive sodium channels in primary cultures of rat skeletal muscle. Since each action potential leads to a large transient increase in cytosolic Ca^{2+} (6), blockade of spontaneous electrical activity will undoubtedly reduce the time-averaged level of cytosolic Ca^{2+}. Thus it is an attractive hypothesis that the observed increase in sodium channel number produced by blockade of electrical activity is mediated by changes in cytosolic Ca^{2+}. The ability of A23187 to decrease TTX-sensitive channel levels gives strong support for this hypothesis. Although we have not directly determined the cytosolic Ca^{2+} levels in these experiments, it seems likely from previous investigations that A23187 increases the level of Ca^{2+} in the cytosolic pool. A23187 markedly increases the permeability of lipid bilayer membranes to Ca^{2+} (28). In skeletal muscle the cytosolic concentration of Ca^{2+} is three to four orders

of magnitude lower than either the extracellular Ca^{2+} concentration or the concentration of Ca^{2+} stored intracellularly in the sarcoplasmic reticulum (6). Thus any increase in the Ca^{2+} permeability of lipid bilayer membranes would allow Ca^{2+} to flow down its electrochemical gradient into the cytoplasm. A23187 has been shown to increase the Ca^{2+} permeability of both sarcolemmal and sarcoplasmic reticulum membranes of mammalian muscle (13, 17). Furthermore, spectrofluorimetric determination of cytosolic Ca^{2+} levels has shown that A23187 increases the concentration of cytosolic Ca^{2+} in intact barnacle muscle (17). A23187 also causes tonic contracture of intact frog skeletal muscle (38). On the basis of these results, it seems highly likely that cytosolic Ca^{2+} levels of cultured muscle cells grown in the presence of A23187 are chronically elevated. Thus blockade of spontaneous electrical activity lowers cytosolic Ca^{2+} and increases the number of TTX-sensitive channels. Conversely, growth in A23187, which almost certainly increases cytosolic Ca^{2+}, decreases the number of TTX-sensitive channels.

Taken together, our findings suggest the presence of a Ca^{2+}-mediated negative feedback loop controlling cellular excitability. Increases in electrical excitability which lead to increased cytosolic Ca^{2+} levels may, in turn, decrease the number of sodium channels and thereby decrease electrical excitability. Conversely, a paucity of electrical activity would lead to an increase in the number of electrically excitable sodium channels. In this way, the cell would be able to maintain a given level of electrical excitability by altering the sodium channel density in response to the frequency of action potentials using changes in the concentration of cytosolic Ca^{2+} as the feedback signal.

The physiological relevance of these results is somewhat uncertain. It may be argued, for example, that treatment with A23187 is an imperfect model of the increased cytosolic Ca^{2+} caused by electrical activity because sarcolemmal action potentials lead to transient rises in cytosolic Ca^{2+}, whereas the presence of ionophore causes a chronically elevated Ca^{2+} level. Nevertheless, recent studies have shown that A23187 treatment is able to mimic motor neuron innervation with regard to the regulation of enzymes involved in intermediary metabolism (22), maintenance of resting membrane potential (9), and acetylcholine receptor (11, 24). The effects on acetylcholine receptors are particularly relevant since receptor density is regulated by electrical activity both *in vivo* and *in vitro* (7). These other results support the view that cytosolic Ca^{2+} is an important intracellular mediator of the effects of electrical activity on a number of muscle properties, including the density of TTX-sensitive sodium channels.

The results presented in the first section on this chapter suggest that neural influences normally act to inhibit the development of TTX-sensitive channels from postnatal days 5–11. The results presented in this section indicate that a similar inhibitory effect is exerted *in vitro* by electrical activity. It is of interest, therefore, to directly compare the development of TTX-sensitive channels in these two experimental systems. For this purpose, the

data presented in Fig. 15.7 have been converted to express the density of channels as femtomoles per milligram of protein. Figure 15.16 compares the development of TTX-sensitive channels observed *in vivo* in innervated and denervated muscle with the development observed *in vitro* in cultures with and without spontaneous contractile activity (from Fig. 15.14). There is a close correspondence between sodium channel development in cultured myotubes displaying spontaneous contractile activity, for example, control cultures, and innervated muscle *in vivo*. Similarly, cultures in which spontaneous contractile activity is blocked by bupivacaine fall on the same curve as denervated muscle *in vivo*. Thus, both *in vivo* and *in vitro*, the reduction of electrical activity leads to a similar increase in the number of TTX-sensitive channels. This comparison suggests that the lack of neuronally driven motor activity in muscles denervated at day 5 *in vivo* may account for the acceleration of sodium channel development observed from days 5 to 11.

Although denervated muscle develops fibrillations that may be analogous to the spontaneous contractile activity observed *in vitro*, it is likely that this type of muscle activity is of a substantially lower magnitude than the normal neuronally driven activity (29). This view is supported by studies of the acetylcholine receptor (AChR) in which exogenous electrical activity, but not endogenous fibrillatory activity, could prevent denervation-induced changes (23). Thus, both in the case of denervation *in vivo* and blockade of spontaneous contractile activity *in vitro*, there is a substantial decrease in the level of electrical and contractile activity and an associated increase in the number of TTX-sensitive channels.

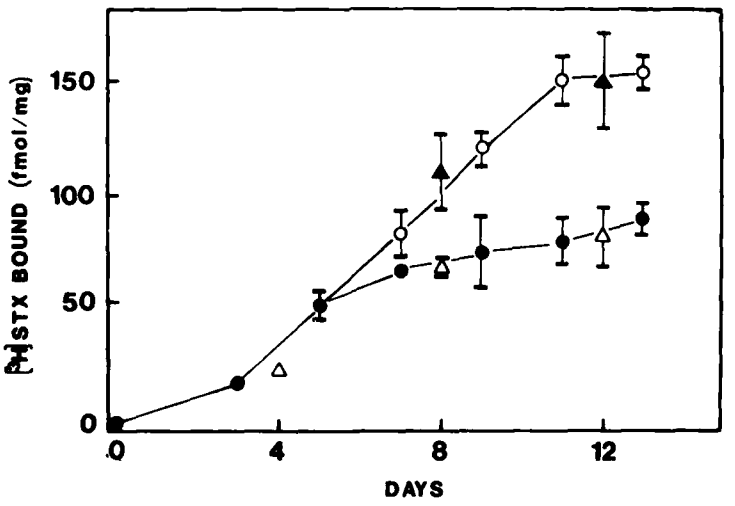

Figure 15.16. Comparison of TTX-sensitive channel development *in vivo* and *in vitro*. The developmental time course of channel development *in vivo* in rat triceps surae is shown for normal muscle (●) and muscle denervated at postnatal day 5 (○) (see Fig. 15.7). The data presented in Fig. 15.14 for control (△) and bupivacaine-treated (▲) cells are shown for purposes of comparison. The units on the ordinate are femtomoles per milligram of total cellular protein. Error bars indicate the s.e.m.

Our *in vitro* results and the comparable effects *in vivo* indicate that the innervation-independent phase of TTX-sensitive channel development is regulated by the level of electrical activity and that this regulation is likely to be mediated by changes in cytosolic Ca^{2+} levels. It is noteworthy that the AChR also appears to be under the influence of this type of regulatory system (24). Furthermore, maturational changes in both the AChR and voltage-sensitive sodium channels occur over a remarkably similar time course (see Fig. 15.3). We believe these similarities are not fortuitous but, rather, reflect important underlying processes by which the muscle cell can coordinate the developmental regulation of proteins integral to synaptic transmission and electrical excitation.

4. CONCLUSIONS

We have investigated the developmental regulation of TTX-sensitive sodium channels in rat skeletal muscle both *in vivo* and *in vitro*. The normal developmental appearance of TTX-sensitive channels in rat triceps surae was determined by measuring the density of high-affinity [^{3}H]STX receptor sites as a function of postnatal age. The regulatory role of innervation was assessed by denervating the triceps surae at various points in the developmental time course and measuring the subsequent changes in the density of TTX-sensitive sodium channels. The results of these experiments indicate that the developmental regulation of the TTX-sensitive sodium channel is biphasic. The first developmental phase leads to the appearance of approximately 50% of the adult level of channels and extends to postnatal day 11. This initial phase of development does not require continuing innervation. Rather, neuronal influences appear to inhibit the accumulation of TTX-sensitive channels during this portion of the development time course. The second phase of development, which occurs from postnatal day 11 to 21, gives rise to the remaining 50% of the adult level and is dependent on continuing innervation.

Our results suggest that the initial innervation-independent phase of development also occurs *in vitro* in uninnervated cultures of fetal muscle cells. These cells have high-affinity STX receptors with similar neurotoxin-binding properties to the receptors associated with TTX-sensitive sodium channels in adult skeletal muscle. The STX receptors found in cultured fetal muscle are almost certainly associated with functional TTX-sensitive sodium channels since these cells display spontaneous contractile activity and neurotoxin-induced Na^+ influx that is inhibited by TTX with essentially the same K_I that is observed for competitive inhibition of [^{3}H]STX binding by TTX. The time course of the *in vitro* development of TTX-sensitive sodium channels is remarkably similar to the time course of channel development *in vivo* after denervation at an early age. Thus cultured fetal muscle may provide a good model system for the study of the regulation of the initial innervation-independent phase of development that occurs *in vivo*.

The regulatory role of electrical activity and cytosolic Ca^{2+} in the development of TTX-sensitive channels was investigated by pharmacological manipulation of cultured fetal muscle cells. Blockade of the spontaneous electrical activity of these cells with the local anesthetic bupivacaine leads to a nearly two-fold increase in the density of TTX-sensitive sodium channels. This increased density of channels is likely to be due to the concomittant reduction of cytosolic Ca^{2+} since treatment with the ionophore A23187, which increases cytosolic Ca^{2+}, markedly decreases channel density. These results suggest the presence of a Ca^{2+}-mediated negative feedback system that modulates the level of electrical excitability. This modulatory effect of electrical activity is a likely explanation for the inhibitory effects of innervation observed *in vivo* during the initial phase of development.

The motor neuron has a profound influence on a wide variety of muscle properties including the three principal proteins involved in neuromuscular transmission: the acetylcholine receptor, acetylcholinesterase, and voltage-sensitive sodium channel (7, 12, 29). Previous work has clearly shown the regulatory effect of innervation on the appearance of TTX-insensitive channels (7, 15, 26, 30). The results presented here indicate that the density of TTX-sensitive channels is also regulated by the motor neuron. One can envision two major mechanisms by which the motor neuron can exert its regulatory influence. The first is that regulatory effects are mediated by the neurally imposed pattern of electrical activity. The second is that chemical mediators may be released by the nerve that exerts a local hormonal effect on the innervated muscle. A review of the current literature suggests that both mechanisms may be important in the regulation of the acetylcholinesterase (42), acetylcholine receptor (7), and TTX-insensitive sodium channel (11, 16). We are uncertain of the mechanism by which motor neuron promotes the continuing development of TTX-sensitive sodium channels in triceps surae after postnatal day 11. The results of our *in vitro* studies indicate that activity *per se* does not promote further development of TTX-sensitive sodium channels but instead has the opposite effect of decreasing the channel density without affecting the general developmental pattern (see Fig. 15.14). If a similar regulatory mechanism is present *in vivo*, as suggested by the comparison of *in vivo* and *in vitro* results presented in Fig. 15.16, then it would be unlikely that electrical activity alone could account for the effects of innervation on the development of TTX-sensitive sodium channels after postnatal day 11. Further studies will be necessary to investigate this fundamental issue fully.

REFERENCES

1. Barchi, R. L. and Weigele, J. B. (1979) *J. Physiol. (Lond.)*, **295**, 383–396.
2. Catterall, W. A. (1976) *Biochem. Biophys. Res. Commun.*, **68**, 136–142.
3. Catterall, W. A. (1977) *J. Biol. Chem.*, **252**, 8669–8678.

4. Catterall, W. A. (1980) *Ann. Rev. Pharmacol. Toxicol.* **20,** 15–43.
5. Catterall, W. A. and Beress, L. (1978) *J. Biol. Chem.*, **253,** 7393–7396.
6. Caputo, C. (1978) *Ann. Rev. Biophys. Bioeng.*, **7,** 63–83.
7. Fambrough, D. M. (1979) *Physiol. Rev.*, **59,** 165–216.
8. Fischbach, G. D. (1972) *Dev. Biol.*, **28,** 407–429.
9. Forrest, J. W., Mills, R. G., Bray, J. J., and Hubbard, J. I. (1981) *Neurosci.*, **6,** 1741–1749.
10. Frelin, C., Vigne, P., and Lazdunski, M. (1983) *J. Biol. Chem.*, **258,** 7256–7259.
11. Greuner, R. and Baumbach, N. (1976) *J. Neurobiol.*, **7,** 513–519.
12. Guth, L. (1968) *Physiol. Rev.*, **48,** 645–680.
13. Hainout, K. and Desmedt, D. C. (1979) *Biochem. Pharmacol.*, **28,** 957–964.
14. Hansen Bay, C. M. and Strichartz, G. P. (1980) *J. Physiol. (Lond.)*, **300,** 89–103.
15. Harris, J. B. and Marshall, M. W. (1973) *Nature New Biol.*, **243,** 191–192.
16. Hasegawa, S. and Kuromi, M. (1976) *Brain Res.*, **119,** 133–140.
17. Kameyama, T. and Ettlinger, J. D. (1979) *Nature*, **279,** 344–346.
18. Kidokoro, Y., Heinemann, S., Schubert, D., Brandt, B. L., and Klier, F. G. (1975) *Cold Spring Harbor Symp. Quant. Biol.*, **40,** 373–388.
19. Krueger, B. K. and Beaustein, M. P. (1980) *J. Gen. Physiol.*, **76,** 387–413.
20. Lawrence, J. C. and Catterall, W. A. (1981) *J. Biol. Chem.*, **256,** 6213–6222.
21. Lawrence, J. C. and Catterall, W. A. (1981) *J. Biol. Chem.*, **256,** 6223–6229.
22. Lawrence, J. C. and Salsgiver, W. J. (1983) *Am. J. Physiol.* **244,** C348–C356b.
23. Lomo, T. and Rosenthal, J. (1972) *J. Physiol. (Lond.)*, **221,** 493–513.
24. McManaman, J. L. and Blosser, J. C. (1982) *Biochem. Biophys. Acta*, **720,** 28–35.
25. Narahashi, T. (1974) *Physiol. Rev.*, 813–889.
26. Pappone, P. A. (1980) *J. Physiol. (Lond.)*, **306,** 377–440.
27. Postma, S. and Catterall, W. A. (1983) *Mol. Pharmacol.* **25,** 219–227.
28. Pressman, B. C. (1976) *Ann. Rev. Biochem.*, **45,** 501–530.
29. Purves, D. (1976) *Int. Rev. Physiol.*, **10,** 125–177.
30. Redfern, P. and Thesleff, S. (1971) *Acta. Physiol. Scand.*, **82,** 70–78.
31. Ritchie, J. M. and Rogart, R. B. (1977a) *Rev. Physiol. Biochem. Pharmacol.*, **79,** 1–51.
32. Ritchie, J. M. and Rogart, R. B. (1977b) *J. Physiol. (Lond.)*, **269,** 341–354.
33. Sastre, A. and Podleski, T. R. (1976) *Proc. Natl. Acad. Sci. USA*, **73,** 1355–1359.
34. Shainberg, A., Yagil, G., and Yaffe, D. (1971) *Dev. Biol.*, **25,** 1–29.
35. Sherman, S. J., Lawrence, J. L., Messner, D. J., Jacoby, K. and Catterall, W. A. (1983) *J. Biol. Chem.*, **258,** 2488–2495.
36. Sherman, S. J. and Catterall, W. A. (1982) *J. Gen. Physiol.*, **80,** 753–768.
37. Stallcup, W. B. and Cohn, M. (1976) *Exp. Cell. Res.*, **98,** 277–284.
38. Statham, H. E., Duncan, C. J., and Smith, J. L. (1976) *Cell Tiss. Res.*, **173,** 193–209.
39. Steinbach, J. H., Merlie, J., Heinemann, S., and Block, R. (1979) *Proc. Natl. Acad. Sci. USA*, **76,** 3547–3551.
40. Takamori, M. Y., Ide, Y., Mori, K., and Tsujihata, M. (1981) *J. Neurol. Sci.*, **50,** 891–894.
41. Tamkun, M. M. and Catterall, W. A. (1981) *Mol. Pharmacol.*, **19,** 78–86.
42. Vigny, M., Koenig, J., and Rieger, F. (1976) *J. Neurochem.*, **27,** 1347–1353.
43. Yaffe, D. (1969) *Curr. Top. Devel. Biol.*, **4,** 37–77.

CHAPTER 16

DEVELOPMENTAL AND REGULATORY ASPECTS OF THE SODIUM- AND POTASSIUM-ION-STIMULATED ATPASE IN AVIAN NERVE AND MUSCLE

DOUGLAS M. FAMBROUGH
BARRY A. WOLITZKY
DAVID W. PUMPLIN
Department of Embryology
Carnegie Institution of Washington
Baltimore, Maryland
and
Department of Anatomy
University of Maryland School of Medicine
Baltimore, Maryland

The sodium- and potassium-ion-stimulated ATPase plays an essential role in a variety of cellular processes. As the major transport mechanism for sodium and potassium in most cells, the Na^+,K^+-ATPase is largely responsible for maintenance of the high intracellular potassium ion concentration needed for a variety of intracellular processes. Together with the selective permeability properties of the plasma membrane, the Na^+,K^+-ATPase, by setting intracellular potassium ion concentration, indirectly sets the transmembrane potential. In addition, especially in excitable cells that have been active and thereby have accumulated excess sodium ions and lost potassium ions, the sodium pump helps to maintain a high resting potential and associated excitability by generating an outward current through its electrogenic transport of ions: exchanging three intracellular sodium ions for two extracellular potassium ions. The involvement of the sodium pump in maintenance of transmembrane potential in excitable cells was recognized and explored by Hodgkin and Keynes (7) in the years immediately following analysis of the action potential in squid axon. The Na^+,K^+-ATPase has remained of special interest to neurobiologists, and its spatial organization and activity in excitable membranes have been explored to some extent. Limiting these explorations has been the lack of convenient ligands for determining the number and distribution of Na^+,K^+-ATPase molecules on individual cells. The major ligand, ouabain, binds in a manner dependent on pumping activity, and the binding is reversible and not stabilized by fixation. In the course of our exploration of excitable cell surfaces with monoclonal antibodies to plasma membrane proteins of nerve and muscle, we identified one of the antigens as the Na^+,K^+-ATPase (4). Monoclonal antibody-24, which binds to the Na^+,K^+-ATPase, binds with high avidity to an epitope on the external face of the plasma membrane, probably located on the β subunit of the Na^+,K^+-ATPase. We have been using this monoclonal antibody and a second monoclonal antibody to the same site (a generous gift from Dr. Thomas Easton) to explore the number and distribution of Na^+,K^+-ATPase molecules on excitable cells and to examine mechanisms of regulation of the Na^+,K^+-ATPase during development and in adult animals. Some of these studies are summarized in this chapter.

1. EVIDENCE THAT MONOCLONAL ANTIBODY-24 RECOGNIZES THE Na^+,K^+-ATPASE

Monoclonal antibody-24 does not inhibit the Na^+,K^+-ATPase and does not inhibit the binding of ouabain to the Na^+,K^+-ATPase. Because solubilization of the Na^+,K^+-ATPase generally destroys ATPase activity, it was not possible to demonstrate directly that monoclonal antibody-24 can be used for selective immunoprecipitation of the Na^+,K^+-ATPase. Thus evidence that monoclonal antibody-24 binds to the Na^+,K^+-ATPase consists of close correlations between the antigen recognized by monoclonal antibody-24 and the

Na^+,K^+-ATPase (3, 4). These correlations include subunit structure and glycosylation characteristics of the antigen, solubility properties of the antigen, presence of the antigen as a major component in microsomal membranes derived from kidney and enriched for Na^+,K^+-ATPase by the method of Jorgensen (8), basolateral distribution of the antigen on cells of kidney tubules and cells of the ducts of duck salt glands, approximately equal numbers of ouabain-binding sites and antigenic sites on tissue-cultured chick myotubes and on erythrocytes, and up-regulation of antigen sites during low-potassium-ion stressing of chick myogenic cells in tissue culture. In addition, the antibody cross-reacts with purified avain salt gland Na^+,K^+-ATPase (a generous gift of Dr. J. A. Reynolds), and antigen purified with the use of monoclonal antibody-24 was used to immunize rabbits, which thereafter produced antisera that react strongly with the β subunit of salt gland Na^+,K^+-ATPase and very weakly with the α subunit of dog pancreas Na^+,K^+-ATPase (a generous gift of Dr. M. Steinberg) on protein blots after electrophoretic transfer of polypeptides from SDS-gels to nitrocellulose sheets. The sum of these observations and details of the distribution of antigen molecules on excitable cells (discussed below) and correlation of antigen with intramembrane particles in freeze fracture replicas (see below) constitute the evidence that the antigen is the Na^+,K^+-ATPase.

It was especially important to establish beyond reasonable doubt that antigen-24 was the Na^+,K^+-ATPase because several of our observations are novel, and others are either at odds with or at least surprising in light of published information on the Na^+,K^+-ATPase. These include observations on biosynthesis and assembly, on cellular distribution, on the possibility of there being multiple molecular forms, and on regulation in skeletal muscle.

2. STUDIES ON NEURONAL Na^+,K^+-ATPASE

In a survey of chicken tissues, using immunofluorescent staining of cryosections to visualize the relative amount of Na^+,K^+-ATPase on different cells, we noted very high levels of Na^+,K^+-ATPase in skeletal muscle, cardiac muscle, kidney, and nervous tissue. We used embryonic chicken brain as a source of Na^+,K^+-ATPase and isolated large amounts of Na^+,K^+-ATPase for biochemical characterization, including determination of subunit structure (Fig. 16.1) and lectin binding (4).

In the nervous system the fluorescent antibody technique revealed a very high level of Na^+,K^+-ATPase on neurons but very little on other cells, including the Schwann cells which myelinate peripheral nerve axons (illustrated in Fig. 16.2).

We were particularly interested in myelinated axons because of an earlier report that the Na^+,K^+-ATPase was confined to the portions of axolemma exposed at Nodes of Ranvier in the knifefish central nervous system (18). This matter is being examined with the aid of fluorescein-labeled monoclonal

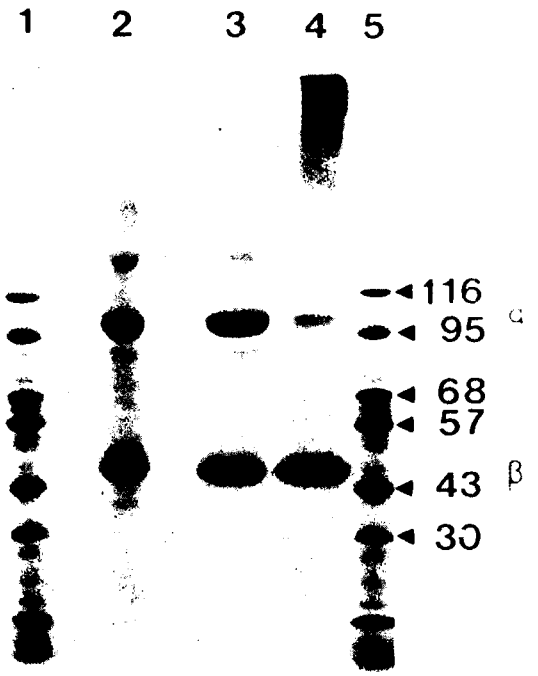

Figure 16.1. Subunit structure of chick brain Na^+,K^+-ATPase. Na^+,K^+-ATPase was purified from a detergent extract of chicken brain membranes by immunoprecipitation with 24-immunobeads and analyzed by SDS-polyacrylamide gel electrophoresis, Coomassie staining. Lanes 1 and 5 are molecular weight standards, with weights in thousands of daltons indicated at right. Lane 2, unreduced sample. Lanes 3 and 4, reduced samples. Sample in lane 4 was heated to 100°C prior to electrophoresis. (From ref. 4.)

antibody. When chicken sciatic nerves are isolated in organ culture and labeled with fluorescent antibody by injection of antibody solution under the perineurium, a strictly nodal localization of bound fluorescent antibody is seen (Fig. 16.3). The question is, does this distribution of bound antibody reflect the true distribution of the Na^+,K^+-ATPase? The answer is that it does not. Another view of the distribution of the Na^+,K^+-ATPase on myelinated nerve fibers is afforded in immunofluorescent-labeled cryosections of peripheral nerve. As shown in Fig. 16.2, the axolemma of all of the nerve fibers in peripheral nerve bundles is brightly labeled in the cryosections. These sections, which are typically about 6–8 μm thick, rarely include a Node of Ranvier. Thus the fluorescence in these sections is due to internodal axolemmal staining. (It is not possible at the level of the light microscope to distinguish between antibody binding to axolemma and to the facing membrane of the myelin. Dr. Herbert Keonig has done a preliminary study in our laboratory, using horseradish peroxidase-labeled monoclonal antibody and immunohistochemistry at the EM level, to reveal that the axolemma is the predominant site of deposition of reaction product when myelinated axons of ciliary nerve are examined.)

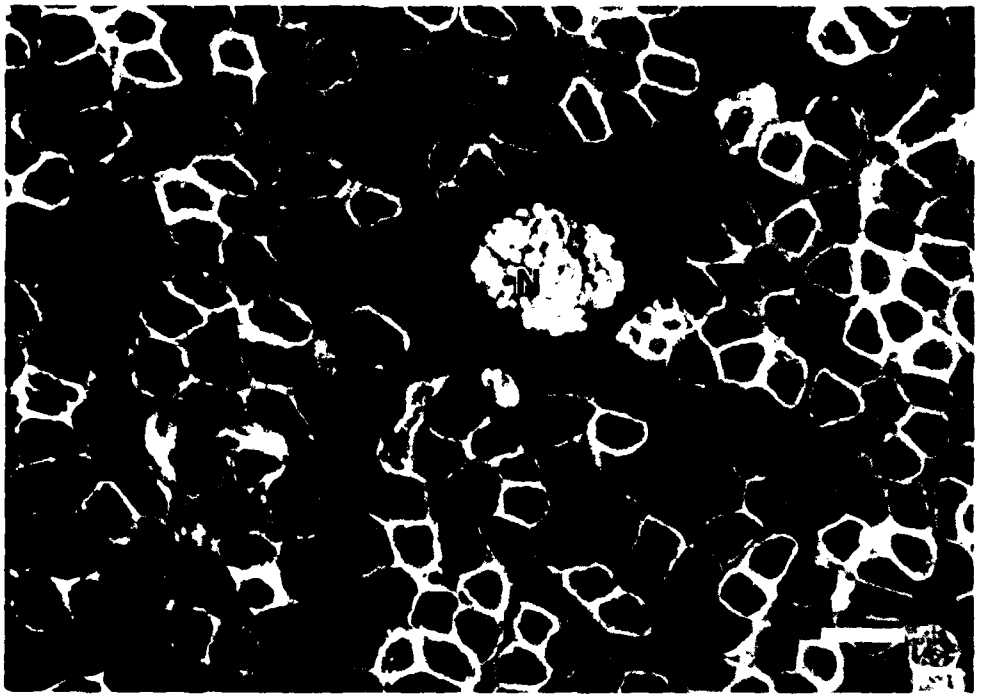

Figure 16.2. Immunofluorescence micrograph of cryosection through chick thigh muscle, illustrating intense staining of the axons in a peripheral nerve bundle (N) and variable staining of muscle fibers with monoclonal antibody-24 and fluorescein-labeled second antibody. Magnification bar = 20 μm. (From ref. 4.)

We have further examined the matter of spatial distribution of Na^+,K^+-ATPase on neurons by studying spinal cord and dorsal root ganglion neurons growing in tissue culture. Dissociated cells plated on a substratum of collagen were examined by autoradiography after labeling the Na^+,K^+-ATPase with iodinated antibody, and a very high level of Na^+,K^+-ATPase was seen on neurons as compared with cells lacking a neuronal morphology (4). To observe the distribution on single growing neurons, dorsal root ganglion cells were plated at low density on polylysine-coated cover slips and grown for about 20 h. Then the cells were labeled with fluorescein-conjugated monoclonal antibody to the Na^+,K^+-ATPase and the cells examined in the fluorescence microscope. Figure 16.4 illustrates typical appearance of embryonic neurons sending out processes in culture. Every portion of the cell surface is labeled, suggesting that there is no preferential localization of the Na^+,K^+-ATPase on the growing neurons.

The growth cones are well endowed with Na^+,K^+-ATPase. As indicated below, the Na^+,K^+-ATPase seems to be mobile in the plasma membrane. Thus the Na^+,K^+-ATPase could arrive at growth cones by diffusion from adjacent plasma membrane or could be inserted directly into the growth cone during expansion of membrane surface area. This is a question we approached several years ago, looking at the incorporation of new α-

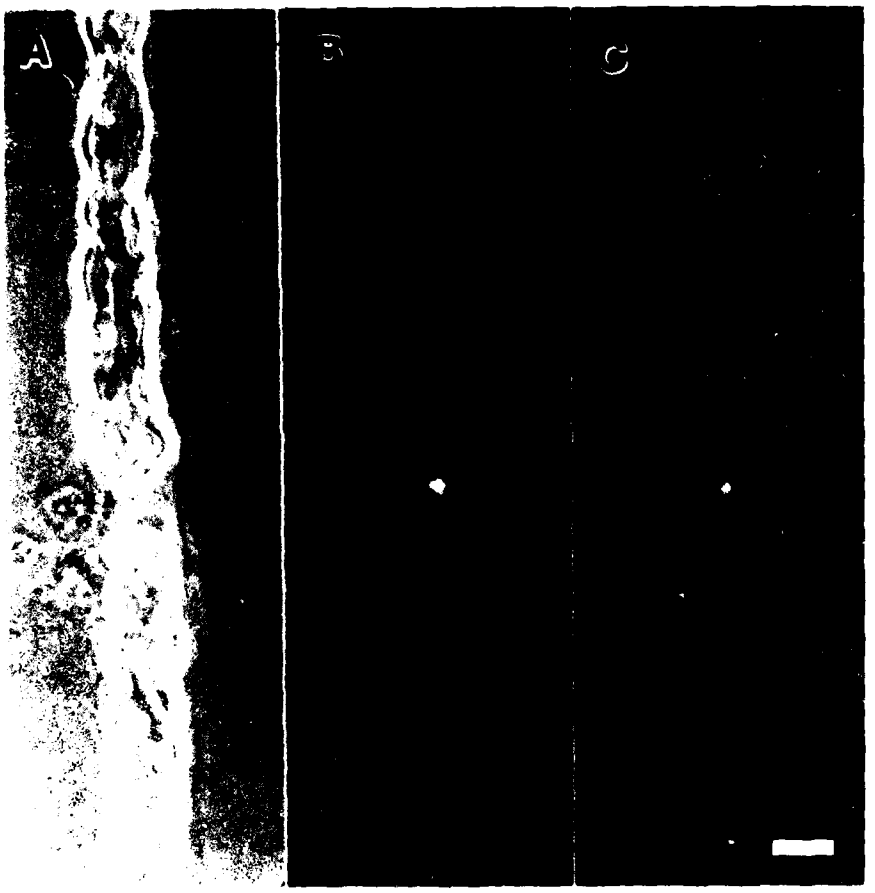

Figure 16.3. Immunofluorescent staining of a Node of Ranvier in an isolated myelinated nerve fiber from chicken sciatic nerve with fluorescein-labeled monoclonal antibody-24. (*A*) Phase micrograph, (*B*) fluorescence micrograph, and (*C*) combined phase and fluorescence. Lack of labeling of internodal axolemmal Na^+,K^+-ATPase by the fluorescent antibody is due to failure of the antibody to gain access to the internodal extra-axolemmal space. Magnification bar = 10 μm.

bungarotoxin receptors into plasma membrane of cultured sympathetic ganglion neurons (1). Monoclonal antibody-24 is a much better ligand than was α-bungarotoxin for such studies: it does not block function, has much higher avidity for its binding site, and can be fluorescently labeled to a much higher specific activity. We plan to examine this question of insertion sites by use of double fluorescent labeling strategies and photobleach-recovery measurements.

Our impression from examination of immunofluorescent-labeled cryosections of neuronal tissue is that there is a fairly uniformly high level of Na^+,K^+-ATPase present on all parts of all neurons. These observations suggest to us the possibility that regulation of the Na^+,K^+-ATPase in neurons may be a different phenomenon than it is in some other cell types. It seems possible that the high level of Na^+,K^+-ATPase in neurons signifies

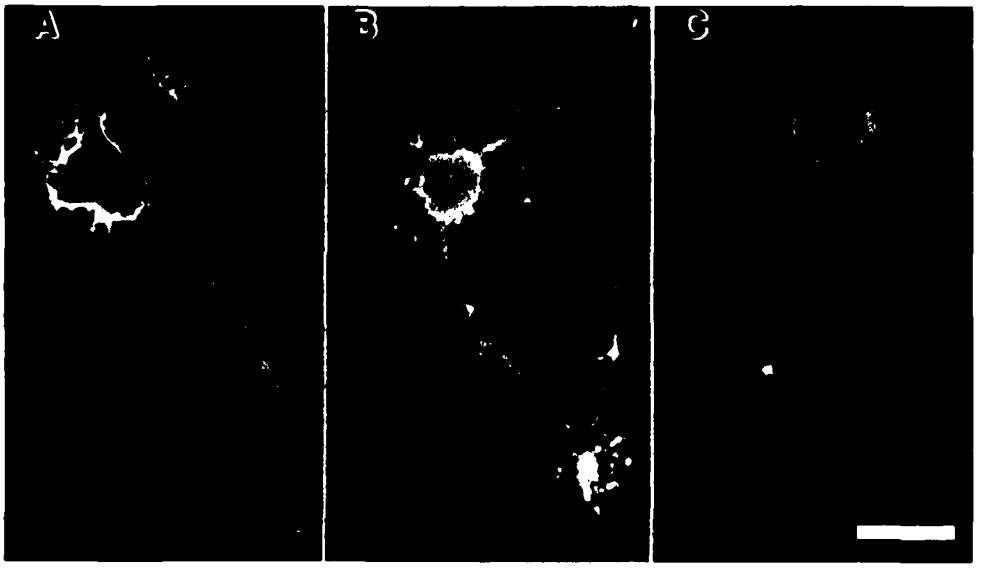

Figure 16.4. Live neurons labeled with fluorescein-conjugated monoclonal antibody-24 during the outgrowth of neurites in tissue culture. Cells from dorsal root ganglia were dissociated by trypsinization and plated on polylysine-coated cover slips and grown in Eagle's minimal essential medium supplemented with 2% embryo extract and 10% horse serum. Immunofluorescent labeling of unfixed cultures was performed about 20 h later. Magnification bar = 20 μm.

constitutive expression of the Na^+,K^+-ATPase at a level sufficient to meet maximal demands of the neuronal cells. Considering the distinctive geometry of many neurons, with processes extending for many thousands of cell body diameters and most of the influx of sodium ions occurring in these processes, it may be that regulation of the number of Na^+,K^+-ATPase molecules in these cells cannot be effected by modulation of biosynthesis and degradation of the Na^+,K^+-ATPase on a fast enough timecourse to be of use to the neurons. This matter merits attention, particularly in light of evidence that up-regulation of the Na^+,K^+-ATPase in Hela cells is accomplished by an inhibition of degradation (11). There is essentially no information on mechanisms of turnover of axolemmal membrane proteins, and therefore such an exploration of regulation of the metabolism of the Na^+,K^+-ATPase in neurons should yield fundamental information about this process.

3. STUDIES ON THE Na^+,K^+-ATPASE OF SKELETAL MUSCLE

3.1. Expression of the Na^+,K^+-ATPase during Myogenesis

Myogenesis involves proliferation of myoblasts and fusion of these to form multinucleate cells termed myotubes. Biosynthesis of contractile proteins specific for skeletal muscle fibers begins at about the time myoblasts end

their proliferative activity and commit to cell fusion, whether or not fusion occurs. This is also true for the muscle specific membrane protein, the acetylcholine receptor. In the case of the Na^+,K^+-ATPase there is, of course, a need for its ion translocation function in all cells, and thus proliferating myoblasts must contain a reasonable number of Na^+,K^+-ATPase molecules. However, there is a substantial rise in level of Na^+,K^+-ATPase during myogenesis, resulting in a particularly high level of this enzyme, as recognized by our monoclonal antibodies, in adult muscle (see below.) Formerly we used monoclonal antibody-24 metabolically labeled by growth of hybridoma-24 in culture medium containing [^{35}S]methionine to measure binding sites on myotubes in culture. Recently we obtained a new hybridoma line from Dr. Thomas Easton that we found to produce a monoclonal antibody that binds to the same site on the Na^+,K^+-ATPase as does monoclonal antibody-24. This new antibody is of lower affinity than antibody-24 but has the advantage that it can be iodinated without loss of activity. Thus we have used [^{125}I]-labeled Easton antibody for measuring number of binding sites in myogenic cells (Fig. 16.5). Binding sights are expressed on a per nucleus basis, for there are many nuclei per myotube. The relation between nuclei and surface area of myogenic cells has not been worked out and is definitely

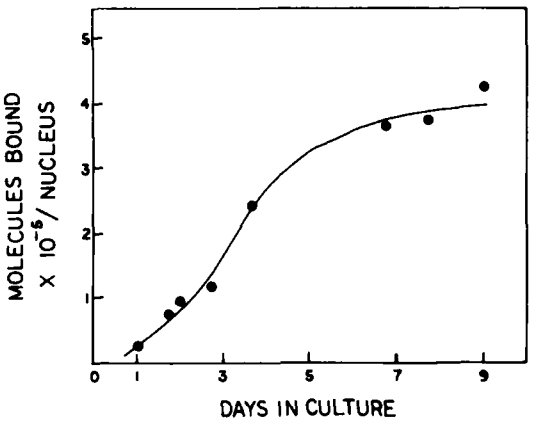

Figure 16.5. The appearance of Na^+,K^+-ATPase on the cell surface during myogenesis in tissue culture. Triplicate cultures were incubated at 20°C for 60 min in HEPES-buffered Eagle's minimal essential medium supplemented with 4% chicken serum and 10% horse serum and containing [^{125}I]-labeled Easton antibody (5 ug/ml). Nonspecific binding was determined by inclusion of 50-fold excess unlabeled antibody in the binding medium. Unbound antibody was removed by washing cultures in Hank's balanced salt solution supplemented with 0.1% bovine serum albumin and precooled to 4°C. Muscle cells were extracted in 1.0 *N* NaOH, and the radioactivity was quantified by scintillation spectrometry. Identical cultures were Giemsa stained, and the numbers of myonuclei were calculated from observation of 15 grid fields examined at × 250 magnification. In these myogenic cultures the starting myoblasts (from 11-day chick embryos) were mechanically dissociated to single cells. These were grown on collagen-coated tissue culture dishes and generally went through one or two cycles of cell division in culture during the first 48 hours before the onset of fusion and differentiation into muscle.

subject to a fair degree of variation depending upon tissue culture conditions. However, these measurements of Na^+,K^+-ATPase molecules per nucleus indicate the trend toward increased numbers of sites per unit area of membrane, which is evident in immunofluorescent-labeling experiments also.

3.2. Regulation of the Na^+,K^+-ATPase in Myogenic Cells

Another noteworthy fact about myotubes in cell culture is that there is considerable variation in the density of Na^+,K^+-ATPase sites from one myotube to the next. This variation may be related to variation in physiological maturity of the myotubes and/or in patterns of spontaneous contractile activity of the myotubes in culture. Our interest in this matter is sparked by our observations that a similar variation in number of Na^+,K^+-ATPase molecules per muscle fiber occurs in adult skeletal muscle (4, and see below).

Myotubes in culture evidence up-regulation of their Na^+,K^+-ATPase. We used the strategy employed much earlier in studies of up-regulation of the Na^+,K^+-ATPase in Hela cells (11, 17) to observe a similar up-regulation in cultured chick myotubes. Some myogenic cultures were switched to a medium containing 0.5 m*M* potassium ions instead of the regular 5.0 m*M*, while companion cultures were switched to the same medium supplemented with potassium ions to the regular level. After 16 to 20 h the numbers of Na^+,K^+-ATPase molecules in these cultures were determined in binding studies with radioactively tagged monoclonal antibody. Although there was considerable variation between experiments, the cells stressed in low-potassium medium possessed significantly more Na^+,K^+-ATPase per myotube nucleus than did control cells, the average up-regulation being about 30% in a large number of experiments. An extended analysis of the mechanism of up-regulation in skeletal muscle is planned. In this system there are voltage-sensitive sodium channels in the plasma membranes that can be opened by veratridine and closed by tetrodotoxin and thus can be used to modulate the entry of sodium into the myotubes. This strategy for modulating intracellular sodium concentration adds extra attraction to the system. The other major attraction of tissue culture systems is the ease with which metabolic studies can be done. In this particular case the availability of monoclonal antibodies to the Na^+,K^+-ATPase makes possible a quantitative analysis of rates of biosynthesis and degradation of the Na^+,K^+-ATPase and also measurements of numbers of molecules in the plasma membrane and in internal membrane systems of the myotubes. Thus we should be able to test all possible formal mechanisms of up-regulation: increased biosynthetic rate, decreased degradation rate, redistribution of molecules from an internal compartment to the plasma membrane, and revelation of masked molecules independent of biosynthesis. Toward this end we have begun a study of metabolism of the Na^+,K^+-ATPase in muscle cultures that has yielded somewhat unexpected information on the biosynthesis and assembly of the Na^+,K^+-ATPase.

3.3. Biosynthesis, Assembly, and Turnover of the Na^+,K^+-ATPase

We have used monoclonal antibody-24 covalently coupled to Sepharose beads (24-immunobeads) for quantitative precipitation and recovery of the Na^+,K^+-ATPase from cultured myotubes, and we have used pulse and pulse-chase labeling strategies with [^{35}S]methionine followed by analysis of the labeled Na^+,K^+-ATPase with SDS-polyacrylamide gel electrophoresis and fluorography for obtaining data on metabolism of the Na^+,K^+-ATPase.

When myotubes are labeled for an extended period with [^{35}S]methionine, the Na^+,K^+-ATPase is found to consist of two major labeled subunits with apparent molecular weights 105,000 and 47,000. We determined that immunoprecipitation of the two subunits with monoclonal antibody (which should bind to only one) was because the subunits were bound together in a stoichiometric complex in the detergent-solubilized state (4). There is no evidence for any homology between the α and β subunits of the Na^+,K^+-ATPase, and it is reasonable to assume that the monoclonal antibody binds either to an epitope on one of the two subunits or to some feature of the molecule generated by interacting α and β subunits. In either case, the coprecipitation of subunits by monoclonal antibody can be used as an operational definition of subunit assembly (3).

Having a method for determining that the subunits are assembled, we analyzed pulse and pulse-chase labeled Na^+,K^+-ATPase. We found that the antibody would precipitate stoichiometric complexes of subunits from cells pulse-labeled for as little as 5 min. In pulse and pulse-chase analysis on a short time scale we found that the α subunit did not change in apparent molecular weight during the chase period, suggesting the lack of significant mass of carbohydrate addition to this subunit. The β subunit underwent a series of three rapid step changes in apparent molecular weight from the polypeptide size of about 32,000 daltons to a relatively stable intermediate with apparent molecular weight 40,000 (Fig. 16.6*a*). This intermediate, which could be converted back to a 32,000 form by endoglycosidase H digestion and thus is a glycosylation intermediate with high mannose oligosaccharide additions (Fig. 16.6*b*), was more slowly converted to the mature, 47,000 molecular weight form (Fig. 16.6*a*), which was resistant to endoglycosidase H and thus contained complex carbohydrates. During these conversions of the β subunit, the ratio of radioactivity in the α subunit compared to that in the β remained constant. Thus we conclude that assembly of subunits is virtually immediate upon completion of polypeptide chain elongation and can even precede the addition of core oligosaccharides to the β subunit (3).

Further analysis of the assembly process suggests that incorporation of radioactivity into Na^+,K^+-ATPase subunits occurs chiefly during the pulse period, with little additional accumulation of radioactivity in the chase period (3). This, together with the constant ratio of label in α as compared to β

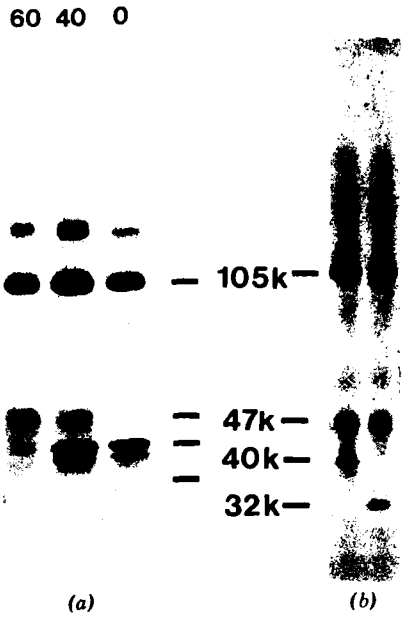

Figure 16.6. Data on the biosynthesis and assembly of Na^+,K^+-ATPase in myogenic cell cultures. Autoradiographs of SDS-polyacrylamide gel electrophoretograms. (*a*) Na^+,K^+-ATPase isolated by 24-immunobead precipitation from extracts of myotubes pulse labeled for 10 min under normal growth conditions with [^{35}S]methionine and then chased for 0, 40, and 60 min in medium with unlabeled methionine (chase times indicated above appropriate lanes.) The α subunit does not shift in apparent molecular weight during the pulse-chase period, while the β subunit undergoes a series of changes in apparent molecular weight due to glycosylations. (*b*) Effect of endoglycosidase H on Na^+,K^+-ATPase subunits. ^{35}S-labeled Na^+,K^+-ATPase-containing β subunit forms with apparent molecular weights 40,000 and 47,000 was subjected to digestion by endoglycosidase H (right lane), resulting in removal of the high-mannose oligosaccharides from the 40,000 dalton β subunit to reduce its apparent molecular weight to about 32,000. The mature 47,000-dalton form was unaffected. (From ref. 3, with permission.)

subunit, suggests that there is not a significant pool of unassembled α and/or β subunits that later are assembled into antigenic complexes of Na^+,K^+-ATPase. Rather, the data are readily explained in terms of rapid association of α and β subunits into stoichiometric complexes. This conclusion appears contradictory to suggestions that there are physically separated cytoplasmic sites for synthesis of α and β subunits, with the α subunits synthesized on free polysomes later uniting with β subunits, synthesized on rough endoplasmic reticulum, to form Na^+,K^+-ATPase molecules (13). Although our data do not rule out separate sites of synthesis of the two subunits, they do suggest a degree of coordination in the biosynthesis-assembly process not apparent from studies of biosynthesis of individual polypeptides by polysomes.

As a first step toward examination of the mechanism of up-regulation in skeletal muscle we have measured the turnover rate of pulse-labeled

Na^+,K^+-ATPase in tissue cultured myotubes under normal culture conditions. The loss of label from the Na^+,K^+-ATPase after pulse labeling with [^{35}S]methionine occurred as a first-order exponential process with a half-time of about 20 h. This is very much slower than the turnover rate reported for HeLa cells (11). We have not yet measured the turnover rate during up-regulation, but we calculate that turnover would have to be inhibited to a very large extent if inhibition of turnover were the sole mechanism involved in up-regulation in the myogenic cells.

3.4. Regulation of the Na^+,K^+-ATPase in Adult Skeletal Muscle

It is evident in Fig. 16.2 that the intensity of immunofluorescent labeling of different muscle fibers within a single muscle is quite variable. The "checkerboard" pattern of labeling intensity illustrated in Fig. 16.2 is reminiscent of the distribution of fiber types within muscles. To investigate the possible relation of various levels of Na^+,K^+-ATPase to fiber types in chick skeletal muscles, we have begun a study in which serial cryosections of skeletal muscles are stained by established histochemical methods to reveal differences in stability of different fiber-type myosin ATPases at extremes of pH (5) or are labeled by fluorescent antibody to reveal the distribution of Na^+,K^+-ATPase. Then the sections are photographed and the photographs aligned. Such alignments demonstrate unequivocally that the fiber types defined by classical staining methods are also differentially endowed with Na^+,K^+-ATPase as revealed with fluorescent antibody (Fig. 16.7).

The different levels of Na^+,K^+-ATPase in different muscle fiber types suggests that up- and down-regulation of the Na^+,K^+-ATPase in skeletal muscle may occur. This suggestion contrasts with the apparent lack of up-regulation of the Na^+,K^+-ATPase in skeletal muscles in the studies of Clausen and colleagues (2, 10), who have shown a generally lower level of Na^+,K^+-ATPase in skeletal muscles of mammals stressed by a low-potassium-ion diet. The correlation of Na^+,K^+-ATPase level with muscle fiber type suggests that there is congruence between level of Na^+,K^+-ATPase and physiological demand for sodium and potassium ion transport in individual muscle fibers. This situation would appear to fit well with our understanding of the motor unit structure of skeletal muscles. Within the muscle mass there are some muscle fibers that are almost continuously active and set the tone of the muscle and thus largely determine the role of the muscle in maintenance of posture. Other muscle fibers, innervated by different motor neurons, are recruited when the muscle is called upon to exert additional force, and some muscle fibers, innervated by yet other motor neurons, are activated only when maximal or near maximal force generation is required for short periods of time. The more continuously active muscle fibers generally have slower twitch speeds, express some different genes for contractile proteins than the other fibers, and have other biochemical and structure

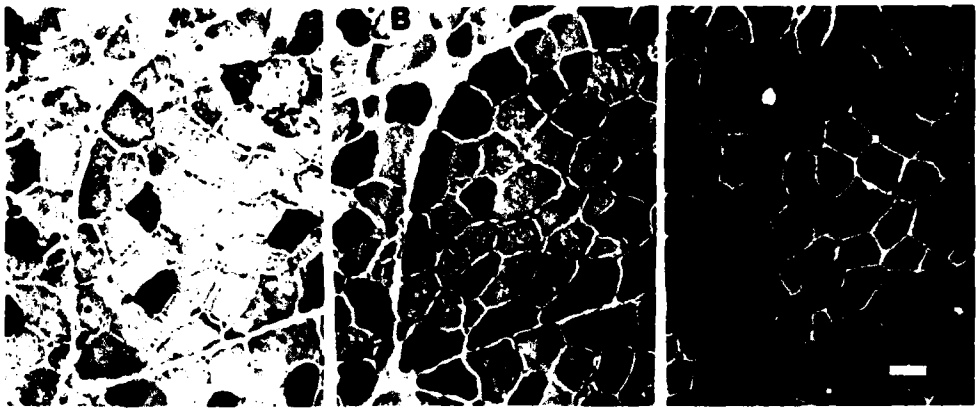

Figure 16.7. Correlation of the levels of Na^+,K^+-ATPase with muscle fiber types in chicken sartorius muscle. Serial transverse cryosections were stained for actomyosin ATPase (*A*, *B*) or binding of monoclonal antibody-24 to the Na^+,K^+-ATPase (*C*). Actomyosin ATPase activity in fast muscle fibers is acid labile, while that of slow muscle fibers is acid stable. Sections were preincubated at pH 4.35 for 30 min (*A*) for 15 min (*B*) before staining. Section in (*C*) was stained with monoclonal antibody-24 followed by fluorescein-labeled second antibody. Note that two types of fast fibers can be distinguished by their differential sensitivity to acid preincubation (*B*). Slow fibers (staining dark in *A* and *B*) contain the lowest levels of Na^+,K^+-ATPase or their surfaces and internal (t-tubule) membranes. The fast fibers with the greater sensitivity to acid pH contain the highest levels of Na^+,K^+-ATPase, whereas the more resistant class contains an intermediate level. Magnification bar = 20 μm.

features that distinguish them as slow fibers. The less continuously active fibers can likewise be subdivided into types based upon similar parameters.

In the muscle illustrated in Fig. 16.7, three fiber types are distinguished by differences in stability of myosin ATPases to acidic pH. It is reasonable to expect that the very different roles played by different types of muscle fibers in muscle activity would require different capacities for ion transport by way of the Na^+,K^+-ATPase. It is possible that these variations in capacity are totally determined by genetically fixed levels of expression of the Na^+,K^+-ATPase. However, it remains equally possible that in addition to some basal level of Na^+,K^+-ATPase there is a modulated component to the muscle fiber's Na^+,K^+-ATPase, and that this modulated component is responsible for much of the fiber type variation we see. According to this hypothesis, we expect that the different levels of Na^+,K^+-ATPase seen in different muscle fibers indicate different levels of demand for ion transport that have existed in the muscle over the past several days. This leads to the prediction that experimentally altered patterns of muscle activity would lead to altered levels of Na^+,K^+-ATPase. We plan to test this hypothesis by examining the levels of Na^+,K^+-ATPase in normal versus tenotomized or denervated or by other means inactivated muscles and in muscles subjected to controlled regimes of activity.

3.5. Correlation of the Na^+,K^+-ATPase and Intramembrane Particles

When living chick myotubes in tissue culture are labeled with fluorescein-conjugated monoclonal antibody-24, an ubiquitous distribution of Na^+,K^+-ATPase on the myotube surfaces is seen (Fig. 16.8*A*). This generalized pattern of fluorescence can be altered to a pattern of small patches (Fig. 16.8*B*) by incubating the fluorescent-labeled myotubes with an antibody directed against mouse IgG. This alteration must result from cross-linking of monoclonal antibody molecules that are bound to Na^+,K^+-ATPase molecules, and the formation of patches indicates that the Na^+,K^+-ATPase molecules are at least somewhat free to move in the plane of the plasma membrane lipid bilayer. The patching is prevented by prior fixation of the cells in formaldehyde fixative (9). The patched pattern is stable for hours while the cells continue to live at 37°C. In this respect this patching is unlike that seen when antibodies to acetylcholine receptors are used to patch the receptor molecules on myotubes. The receptors are rapidly interiorized and are degraded at a much accelerated rate after antibody cross-linking. We have not measured turnover of the Na^+,K^+-ATPase after antibody cross-linking, but we expect that an acceleration of turnover will not be seen. A variety of control experiments established that the patching of Na^+,K^+-ATPase molecules did not sweep together other membrane antigens and that patching of each of three other membrane antigens with monoclonal antibodies and antimouse IgG did not cause clustering of the Na^+,K^+-ATPase.

We have carried out a freeze-fracture study of myotubes treated as described (12). This study revealed that the fluorescent patches generated by double antibody treatment were spatially congruent with clusters of intramembrane particles (IMPs) seen in the freeze-fracture replicas of the same myotubes (Fig. 16.9). The clustered particles represented up to 50% of the IMPs in the replicas, or up to 400 IMPs per square micrometer of surface membrane. About 80% of the clustered particles were in the P-face replicas. The distribution of particle diameters for the clustered particles was virtually identical to the distribution of particle diameters for the entire population of IMPs on the myotubes.

The correlation of IMPs and Na^+,K^+-ATPase may be relevant to observations made by Schotland and co-workers (14, 15) on the numbers of IMPs in freeze-fracture replicas of normal and dystrophic human muscle fibers. These investigators reported lower IMP densities for the dystrophic muscles. Our freeze-fracture study, identifying a large fraction of the IMPs as related to the Na^+,K^+-ATPase, suggests an explanation for this difference in densities. As discussed before, our observations on levels of Na^+,K^+-ATPase in cultured myotubes and in adult skeletal muscle fibers suggest the possibility that the Na^+,K^+-ATPase is subject to up- and down-regulation in response to the needs of the muscle fibers for ion transport. We expect that normal and dystrophic muscles would be subject to different patterns and degrees of

Figure 16.8. Fluorescence micrographs of tissue cultured chick myotubes, illustrating the generalized distribution of Na^+,K^+-ATPase molecules on a myotube surface labeled with fluorescein-conjugated monoclonal antibody-24 (*A*) and the patching of these fluorescent antigen-antibody complexes (on a different myotube) by subsequent incubation with antimouse IgG serum (*B*).

Figure 16.9. Correlation of intramembranous particles with the Na^+,K^+-ATPase on tissue cultured chick myotubes. (*A*) and (*B*) illustrate a freeze-fracture replica (P-face) of a very small myotube with Na^+,K^+-ATPase molecules patched by double-antibody labeling. In (*B*) the patched areas are outlined. (*C*) consists of the inset map of the same replica at much lower magnification and a fluorescence micrograph of the same myotube made before fixation and freeze fracturing. The inset map is aligned so that correspondence between mapped areas of clustered IMPs (dark areas on map) and fluorescent patches of antibody bound to the Na^+,K^+-ATPase should be apparent. (Figure remade from data in ref. 12.)

usage and might represent somewhat different degrees of muscle maturation. These differences we would expect to be manifested in different levels of Na^+,K^+-ATPase, and thus the replicas of the freeze-fractured muscle biopsies should reflect this difference in different numbers of IMPs.

4. EVIDENCE FOR MULTIPLE MOLECULAR FORMS OF Na^+,K^+-ATPASE

The ability of 24-immunobeads to precipitate Na^+,K^+-ATPase pulse labeled for only a few minutes is consistent with the observation that antibody-24 can be used to immunoprecipitate the Na^+,K^+-ATPase from cultured myotubes pulse labeled with [^{35}S]methionine in the presence of tunicamycin [which blocks lipid-linked oligosaccharide addition to the β subunit (4)]. In both cases an unglycosylated β subunit form with apparent molecular weight about 32,000 was seen, suggesting that this is the true size of the β polypeptide in chicken muscle. These results also demonstrate that the monoclonal

antibody recognizes some aspect of protein structure of the Na^+,K^+-ATPase, since these immunoprecipitations were done on material before posttranslational modifications occurred. Because antibody-24 does not recognize either subunit after denaturation of the Na^+,K^+-ATPase and does not detect either subunit on protein blots, we are not sure of which subunit is recognized by the antibody. However, there is one experiment which suggests that the antibody interacts with the β subunit. When Na^+,K^+-ATPase is bound to 24-immunobeads and the beads are washed with a mixed micellar detergent containing 0.1% SDS and 0.05% Triton X-100, the α subunit slowly dissociates from the beads, leaving a preponderance of β subunit still bound. These aspects of the binding of the monoclonal antibodies to the Na^+,K^+-ATPase become important in interpreting a discrepancy between binding of antibody and ouabain to chicken fibroblasts and in further interpreting the immunofluorescence microscopy of chicken tissues.

During our experiments to identify the antigen recognized by monoclonal antibody-24, we were puzzled by the apparent lack of binding of antibody to certain cell types which we expected to have a reasonably high level of Na^+,K^+-ATPase, such as Schwann cells, capillary endothelial cells, and interstitial fibroblasts. Parallel binding studies with [^{3}H]ouabain and [^{35}S]methionine-labeled monoclonal antibody showed that chick myotubes in cell culture displayed the same number of ouabain-binding sites and antigen sites within experimental error; there were about 25 times more ouabain-binding sites than antibody sites on cultured chick fibroblasts (4). This discrepancy held when we redid the binding experiments, defining specific ouabain binding as potassium ion inhibitable binding rather than saturable binding.

This discrepancy, together with the strong evidence that monoclonal antibody-24 does recognize the Na^+,K^+-ATPase on neurons, muscle fibers, and kidney cells, leads us to the conclusion that there must be a form of the Na^+,K^+-ATPase on fibroblasts (and possibly on other cell types) that is not recognized by the antibody. Since the antibody recognizes some aspect of protein structure of the Na^+,K^+-ATPase (see previous discussion), the possibility suggests itself that there may be multiple forms of Na^+,K^+-ATPase encoded in different genes. An alternate possibility that the epitope on the Na^+,K^+-ATPase recognized by monoclonal antibody-24 is sequestered in certain cell types was examined by making cryosections of muscle and extracting them with various solutions in attempts to reveal latent sites on the fibroblasts and Schwann cells, but no latent sites were found (4). This result, of course, does not eliminate the possibility.

Other evidence for multiple forms of the Na^+,K^+-ATPase has come from binding studies (see, for example ref. 6) and from the work of Sweadner (16), which included both binding data and evidence for electrophoretically different α subunits of myelinated axons of the central nervous system compared with astrocytes and with sympathetic neurons grown in tissue culture.

The existence of multiple forms of the Na^+,K^+-ATPase will complicate analysis of tissue distributions and up-regulation. It is possible that some cell types express a mixture of forms, and it is possible that they respond differently to physiological signals. The problem may require the use of monoclonal antibodies specific to each form of Na^+,K^+-ATPase. Solution to the problem of multiple forms is likely to come in part from studies at the nucleic acid level.

ACKNOWLEDGMENTS

Research in the authors' laboratories is supported by grants from the National Institutes of Health to D. M. Fambrough and D. W. Pumplin and by a Muscular Dystrophy Association Research Fellowship to B. A. Wolitzky.

REFERENCES

1. Carbonetto, S. and Fambrough, D. M. (1979) *J. Cell Biol.*, **81,** 555–569.
2. Clausen, T., Hansen, O., Kjeldsen, K., and Norgaard, A. (1982) *J. Physiol. (Lond.)*, **333,** 367–381.
3. Fambrough, D. M. (1983) *Cold Spring Harbor Symp. Quant. Biol.*, **47,** in press.
4. Fambrough, D. M. and Bayne, E. K. (1983) *J. Biol. Chem.*, **258,** 3926–3935.
5. Guth, L. and Samaha, F. J. (1969) *Exp. Neurol.*, **25,** 138–152.
6. Hansen, O. (1976) *Biochim. Biophys. Acta,* **433,** 383–392.
7. Hodgkin, A. L. and Keynes, R. D. (1955) *J. Physiol. (Lond.)*, **128,** 28–60.
8. Jorgensen, P. L. (1974) *Biochem. Biophys. Acta,* **356,** 36–52.
9. McLean, I. W. and Nakane, P. K. (1974) *J. Histochem. Cytochem.*, **22,** 1077–1083.
10. Norgaard, A., Kjeldsen, K., and Clausen, T. (1981) *Nature*, **293,** 739–741.
11. Pollack, L. R., Tate, E. H., and Cook, J. S. (1981) *Am. J. Physiol.*, **241,** C173–C183.
12. Pumplin, D. W. and Fambrough, D. M. (1983) *J. Cell Biol.*, **97,** 1214–1225.
13. Sabatini, D., Colemen, D., Sabban, E., Sherman, J., Morimoto, T., Kreibish, G., and Adesnik, M. (1982) *Cold Spring Harbor Symp. Quant. Biol.*, **46,** 807–818.
14. Schotland, D. L., Bonilla, E., and Wakayama, Y. (1980) *Muscle Nerve*, **3,** 21–27.
15. Schotland, D. L., Bonilla, E., and Wakayama, Y. (1981) *Acta Neuropathol.*, **54,** 189–197.
16. Sweadner, K. J. (1979) *J. Biol. Chem.*, **254,** 6060–6067.
17. Vaughan, G. L. and Cook, J. S. (1972) *Proc. Natl. Acad. Sci. USA*, **69,** 2627–2631.
18. Wood, J. G., Jean, D. H., Whitaker, J. N., McLaughlin, B. J., and Albers, R. W. (1977) *J. Neurocytol.*, **6,** 571–581.

INDEX

AD-A166 003 REGULATION & DEVELOPMENT OF MEMBRANE TRANSPORT PROCESSES(U) MEDICAL UNIV OF SOUTH CAROLINA CHARLESTON J S GRAVES 15 MAY 85 AFOSR-TR-86-0142 1/4

UNCLASSIFIED F/G 6/16 NL

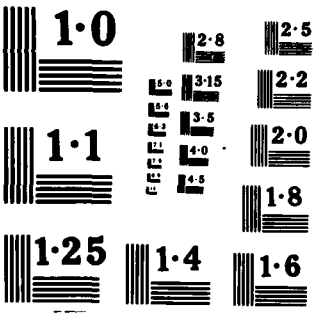
1·0
1·1
1·25
1·4
1·6
1·8
2·0
2·2
2·5
2·8
3·15
3·5
4·0
4·5

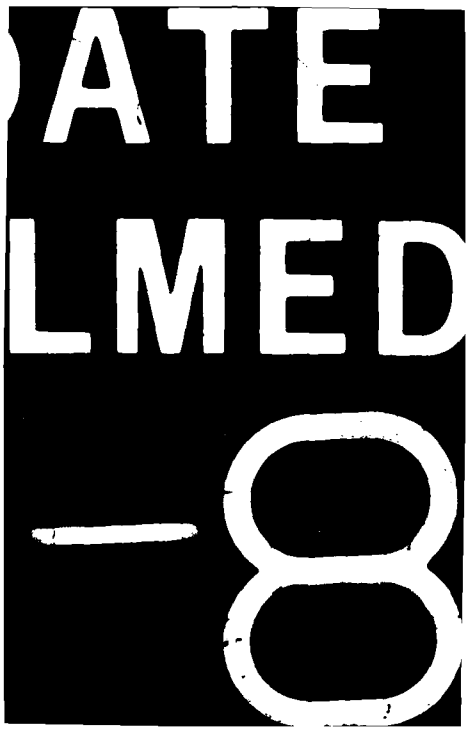
ATE
LMED
8